Development, Analysis and Testing of Innovative Mechanical Prestressing Anchors for CFRP Plates for Structural Rehabilitation and Retrofitting

by

Faizul M. Mohee

A thesis

presented to the University of Waterloo

in fulfillment of the

thesis requirement for the degree of

Doctor of Philosophy

in

Civil Engineering

Waterloo, Ontario, Canada, 2017

AUTHOR'S DECLARATION

I hereby declare that I am the sole author of this thesis. This is a true copy of the thesis, including any required final revisions, as accepted by my examiners.

I understand that my thesis may be made electronically available to the public.

ABSTRACT

This thesis presents the development, analysis and experimental investigation of three innovative, easy-to-install, low cost, epoxy-free, mechanical, friction-based, compact, high-strength, prestressing anchors for carbon fibre-reinforced-polymer (CFRP) plates. Two anchors (anchor #1 and #2) were developed to prestress the popular and commercially available 50 mm × 1.2 mm CFRP plates with 2,800 MPa strength, while the third anchor (anchor #3) was for the 50 mm × 1.4 mm CFRP plates with 2,900 MPa strength. Two anchors (anchor #1 and #3) were made of heat-treated H13 steel. Anchor #2 was the corrosion resistant anchor, and it was made of heat-treated 440C stainless steel. Each anchor consists of a CFRP plate, two annealed copper sleeves, two steel wedges and a steel barrel.

The novel CFRP plate anchors were designed and analyzed by means of: (1) experimental friction tests; (2) finite element numerical modelling; (3) mathematics-based analytical modelling; and (4) experimental investigations of the anchor prototypes.

Friction tests were conducted to characterize the tribological behaviour and to determine the coefficient of friction values between the CFRP plate and two types of copper plates (as-received and annealed). Finite element numerical models were developed to investigate the mechanics of the three anchors. A parametric study, using the numerical models, was carried out in order to optimize the anchor design. A unique mathematics-based analytical model was developed to predict the contact pressure distribution on the CFRP plate inside the anchor under loading. A manufacturability study was also conducted for the new anchors including the selection of materials, the heat-treatment procedure and 3-D rapid prototyping.

This thesis also presents the experimental results of twenty-nine tension tests to measure the performance of the anchors under loading. The new anchors were optimized through a sequential testing program for different design parameters. All three new anchors carried a load of more than 100% of the guaranteed ultimate tensile strength of the CFRP plate without any premature failure or slip of the CFRP plate from the anchor. The average failure load was

187±6 kN, 187±5 kN and 231±6 kN for anchor #1, #2 and #3, respectively. The failure mode of all of the anchors was the tensile rupture of the CFRP plate at its free length outside of the anchors. The results show that the anchors do not require any pre-setting equipment.

The new anchors can be used for new construction and for the repair, rehabilitation and retrofitting of aging infrastructure by prestressing the CFRP plate in bridges, buildings, tunnels, dams, marine structures and other structures.

ACKNOWLEDGEMENTS

I would like to thank my supervisor Dr. Adil Al-Mayah; and my former-supervisors: Dr. Alan Plumtree and late Dr. Khaled Soudki for their sincere guidance all the way.

I would like to acknowledge NSERC (for NSERC PGS-D3 scholarship) and the University of Waterloo (for President's Scholarship) for their funding for this research work. I also would like to acknowledge SIKA Canada Inc. for their CFRP plate donations for this research project. I also would like to thank Ontario Society of Professional Engineers (OSPE), Canadian Prestressed Concrete Institute (CPCI) and Canadian Transportation Research Forum (CTRF) for their scholarships; and the University of Waterloo Civil and Environmental Engineering Department for the 'Semester Performance Award' twice.

I would like to thank my friend, Marina Freire-Gormaly for her help all the way. Without her moral and analytical help and encouragements all the way, it would have been very difficult for me to achieve all of the accomplishments during my PhD studies.

I would like to thank my mother (Aeysha Hoque), my father and my brother for all of their continuous moral support all the way – for pushing me hard to do the PhD.

I would like to thank Rick Forgett, Mark Kuntz, Phil Laycock, Charlie Boyle, Jorge Cruz, Karl Janzen and Graeme Adair in the Machine Shop (for making the anchor prototypes and machine parts); Doug Hirst, Richard Morrison and Rob Sluban in Structural Engineering laboratory (for the tension tests); Kevin and Paul from IT; Richard Gordon in Mechanical Engineering laboratory (for friction and roughness tests) and Mark Griffett (for annealing and hardness tests) in Materials laboratory for their help through out this research program.

A special thanks is due to my former roommate, Dr. Andre Erler for his advices. I also would like to thank my friends: Dr. Roshanak Banan, Dr. Mihaela Vlasea, Jangchuk Tashi, Kambiz Aghassi, Adnan Azam, Dr. Rayed Alyousef, Ayman Shihata, Dr. Rizwan Azam, Sabah Hassan, Mohammad Mahdi Fazaeli, Brendan Shapton, Mohamed Enshashi, Dr. Noran Wahab, Mina Lee and Matin Parchei-Esfanai for helping me in different times.

DEDICATION

I am dedicating my PhD thesis to the following people:

1. Late Dr. Khaled Soudki, my first PhD supervisor at University of Waterloo. Without him, I might not end up doing this PhD study at all. He was the one who encouraged me and motivated me to do PhD after I won the NSERC PGS-D3 scholarship in 2012. I talked to him in late-2012 over email, phone and in-person and he motivated me to do PhD even though I was doing a very good job at that time (Hatch in Mississauga).
2. Late Susan Lee, one of my closest friends who died in December 2016, just 10 days before my PhD Defense, and I needed to attend her funeral only 3 days before my PhD defense. She was one of my closest and kindest friends in my last 10.5 years of stay in Canada. She was my friend from University of Toronto Grad House residence. She trained me a lot for Canadian English pronunciation and public speaking skills.
3. Late Niaz Ahmed, one of my closest friends in my life, who was also considered the most talented students in my year in whole Bangladesh; and who died in a very early age in 2000.
4. My mother, my father and my brother – all three of them continuously pushed me to do this PhD degree.

TABLE OF CONTENTS

LIST OF FIGURES

LIST OF TABLES

CHAPTER 1
INTRODUCTION

1.1 GENERAL BACKGROUND AND MOTIVATION

With the rapidly increasing demand for large infrastructure projects, and with the aging infrastructure (bridges, buildings and tunnels), the repair, rehabilitation and retrofitting of the infrastructure is a major focus of the government organizations in North America. The continuously reducing level of services due to structural failures and damages is a growing concern. Several bridges, highway overpasses and other structures have collapsed in the last few years in North America [1]. Reid [2] cited three major reasons for the recent structural collapses and the impending infrastructure crisis. First, there was a construction boom during the post-second world war period. Many structures in Canada and the United States were built 40-50 years ago. Standing for over 50 years, these structures have experienced significant decay and corrosion; and in some cases have suffered continuous neglect in the intervening period. Second, the population has also grown substantially, resulting in dramatic increases in both demand and loading on these structures. Third, governments cannot afford to spend the billions of dollars required to replace the aging infrastructure. According to Federation of Canadian Municipalities (FCM) [1], Canada's three levels of government require $123 billion to repair, rehabilitate and retrofit the country's infrastructure, and further delay in repair will accelerate decay in the existing infrastructure. Therefore, it is crucial to develop innovative and cost-effective tools to repair, rehabilitate and retrofit the aging infrastructure.

1.2 PROBLEM STATEMENT

The impending infrastructure crisis is driving the development of innovative and cost-effective structural materials and tools to repair, rehabilitate and retrofit structures. A composite material, fibre-reinforced-polymer (FRP), has been identified as a suitable material for the rehabilitation and retrofitting of structures. FRP has a high tensile strength, non-corroding behaviour, low weight and no magnetic conductivity. Compared to the other FRPs, carbon

fibre-reinforced-polymer (CFRP) has a higher tensile strength, a higher modulus of elasticity, a longer fatigue life and better creep properties. Different forms of CFRP composites have been used by structural engineers, including plates, rods, and sheets. The CFRP plate has an ultimate tensile strength and a modulus of elasticity higher than that of the CFRP rod, because of a higher fibre content in the CFRP plate. However, there are a number of challenges associated with its structural applications. Finding a suitable reusable anchor system, capable of carrying the full tensile strength of the CFRP plate, is one of these challenges. In order to utilize the full tensile capacity (2,800 MPa) of the CFRP plate, the plate requires to be prestressed; and an end-anchor is required in order to transfer the forces from the CFRP plate to the structure [3]. However, there is no efficient and high-strength anchor available for CFRP plates. The existing CFRP plate anchors have several major disadvantages as described below:

1. Utilization of only a small fraction of the ultimate tensile strength of the CFRP plate [4], [5];
2. Long waiting time for the epoxy to cure, up to one week [4], [5];
3. Long anchorage length because of use of epoxy, *e.g.*, as long as one meter [6];
4. Requirement of extra heating machines to accelerate the curing process [6];
5. Several complicated installation steps [6], [7];
6. Complicated and hard-to-manufacture design of the anchor [8];
7. Not reusable [4], [5];
8. Heavy weight [9].

Therefore, the development of a novel, mechanical, epoxy-free, short, cost-effective and high-strength anchor, having no premature failure or slippage of the plate from the anchor under a 2,800 MPa tension load, was required to grip and prestress the CFRP plates; and undertaken in this research.

1.3 RESEARCH OBJECTIVES AND GOALS

The primary objective of this research is to develop an innovative, practical, economical, non-corroding, epoxy-free, compact (≤110 mm long) and high-strength (≥2,800 MPa) prestressing anchor for the most popular and commercially available 50 mm × 1.2 mm carbon fibre-reinforced-polymer (CFRP) plate that can carry the full capacity of the CFRP plate (2,800 MPa) without any premature failure or slippage of the plate.

The objectives of this research program are:

1. Experimental investigation of the friction properties of the CFRP plate in contact with as-received and annealed copper plates to be used in the numerical model of the anchor;
2. Development, analysis and optimization of a finite element numerical model of an innovative anchor to grip and prestress the CFRP plates;
3. Development of a mathematics-based analytical model to predict the contact pressure distribution on the CFRP plate inside the anchor, and to validate the numerical model;
4. Performing a parametric study to optimize the anchor design; and also investigating the manufacturability of the newly developed anchor;
5. Experimental investigation of the newly developed anchor to verify the numerical model results; and to show the practical applicability of the new anchor;
6. Proposing a final design of the novel, epoxy-free and high-strength anchor that can carry a load equivalent to the full capacity of the CFRP plate (2,800 MPa) without any premature failure or slippage of the plate.

1.4 ANCHOR RESEARCH CRITERIA

There are several criteria to be fulfilled for an effective design of the new CFRP plate anchor. These criteria include the following:

1. The anchor should be epoxy-free to ensure no waiting time for the epoxy to set.
2. The anchor should not require any heat treatment of the beam/slab for its installation.
3. There should not be any galvanic reaction inside the anchor [10].
4. The ultimate tensile strength of the anchor should be at least 95% of the guaranteed ultimate tensile strength of the CFRP plate (2,800 MPa) [3].
5. The CFRP plate should not exhibit any significant slip from the anchor under the failure load;
6. The von Mises stress of the anchor components should be less than the yield strength of the anchor material.
7. The contact pressure in the CFRP plate under failure load should be less than 546 MPa (the transverse strength of the 1.2 mm thick CFRP plate) at the loading end to avoid premature failure of the CFRP plate inside the anchor [11].
8. For ease of application, the length of the anchor should be less than 110 mm [3].

1.5 RESEARCH SCOPE

This research focused on the development of an epoxy-free, mechanical, friction-based anchor for the CFRP plates. The new anchors were developed for the popular 50 mm wide and 1.2-1.4 mm thick CFRP plates. These new anchors were developed primarily for new construction and structural repair, rehabilitation and retrofitting of aging infrastructure. The research work focused on the experimental investigation of the friction characteristics between the CFRP plate and the sleeve material, the mathematics-based analytical modelling of the contact pressure on the CFRP plate inside the anchors, the finite element based numerical modelling and the parametric study of the anchors, and the experimental investigation of the newly developed anchors. The experimental investigation program concentrated on the static tensile capacity of the three new CFRP plate anchors.

1.6 THESIS CONTRIBUTIONS

The main contribution of this PhD research work was that three innovative, mechanical, friction-based, short (100 mm long), high-strength (≥2,800 MPa) anchors were developed, analyzed, optimized and tested for prestressing the 50 mm wide CFRP plates. The first anchor (anchor #1) was developed to prestress the 1.2 mm thick CFRP plates. The second anchor (anchor #2) was the corrosion resistant option for prestressing the 1.2 mm thick CFRP plates. The third anchor (anchor #3) was developed for prestressing the 1.4 mm thick and high modulus (210,000 MPa) CFRP plates.

Another contribution is the comprehensive tribological characterization between the CFRP plate and the sleeve plate. The frictional behaviour of CFRP plates in contact with as-received and annealed copper plates was characterized experimentally within the contact pressure range of 50-175 MPa. Within this range, the static coefficient of friction between the CFRP plate and the as-received copper plate was found as 0.31. The coefficient of friction between the CFRP plate and the annealed copper plate decreased from 0.39 to 0.30 with the increase of contact pressure. The shear stress vs. normal stress relationship obtained for the as-received copper plate was: $\tau = 0.31\ \sigma$. The relationship for the annealed copper plate was: $\tau = 1.02\ \sigma^{0.76}$.

A mathematics-based analytical model for the anchor was developed. The contact pressure on the CFRP plate surface inside the anchor was calculated using the analytical model.

The finite element numerical models of the new anchors were created, analyzed and optimized for different design parameters. The longitudinal profile radius of the barrel and the wedge, the length of the barrel and the wedge, the thickness of the barrel and the wedge, the pre-setting distance and the interference distance between the barrel and the wedge at the loading end had significant effects on the anchor performance. During numerical modelling, it was ensured that the anchor research criteria, given in section 1.4, were fulfilled.

Prototypes of the new anchors were made and experimentally tested. Based on the tension test results, the anchor #1 and the corrosion resistant anchor #2 exceeded the tensile capacity of the

1.2 mm thick CFRP plate (2,800 MPa); and the anchor #3 was capable of prestressing the 1.4 mm thick high modulus CFRP plate to its ultimate tensile strength (2,900 MPa). The failure mode of all of the anchors was the tensile rupture of the CFRP plate outside of the anchor at its free length. There was no significant slip of the CFRP plate from the anchor under the failure load. The experimental results showed that the new anchors would not require any extra pre-setting equipment for the installation of the anchors at the site.

1.7 ORGANIZATION OF THE THESIS

This thesis is organized into nine chapters. The motivation, the problem statement, the research objectives, the scope, the research criteria and the contributions are highlighted in Chapter 1. Chapter 2 provides a background study, a literature review of the existing CFRP plate anchors and a brief comparison among them. All of the relevant theories and previously performed numerical and experimental methods for the development of the different types of CFRP plate anchors are also described. It also presents a discussion on the properties of CFRP plates. Chapter 3 presents the methodology of the research work and the basic anchor design concept. Chapter 4 includes the details of the friction test between the CFRP plate and two types of copper plates, the experimental program, test specimen, sample preparation, instrumentation, test setup and procedure, methodology of the test, test results and discussions. Chapter 5 illustrates the finite element based numerical modelling of the new CFRP plate anchors using Abaqus software. It shows the boundary conditions, loading conditions, all of the input and output parameters, development of the base anchor, analysis and optimization process of the anchor for different design parameters, analysis of the anchor for manufacturability and the analysis results for the final designs of the anchor. In Chapter 6, the mathematics based analytical modelling of the anchor is given. The tension test program, test setup, instrumentation, test specimen, sample preparation, test parameters and procedure are given in Chapter 7. Chapter 8 provides the experimental results and discussions. The conclusions and recommendations are presented in Chapter 9.

CHAPTER 2
LITERATURE REVIEW AND BACKGROUND

2.1 INTRODUCTION

Over the last three decades, fibre-reinforced-polymer (FRP) has been introduced as a mainstream solution for the structural rehabilitation and retrofitting of aging infrastructure. This is a multi-billion-dollar industry globally; and it is leading to a continuous growth of demand for FRP materials. This is due to the high tensile strength, non-corroding property, good chemical stability in hostile environment and light weight of FRP [12]. A number of FRP materials have been developed using various types of fibres. These include carbon FRP (CFRP), glass FRP (GFRP), aramid FRP (AFRP), and basalt FRP (BFRP) [13]–[16]. In recent years, many review articles were published on the properties of FRP materials [17]–[19], their use in concrete [20]–[31] and steel structures [32]–[35], and their application in near surface mounted (NSM) systems [36], [37]. The CFRP material has a higher tensile strength, a higher modulus of elasticity, a longer fatigue life and better creep properties than the other FRP materials [6], however, its cost is also the highest [6]. The CFRP has an elastic modulus of 75-105% of that of steel, while the elastic moduli of other FRP materials are about 25-30% of steel. The CFRP material is available in different forms including round bars, plates and sheets. The CFRP plate has an ultimate tensile strength and modulus of elasticity higher than the CFRP round bars because of its higher fibre content [38]. The CFRP plates are easier to install under concrete, steel or composite beams and slabs because of its flat shape and larger total surface area, compared to the CFRP round bars.

One of the main challenges for the wide structural applications of CFRP plates is its attachment to the structure. Without adequate gripping, the plates detach from the structure [4], [5], [38]–[40]. The unanchored plates, mounted to the beam surface using epoxy, debond like a ‘zipper’ from the ends [40]. According to ACI 440.4 [39], for the prestressed CFRP plates, a special

end-anchor is necessary in order to transfer the forces from the CFRP plate to the concrete beam or slab surface. An end-anchor prevents the premature peeling-off failure of the CFRP plate from the beam. Garden and Hollaway [4] showed that the CFRP plate anchors improved the combined action between the CFRP plate and the concrete beam. They also showed that a prestressing end anchor prevented the 'cover separation' failure in the concrete structures (Fig. 2.1). In this failure mode, the full thickness of the concrete-cover separated throughout the shear span of the concrete beam. This failure was initiated by a CFRP plate end shear crack close to the support of the concrete beam. Garden and Hollaway [4] recommended the use of anchors for CFRP plates in structures to prevent the 'cover separation' failure. Hence, it is necessary to secure the ends of CFRP plates in beams by means of an anchor system [40].

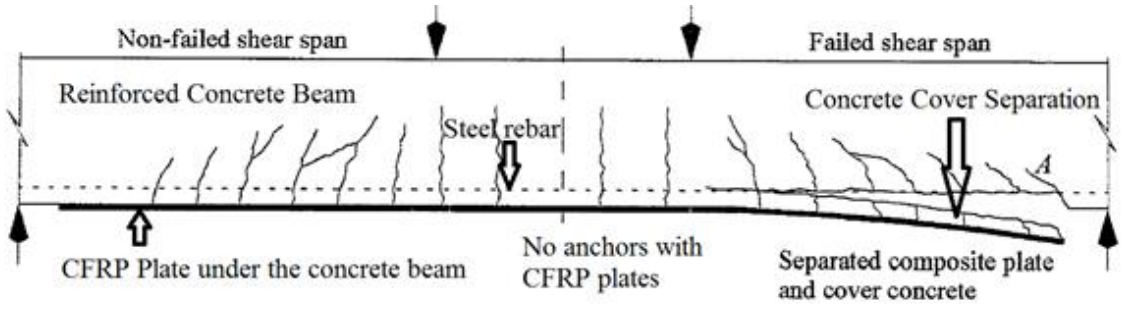

Figure 2.1: Cover separation failure because of not using an end anchor with CFRP plate [4].

Furthermore, in order to utilize the high tensile strength of the CFRP plate, prestressing of the plate is required. Prestressing can utilize the high tensile strength of the CFRP plate [39]. In addition, prestressing ensures reduced deflection and reduced cracking (delayed cracks and less crack width), resulting in an effective stress redistribution, thus delaying the failure of the concrete beams reinforced with CFRP plates [39]. The cracking and ultimate loads are higher in prestressed CFRP strengthened beams compared to non-prestressed CFRP strengthened beams. Prestressing the CFRP plates enhances the fatigue resistance of the concrete beams and slabs by reducing the crack width in the tension zone of the beam. Prestressing creates a compressive stress in a beam section. Prestressing also creates a bending moment: compression

in the lower part and tension in the upper part of the beam. With these extra stress components, the overall carrying capacity of the beam increases.

However, the conventional anchors and clamps used for steel plates can crush the CFRP at its load bearing area, leading to a premature failure of the plate at the anchor point. This is mainly attributed to low transverse compressive strength of the CFRP. Different anchor systems have been studied including, anchors for the externally-bonded FRP sheets [41], [42] and anchors for the CFRP round bars [43], [44]. Furthermore, a significant amount of research work has been carried out worldwide over the last 25 years on the development of CFRP plate anchors. However, there is limited information regarding CFRP plate anchors. This chapter presents: (i) a brief overview of the available CFRP plate anchors and their characteristics; (ii) the common failure modes; (iii) a comparative analysis of the existing CFRP plate anchors; and (iv) a discussion on the research needs. This chapter has been adapted from Mohee *et al.* [3].

2.2 METHODOLOGY

Several terms have been used in literature to describe the rectangular cross section thin CFRP plates. These terms include 'CFRP plate' [38], 'CFRP strip' [8], 'CFRP tape' [45], 'CFRP laminate' [46], [47], 'strip-shaped tensional member' [48], [49] and 'band-shaped tensional member' [50]. In this thesis, the material is termed as 'CFRP plate'. Several terms in the literature have also been used to describe the prestressing anchor for CFRP plates including 'anchor' [44], 'anchorage' [44], 'anchoring device' [47], 'grip' [8], 'prestressing device'[44], 'reinforcement device' [40], 'clamping device' [50] and 'prestressing system' [38]. In this thesis, the term CFRP plate 'anchor' is used.

2.3 CFRP PLATE PROPERTIES

CFRP plates can be used in concrete [20]–[31], steel [32]–[35], timber [51] and masonry [52] structures. The CFRP plate is an orthotropic material. The volumetric fibre content in the CFRP

plate is 68%-70%. Presently, the available CFRP plates have widths between 15 mm and 150 mm with thicknesses between 1.2 mm and 1.4 mm. The ultimate tensile strength of the CFRP plate varies between 1,300 MPa and 2,900 MPa; and the modulus of elasticity ranges between 131,000 MPa and 300,000 MPa (Table 2.1). Figure 2.2 shows a CFRP plate; and Table 2.1 gives the properties of available CFRP plates [38], [53], [54].


(a)


(b)

Figure 2.2: (a) A roll of CFRP plate; (b) a 1.2 mm thick CFRP plates.

2.4 RESEARCH SIGNIFICANCE FOR CFRP PLATE ANCHOR

A correctly designed CFRP plate anchor can significantly contribute to the repair, rehabilitation and retrofitting of infrastructure by prestressing the CFRP plate reinforcement on corroded bridges, buildings, tunnels, seaport and other structures. An effective CFRP plate anchor can also be used for the design of lighter and fuel-efficient cars, ultra-high-speed trains, airplanes, satellites and ships.

Table 2.1: Properties of CFRP plates available in the North American market

Manufacturer	Type	Dimension (mm × mm)	Ultimate strength (MPa)	Modulus of elasticity (MPa)	Ultimate strain (%)	Fibre content (%)
SIKA Canada Inc. [38]	S	100 × 1.2 80 × 1.2 50 × 1.2	2,800	165,000	1.7	68
	M	90 × 1.4	2,400	210,000	1.35	68
	H	50 × 1.4	1,300	300,000	0.45	68
Hughes Brothers [53]	Aslan 400	100 × 1.4 50 × 1.4	2,400	131,000	1.87	70
S&P [54]	150/2000	150 × 1.4 50 × 1.2	2,800	170,000	1.6	68
	200/2000	120 × 1.4 50 × 1.4		205,000	1.35	

2.5 POTENTIAL FAILURE MODES OF CFRP PLATE ANCHORS

Several failure modes of CFRP anchors installed in reinforced concrete beams have been reported by ACI 440.4 [39], El-Mihilmy and Tedesco [55], Garden and Hollaway [4], Schmidt *et al*. [44], Arduini and Nanni [56], Taljsten et. al. [57], [58], Saadatmanesh and Malek [59], Oehlers *et al*. [60], [61], Smith *et al*. [62], [63], Teng *et al.* [33], [64] and Pham and Al-Mahaidi [65]. The most common failure modes of these anchors under prestressing tensile load are:

1. Debonding at the concrete-epoxy interface (Fig. 2.3a). The CFRP plate detaches from the beam due to the high shear stress in the surface exceeding the shear strength of the concrete-epoxy interface [55]. This is also called the 'peeling off' failure.
2. Debonding at the CFRP plate-epoxy interface. Shear stress in the surface exceeds the shear strength of the CFRP-epoxy interface [55].
3. Concrete 'cover separation' failure – the anchor and the CFRP plate are forced out of the beam along with the concrete clear cover under the steel rebar [41].
4. Tensile rupture of the CFRP plate just outside the anchor (outside a distance equivalent to three diameters of the anchor) (Fig. 2.3b). This is the most acceptable failure mode, since the tensile capacity of the CFRP plate is reached [39], [55].
5. Local crushing of the CFRP plate inside the anchor due to stress concentration [39].
6. Slippage of the CFRP plate from the anchor (Fig. 2.3c). The CFRP plate slips out of the anchor and leads to a complete loss of the prestressing force [39], [55].
7. Cracking and crushing of the anchor under loading (Fig. 2.3d).
8. Fatigue failure of the anchor under cyclic or repeated loads.

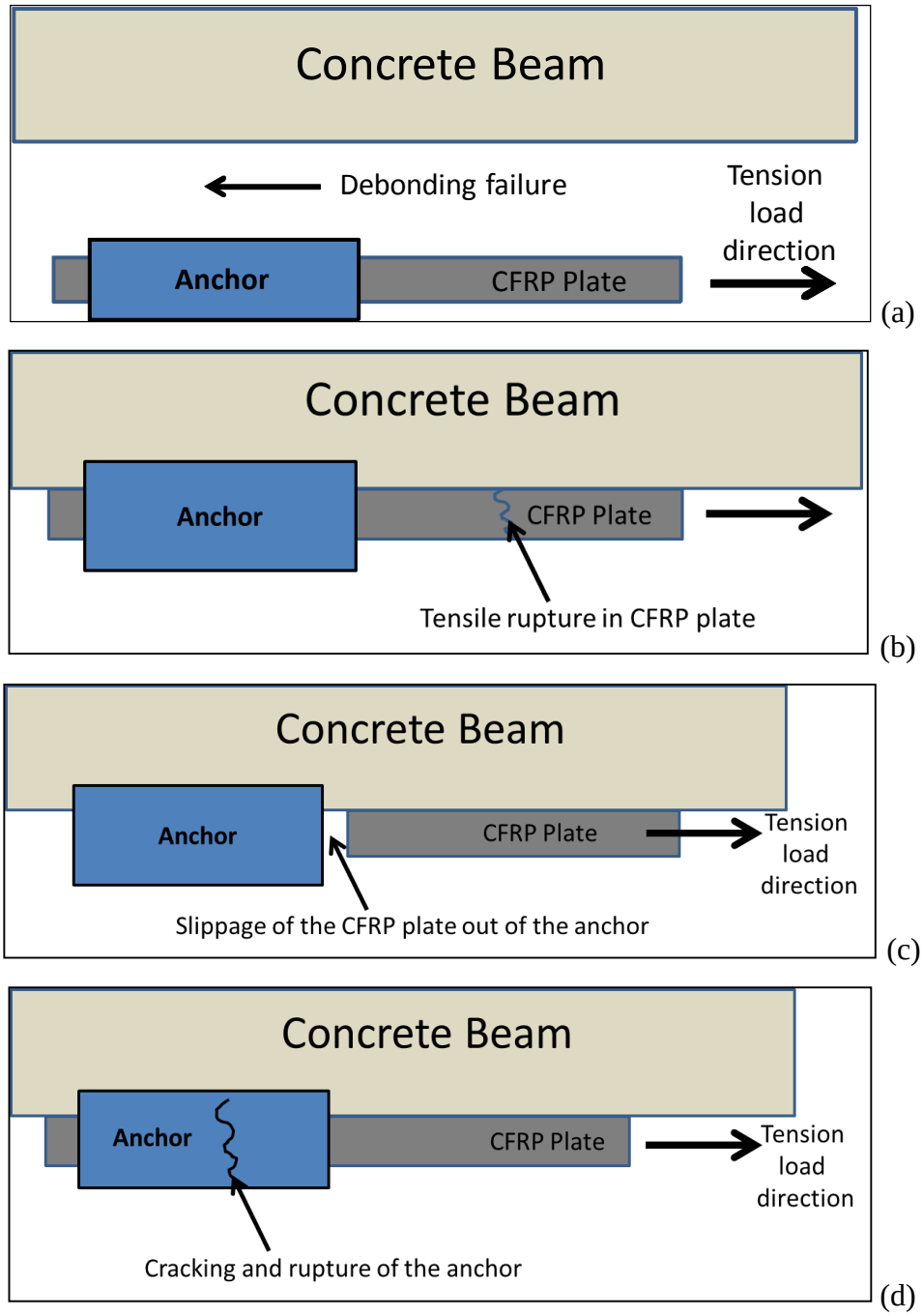

Figure 2.3: (a) Debonding failure of anchor; (b) tensile rupture of the CFRP plate; (c) slippage of the CFRP plate out of the anchor; and (d) cracking and rupture of the anchor.

2.6 EXISTING CFRP PLATE ANCHORS

Several anchors have been developed for gripping and prestressing CFRP plates in recent years. The existing CFRP plate anchors can be divided into two major categories: epoxy-based anchors and mechanical anchors (bolt-based or friction-based). The advantages and disadvantages of the design concepts and the failure modes of all anchors are considered in this section.

2.6.1 Epoxy based Anchors

Most of the existing CFRP plate anchors are epoxy-based. Triantafillou *et al*. [5] used epoxy to anchor 0.5 mm thick CFRP plates as a flexural reinforcement for wood structures. This anchor contained a 0.75–1.25 mm thick and 100 mm long epoxy layer. However, it carried only 30% of the ultimate tensile strength of the plate. Garden and Hollaway [4] presented another adhesive-based anchor with a thicker (2 mm thick) adhesive layer, but the prestressing efficiency was only 50% of the ultimate tensile strength of the CFRP plate. Jumaat and Alam [66] designed another epoxy-based anchor. It consisted of two L-shaped steel plates (each 2 mm thick) glued to the concrete beam with an anchor length of 200 mm (Fig. 2.4). The ultimate failure load was 54% of the CFRP plate's capacity. The failure mode was a premature shear failure in the concrete beam.

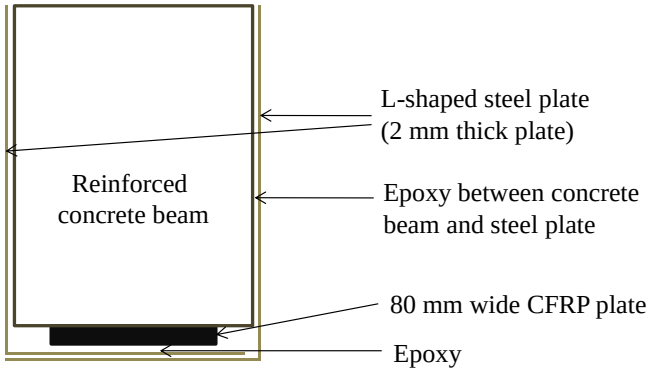

Figure 2.4: Cross section of the anchor from Jumaat and Alam (adapted from [66]).

Rytter *et al*. [7] and Kulakov *et al.* [67] designed an epoxy-based anchor, where the CFRP plate was split into two parts along the anchor. A 100 mm long aluminum wedge was inserted in the split and glued to the two parts using an anchor filling mixture (Fig. 2.5) consisting of 55% (by volume) ciba epoxy resin, 40% glass beads of 100-150 μm diameter, and 5% milled carbon fibres. Heating was required for the curing process. In order to limit the compressive transverse stress, the vertex angle of the wedge was kept at 10º for the wedge: 5º in each side of the CFRP plate axis. This anchor had a maximum tensile strength of 95.7 kN, which was 76% of the 15 mm wide and 0.5 mm thick CFRP plate's capacity. The failure mode was tensile rupture of the CFRP plate just outside of the anchor. Multiple curing stages were necessary, including splitting the thin CFRP plate into half, preparing the anchor material mix in the correct proportion, and placing the wedge at an exact angle. Rytter *et al.* [7] also showed that the geometry and the mechanical properties (modulus of elasticity and Poisson's ratio) of the anchor had a significant influence on the stresses acting on the anchor.

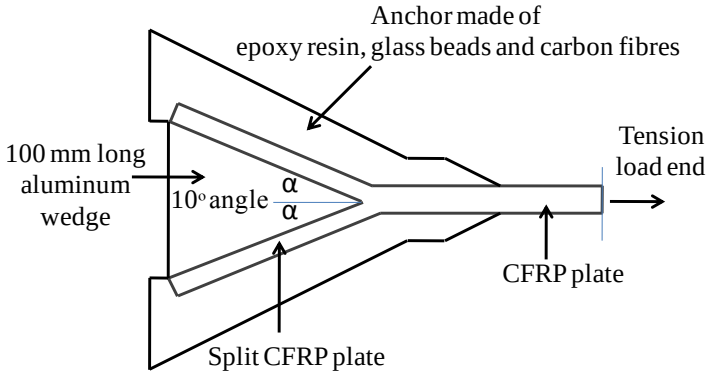

Figure 2.5: Longitudinal section of the anchor from Rytter *et al.* [7] (adapted from [7]).

Schwegler [40] introduced an epoxy-based anchor, where the CFRP plate was split into three or more parts at the end, and placed inside the anchor grooves. The split CFRP plate was then attached to the anchor with epoxy inside the grooves (Fig. 2.6). Splitting the thin CFRP plates (1.2 mm or 1.4 mm) into three or more sections was complicated at the construction site. It also used epoxy that required approximately seven days for curing to reach full strength. Since

this anchor used epoxy as a bond, it was not suitable for reuse. The ultimate capacity of the anchor was also not reported.

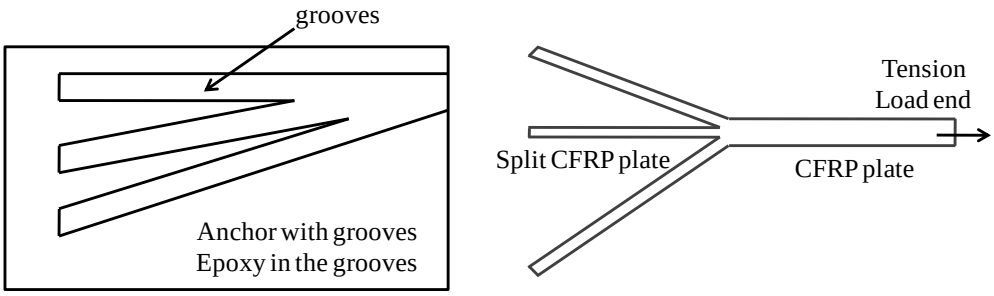

Figure 2.6: Longitudinal section of the anchor from Schwegler [40] (adapted from [40]).

An anchor patented by Yuzuru *et al*. [68] was made of mild steel; 150–400 mm long, 50–200 mm wide and 30–60 mm thick (Fig. 2.7). The anchor had an opening in the cross section. The opening had a width of 40-105 mm and a semi-circular arc of 5-15 mm radius at all four corners (Fig. 2.6). The surface of the CFRP plate was roughed by the application of adhesive on the plate, and 0.1-5 mm diameter silica sand or crushed stone layer on the adhesive. The space between the anchor and the CFRP plate was filled with a paste consisting of cement, silica fume and water. The capacity of the anchor was not reported.

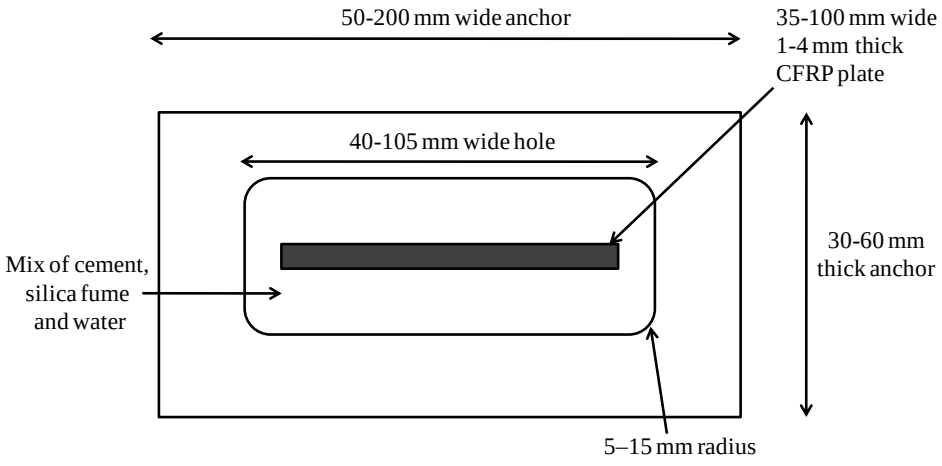

Figure 2.7: Cross section of the anchor from Yuzuru *et al.* [69] (adapted from [69]).

In the commercially available 'SIKA StressHead' anchor [38], the CFRP plate was bonded to an elliptically shaped 'StressHead' (60 mm × 80 mm elliptical cross section and 110 mm length) at both ends of the plate (Fig. 2.8). The CFRP plate was fixed to a steel framework that was placed in a hole, drilled inside the concrete beam. The CFRP plate was then mechanically prestressed by the 'StressHead' [38]. The prestressing loss was <0.1%. It took one week time for the epoxy to cure completely in order to manufacture this anchor in the factory's controlled environment [70]. This anchor had strength of 1540 MPa, which was 55% of the ultimate tensile strength of the CFRP plate. The anchor required at least 35 mm of concrete clear cover in the structure to be installed.

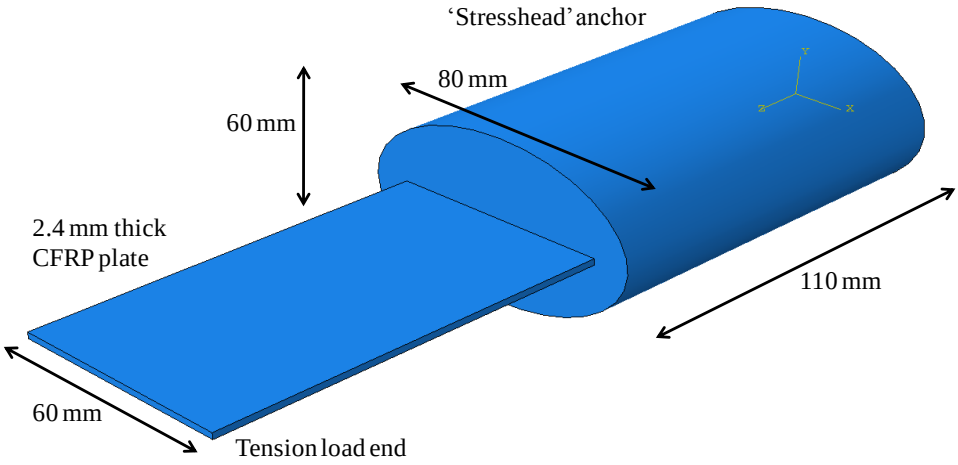

Figure 2.8: The 'stresshead' anchor from SIKA [38] (adapted from [70]).

The epoxy-based 'gradient anchor', developed by the researchers in ETH Zurich (*i.e.*, Michels, Czaderski and Motavalli), required heat-treatment of the concrete beam/slab before the epoxy application [6], [71]–[78]. The thickness of the S&P 220 epoxy layer was 2.63 mm. The heat-treatment was carried out at 90°C for approximately 2 hours, followed by a cooling down period. The heat-treatment accelerated the curing process of the epoxy; and thus the installation time of the anchor was less than epoxy-based anchors with no heat-treatment. The anchor length was 800 mm for attaining a prestress force of 120 kN, which was 36% of the ultimate

tensile strength of the CFRP plate. This anchor required phased heating and cooling the concrete beam before application. In the first step, 300 mm length of the structure was heated and the epoxy was cured within this length; and a prestress force of 50 kN was developed (Fig. 2.9). In each of the next two subsequent steps, a 35 kN prestress force was developed at a 200 mm long cured epoxy segment (Fig. 2.9). The last 100 mm length was stress-free. The installation of this anchor required over 4 hours [76]. A long term (13 year) experimental investigation of the anchor was performed and a 0.55% prestress loss was observed [76]. This anchor did not require any steel base plate for installation in the reinforced concrete beam. The size of the anchor and the curing process are the main challenges associated with the practical application of this system. This anchor is commercially available [79] together with the previous anchors from the same company [46], [80]–[82].

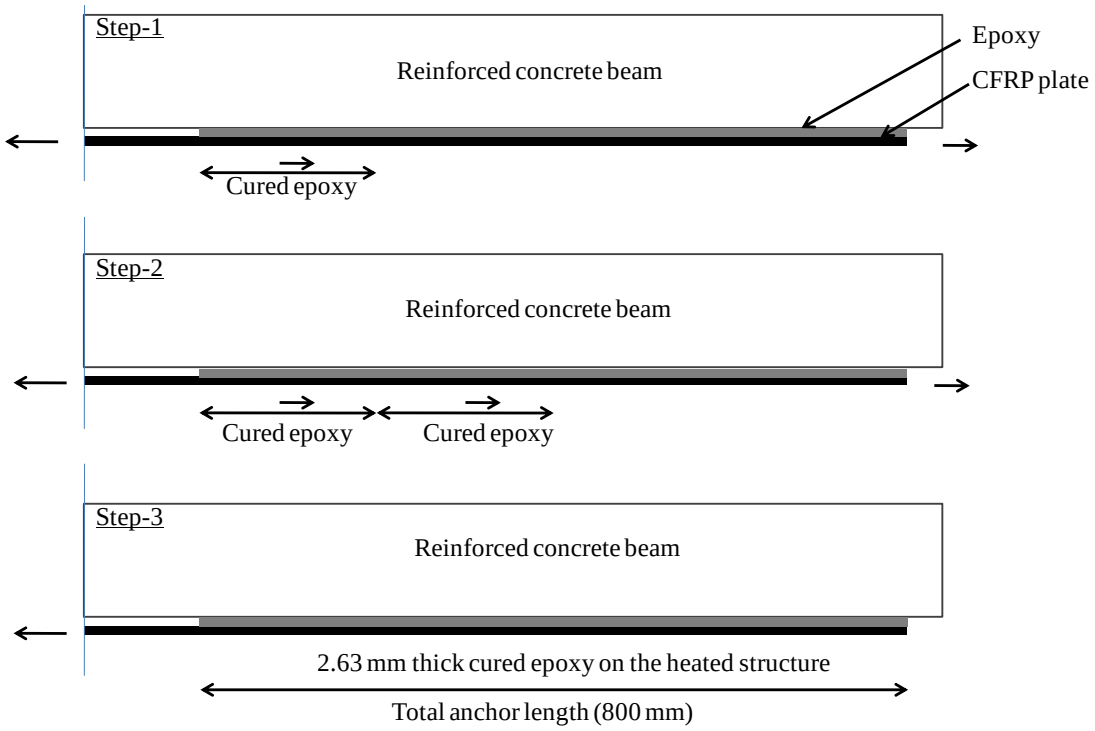

Figure 2.9: CFRP plate anchor developed by Michels *et al*. [76]: the phased heating, cooling, and prestressing force development (adapted from [76]).

2.6.2 Epoxy and Friction based Anchor

Burtscher [9], [83] introduced a wedge anchor using both friction and epoxy (Fig. 2.10). This anchor included epoxy in the CFRP-wedge interface, and used steel-steel friction in the barrel-wedge interface. This anchor had an 8 kg mass and a slope of 8º for both wedge and barrel. The wedges were made of steel and epoxy. The steel and epoxy had variable depths. On the wedge-CFRP plate surface, epoxy was applied and a ribbed surface was produced in the epoxy surface. The ribbed surface in the wedge was formed by grooves made with a triangular cross section (1 mm height) normal to the tension loading direction. The thickness of epoxy decreased from the tension load end to the free end, and vice versa for the wedge thickness. The lateral stiffness of the wedges increased from the loaded end to the free end along the longitudinal direction. This was due to the varying thickness of the steel and epoxy layers in the wedge. Since the epoxy was softer with a lower modulus of elasticity than steel; the stiffness of the wedge was primarily governed by the thickness and elastic properties of the steel part. While designing this anchor, the focus was to control the contact pressure and the tensile stress, primarily at the CFRP-wedge interface. Using a Finite Element model, Burtscher [9] showed that the contact pressure on the CFRP plate was the highest close to the free end, and gradually decreased towards the tension loading end (Fig. 2.10). On the contrary, the tensile stress on the CFRP plate was the highest close to the tension load end, and gradually decreased towards the free end [9]. Vorwagner *et al*. [84]–[88] showed the application of the anchor from Burtscher [9] secured with the near surface mounted (NSM) method. With the NSM method, this anchor required an edge distance of at least four times the CFRP plate width.

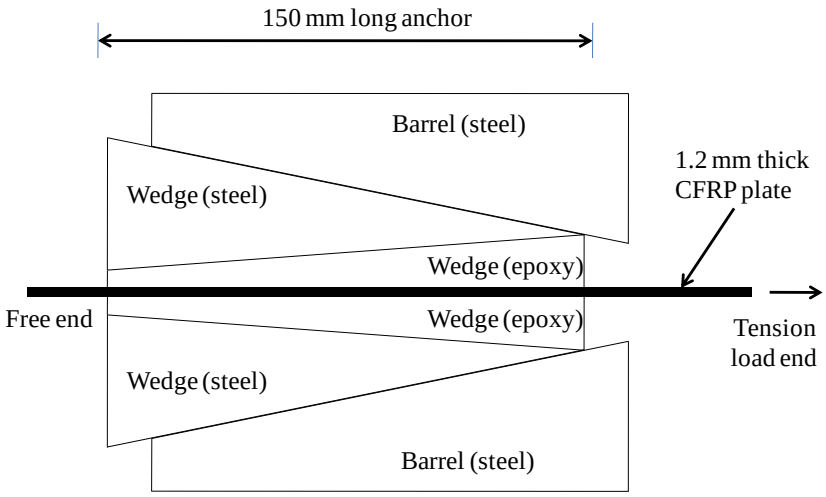

Figure 2.10: Longitudinal section of the CFRP plate anchor from [9] (adapted from [9])

2.6.3 Mechanical Bolt based Anchor

Duthinh and Starnes [89] proposed a clamping anchor using a steel plate and bolts. The bolts were torqued to 400 N.m. Andra and Maier [48]–[50], [90]–[94] developed a clamping anchor, which was a combination of clamping and bonding anchors. This anchor consisted of four steel plates: a base plate, a clamping plate, a temporary clamping plate and a fixed clamping plate. The CFRP plate was sandwiched between two steel clamping plates. The clamping plates were bolted with each other and the anchor was loaded to prestress the CFRP plate. A fixed plate was then bolted to the anchor to keep the CFRP plate in the stressed condition and the temporary plate was removed. Two adhesives were used – first, a high deformation modulus adhesive during the temporary stage, and then a low deformation modulus adhesive during the permanent stage. A cavity (500 mm × 300 mm × 35 mm) was cut into the concrete, and a base plate was placed inside the cavity. The base plate transferred the prestress force from the anchor to the concrete. The corrosion problem in this anchor was overcome by spraying an anti-corrosion adhesive layer on the steel anchor surface. In their later patent in 2010, Andra *et al.* [49] improved the design of the anchor by placing an extra traction device and a

positioning device in the anchor. The positioning device was a threaded anchor bar connecting the clamping plate with the base plate to keep them in fixed positions. The traction element was an extra adhesive layer under the steel base plate. The steel base plate was connected to the concrete beam by an adhesive layer and bolts. Andra *et al.* [49] did not report the capacity of their anchors. However, the latest version of the anchor [48] is currently not available; although it reported a strength of 1587 MPa; which is 57% of the ultimate tensile strength of the CFRP plate.

Another bolt based anchor is available [54], [95], [96] which requires that the concrete substrate is first cleaned and bolt holes drilled in the bottom of the concrete beam. Then the CFRP plate is placed under the beam. Afterwards, a steel base plate is placed under the CFRP plate. Subsequently, the CFRP plate is prestressed and clamped to the concrete beam using an aluminum supporting frame and a bolt-based mobile clamping unit. Finally, the CFRP plate is attached to the concrete beam using the S&P 220 resin.

Franca and Costa [47], [97] designed an anchor not requiring a hole in the bottom of the concrete beam. There were two 12 mm thick V-shaped plates in the anchor. Steel cylinders, connected to the concrete beam through the hole of the V-shaped plates, supported the anchor. Under the prestressing load, one arm of the V-shaped plate was in tension and the other arm was in compression. Stöcklin and Meier [98]–[100] introduced another anchor, where two big wheels were connected to the bottom of the concrete beam using anchor bolts. The CFRP plate was wrapped around the wheels and clamped at its ends. The plate was prestressed by rotating one or both wheels. The CFRP plate was first prestressed and then bonded to the bottom of the concrete beam using epoxy. Since this anchorage system requires two big wheels at the two ends of the concrete beam, this is not a practical solution for retrofitting and rehabilitation work.

2.6.4 Mechanical Bolt and Friction based Anchor

An anchor system consisting of two anchors was introduced by Figeys *et al*. [46], [101]–[104] – a temporary active anchor and a permanent passive anchor. The anchors were made of steel. A load transfer layer, made of AFRP plate, was bonded to the CFRP plate. This load transfer layer prevented the CFRP plate from slipping inside the anchor. A steel tab of 10 mm × 10 mm × 90 mm size was welded to the steel anchor and put inside a cut in the concrete. Four 70-120 mm long M20 bolts and an adhesive layer connected the anchor to the concrete. The steel tab, the M20 bolts, and the epoxy adhesive together transferred the prestress force from the anchor to the concrete (Fig. 2.11). The number of steps in the installation process was limited. The capacity of this anchor was 200 kN (1429 MPa), which represented 51% of the ultimate tensile strength of the CFRP plate.

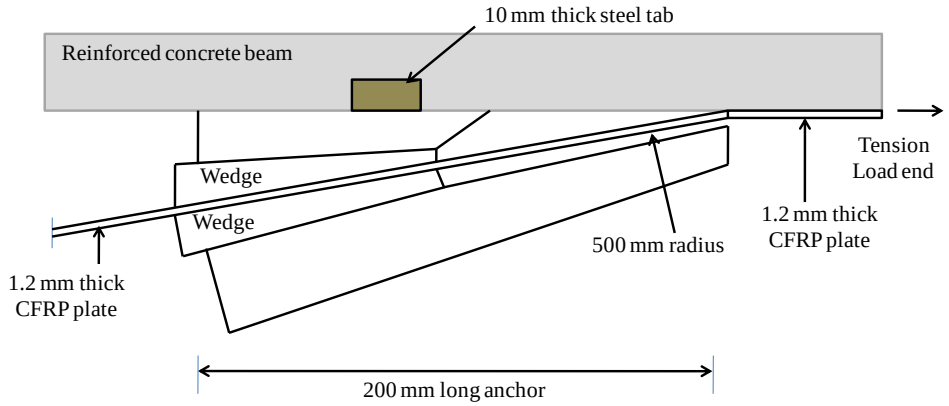

Figure 2.11: CFRP plate anchor from Figeys *et al*. [46]. (adapted from [46])

Guo [105] proposed an anchor using the three basic components: epoxy, bolts and friction. The design of this anchor used a steel barrel, two steel wedges and two aluminum sleeves. The anchor's barrel and wedge had a tapered profile. The CFRP plate and the aluminum sleeves were attached to each other by an adhesive. Friction acted at the surface between the tapered

steel barrel and wedges. However, there is no information available regarding the strength, length, weight, taper angle and friction details of this anchor.

2.6.5 Mechanical Friction based Anchor

The friction behaviour of the CFRP plate was investigated by Mohee *et al*. [106]. A friction-based duralumin-made anchor was patented by Portnov *et al*. [8], [107]–[111]. The anchor was developed based on three basic assumptions: (1) a constant coefficient of friction between the CFRP plate and the anchor surfaces, (2) absolute rigidity of the anchor, and (3) zero relative displacements of the two parts of the anchor during the tension loading. The anchor had an upper and a lower section connected through fastening bars and screws (Fig. 2.12). The top part of the anchor had a curved bottom and the bottom part had a curved top – both having the same curvature. The CFRP plate was placed between the two anchor parts, pressed from top and bottom; and the CFRP plate also had the same longitudinal curve. In this anchor, the tensile load in the CFRP plate was transferred by the shear stresses in the plate surface. These shear stresses were generated by friction during micro-slipping of the CFRP plate inside the anchor. A 65 mm long and 1.5 mm thick GFRP strip was also attached to the end of the CFRP plate to protect the CFRP plate from slippage [107], [112]. There was zero curvature at the tension load end of the plate, where the peak tensile stress was expected; hence zero bending moment at this point. The longitudinal curvature increased gradually along the length. The maximum curvature was at the free end of the anchor. The maximum curvature led to the maximum bending stress in the CFRP plate at the free end, indicated in Fig. 2.12. The reason for the alternate upward and downward curves was to impose the stress downward and upward alternately, instead of developing all of the stresses in one direction. The tensile stresses gradually decreased from the tension load end, and the bending stress gradually increased from this end over the length of the anchor. Thus the total stress was limited to the ultimate tensile strength of CFRP plate all over the length [8].

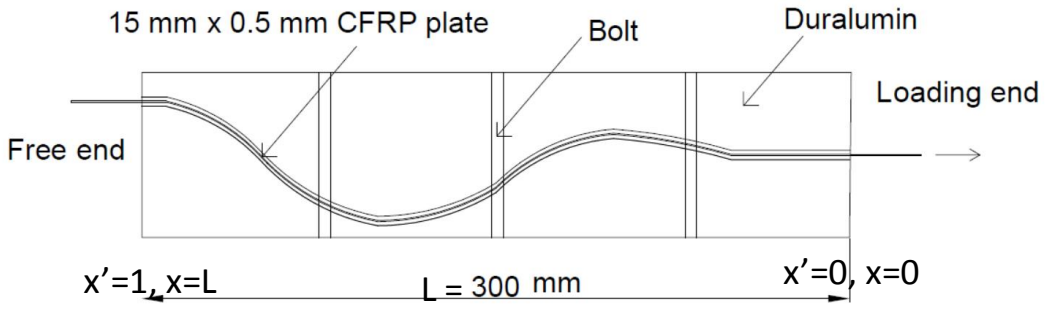

Figure 2.12: CFRP plate anchor from Portnov *et al.* [8]. (adapted from [8])

2.7 COMPARISON OF THE CFRP PLATE ANCHORS

A comparative discussion on all of the available CFRP plate anchors is presented in this section. Tables 2.2-2.5 show the comparison among the anchors for different parameters.

2.7.1 Commercial Availability

Although several CFRP plate anchors have been developed, very few are available commercially (Table 2.2). Two anchors, 'SIKA LEOBA'[38] and 'SIKA stresshead' [38], are commercially available, although the 'LEOBA' anchor is currently not available in the North American market anymore. The 'gradient anchor', developed in Switzerland, [6], [71]–[78] is commercially available through the company, S&P. The anchors from Schwegler [40], Franca and Costa [47] and Andra and Maier [49] are also available in Europe [95], [96]. The anchor developed by Burtscher [9], [83] is also commercially available in Europe.

Table 2.2: List of the commercially available CFRP plate anchors

Inventor of the Anchor	Commercial availability
Burtscher [9], [83]	Available
SIKA Leoba [38]	Available
SIKA Stresshead [38]	Available
Gradient Anchor [6]	Available
Schwegler [40]	Available
Andra and Maier [49]	Available
Franca and Costa [47]	Available
S&P [96]	Available

2.7.2 Use of Epoxy

Most of the CFRP plate anchors are epoxy-based. Different epoxy thicknesses have been used ranging between 0.75-1.25 mm [5], 2 mm [4], and 2.63 mm [6]. None of these epoxy-based anchors are reusable. These anchors are longer (165-800 mm long) than the non-epoxy based anchors (Table 2.4). All of the epoxy-based anchors have significantly longer installation times than the non-epoxy based anchors. For the 'gradient anchor' [6], the installation time is shorter than the other epoxy-based anchors, but it requires an extra heating device and heat-treatment of the concrete structure before placing the anchor. Many of the inventors recommended the development of a more efficient anchor [4], [8], [66].

2.7.3 Anchor Material

The majority of the epoxy-less anchors are made of steel, and use steel base plate and bolts (Table 2.3). Some anchors use aluminum support frames. One anchor [8] is made of duralumin (93.5% aluminum, 4.4% copper, 1.5% Magnesium and 0.6% Manganese, by weight). The typical yield strength of duralumin is 450 MPa. However, duralumin is susceptible to

corrosion. Another anchor [7] consists of an aluminum wedge and thermoplastic adhesive; and the anchor is a mix of ciba epoxy resin, glass beads and milled carbon fibres (Table 2.3). Since aluminum and aluminum alloys are susceptible to galvanic corrosion, when they are in contact with the CFRP plate [113], they are unsuitable material for a CFRP plate anchor. The anchor of Yuzuru *et al*. [68] is made of steel; and the void inside the anchor is filled with a paste of cement, silica fume and water mix. Two of the anchors [8], [46] also use AFRP layers. Some anchors [7], [68] require a precise mixing of several materials, which is time consuming and costly.

Table 2.3: Anchor materials

Inventor	CFRP Plate Anchor Materials
Burtscher [9], [83]	Steel and epoxy
Figeys *et al*. [46]	Steel, steel tab, steel bolts, AFRP plate, aluminum plate
Franca and Costa [47]	Steel frame
Portnov *et al*. [8]	Duralumin, steel bolts, AFRP sheet
Rytter *et al*. [7]	Aluminum, a mix of 55% ciba epoxy resin, 40% glass beads and 5% milled carbon fibres, thermoplastic adhesive
Schwegler [40]	Steel and epoxy
SIKA Stresshead [38]	Steel, steel bolts
S&P [54], [95], [96]	Steel base plate, aluminum supporting frame, steel bolts
Yuzuru *et al*. [68]	Mild steel, a mixture of cement, silica fume and water

2.7.4 Anchor Length

Table 2.4 shows that the anchor length varies between 110 mm and 800 mm - the 'stresshead' anchor [38] has the smallest length of 110 mm. The anchor from Burtscher [83] is the second smallest (150 mm of long), followed by the 165 mm long anchor from Rytter *et al*. [7]. The

friction-based anchor from Portnov is 300 mm long. The LEOBA anchor [38] has a length of 500 mm and the epoxy-based 'gradient anchor' [6] is 800 mm long.

2.7.5 Strength of the Anchors

The comparative strengths of the existing anchors are presented in Table 2.4. Strength-wise, the anchor from Portnov *et al*. [8] has the highest capacity of 2768 MPa, which is very close to the ultimate tensile capacity of CFRP plate of 2,800 MPa [38]. The ultimate strain of the anchor is 1.6%. However, the length of this anchor is 300 mm; and can grip only 15 mm wide and 0.5 mm thick plates. For the 1.2 mm thick CFRP plates, the anchor from Burtscher [9] can achieve the ultimate tensile strength of the CFRP plate; but for the 2.5 mm thick CFRP plates, this anchor can carry 84-87% of the ultimate tensile strength. However, this anchor can grip only the 15 mm wide CFRP plates, not the wider plates. Most of the other CFRP plate anchors have lower ultimate tensile strength. The tensile strength of the 'LEOBA' anchor [38] is 170-200 kN, which represents 48-57% of the ultimate tensile strength of the CFRP plate. The prestress loss in this anchor was 0%. The tensile strength of the 'Stresshead' anchor [38] is 1,540 MPa, which corresponds to the total tensile force of 220 kN. This tensile strength of the anchor is 55% of the ultimate tensile strength of the CFRP plate. The anchor from Duthinh and Starnes [89] carry 60% load of the ultimate strength of CFRP plates. The anchor from Rytter *et al*. [7] has a tensile strength of 95.7 kN, which is equivalent to an ultimate strength of 2,130 MPa. This corresponds to the 76% of the strength of CFRP plate. The prestress force in the 'gradient anchor' [6] is applied in three steps: 300 mm, 200 mm and 200 mm of anchor lengths achieving 50 kN, 35 kN, and 35 kN prestress forces, respectively. The anchor is able to provide a 0.6% prestrain to the CFRP plate, which is 36% of the ultimate strain of the CFRP plate. The anchor of Figeys *et al*. [46] carry a maximum of 200 kN prestress force, which represents 51% of the ultimate tensile strength of the CFRP plate.

Table 2.4: A comparative table for all available CFRP plate anchors

Type of anchor	Inventor	Length (mm)	Width/ Height (mm)	Mass (kg)	Ultimate tensile strength (MPa)
Epoxy	Jumaat and Alam [66]	200	-	-	1215
	Rytter *et al.* [7]	165	20	-	2130
	Stresshead [38]	110	80 × 60	0.55	1540
	Yuzuru *et al.* [68]	150-400	50-200 × 30-60	-	-
	Michels *et al.* [6]	800	-	-	1000
Epoxy and friction	Burtscher [9]	150	-	8	2352
Bolt	SIKA Leoba [38]	500	-	-	1587
Bolt and friction	Figeys *et al.* [46]	200	200	-	1429
Friction based	Portnov *et al.* [8]	300	-	-	2768
CFRP Plate [38]					2800

2.7.6 CFRP Plate Size

Different anchors have been developed for different CFRP plate sizes. Due to the dimension limitations and stress concentration on the CFRP plate inside the anchor, an anchor developed for a particular size of CFRP plate cannot grip a different size CFRP plate. The anchors for

narrower (*i.e.*, 15 mm) plates can achieve a higher ultimate tensile capacity than the anchors for wider (*i.e.*, 80-100 mm) plates (Table 2.4 and 2.5). Among the high-strength anchors, the anchor of Burtscher [9] is for 15 mm × 1.2 mm plates, and the one from Portnov *et al*. [8] is for 15 mm × 0.5 mm plates. In addition, the anchor from Figeys *et al*. [46] can grip the 100 mm × 1.4 mm CFRP plates. The LEOBA anchor has been developed for the 90 mm x 1.4 mm plates and the stresshead anchor is for 60 mm × 2.4 mm plates. The most popular CFRP plates in the North American market are 100 mm × 1.2 mm, 80 mm × 1.2 mm and 50 mm × 1.2 mm plates. There is no high strength anchor available for these popular but wider CFRP plates that can carry the full tensile capacity of the CFRP plates.

Table 2.5: Type of CFRP plates used in the anchors

Type of anchor	Inventor	Dimension of CFRP plate used	
		Width (mm)	Thickness (mm)
Epoxy based	Triantafillou *et al*. [5]	44	0.5 – 0.75
	Garden and Hollaway [4]	67	0.87
	Jumaat and Alam [66]	80	1.2
	Rytter *et al*. [7]	15	0.5
	Yuzuru *et al*. [68]	35 – 100	1 – 4
	SIKA Stresshead [38]	60	2.4
	Michels *et al*. [6]	100	1.2
Epoxy and friction based	Burtscher [9]	15	1.2 – 2.5
Bolt based	SIKA LEOBA [38]	90	1.4
Bolt and friction-based	Figeys *et al*. [46]	100	1.4
Friction based	Portnov *et al*. [8]	15	0.5

2.7.7 Manufacturing and Installation Steps

Some of the CFRP plate anchors require complicated manufacturing process [8],[7]. Some anchors have wavy longitudinal profile, and it is not realistic to compress a wider and thicker CFRP plate into curved longitudinal shape [8]. Other anchors require the mixing of an exact proportion of multiple materials into an exact geometry shape during the manufacturing process [7],[68].

Some of the anchors have complicated installation procedures. Some anchors require the CFRP plate to be split into two [7], and up to four parts [40]; and require the wedge to be inserted into an exact angle (5º in each side of the CFRP plate axis) [7]. Another anchor requires multiple step curing and pre-heating of the structure before the installation of the anchor [6]. Furthermore, all epoxy-based anchors require a long installation time (up to one week) for the epoxy to cure.

2.7.8 Measures How to Fix Anchors to the Structure

Different measures were used to attach anchors to the structure. All of the anchors from Andra and Maier [48]–[50], [90]–[94] used base plates and clamping bolts to connect to concrete beams. Most of the epoxy-based anchors used epoxy to connect the CFRP plate to the concrete structure. The 'stresshead' [38] anchor used the epoxy-made head to connect to the beam mechanically; and the head was fixed to the concrete beam using bolts. Some anchors (*i.e.*, Schwegler [40], Yuzuru *et al*. [68]) were placed in a recess made in the concrete beams. The anchor from Franca and Costa [47], [97] used V-shaped steel plates and steel cylinders to connect their anchor to the concrete beam. Stöcklin and Meier [98]–[100] used two big wheels at each end under the concrete beam to prestress the CFRP plate; and the wheels were connected to the beam using steel bolts.

2.7.9 Typical Projects using CFRP Plate Anchor

The CFRP plate anchors were used for new construction and repair, rehabilitation or retrofitting of aging structures.

New construction included building, bridge, underground parking and underground tunnel projects. The 'LEOBA' CFRP plate anchor was used in several new construction projects including a bank building project at Langen near Frankfurt, Germany [38]. The SIKA ‘stresshead’ CFRP plate anchor was used in several projects that included the Trade building project in Amsterdam, Netherlands [38]. S&P CFRP plate anchor was used for the construction of a new primary school building in Nebikon, Switzerland.

Repair, rehabilitation and retrofitting included building, bridge, underground parking and underground tunnel projects. They also included the seismic retrofitting of structures. The 'LEOBA' CFRP plate anchor was used in a bridge repair project over the Lauter river near Gomadingen in Baden-Württemberg state in Germany and the ‘Fina’ high-rise building project in Frankfurt, Germany [38]. The ‘stresshead’ CFRP plate anchor was used in several projects that include the Lucerne Police Headquarters building project in Switzerland and the Sung San Bridge project in Seoul in South Korea [38]. The S&P CFRP plate anchor was used for the repair of an underground garage in Kasparstrasse, Switzerland in 2014 [96]. A total of 44 prestressed CFRP plates of 150/2000 type, 100mm × 1.4 mm size and four-meter-long each, were installed in the third basement level in the parking lot and placed in the upper deck surface. Un-prestressed CFRP plates were used for seismic retrofitting in a 50-year-old residential building project in Pilgerstresse, Switzerland. They were also used for the restoration of a pedestrian underpass project in Bodenstrasse, Switzerland in 2014. Repair of a 40 year old concrete “Viadotto delle Cantine a Capolago” bridge in southern Switzerland was performed using CFRP plates prestressed by ‘gradient’ anchor in 2007 [71]. Six CFRP plates of 50 mm by 1.2 mm × 15.5 m length in each girder were used. Each of the CFRP plates was prestressed at 1,000 MPa.

2.8 CONCLUSIONS AND RESEARCH NEEDS

It is evident that there is a wide range of different CFRP plate anchors available which are diverse in terms of materials used, geometry, strength, performance, design parameters and failure modes. Anchors for smaller width (*i.e.,* 15 mm) CFRP plates have a higher ultimate tensile strength than the anchors for wider (*i.e.,* 50 mm) plates. The epoxy-based anchors carry a small fraction (35-60%) of the ultimate tensile strength of the CFRP plate. The mechanical anchors carry a higher ultimate tensile load than the epoxy-based anchors. In addition, the epoxy-based anchors have a longer anchor-length and installation time. Therefore, a mechanical anchor is the most efficient option. A majority of the existing anchors require unconventional manufacturing and complicated installation steps, and thus become highly expensive.

No high-strength CFRP plate anchor has yet been developed for the popular 50 mm × 1.2 mm CFRP plates that is capable to carry its ultimate tensile strength (2,800 MPa). Furthermore, no CFRP plate anchor has yet been developed that is economically and practically competitive, compared to the existing steel post-tensioning anchors. Therefore, it can be concluded that the development of an innovative, easy-to-use, epoxy-free, high-strength (≥2,800 MPa tensile strength) and short (≤110 mm long) anchor for CFRP plates of 50 mm width and 1.2 mm thickness is required. Consequently, such an anchor was developed in this PhD research work.

CHAPTER 3
METHODOLOGY AND DESIGN CONCEPT

3.1 METHODOLOGY

This chapter discusses the methodology of this research project to develop, analyze, optimize and test an innovative CFRP plate anchor that is compact, easy to use, and able to carry the high tensile strength of the CFRP plate. The methodology covers the analytical modelling, the numerical modelling and the experimental investigation. The experimental investigation includes two major tests: first, the friction test between the CFRP plate and two types of copper plates; and second, the tension test of prototypes of the newly developed anchors. Figure 3.1 shows the methodology of this research program in a flowchart.

Through the friction tests, the frictional behaviour of the CFRP plate in contact with as-received and annealed copper plates was characterized. The shear stress vs. contact pressure relationship was explored for both types of copper plates. The coefficient of friction values between the CFRP plate and the two types of copper plates were determined.

A base numerical model of the new CFRP plate anchor, based on the finite element method (FEM), was developed using Abaqus software. From the friction test results, the coefficient of friction value (μ) obtained between the CFRP plate and the annealed copper sleeve plate was used as an input parameter into the numerical model (Fig. 3.1).

A unique mathematical model was developed to predict the contact pressure on the CFRP plate inside the anchor under loading; and also to predict a preliminary thickness of the anchor. The model included all anchor components namely: CFRP plate, sleeve, wedge and barrel.

A detailed parametric study, using the numerical model, was conducted in order to optimize the design of the CFRP plate anchor (Fig. 3.1). Different design parameters were investigated, including the pre-setting distance, the length of the anchor, the interference distance along the Y-direction between the barrel and the wedge end points at the loading end ($D_{w.l.} - D_{B.l.open}$ in

Fig. 3.2), the longitudinal curvature of the barrel and the wedge, and the thickness of the barrel and the wedge. The parametric study was used to develop an optimized design of the shortest and the lightest anchor carrying the full capacity of the CFRP plate without any premature failure or slippage.

The manufacturing process of the anchor was also explored and an easier manufacturing process was finalized. The anchor design and the numerical models were updated and analyzed accordingly. The exact material (*i.e.*, the exact grade and the heat treatment process of steel and copper to achieve the required strength) used to make the anchor was also identified in this thesis. Furthermore, two 3D-printed prototypes of the new anchor were made and used in order to design different components and equipment used in the tension test process before manufacturing the actual anchors.

Based on the numerical modelling, analysis, parametric study and manufacturability-study results, prototypes of three newly developed anchors were made and tested for their tension capacity and failure modes (Fig. 3.1). A total of twenty-nine tension tests were carried out. The research steps are shown in a flowchart in Fig. 3.1. All of these research steps are discussed step-by-step in the subsequent chapters in this thesis.

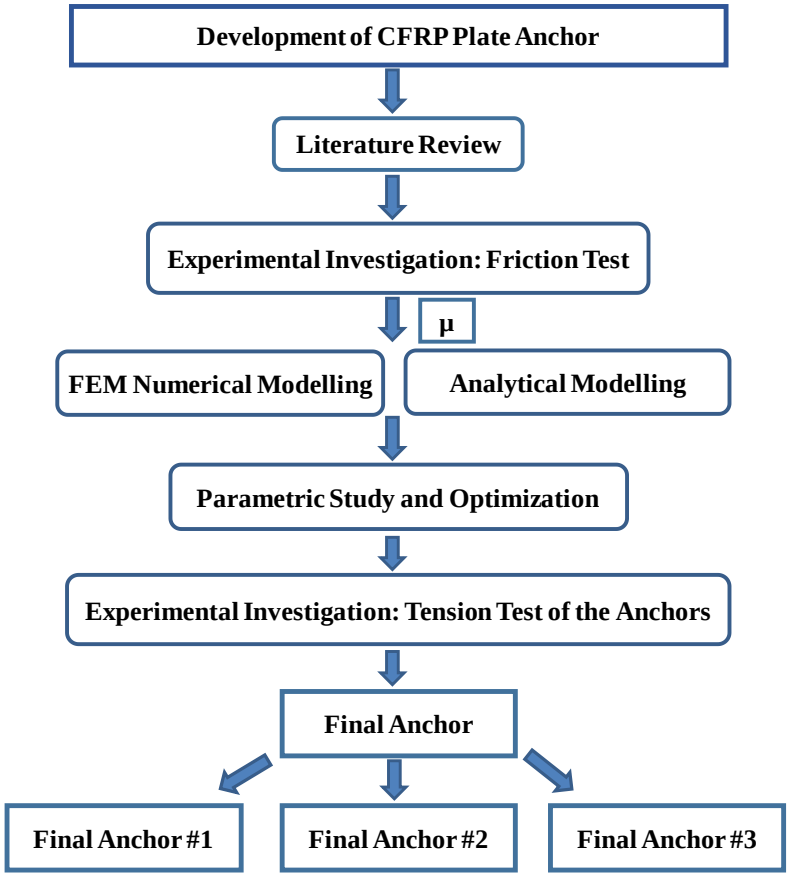

Figure 3.1: Flowchart of the methodology of the research program

3.2 DESIGN CONCEPT OF THE ANCHOR

The development of the novel CFRP plate anchor started with a conceptual design of the anchor. This friction-based mechanical anchor does not require any epoxy or adhesive. Hence, it requires no curing time that is normally needed in resin or epoxy-based anchors that delays the construction significantly. In addition, the minimum required length for the epoxy-based anchors is high (as long as one meter long). Therefore, a mechanical wedge-anchor was chosen for this research.

Based on the literature review, a circular-profile wedge-anchor (Fig. 3.2) was adopted due to its efficiency in reducing the stress concentration that frequently caused premature failure of CFRP materials inside the previously developed anchors. The new CFRP plate anchor consists of a CFRP plate, two annealed copper sleeves, two steel wedges and a steel barrel (Fig. 3.3).

The CFRP plate is a soft and orthotropic material; and it is weak in the transverse direction. Therefore, a soft layer is required to protect the plate from rupture caused by direct contact with hard steel. The sleeve layer can be copper, aluminum, annealed copper or annealed aluminum. Since aluminum, in presence of CFRP, can cause galvanic corrosion, aluminum was not considered in this anchor. Between as-received copper and annealed copper, annealed copper is softer [106]. In addition, it was expected that softer annealed copper would have a higher coefficient of friction than as-received copper [106]. Therefore, annealed copper was used as the sleeve material.

The basic principle of anchoring CFRP materials for prestressing application is to apply uniform transverse pressure on the CFRP in order to grip it [114]. According to the 'soft zone concept' [43], [115], the stiffness of the anchor should be varied along the longitudinal profile in order to avoid any premature failure of the CFRP inside the anchor. Furthermore, according to the 'differential angle concept' [116], the difference in angle of the wedge and the barrel along their longitudinal profile should be as small as possible (less than 4^{o}) in order to avoid any premature failure of the anchor.

Therefore, one of the primary objectives of this anchor design was to ensure an uniform total pressure distribution on the CFRP plate along the anchor-length. The tensile stress was the maximum at the loading end of the CFRP plate. In order to maintain the total stress uniform and within the allowable limit all over the length of the CFRP plate inside the anchor, the longitudinal profile of the anchor was designed appropriately. Therefore, as shown in Fig. 3.2, a circular longitudinal profile for both the wedges and the barrel, with the same radius (R) and center (C), was chosen. The center of the circular curve (C) was considered along the line of

the barrel end at the loading end. The circular profile was chosen such that the tangent of the surface was the lowest (zero) at the loading end and the highest at the free end. The interference distance between the barrel end and the wedge end at the loading end of the anchor (as shown by the $D_{w.l.} - D_{B.l.open}$ distance in Fig. 3.2) should also be as small as possible. The circular profile of the wedge and the barrel was chosen such that the contact pressure on the CFRP plate was the minimum at the tension load end and the maximum at the free end (or, the pre-setting end) (Fig. 3.2, 3.3, 3.4b). These phenomena in the anchor design would overcome any stress concentration at the loading end of the anchor; and thus resist any premature failure of the anchor.

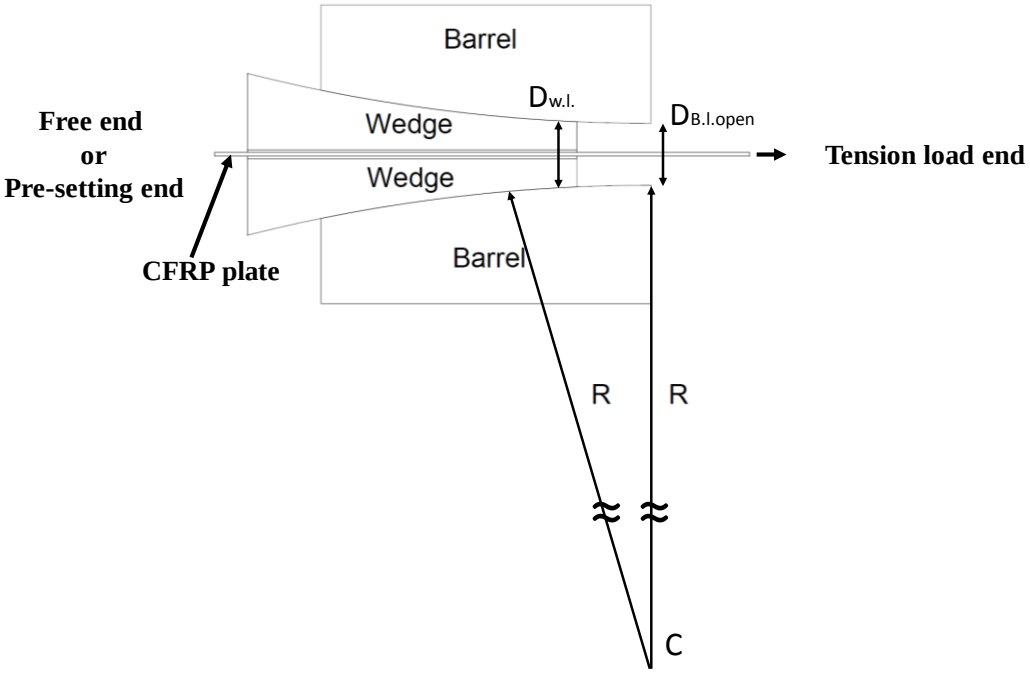

Figure 3.2: The schematic longitudinal circular profile of the barrel and the wedges.

The exact material selection for the manufacturing of the anchor is also very important in order to ensure that the anchor would act according to the theoretical behaviour. The manufacture-ease should also be considered for an easy and cost-effective manufacturing of the anchor (Fig. 3.3b). Figure 3.3 shows the three-dimensional view of the anchor: the solid anchor

(Fig. 3.3a) and the bolted anchor for manufacturing ease (Fig. 3.3b). The cross-sectional view and the longitudinal view of the anchor are also shown in Fig. 3.4a and 3.4b, respectively.

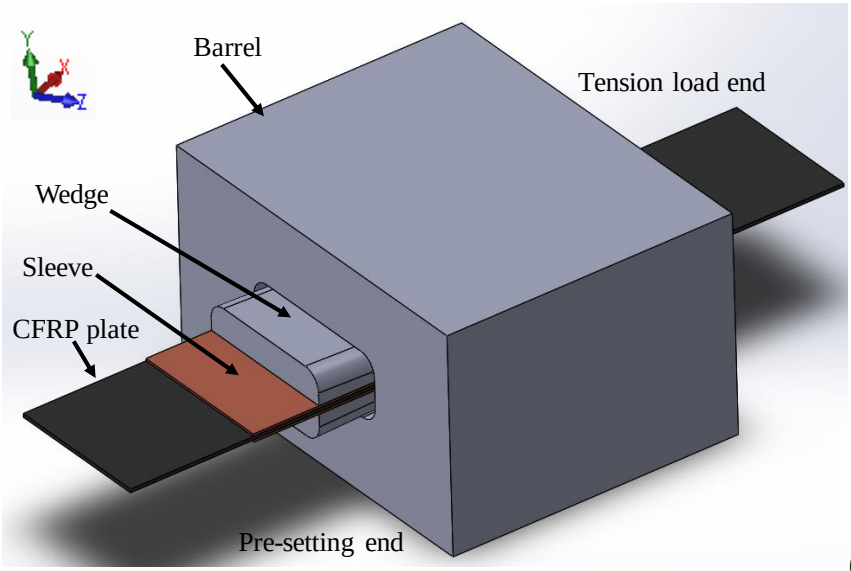

(a)

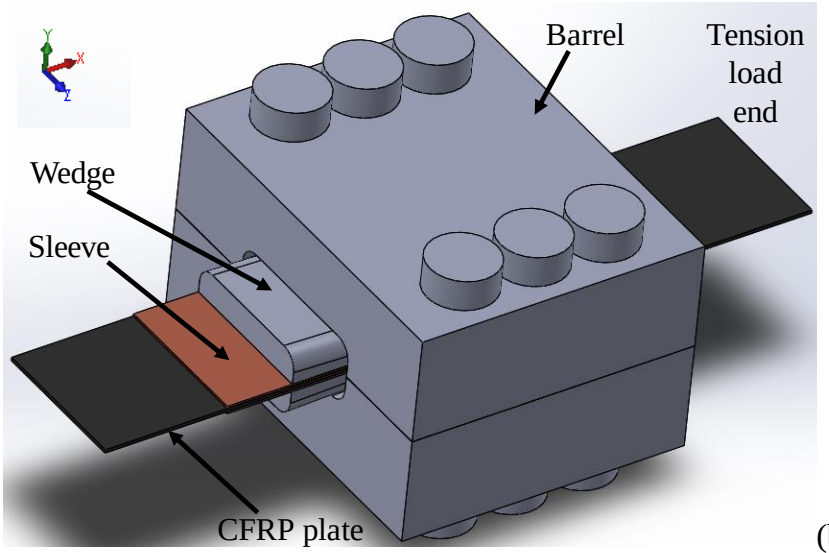

(b)

Figure 3.3: The three-dimensional isometric view of the CFRP plate anchor model: (a) the solid anchor without bolts, and (b) the anchor with bolts for manufacturing ease.

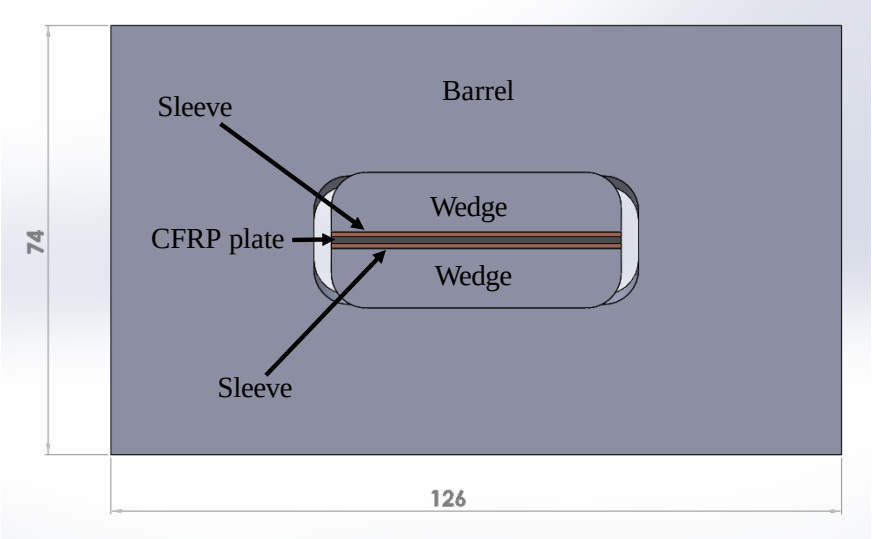

(a)

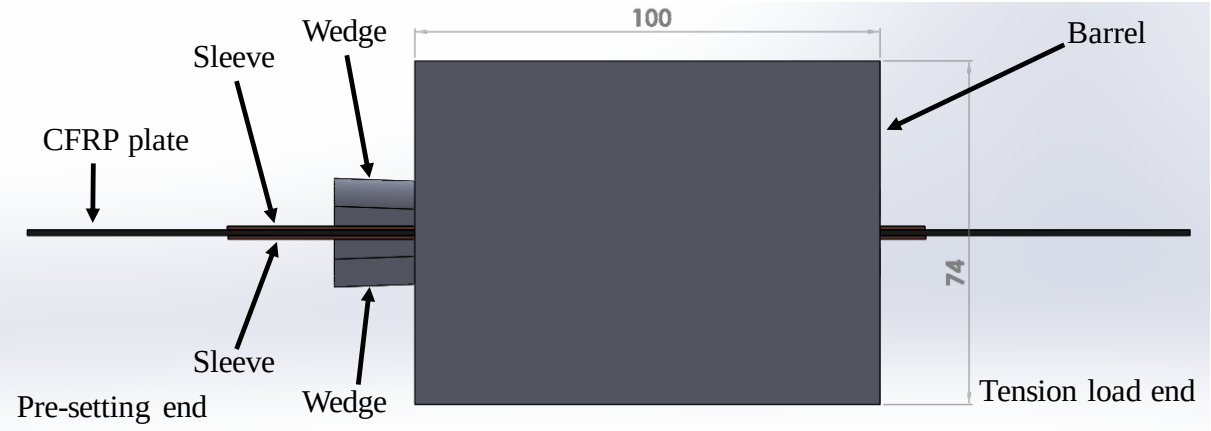

(b)

Figure 3.4: The new CFRP plate anchor with different components and dimensions: (a) the cross sectional view, and (b) the longitudinal view.

3.3 ANCHOR DESIGN PARAMETERS

The primary design basis of the CFRP plate anchor in this thesis is friction. Therefore, the coefficient of friction between the different components of the anchor is one of the most important input parameter in the numerical model. There are three coefficient friction values in the three interfaces inside the anchor: (1) between the CFRP plate and the sleeve; (2) between the sleeve and the wedge; and (3) between the wedge and the barrel.

The same longitudinal curve radius (R in Fig. 3.2) was used for both barrel and wedges for the simplicity of the manufacturing of the anchor. The interference distance between the barrel end and the wedge end at the loading end of the anchor is another important design parameter. This parameter is shown as $D_{w.l.} - D_{B.l.open.}$ distance in Fig. 3.2.

A pre-setting load is required to be applied on the wedges before applying the tension load on the CFRP plate. This is performed to set the wedges inside the anchor before the application of load. If there is no pre-setting load, there is a likelihood that the CFRP plate may slide out of the anchor without taking any load. This also requires to be tested experimentally.

One of the primary objectives of this research is to develop a compact anchor. A long anchor has high manufacturing and installation cost and difficult to transport. Although a short anchor-length is desired, a certain length is required to avoid any major stress concentration inside the anchor; and also to accommodate a potential slip of the wedges within the length of the anchor. The barrel length and the wedge length were kept same in this thesis. The thicknesses of the barrel and the wedges are important anchor design parameters. A thicker barrel provides a stronger confinement of the anchor. But a thicker barrel makes the anchor heavier. A thinner barrel is susceptible to stress concentration inside the anchor, and may fracture. Therefore, obtaining an optimum thickness for both barrel and wedge is necessary.

Finally, an optimum design of the CFRP plate anchor was obtained by considering and optimizing all of the above mentioned anchor design parameters (Fig. 3.3 and 3.4).

CHAPTER 4
FRICTION TEST

4.1 GENERAL

The unidirectional orthotropic carbon fibre-reinforced-polymer (CFRP) plate is weak in the transverse direction. In order to save the CFRP plate from failure under shear stress while in contact with hard steel surface inside the anchor, a soft layer is required to protect the CFRP plate. Copper plates can act as a soft layer inside the anchor. Other common soft materials such as aluminum may cause galvanic corrosion while in contact with the CFRP plate; and thus cannot be considered for this purpose. Therefore, the coefficient of friction between the CFRP plate and the copper plate is an important parameter for designing friction-based anchors for CFRP plates. However, the literature lacked coefficient of friction values between CFRP and copper plates. Therefore, an experimental investigation was required to determine the coefficient of friction between CFRP plates and different types of copper plates.

To determine the coefficient of friction between CFRP plates and different types of copper plates, the tribological properties of the two materials must be understood. CFRP plates have specific tribological properties that include self-lubrication characteristics [117]. There are a number of factors that affect the coefficient of friction between fibre-reinforced-polymer (FRP) and other materials. These factors include: (1) the polymer of the CFRP plate, (2) normal stress applied, (3) hardness of the materials in contact, (4) surface topography, (5) temperature, (6) presence of wear particles and dust at the interface, (7) microstructure of materials, (8) lubricants, (9) apparent contact area, and (10) the direction of the fibres and the direction of sliding [118], [119].

There are a number of friction models available to determine the coefficient of friction. The coefficient of friction (μ) can be calculated by Amonton's law [120]: $\mu = T/N$, where N and T are the normal force and the friction force, respectively. Howell [121] and Howell and Mazur

[122] proposed an equation for the relationship between the friction force (T) and the normal force (N) for the viscoelastic (*i.e.*, CFRP) materials, $T=aN^b$, where the friction index (b) was 0.8-1.0. The friction equation, $T=\mu N$ is a special case of the equation $T=aN^b$, where $b=1.0$ (Howell 1953). Since unidirectional CFRP is an anisotropic material, Hertzian theory and other contact theories are not valid for FRPs [117]. Al-Mayah [114] investigated the effect of transverse compressive strength on the friction properties of CFRP and found that there was no effect of the transverse compressive strength of CFRP while in contact with different materials.

CFRP plates have different friction behaviour compared to other FRP materials. The friction and wear properties of eight different types of FRPs were measured by Tsukizoe and Ohmae [123]. They showed that the CFRP had a lower wear rate and coefficient of friction than that of glass fibre-reinforced-polymer (GFRP) and steel fibre-reinforced-polymer (SFRP) [123]. The friction behaviour of three types of FRPs (carbon, glass and aramid fibres) in contact with aluminum was tested [124]. The wear rate of FRP materials was affected by the level of contact pressure. At low contact pressure (<20 MPa), the wear rate remained fixed. However, the wear rate increased at high contact pressure (>20 MPa) [124], [125]. The coefficient of friction decreased with increase of contact pressure [126].

Hardness of the counterface material has a significant effect on the tribological properties of high strength CFRPs [127]. The softer the counterface material is, the higher the coefficient of friction [127]. Friction of FRPs against a metal surface is also influenced by the ploughing action, and there is a mutual transfer of materials between the sliding surfaces [128]. With the increase of surface roughness of the counterpart material, separation occurs between the fibre and the polymer [129]. Most of the transferred materials during sliding of CFRPs are the polymers, not the carbon fibres [130]. Sung and Suh [131] examined the effect of fibre orientations for carbon fibre and concluded that the wear volume was the highest when the sliding direction was perpendicular to the fibre axis of CFRP, and the wear volume was the lowest when the sliding direction was parallel to the fibre axis. In addition, the tribological

properties of FRPs were significantly affected by the selection and volumetric content of fibre [130]. The wear volume decreased with the increase of the volumetric fibre content [132].

Temperature also had a significant effect on the frictional properties of epoxy in contact with metals [133]. Myshkin *et al*. [134] reviewed the literature and summarized the effect of temperature and sliding velocity on the frictional properties of FRPs. The temperature dependence was above the glass transition temperature, since the epoxy softened and stuck to the metal surface resulting in stick-slip behaviour and a higher wear rate [133]. There was a linear relationship between the coefficient of friction and the shear modulus of epoxy at the glassy temperature region [133]. The rise of temperature in FRP during friction testing was associated with a rise of the friction force [135].

Although the friction behaviour between CFRP plates and copper plates has not been studied, the friction behaviour between CFRP plates and different metals has been investigated. The frictional behaviour of CFRP in contact with steel depends on the type of carbon fibres – high strength fibre or high modulus fibre [132]. The wear volume increases with the increase of the sliding distance and the sliding velocity[132]. The coefficient of friction between CFRP and stainless steel in the contact pressure range of 150-375 MPa is 0.06-0.26 [136]. Schön [137]–[139] reported a coefficient of friction of 0.23 between CFRP plate and aluminum plates. In contrast, Portnov *et al*. [8] reported a coefficient of friction of 0.1 between CFRP plate and duralumin plate.

CFRP plates and copper plates as the counterface material have not been studied whereas carbon fibres and CFRP round bars in contact with copper have been investigated. Roselman and Tabor [140] measured a static coefficient of friction of 0.5 between high strength carbon fibre (not CFRP) and copper under a small normal load (10^{-5} N). Al-Mayah *et al*. [113], [114], [141], [142] measured a coefficient of friction of 0.24 between CFRP round bars and annealed copper round sleeves.

Since polymers deform visco-elastically under tension, the tribological behaviour of CFRP depends not only on the normal load, but also on the geometry of the specimen [126]. In addition, due to the complexity of friction mechanism, the contact geometry of the friction test samples must be similar to the application of the materials [143]. Therefore, an investigation of the friction between the CFRP plate and the two types of copper plates is required because of the geometry (from circular rod in previous work to rectangular plate used in the current study). In addition, the surface of CFRP rod has an epoxy outer layer, while the surface of CFRP plate has fibres very close to the surface. Furthermore, the CFRP plate is relatively smoother than round CFRP rods due to helical deformation added to the bar to increase its bond performance with concrete.

The objective of this experimental investigation is to determine the coefficient of friction between the CFRP plate and the two types of copper plates – as-received and annealed. A study on the shear stress vs. normal stress relationship has been carried out. The friction and sliding mechanisms have also been studied to obtain an in-depth knowledge of their contact behaviour. This chapter has been adapted from Mohee *et al.* [106].

4.2 TEST SPECIMENS

4.2.1 Carbon Fibre-Reinforced-Polymer Plate

The unidirectional orthotropic CFRP plate is composed of 68% (by volume) carbon fibre with epoxy matrix. The CFRP plate used in this work has a thickness of 1.2 mm, which is the most widely used CFRP plate. The CFRP plates have a surface texture on one face in order to facilitate the structural adhesives for easily connecting to the concrete beams. The tensile strength of the CFRP plate is 2,800 MPa. The longitudinal modulus of elasticity is 165,000 MPa and the transverse modulus of elasticity is 9,500 MPa. The ultimate strain of CFRP plate is 1.7% and the density of CFRP plate is 1.5 gm/cm^3. Table 4.1 shows the different properties of the CFRP plates provided by SIKA [38]. Figure 4.1 shows the 1.2 mm thick

CFRP plate. The average hardness of the CFRP plate is 80±1 on the HR15TS Rockwell superficial hardness scale. The average surface roughness of CFRP plate surface is 0.43 µm in the smoother surface and 1.72 µm in the rougher surface.

Figure 4.1: A 1.2 mm thick and 20 mm wide CFRP plate.

4.2.2 Copper Plate

The copper plates used for the friction tests were 0.81 mm thick. Copper has a modulus of elasticity of 131,000 MPa and Poisson's ratio of 0.31. The ultimate strain of copper plate is 25%. Two types of copper plate were used for the friction test – as-received and annealed.

4.2.3 Annealing of Copper Plates and Hardness Test

In order to obtain a soft copper, the plates were annealed at a 500º C oven for one hour [144], and then air-cooled to room temperature. The hardness of both types of copper plates was determined using the Rockwell superficial micro-hardness tester machine with a 15 kg mass and 1.59 mm diameter ball. Table 4.2 gives the hardness results obtained for both types of copper plates. The average hardness of the as-received and annealed copper plates were 67±7 and 34±4 on the HR15TS Rockwell superficial hardness scale, respectively. The average surface roughness of the as-received and annealed copper plates was 0.27 µm and 1.49 µm, respectively.

Table 4.1: Properties of the CFRP plate for the friction tests

Parameter	Values
Dimension (width × thickness) (mm × mm)	20 × 1.2
Longitudinal ultimate tensile strength, f_u (MPa)	2,800
Longitudinal modulus of elasticity, E (MPa)	165,000
Ultimate strain, ε_{ult} (%)	1.7
Fibre content (%)	68
Density, ρ (gm/cc)	1.5

Table 4.2: Hardness of the test materials

Material	Average hardness (± standard deviation) (in the Rockwell superficial HR15TS scale)
As-received copper plate	67 ± 7
Annealed copper plate	34 ± 4

4.3 FRICTION TEST SAMPLE PREPARATION

For the friction test, CFRP plate samples 580 mm long, 20 mm wide and 1.2 mm thick were used (Fig. 4.2). The length of the CFRP plate was determined from the distance between the gripping end and the free end of the friction test machine. Both the as-received copper and annealed copper plates were tested. At the friction end, two 50 mm long, 20 mm wide and 0.8 mm thick copper plates were used. The friction test area was 15 mm in length by 20 mm in width (Fig. 4.2). L-shape copper plate shoulders were epoxied to the copper plates in order to prevent any movement of the plates during the friction tests.

Due to the relatively smooth surface of CFRP plates, the friction test machine initially could not grip the CFRP plate at the "non-testing" end; and the plate slipped during the test. This was resolved by gluing the CFRP plate to two 80 mm long copper plates using epoxy.

4.4 INSTRUMENTATION AND APPARATUS

Two steel clamping plates (15 mm × 100 mm area) were installed in the friction test machine in order to apply the normal load. One clamping plate was at the top and the other was at the bottom of the CFRP plate (Fig. 4.3). The steel clamping plates had a hardness of 45 (Rockwell C scale). The steel clamping plates were designed to fulfil the following purposes: (1) to provide a 15 mm long normal stress application area; (2) to avoid slippage between steel (friction test machine) and copper plates by supporting the L-height (the extra height of the copper plate resisting any movement of the copper plate under the horizontal load); (3) to utilize the whole 20 mm width and thus the whole capacity of the CFRP plate; and (4) to ensure friction between the CFRP plate and the copper plates without breaking the CFRP plate during the test.

A built-in linear variable differential transformer (LVDT) and load cell were installed in the friction test machine at the pulling end. The maximum capacity of the load cell was 44.5 kN as mentioned.

4.5 EXPERIMENTAL SETUP AND PROCEDURE

The CFRP plate, all of the copper plates and machine steel clamping plates were cleaned thoroughly with isopropanol before each test. The gripping device was tightened to grip the CFRP plate at one end (Fig. 4.4). At the testing end, a pre-defined normal stress (Table 4.3) was applied through the two steel clamping plates on the 15 mm × 20 mm area of the two copper plates and the CFRP plate. There was a delay of 30 seconds in order to stabilize the normal stress on the test samples before the horizontal (pullout) force was applied. In each test, the contact pressure remained constant and the horizontal pullout force was increased. The

horizontal force was applied (Fig. 4.4) until either the machine maximum allowable sliding distance of 98 mm (stroke) was reached, or the CFRP plate broke. During the application of the horizontal force, the copper plates remained in place, and the CFRP plate slid between the two copper plates (Fig. 4.4). A normal load rate of 2 kN/sec and a horizontal displacement rate of 25 mm/sec were used in all tests. The scan rate was 1000 scans/ second, and the number of scans was 200 on average per plot point, and the duration was 30 seconds. The coefficient of friction was determined using equation (4.1) and a summary of the friction test input parameters is given in Table 4.3.

Table 4.3: The friction test matrix

Normal stress (MPa)	Friction area (mm × mm)	Normal force (kN)	Number of samples
50	15 × 20	15	3
75		22.5	3
100		30	3
125		37.5	3
150		45	3
175		52.5	3

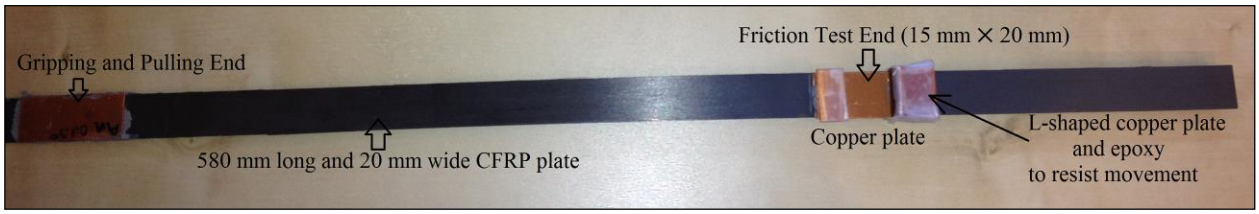

Figure 4.2: Prepared friction test samples: CFRP plate (black) and copper plate (red).

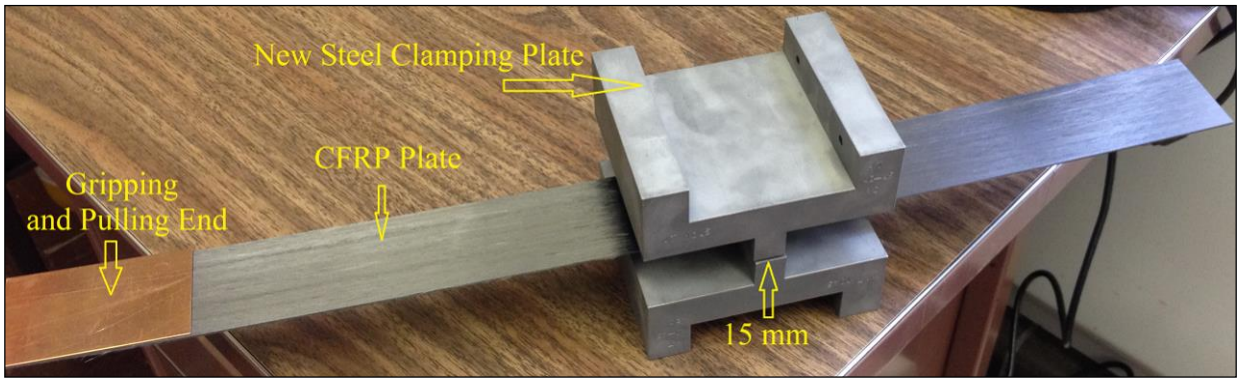

Figure 4.3: The steel camping plates and a CFRP plate showing the test setup.

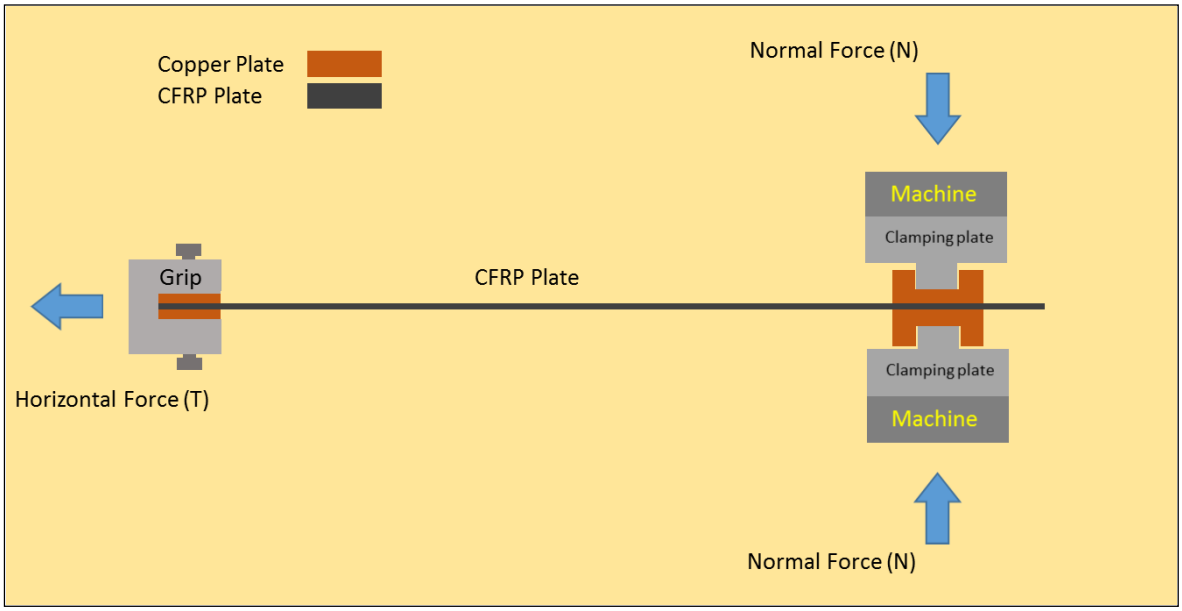

Figure 4.4: Schematic diagram of the friction tests showing the steps (not drawn to scale).

4.6 METHODOLOGY OF THE FRICTION TEST

As shown by Schön [138], the coefficient of friction between the CFRP plate and the two counterface material plates may be calculated from the following equations:

$$\mu = \frac{T_{max}}{2N} \tag{4.1}$$

$$\mu = \frac{\tau}{\sigma} \tag{4.2}$$

where, μ is the coefficient of friction, N is the total normal force perpendicular to the CFRP plate and the counterface material plate, and T_{max} is the total horizontal (pullout) force applied at the CFRP plate end, as shown in Fig. 4.5. The normal force is multiplied by two, because the CFRP plate has two contacting surfaces. Figure 4.4 shows the schematic diagram of the friction test setup.

To calculate the static friction, T_{max} is the force required for moving and sliding a stationary object, which was the first peak horizontal force value (seen Fig. 4.6 and 4.8). The first peak of the horizontal force was used to calculate the coefficient of friction.

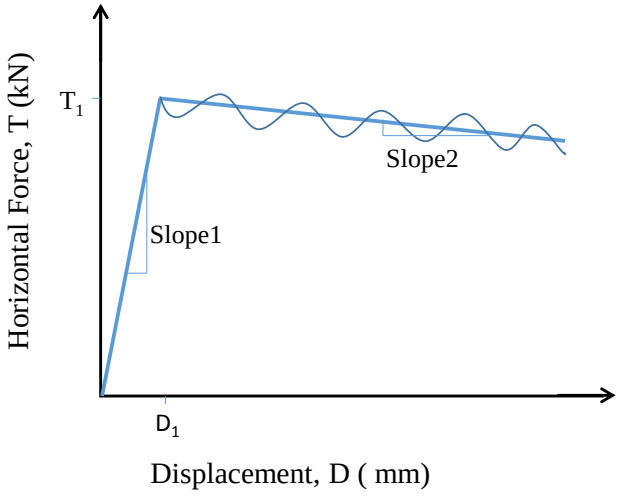

Figure 4.5: The schematic diagram of the slipping behaviour between the CFRP plate and the two types of copper plates.

4.7 RESULTS

The friction tests were performed under different normal stresses ranging from 50 MPa to 175 MPa. However, a small number of samples were tested using a higher normal stress (>175 MPa). The CFRP plates broke after a total displacement of 30-50 mm before reaching the peak load under >175 MPa normal stress, where fracture in the CFRP plate controlled the friction behaviour. For this reason, test results above the 175 MPa were not in the scope of this chapter.

The friction tests between the CFRP plate and as-received copper plates were carried out at normal stresses of 50 MPa, 100 MPa, 150 MPa and 175 MPa. Figure 4.6 shows the horizontal pullout force vs. displacement for the above-mentioned normal stresses for as-received copper plates. The horizontal pullout force increased linearly with displacement until sliding began (Fig. 4.6). After reaching the peak horizontal force value, either the CFRP plate continued to slide (under 50-100 MPa contact pressure) until it reached the stroke length of 98 mm, or the CFRP plate broke (under 150-175 MPa contact pressure). The initial horizontal force vs. displacement slope (slope1 in Fig. 4.5) remained constant with the increase of contact pressure (Fig. 4.6, 4.8 and 4.12). After reaching the peak value, the downward horizontal force vs. displacement slope (slope2 in Fig. 4.5) increased with the increase of contact pressure (Fig. 4.6, and 4.12). Furthermore, at a higher contact pressure, a higher peak of the horizontal force was obtained (Fig. 4.6).

There was an initial displacement (D1) at the beginning of the friction tests as shown in the schematic horizontal force vs. displacement curve in Fig. 4.5. This is dominated by the elastic elongation of the CFRP plate. However, there are other minor mechanisms contributing to this displacement such as (1) deformation of the apparatus (friction test machine); (2) shear deformation of the samples (CFRP plate and copper plates); and (3) breakage mechanism of the micro-welding between the two surfaces. The maximum elastic elongation of the CFRP plates before failure was estimated. The friction test sample length was 365 mm. The ultimate

strain of the CFRP plate, as given by the manufacturer, was 1.7%. Therefore, the maximum possible elongation in the CFRP plate before failure was 6.2 mm under 2800 MPa tensile stress.

Figure 4.7 shows the shear stress vs. normal stress relationship for the as-received copper in the friction test. The following shear stress vs. normal stress relationship was obtained between the CFRP plate and the as-received copper plate (Fig. 4.7):

$$\tau = 0.31\ \sigma \qquad (4.3)$$

where, τ represents the shear stress and σ the normal stress. The equation represents a very close relationship among all of the test data ($R^2 = 0.97$). The coefficient of friction remained constant with the increase of normal stress (Fig. 4.7 and Table 4.4).

Table 4.4: The friction test results between CFRP plate and as-received copper plate

Normal stress (MPa)	Mean coefficient of friction
50	0.31 ± 0.04
100	0.31 ± 0.03
150	0.31 ± 0.01
175	0.30 ± 0.02

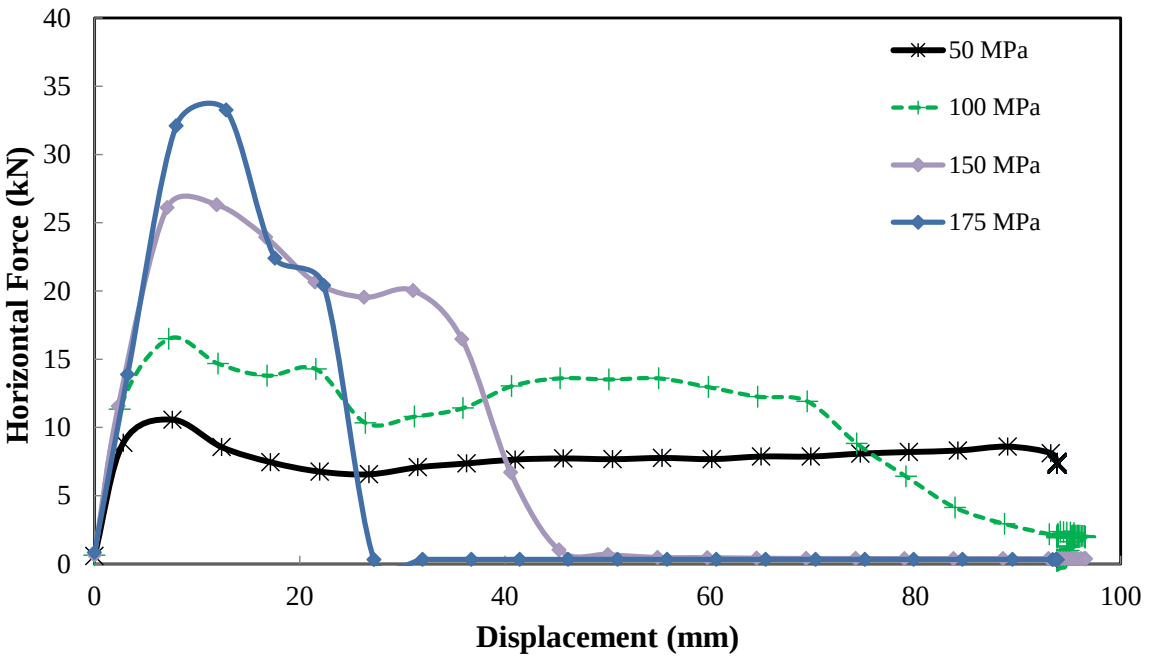

Figure 4.6: The horizontal (pullout) force vs. displacement curves for different normal stresses (50, 100, 150 and 175 MPa) for as-received copper plates in the friction tests.

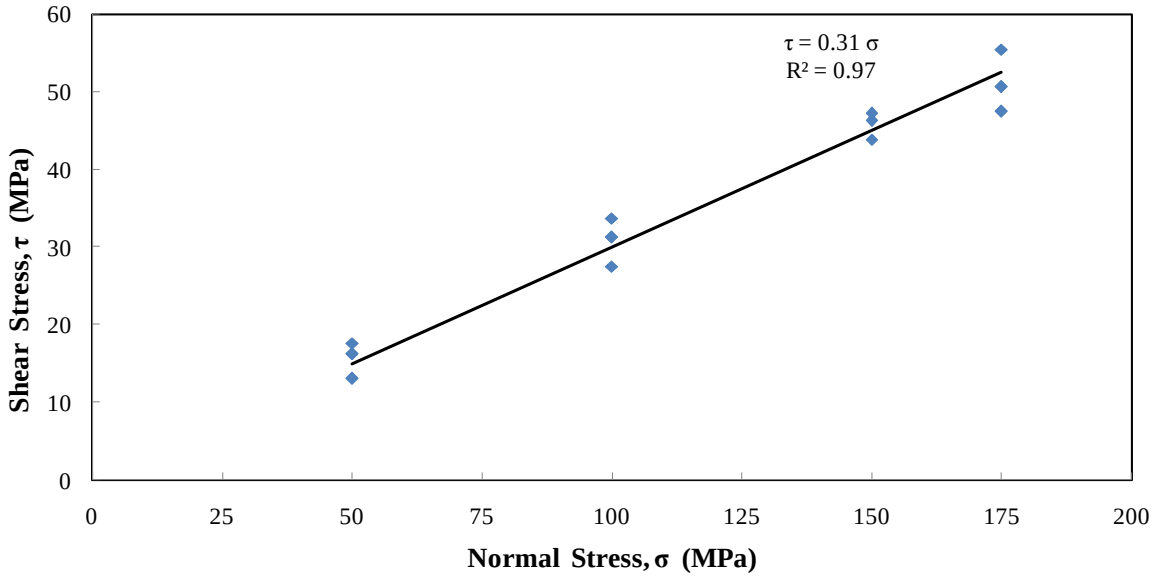

Figure 4.7: The Shear stress vs. normal stress for as-received copper.

Friction tests were also carried out to determine the coefficient of friction between the CFRP plate and the annealed copper plates. Figure 4.8 shows the horizontal force vs. displacement curves for different normal stresses (between 50 MPa and 175 MPa) for the annealed copper plates. From Fig. 4.9, a shear stress vs. normal stress relationship was also obtained for friction between the CFRP plate and the annealed copper plate using the modified version of Howell's equation:

$$\tau = 1.02\ \sigma^{0.76} \qquad (4.4)$$

where, τ represents the shear stress and σ represents the normal stress ($R^2 = 0.92$).

Table 4.5 gives the coefficient of friction for different normal stresses between the CFRP plate and the annealed copper plates. More details of the friction test results and the effects of different test factors are given in the discussion.

Table 4.5: The friction test results between CFRP Plate and annealed copper plate

Normal stress (MPa)	Mean coefficient of friction
50	0.39 ± 0.06
75	0.38 ± 0.02
100	0.35 ± 0.02
125	0.35 ± 0.03
150	0.31 ± 0.01
175	0.30 ± 0.01

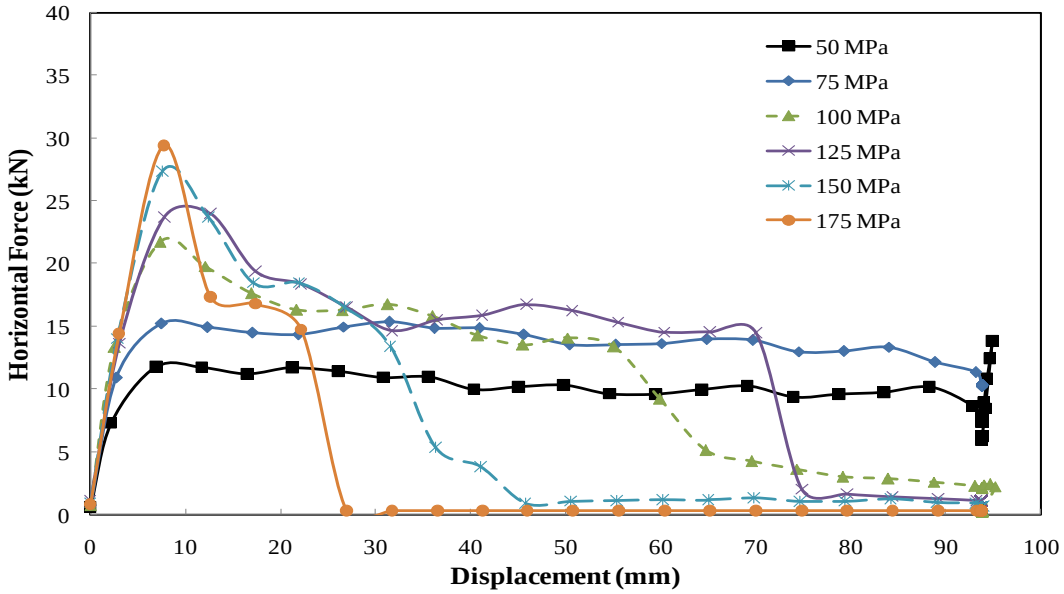

Figure 4.8: The horizontal (pullout) force vs. displacement curves for different normal stresses (50, 75, 100, 125, 150and 175 MPa) for annealed copper plates.

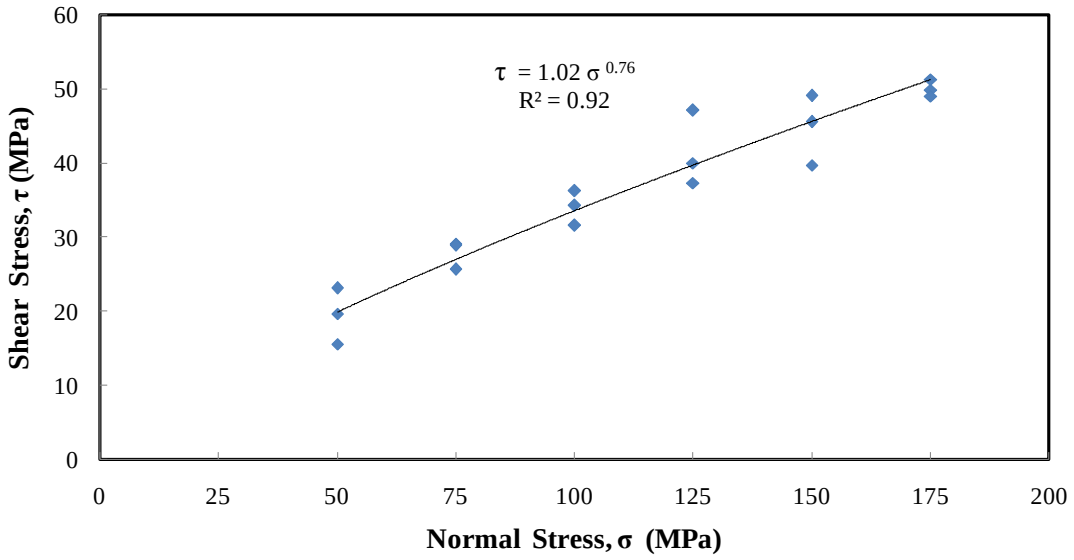

Figure 4.9: Shear stress vs. normal stress for annealed copper.

Figure 4.10 portrays the relationship between the coefficient of friction and normal stress for both as-received copper (solid line) and annealed copper plates (dotted line). For as-received copper plates, the coefficient of friction value remained constant (0.31) between 50 MPa and 175 MPa. However, the coefficient of friction for the annealed copper decreased gradually from 0.39 to 0.30 with the increase of normal stress.

Figure 4.11 illustrates the relationship between the maximum sliding distance and the normal stress for both as-received copper (solid line) and annealed copper plates (dotted line). For both type of copper plates, the maximum sliding distance decreased with the increase in normal stress. The maximum sliding distance is the distance the CFRP plate slid between the two copper plates under loading until the plate broke or reached the stroke length. Figure 4.14a shows the maximum sliding distance on the test sample after the test.

Comparative friction test results are shown in Fig. 4.12 for the as-received copper and annealed copper. From Fig. 4.12, it can be observed that the peak of the horizontal force vs. displacement curve is higher for annealed copper plates compared to the as-received copper plates for 50 MPa and 100 MPa normal stresses. Hence, annealed copper has a higher coefficient of friction than as-received copper during the initial sliding friction with the CFRP plate between 50 MPa and 150 MPa normal stress range, as shown in Fig. 4.13.

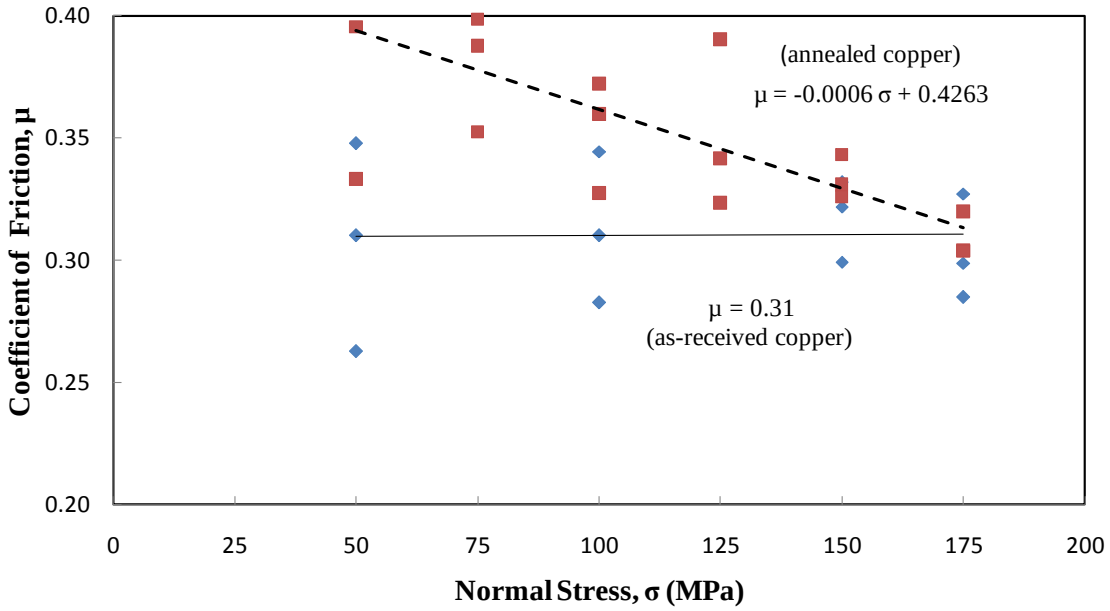

Figure 4.10: The variation of coefficient of friction with normal stress for as-received and annealed copper plates.

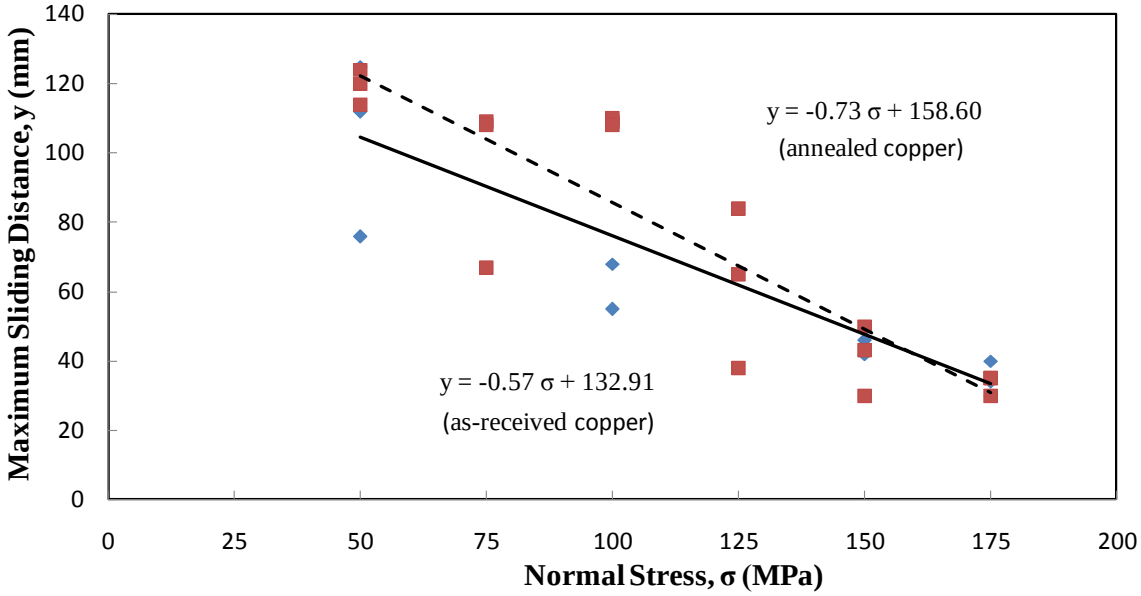

Figure 4.11: The maximum sliding distances for different normal stresses for as-received and annealed copper plates.

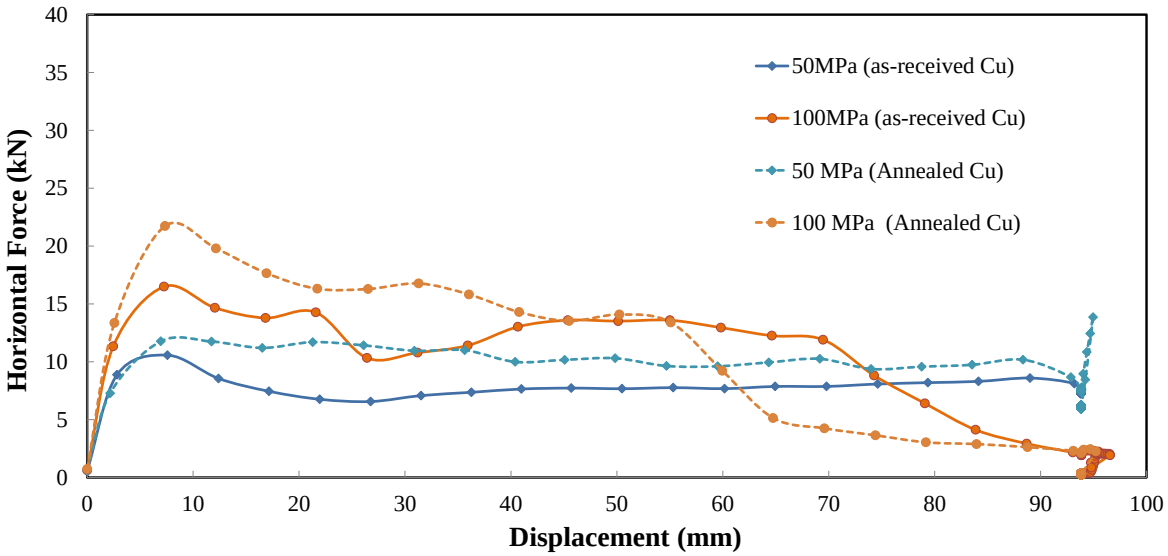

Figure 4.12: The horizontal force vs. displacement curves for 50 MPa and 100 MPa normal stresses for both as-received (solid lines) and annealed copper plates (dotted lines).

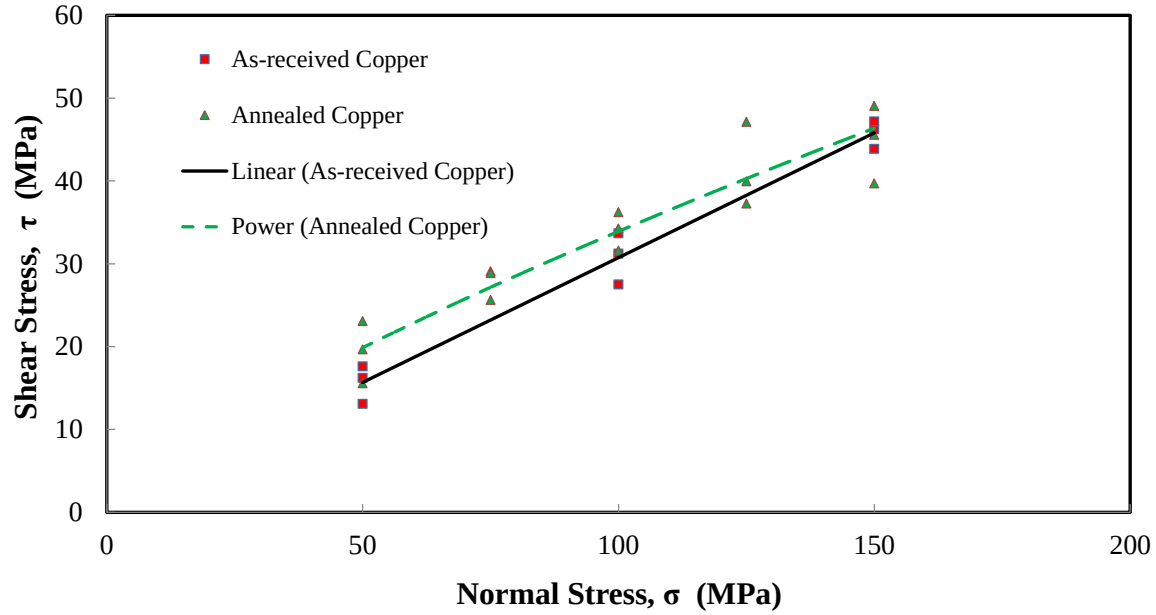

Figure 4.13: The shear stress vs. normal stress curves for as-received copper (solid line) and annealed copper (dotted line).

4.8 DISCUSSION

4.8.1 Coefficient of Friction

In the contact pressure range of 50-175 MPa, the coefficient of friction between the CFRP plate and the as-received copper plates is a constant value of 0.31. However, the coefficient of friction between the CFRP plate and the annealed copper plates varies between 0.39 and 0.30 decreasing with increase of the contact pressure. A similar decrease of coefficient of friction with increasing contact pressure for FRP/aluminum surface has also been observed by [137]–[139]. The friction equations (Equations 4.3 and 4.4) are in accordance with Howell's equation for the friction of viscoelastic materials, with the friction index (*b*) varying between 0.76 and 1.0 [121], [122]. The coefficient of friction between the CFRP plate and the two types of copper plates can be used for the development of different friction-based equipment for CFRP plates (*e.g.,* CFRP plate anchors) and can also be used as a benchmark for other similar geometry of composite/metal contact behaviour.

4.8.2 Effect of Material Hardness

The initial peak horizontal force is higher for the softer annealed copper plates than that of the as-received copper plates (Fig. 4.12). This phenomenon has also been observed in previous studies on other composite materials [113], [114], [127], [141]. Consequently, the coefficient of friction values are higher for the softer annealed copper plates than that of the harder as-received copper plates for the same contact pressure (Table 4.4 and 4.5). This is because the softer annealed copper plates deform and fill gaps between the asperities providing a larger real contact surface area with the CFRP plate resulting in a higher coefficient of friction and shear stress. Since the shear stress and coefficient of friction values are higher for the softer annealed copper plates, the slippage distance of a CFRP plate between two copper plates will be less for the softer annealed copper plates.

4.8.3 Effect of Contact Pressure

Contact pressure has a significant role on the coefficient of friction. In the case of as-received copper plates, the coefficient of friction remained constant at the investigated contact pressure range of 50-175 MPa (Fig. 4.10 and Table 4.4). However, the coefficient of friction decreased with the increase of contact pressure for annealed copper from 0.39 to 0.30 in the same contact pressure range (Fig. 4.10 and Table 4.5). The shear stress also increased with the increase of contact pressure for both as-received (Fig. 4.7) and annealed copper (Fig. 4.9). This trend of increasing shear stress with the increase of contact pressure and decreasing coefficient of friction with the increase of contact pressure was consistent with other composite/metal contact [124]–[126]. As the contact pressure increased, the actual contact area between the two surfaces increased until it reached its constant maximum level.

Asperities are small projections of the harder material that enter into the softer material. When the horizontal pullout force is applied, asperities resist the horizontal force, and break. The two surfaces then slid against each other. With the increase of the actual contact area, the horizontal force/displacement initial slope increased (Fig. 4.6 and 4.8), and the maximum initial shear stress also increased. At a very high normal stress (150-175 MPa), the actual contact area became the same as the total apparent contact area, and there was no further increase of the actual contact area. The additional normal stress then fractured the CFRP plate. Hence, the maximum sliding distance before failure also decreased with the increase of contact pressure for both the as-received and annealed copper (Fig. 4.11). The sliding distance represented the slippage distance of the CFRP plate from the middle of two copper plates. Since an anchor fails if the CFRP plate slips out of the two copper plates inside the anchor, the sliding distance is a very important parameter for the development of the planned CFRP plate anchor.

4.8.4 Friction and Sliding Mechanisms

In order to characterize the tribological behaviour between the CFRP plate and the two types of copper plates, the sliding mechanism between them was investigated. Figures 4.14 and 4.15 illustrate the post-test samples: CFRP plates and as-received copper plates under normal stress of 50 MPa (Fig. 4.14a), 100 MPa (Fig. 4.15a) and 150 MPa (Fig. 4.14b)**.** As the contact pressure was applied, the asperities from the copper plate entered into the CFRP plate (Fig. 4.14a). With the application of horizontal pullout force, ploughing occurred on the CFRP plate surface and increased with the increase of contact pressure. After the CFRP plate slid for 30-50 mm between the two copper plates (Fig. 4.14a), CFRP debris accumulated at the interface creating an obstacle to sliding (Fig. 4.14b). The wear volume and the debris accumulation were minimal in the beginning of the test. The ploughing and the debris accumulation increased with the increase of the sliding distance (Fig. 4.14a). Hence, the initial highest shear stress value was used to calculate the coefficient of friction. Therefore, the calculation of the coefficient of friction was not affected by transfer of wear materials (copper asperities or CFRP debris). This method was also used for determining the coefficient of friction between composite and aluminum [137]–[139]. The phenomenon of the increase of ploughing and wear volume with the increase of the sliding distance was also observed for CFRP/steel interaction [132].

Stick-slip behaviour was observed during the friction tests. At a lower contact pressure (50-100 MPa), a large amount of sliding (100-130 mm) occurred between the CFRP plate and the copper plates; and a large volume of debris accumulated on the CFRP-copper interface. Sticking also occurred at the CFRP-copper interface. The stick and slip behaviour under a normal stress of 100 MPa is shown in Fig. 4.15. Figure 4.15a shows the test sample after the friction test; and Fig. 4.15b shows the representative horizontal force vs. displacement graph with the stick-slip behaviour. Accumulation of debris resisted the horizontal force and causes sticking. After the debris was cleared by the horizontal force, sliding occurs. This phenomenon

was repeated several times during the friction test. This stick-slip friction behaviour was not clearly visible on the specimens at very high contact pressure (150-175 MPa) after the tests, because of the ploughing and CFRP debris accumulation on the copper plates (Fig. 4.14b). The failure pattern of the CFRP plates under 150 MPa normal stress is illustrated in Fig. 4.16. At 150 MPa contact pressure, after sliding for 30-50 mm, the carbon fibres tended to spread and break. Figure 4.17 depicts the general mechanism of ploughing and wear of CFRP plate, debris accumulation on copper plates and the reduction of CFRP plate cross-section during the friction tests. This type of stick-slip behaviour was also observed during the frictional behaviour of other composite materials [133].

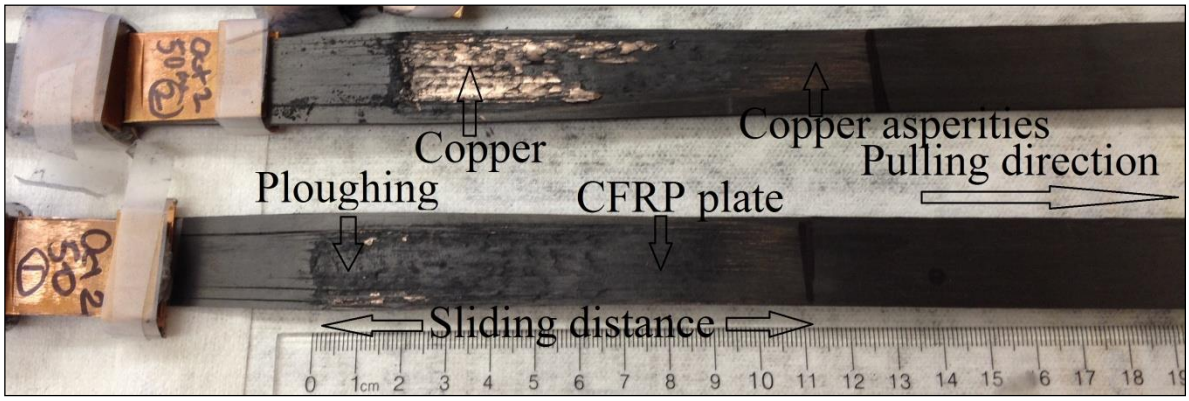

(a)

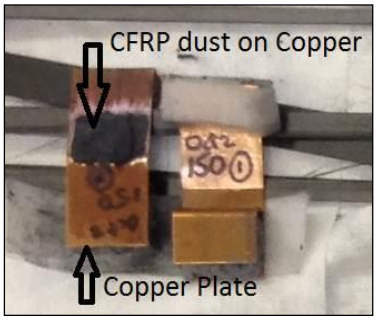

(b)

Figure 4.14: (a) Samples after the friction test between CFRP Plate and as-received copper plate under 50 MPa contact pressure; (b) carbon debris was accumulated on the copper plate surface after the friction test using 150 MPa contact pressure.

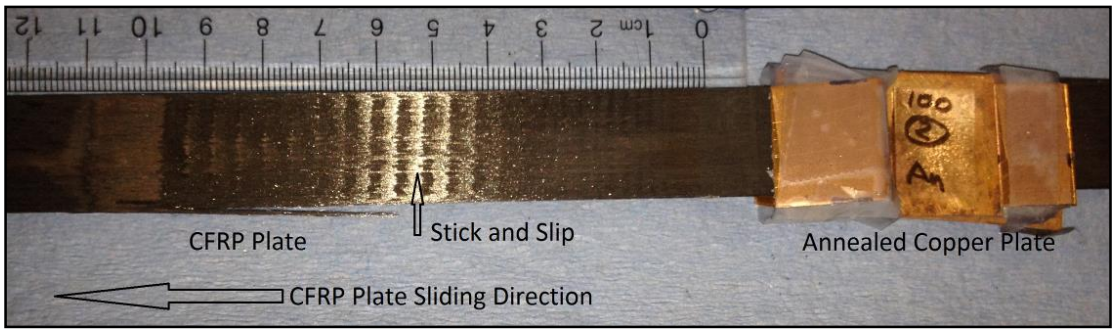

(a)

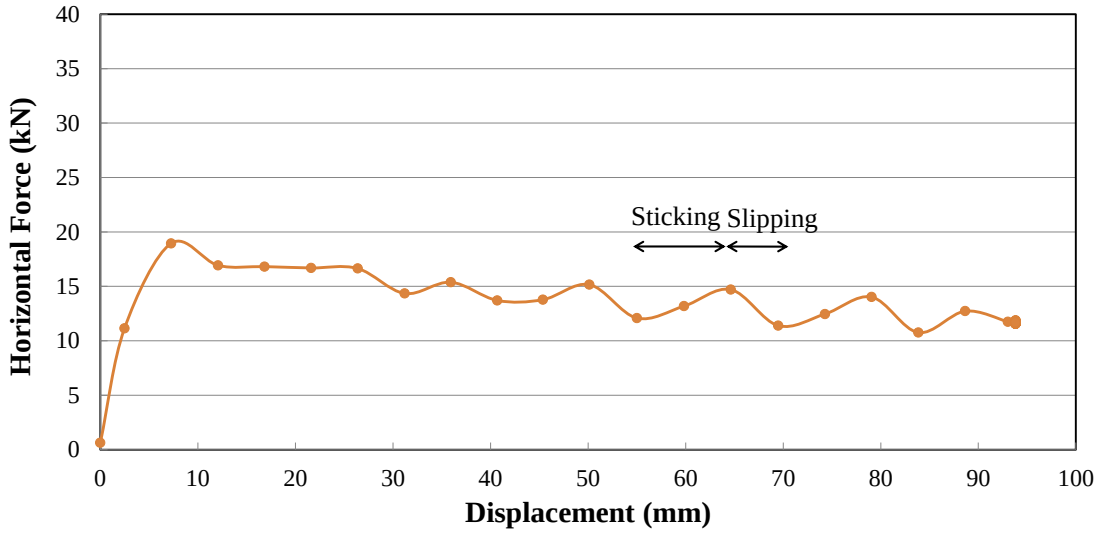

(b)

Figure 4.15: (a) Friction Test sample after the test for 100 MPa contact pressure for annealed copper, (b) horizontal force vs. displacement curve showing the stick and slip behaviour.

Figure 4.16: The CFRP plates failed in tension after sliding for certain distances – all three samples in this figure have been tested for 150 MPa normal stress.

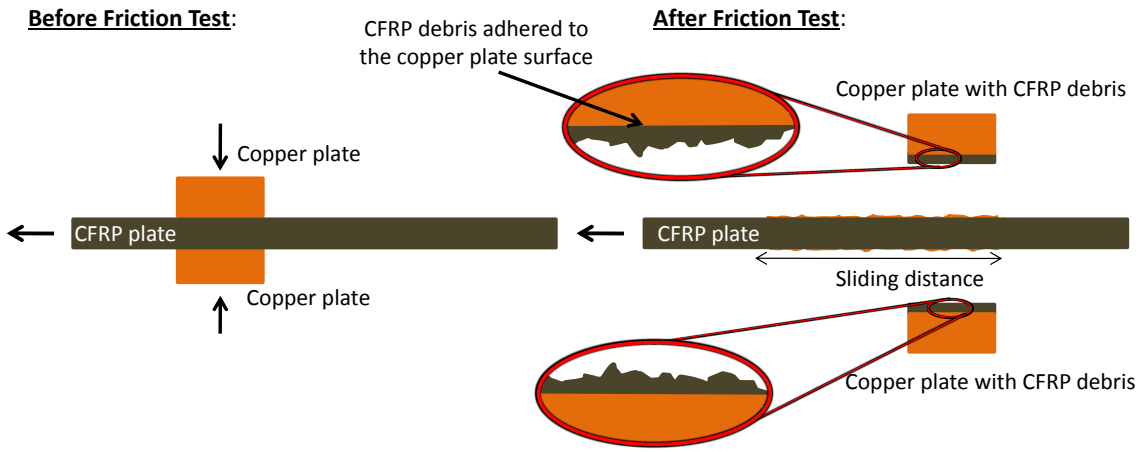

Figure 4.17: General mechanism of ploughing of CFRP plate, debris accumulation on copper plates and reduction of CFRP plate cross-section during friction tests.

The maximum tensile strength of CFRP plate, given by the manufacturer, is 2800 MPa, which is equivalent to 67.2 kN force for a 20 mm × 1.2 mm cross section plate. The CFRP plates did not break during the friction tests under lower (*i.e.*, 50-150 MPa) contact pressures. However, the CFRP plates broke at a lower load (between 28 kN and 34 kN) for both types of copper plates under 175 MPa contact pressure. During friction testing under a higher contact pressure (175 MPa), the CFRP plate was gradually reduced and the cross section (thickness) of the plate gradually was reduced to a smaller cross section before failure, and thus it failed in lower breaking force. In addition, 100 mm wide CFRP plates were cut into 20 mm wide friction test samples; and during this process, some side-fibres were cut causing the reduction of strength of the plate. Therefore, with the increase of contact pressure and decrease of coefficient of friction (Table 4.4 and 4.5), the maximum horizontal pullout force (breaking force) also increased.

4.9 CONCLUSIONS

The frictional behaviour of CFRP plates in contact with as-received and annealed copper plates was characterized within the contact pressure range of 50-175 MPa. Within this contact pressure range, the static coefficient of friction between the CFRP plate and the as-received copper plate was 0.31. The coefficient of friction between the CFRP plate and the annealed copper plate decreased from 0.39 to 0.30 with the increase of contact pressure. The softer annealed copper plates exhibited a higher coefficient of friction value (0.39 to 0.30) than the harder as-received copper plates (0.31 to 0.30). The shear stress vs. normal stress relationship was also obtained at the contact pressure range of 50 MPa-175 MPa. For the as-received copper plate, the relationship was: $\tau = 0.31\sigma$. For the annealed copper plate, it was: $\tau = 1.02\ \sigma^{0.76}$. This chapter also portrayed a visual record of ploughing, wear, debris accumulation and stick-slip behaviour for the friction between CFRP plates and copper plates.

The friction behaviour between the CFRP plate and the two types of copper plates can be used for the development of a new and innovative anchorage system for composite materials, which can be used for structural rehabilitation and retrofitting and for the design of lighter and more fuel-efficient cars, airplanes and satellites. In addition, this information can be utilized in several industries, *e.g.,* geotechnical engineering, biomedical engineering, automotive, aviation, space and shipbuilding industries.

CHAPTER 5
NUMERICAL MODELLING

5.1 INTRODUCTION

Several CFRP plate anchor systems of different concepts were numerically modelled using the finite element method (FEM). This three-dimensional numerical modelling was performed in order to develop a base design of the CFRP plate anchor system. The base model was then optimized to design an efficient mechanical CFRP plate anchor. The geometric configurations of the anchors, material properties of different components of the anchors, boundary conditions and loading conditions are presented in this chapter. A parametric study was conducted. The results are presented and discussed. This chapter has been adapted from Mohee *et al.* [145].

5.2 THREE DIMENSIONAL FEM BASED ANCHOR MODELLING

5.2.1 General Configuration

A three dimensional finite element model for the CFRP plate anchor using Abaqus software (from Dassault Systèmes Simulia Corp.) was developed. The model was developed primarily for the 50 mm × 1.2 mm CFRP plate. A detailed parametric analysis and optimization study were performed with different input parameters to obtain an efficient anchor that is easy to use, reusable, epoxy-free, compact, capable to carry high tensile strength of the CFRP plate, corrosion resistant and inexpensive.

As stated in Chapter 3, the new CFRP plate anchor consists of a CFRP plate, two annealed copper sleeves, two steel wedges and a steel barrel, as shown in Fig. 5.1. Since the preliminary anchor was symmetric along both Y and Z axes in the cross section, for simplicity and faster analysis, one-quarter of the anchor was modelled and analyzed (Fig. 5.1a). In the figures and Table 5.1, X-axis (or, direction 1) was the longitudinal direction (parallel to the fibre direction of the CFRP plate), and Y-axis (direction 2) and Z-axis (direction 3) were the transverse

directions (normal to the fibre direction of the CFRP plate). During the manufacturing stage of the anchor, for ease of manufacturing of the barrel, the barrel was made of two identical parts that were connected by six high strength bolts after manufacturing (Fig. 5.1b). These bolts were for manufacturing purpose only and need not be tightened every time.

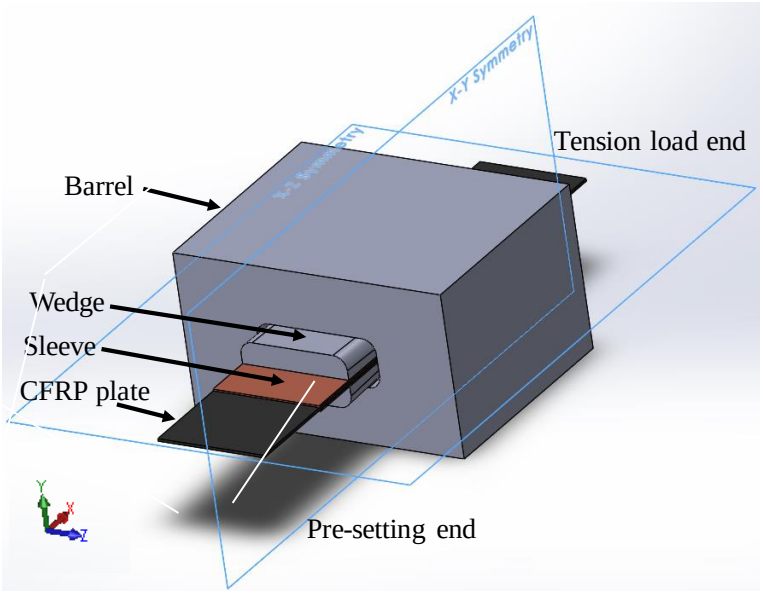

(a)

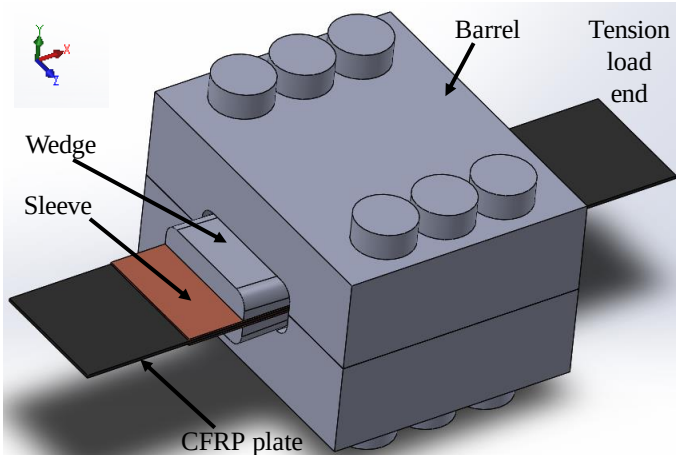

(b)

Figure 5.1: The three dimensional view of the anchor with different components: (a) the solid anchor along with the two symmetry planes (XY and XZ) for the numerical modelling of one-quarter of the anchor, and (b) the bolted anchor with two-part barrel and six bolts.

5.2.2 Material Properties

The material properties of different parts of the anchor are listed in Table 5.1 [9], [38], [146], [147]. The CFRP plate was modelled as an orthotropic material. The annealed copper sleeve, the steel wedge and the steel barrel were modelled as isotropic materials. The anchor performance was studied using both elastic and elastic-plastic properties of the annealed copper sleeves. Since the steel was heat-treated and hardened, there was no significant plastic deformation of steel. Therefore, the steel used in the wedge and the barrel was modelled as an elastic material.

Table 5.1: Properties of the CFRP plate anchor components

<table>
<tr><td>Parameter</td><td>CFRP plate</td><td>Sleeve</td><td colspan="2">Wedge and Barrel</td></tr>
<tr><td>Material</td><td>CFRP</td><td>Annealed Copper</td><td>Heat treated H13 Steel</td><td>Heat treated 440C stainless steel</td></tr>
<tr><td>Ultimate tensile strength, f_u (MPa)</td><td>2,800</td><td>210 (f_y=45)</td><td>1,580 (f_y=1,366)</td><td>1,975 (f_y=1,896)</td></tr>
<tr><td>Longitudinal modulus of elasticity, E_1 (MPa)</td><td>165,000</td><td rowspan="2">117,000</td><td rowspan="2">210,000</td><td rowspan="2">210,000</td></tr>
<tr><td>Transverse modulus of elasticity, E_2, E_3 (MPa)</td><td>9,500</td></tr>
<tr><td>Long. Poisson’s ratio, v_{12}, v_{13}</td><td>0.17</td><td rowspan="2">0.31</td><td rowspan="2">0.3</td><td rowspan="2">0.283</td></tr>
<tr><td>Transverse Poisson’s ratio, v_{23}</td><td>0.45</td></tr>
<tr><td>Longitudinal shear modulus, G_{12}, G_{13} (MPa)</td><td>5,500</td><td rowspan="2">46,000</td><td rowspan="2">81,000</td><td rowspan="2">83,900</td></tr>
<tr><td>Transverse shear modulus, G_{23} (MPa)</td><td>3,275</td></tr>
<tr><td>Ultimate strain, ε_{ult} (%)</td><td>1.7</td><td>60</td><td>9</td><td>9</td></tr>
</table>

5.2.3 Model Meshing

A three-dimensional and eight-node hexahedral (brick) solid element (C3D8R in Abaqus) was used to model the anchor. The 'structured' mesh generation technique, along with the hexahedral element shape option, was used to model the CFRP plate, the sleeve and the wedge. The 'sweep' mesh generation technique, along with the hexahedral element shape option, was used for the barrel. The 'structured' technique is usually used for meshing rectangular prisms. This technique creates regular shaped (*i.e.*, brick) meshes in objects. On the contrary, the 'sweep' technique is used to generate meshes for complex shaped solids. In this technique, meshes are generated in one element layer of object; and then the meshes are copied in a sweep path to create meshes in the whole object.

A convergence study was carried out to investigate the effect of element size on the anchor performance at 3 mm pre-setting and 2,800 MPa tension load (Fig. 5.2 and Table 5.2). For this convergence study, an anchor with a longitudinal curve radius of 3,000 mm, an interference distance of 0.05 mm, an anchor-length of 100 mm and a minimum barrel thickness of 25.93 mm was used. Different mesh element sizes were investigated, including 6 mm × 6 mm, 4 mm × 4 mm, 2 mm × 2 mm, 1.5 mm × 1.5 mm and 1.2 mm × 1.2 mm. A coarser mesh resulted in a less accurate result, since it did not cover all of the points in the anchor model. On the contrary, a finer mesh made the numerical analysis significantly more time consuming, and sometimes outside of the computational capacity of a desktop computer (Table 5.2). It was concluded that 2 mm × 2 mm mesh size with 46,305 elements was the optimum mesh size because it provided high accuracy with acceptable computation time (Table 5.2 and Fig. 5.2). The number of elements in the solid anchor without bolts, the anchor with bolts (anchor #1), the bolted stainless steel anchor (anchor #2) and the bolted anchor for 1.4 mm thick CFRP plates (anchor #3) were 46305, 37759, 33994 and 38539, respectively.

Table 5.2: Convergence study for different mesh sizes in the anchor FEM model under a pre-setting distance of 3 mm and tensile load of 2,800 MPa

Mesh size (mm)	Analysis time (Hours: Min)	No. of elements	CFRP plate max. contact pressure (MPa)
6 × 6	2 min	2,939	378
4 × 4	3 min	7,170	393
2 × 2	38 min	46,305	393
1.5 × 1.5	3 hours: 54 min	106,792	393
1.2 × 1.2	15 hours: 44 min	198,012	393

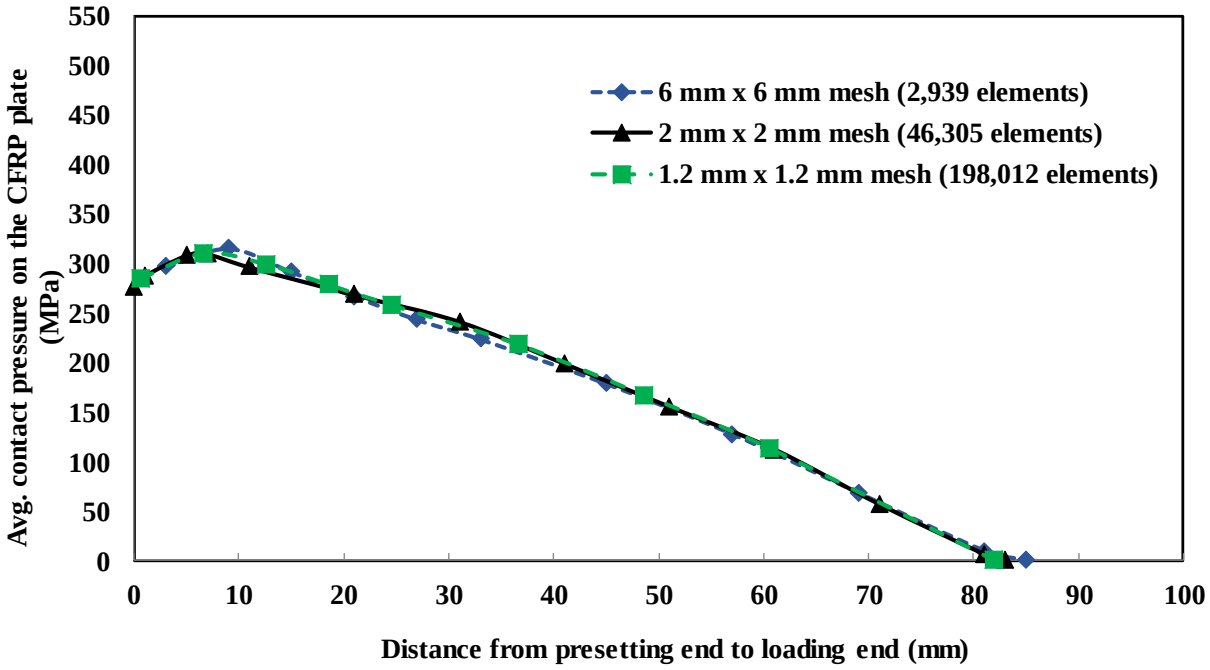

Figure 5.2: Mean contact pressure distribution on CFRP plate using different element sizes - convergence study of the FEM model at 3 mm pre-setting and 2,800 MPa tension load.

5.2.4 Contact Surface and Friction

The numerical model consisted of three surface-to-surface contact interfaces among the different components of the anchor. These interfaces were: (i) CFRP plate-sleeve, (ii) sleeve-wedge, and (iii) wedge-barrel. Based on the results of comprehensive experimental investigation performed in this research and described in Chapter 4, a coefficient of friction of 0.3 was used at the contact surface between the CFRP plate and the annealed copper sleeve. Based on the literature review [148], the coefficient of friction of 0.4 was used at the sleeve-wedge interface to simulate a strong grip between the annealed copper sleeve and the sandblasted wedge. The third contact surface was at the circular profile surface between the steel barrel and steel wedge. Lubricant was used on this interface in order to reduce the coefficient of friction to facilitate the movement of the wedge into the barrel to ensure a full grip of the CFRP plate inside the anchor. Based on the literature review [149], in the parametric analysis numerical models and in the final anchor models, a coefficient of friction value of 0.07 was used in this barrel-wedge interface. After completing all of the experimental investigations, another new set of numerical analysis was carried out on the bolted anchors #1, #2 and #3. A coefficient of friction of 0.01 was used at the barrel-wedge interface [114], [148] in the final set of numerical models in order to simulate a behaviour observed in the experiments.

5.2.5 Boundary Conditions

Different sets of boundary conditions were used in the model. A boundary condition was applied on the barrel base (B1-B2-B3-B4-B5-B6 surface in Fig. 5.3a) near the loading end of the CFRP plate to restrain the movement of the anchor in the X-direction. This boundary condition represented the support provided by the steel base plate in the tension test machine on which the anchor was placed during the test.

Boundary conditions were applied to represent the two symmetry planes (XY and XZ planes) in the model (Fig. 5.3b). The top surface of the CFRP plate (the C1-C4-C5-C6 surface in Fig. 5.3b) was restrained from moving upwards (towards the Y-direction). The symmetry surface (the C1-C2-C3-C4 surface in Fig. 5.3b) of the CFRP plate was prevented from moving towards the Z-direction. Similarly, the symmetry surfaces of the sleeve (the S1-S2-S3-S4 surface in Fig. 5.3b), the wedge (the red color W1-W2-W3-W4 surface) and the barrel (the red color B1-B2-B7-B8 surface in Fig. 5.3b) were prevented from moving towards the Z-direction. The barrel sidewall symmetry surface (the red color B5-B4-B9-B10 surface in Fig. 5.3b) was also supported against upward movement (towards Y-direction).

The three bolted anchor models had the same boundary conditions in all components except the top surface of the barrel sidewall (B5-B4-B9-B10 surface). This was changed from the symmetry boundary condition to the bolted boundary conditions. These additional bolted boundary conditions were applied to restrict the movement of all three bolt-head surfaces in the Y-direction; and the movement of all three bolt-bolthole cylindrical interfaces in the X and the Z-directions, as shown in Fig. 5.3c.

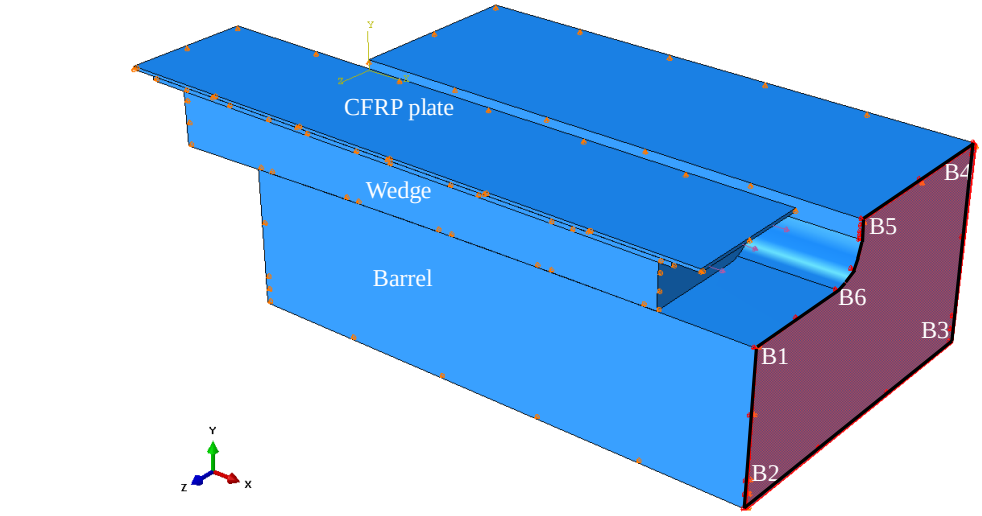

(a)

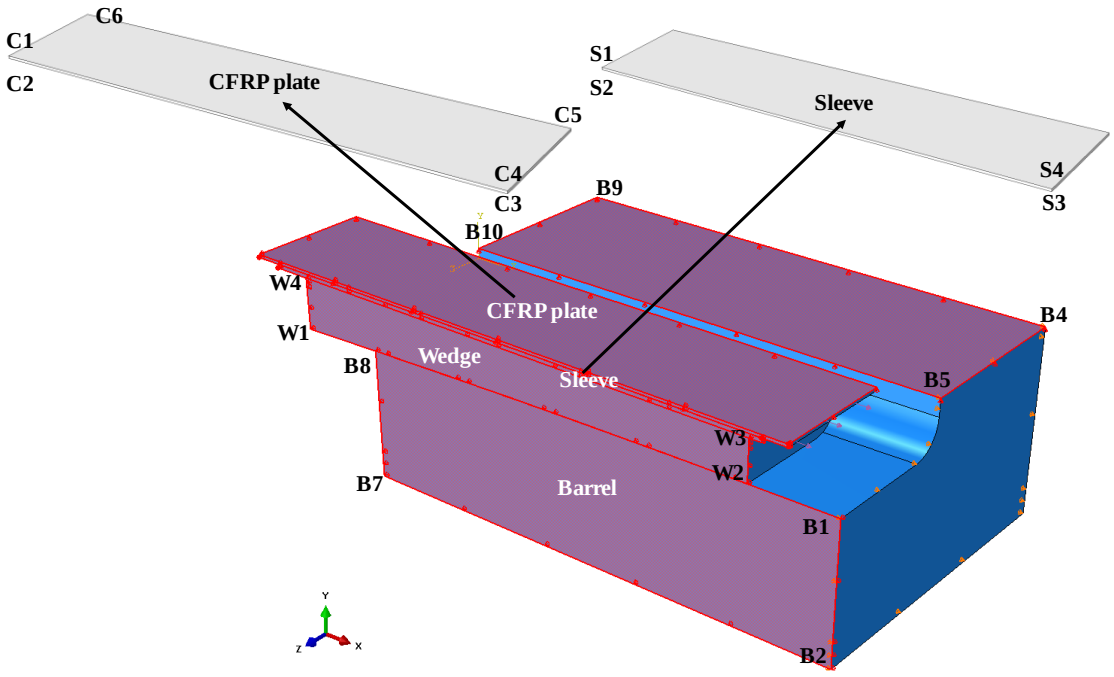

(b)

Figure 5.3: Boundary conditions (a) in the X-direction in the barrel end wall; (b) for symmetry (since it is one-quarter of the CFRP plate anchor); (c) The extra boundary conditions for the bolted anchors: along Y-direction at the bolt-head or nut surfaces, and along X and Z directions in the bolt-bolthole surfaces.

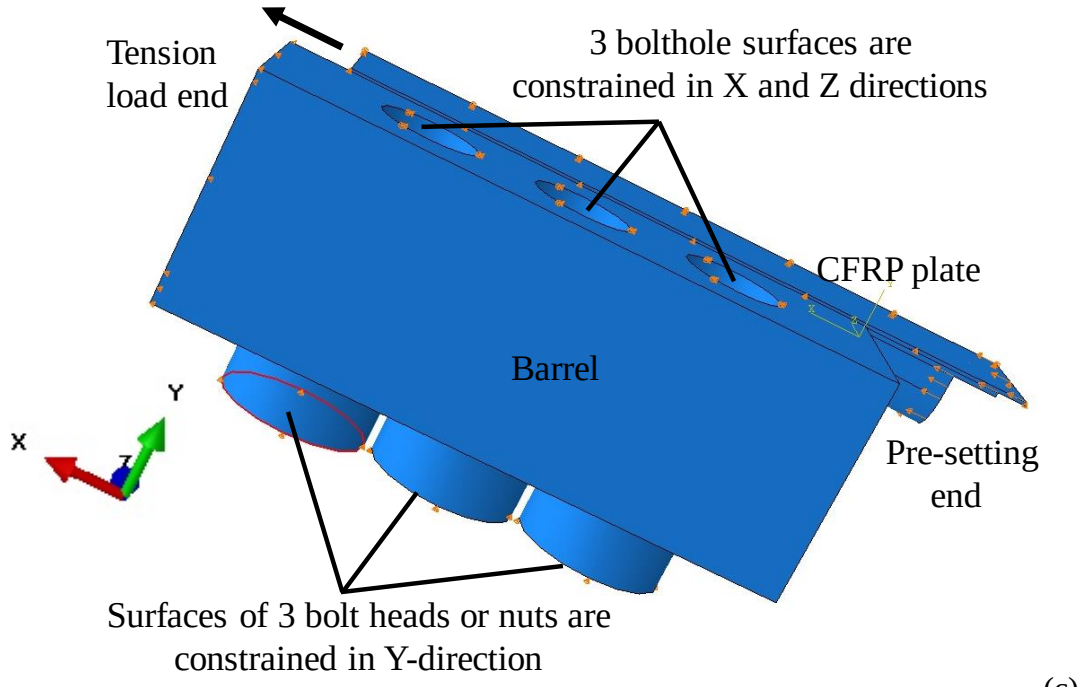

(c)

Figure 5.3 (c): The extra boundary conditions for the bolted anchors: along Y-direction at the bolt-head surfaces, and along X and Z directions in the bolt-bolthole surfaces.

5.2.6 Loading Conditions

Two loading stages are required for the anchor application in the field, namely: (i) the pre-setting load on the wedge in order to set the wedge inside the anchor, and thus to avoid a potential slippage of the CFRP plate from the anchor; and (ii) the tension load on the CFRP plate at the loading end of the anchor. These loading stages were simulated in the numerical model, as shown in Fig. 5.4a and b, as the pre-setting (step-1) and the tension load (step-2), respectively. In all of the figures, the X-axis represents both the pre-setting and the tension force direction, and the Y-axis represents the vertical direction. Displacement control was used while applying the pre-setting load in order to monitor and ensure an exact movement of the wedge inside the barrel, similar to the actual pre-setting distance used in tension test in the

laboratory. A range of pre-setting distances between 0.32 mm and 14 mm were applied on the wedge surface at the pre-setting end of the anchor, as shown in Fig. 5.4a. This was followed by the tension load step at which the ultimate tensile stress of 2,800 MPa of the CFRP plate was applied at the loading end of the CFRP plate (Fig. 5.4b).

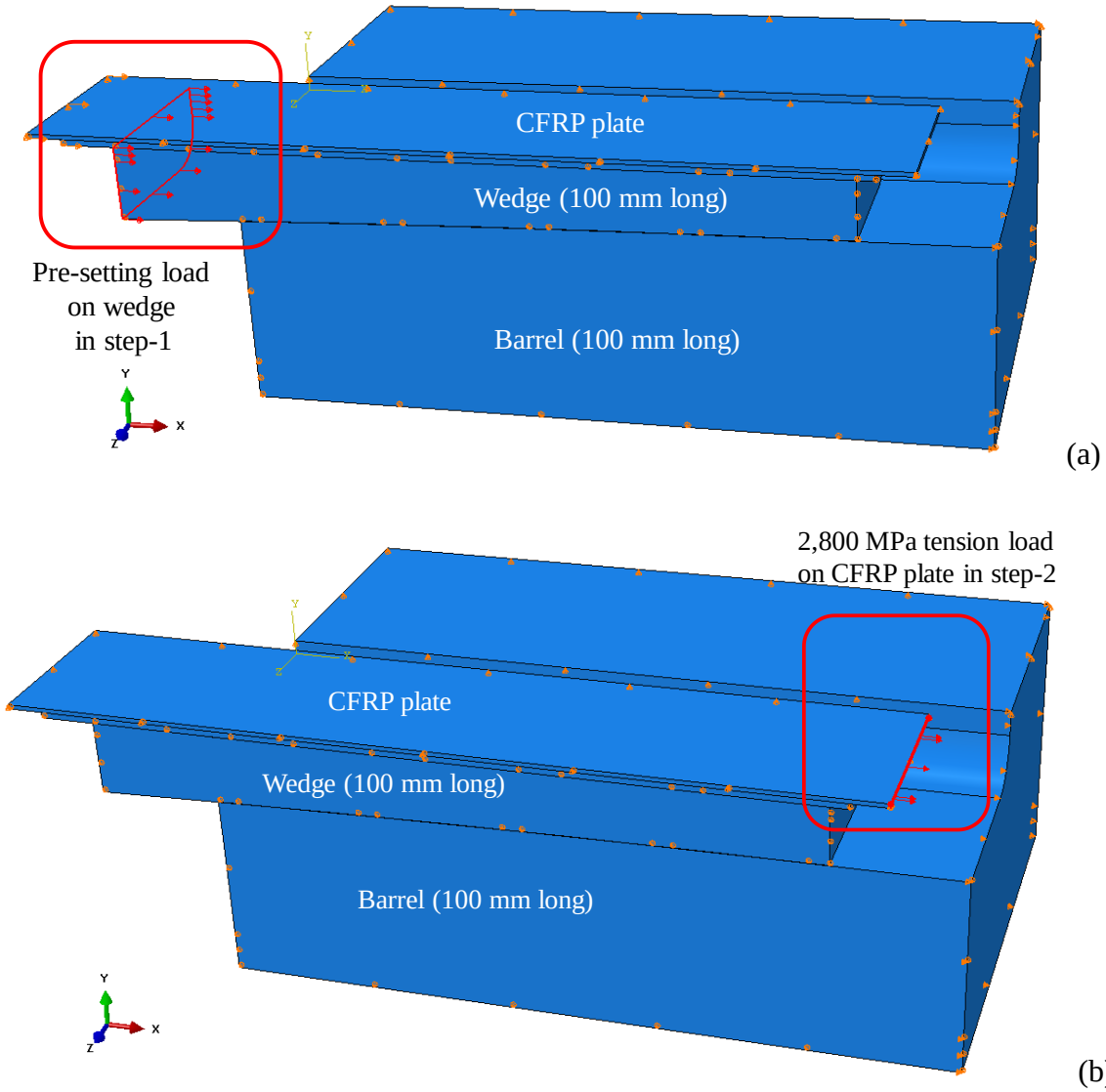

Figure 5.4: The applied loads in the anchor model: (a) the pre-setting load on the wedge in step-1 load; and (b) the 2,800 MPa tension load on the CFRP plate in step-2 load.

5.3 DESIGN PARAMETERS AND FAILURE CRITERIA

The contact pressure on the CFRP plate has a significant role on the performance of the anchor system under loading. This is mainly attributed to the weakness of the CFRP plate in the transverse direction; and any stress concentration can cause a premature failure of the CFRP plate inside the anchor. In addition, for a functional anchor design, the contact pressure must be the highest at the pre-setting end; and decrease gradually over the length of the CFRP plate to the lowest contact pressure at the tension load end. Furthermore, the contact pressure on the CFRP plate inside the anchor should be large enough to grip the CFRP plate properly without any sliding of the CFRP plate. On the contrary, the contact pressure on the CFRP plate should be less than 546 MPa, which is the compressive strength of the CFRP plate [11] to prevent premature rupture of the CFRP plate inside the anchor.

Since the CFRP plate is an orthotropic material, the von Mises stress cannot be used as an output parameter for the CFRP plate. Two failure mechanism theories, namely: the 'Maximum Stress Theory' and the 'Tsai-Hill Theory', were used in order to determine if the orthotropic CFRP plate would fail inside the anchor at 2,800 MPa tension load.

According to the 'Maximum Stress Theory' for orthotropic materials [150], the failure occurs if one of the stresses exceeds the corresponding ultimate strength of the material in that particular direction. In order to avoid failure under tension load, the material should satisfy the following:

$$\sigma_L \leq \sigma_{Lu}$$

$$\sigma_T \leq \sigma_{Tu}$$

$$\tau_{LT} \leq \tau_{LTu} \qquad (5.1)$$

Where, σ_L is the longitudinal tensile stress, σ_{Lu} is the ultimate longitudinal tensile strength of the material, σ_T is the transverse stress, σ_{Tu} is the ultimate transverse strength of the material, τ_{LT} is the shear stress and τ_{LTu} is the ultimate shear strength of the material.

According to the 'Tsai-Hill theory' for orthotropic material for plane stresses [150], the failure criterion is:

$$\left(\frac{\sigma_L}{\sigma_{Lu}}\right)^2 + \left(\frac{\sigma_T}{\sigma_{Tu}}\right)^2 - \frac{\sigma_L . \sigma_T}{{\sigma_{Lu}}^2} + \left(\frac{\tau_{LT}}{\tau_{LTu}}\right)^2 \leq 1 \tag{5.2}$$

Where, σ_L is the longitudinal tensile stress, σ_{Lu} is the ultimate longitudinal tensile strength of the material, σ_T is the transverse stress, σ_{Tu} is the ultimate transverse strength of the material, τ_{LT} is the shear stress and τ_{LTu} is the ultimate shear strength of the material.

From the FEM model results, it was found that the shear stress (τ_{LT}) values were negligible (<10 MPa) compared to the ultimate shear strength of the CFRP plate (120 MPa) in all models. Hence, the $\left(\frac{\tau_{LT}}{\tau_{LTu}}\right)^2$ term was always very small: $(\left(\frac{10}{120}\right)^2 = 0.007)$. In addition, this shear stresses were also not co-located with the high tensile stresses. Therefore, the shear term (τ_{LT}) was ignored in the above equations during the failure criteria calculations for both of the theories for the anchor design in this thesis.

The von Mises stresses in the barrel and the wedge are critical parameters for the anchor design. For a functional anchor design, the maximum von Mises stresses in the barrel and the wedge should be less than the yield strength of the material to be used for manufacturing the anchor. This will ensure that no cracking and no plastic deformation in the barrel and the wedge would occur under full loading (2,800 MPa).

The length and the weight of the anchor are also very important. The anchor should be as short and as light as possible. This will ensure the ease of use of the anchor during the installation, and a reduced manufacturing and transportation cost.

5.4 RESULTS

The final CFRP plate anchor design was selected to ensure that there was no significant stress concentration in the CFRP plate or any other components of the anchor under a load equivalent to the ultimate tensile strength of the CFRP plate (2,800 MPa). The anchor required some displacement of the wedge in order to set the wedge inside the anchor under loading (self-seating distance). The design was also selected such that there was no slippage of the CFRP plate from the anchor (no slippage with respect to the wedge). The impact the design parameters (*i.e.*, length of the anchor, longitudinal curvature of the barrel and the wedge, interference distance between the barrel and the wedge at the loading end, pre-setting distance, thickness of the barrel and the wedge, and thickness of barrel sidewall) had on the anchor performance was investigated in order to obtain the optimal design of the anchor.

The contact pressure and the longitudinal stress distributions on the CFRP plate inside the new anchor under a 3 mm pre-setting distance and 2,800 MPa tensile stress are shown in Fig. 5.5(a) and 5.5(b). The contact pressure on the CFRP plate was distributed over the whole length and width of the CFRP plate that was inside the anchor. As shown in Fig. 5.5(a), there was no stress concentration in the CFRP plate near the loading end indicating that the CFRP plate would not fail due to stress concentration. In addition, the maximum contact pressure in the CFRP plate was 393 MPa at the pre-setting end of the plate, which was less than the 546 MPa limit. The longitudinal stress (S11) was examined for the CFRP plate (Fig. 5.5b), and compared with the ultimate tensile strength of the CFRP plate (2,800 MPa) following the maximum stress theory. Figure 5.6 illustrates the mean contact pressure and the mean longitudinal stress distribution on the CFRP plate along the length of the plate under 3 mm pre-setting and 2,800 MPa tension load.

Two failure mechanism theories, named by the ‘Maximum Stress Theory’ and the ‘Tsai-Hill Theory’ were used to determine if the orthotropic CFRP plate inside the newly developed anchor would fail at 3 mm pre-setting and 2,800 MPa tension load. Table 5.3 shows that the

failure criteria of the CFRP plate inside the anchor under loading at all points of the CFRP plate satisfied both equation (5.1) and (5.2) given by the 'Maximum Stress Theory' and the 'Tsai-Hill Theory'. In Table 5.3, the 0 mm and the 100 mm represent the pre-setting end and the tension load end of anchor, respectively. There was no failure anywhere in the CFRP plate inside the anchor under loading (Table 5.3).

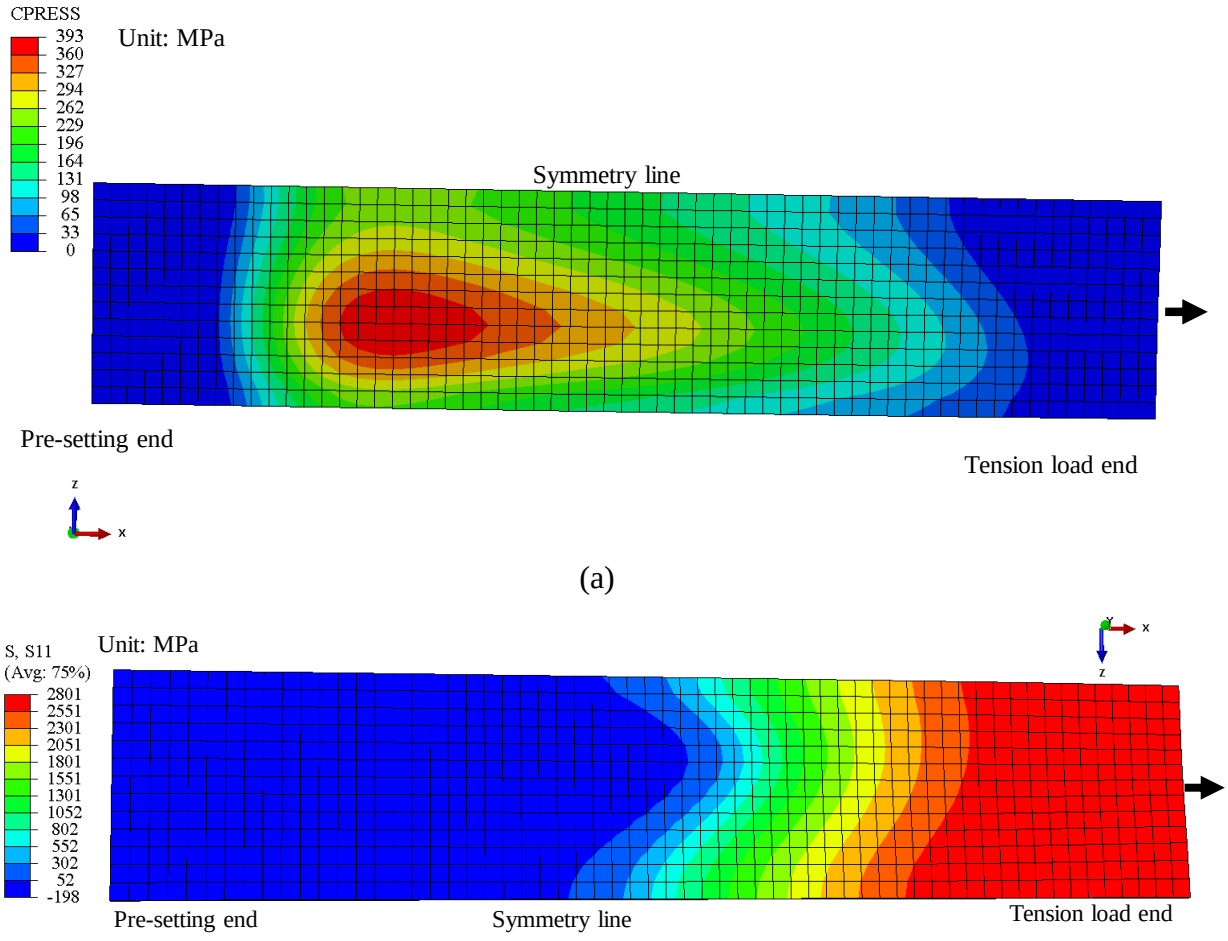

Figure 5.5: (a) The contact pressure distribution; and (b) the longitudinal stress distribution on the CFRP plate (one-quarter) inside the anchor under 3 mm pre-setting and 2,800 MPa tension load.

Table 5.3: Checking the failure criteria of the CFRP plate in the solid anchor at a pre-setting distance of 3 mm and 2,800 MPa tension load using the 'Maximum Stress Theory' and the 'Tsai-Hill Theory'.

Distance in anchor, X (mm)	Mean Contact Pressure on CFRP plate (MPa)	Mean Tensile Stress in CFRP plate (MPa)	Checking failure 'Maximum Stress Theory'	Checking failure 'Tsai-Hill Theory'
0	276	N/A	$\sigma_L < \sigma_{Lu}$, $\sigma_T < \sigma_{Tu}$, OK	0.255 <=1, OK
1	287	N/A	$\sigma_L < \sigma_{Lu}$, $\sigma_T < \sigma_{Tu}$, OK	0.277 <=1, OK
5	308	N/A	$\sigma_L < \sigma_{Lu}$, $\sigma_T < \sigma_{Tu}$, OK	0.319 <=1, OK
11	297	N/A	$\sigma_L < \sigma_{Lu}$, $\sigma_T < \sigma_{Tu}$, OK	0.295 <=1, OK
21	269	0	$\sigma_L < \sigma_{Lu}$, $\sigma_T < \sigma_{Tu}$, OK	0.242 <=1, OK
31	241	142	$\sigma_L < \sigma_{Lu}$, $\sigma_T < \sigma_{Tu}$, OK	0.194 <=1, OK
41	199	867	$\sigma_L < \sigma_{Lu}$, $\sigma_T < \sigma_{Tu}$, OK	0.207 <=1, OK
51	156	1,733	$\sigma_L < \sigma_{Lu}$, $\sigma_T < \sigma_{Tu}$, OK	0.430 <=1, OK
61	112	2,340	$\sigma_L < \sigma_{Lu}$, $\sigma_T < \sigma_{Tu}$, OK	0.707 <=1, OK
71	57	2712	$\sigma_L < \sigma_{Lu}$, $\sigma_T < \sigma_{Tu}$, OK	0.929 <=1, OK
81	6	2,800	$\sigma_L < \sigma_{Lu}$, $\sigma_T < \sigma_{Tu}$, OK	0.998 <=1, OK
92	0	2,800	$\sigma_L < \sigma_{Lu}$, $\sigma_T < \sigma_{Tu}$, OK	1.000 <=1, OK
100	0	2,800	$\sigma_L < \sigma_{Lu}$, $\sigma_T < \sigma_{Tu}$, OK	1.000 <=1, OK

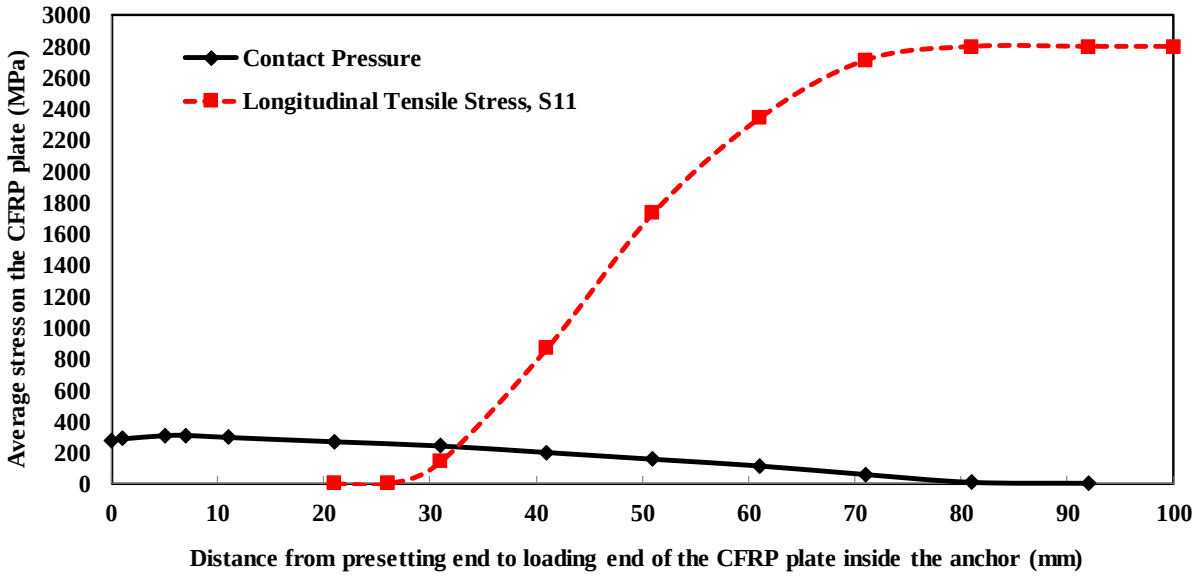

Figure 5.6: The mean contact pressure and longitudinal pressure distribution in CFRP plate.

The displacement distribution along the CFRP plate is shown in Fig. 5.7(a) using 3 mm pre-setting and 2,800 MPa tension load. As expected, the displacement was gradually distributed along the CFRP plate. The maximum combined displacement and extension of the wedge, the sleeve and the CFRP plate was 8.45 mm at the loaded end (Fig. 5.7a). Most of this displacement was due to the sliding of the wedge inside the anchor (7.62 mm), as shown in Fig. 5.7(b). Out of this 7.62 mm of wedge displacement, 3 mm was due to the application of the 3 mm pre-setting load. The remaining 4.62 mm was the sliding distance of the wedge with respect to barrel; and this sliding distance was required to self-seat the wedge inside the anchor. From Fig. 5.7a and 5.7b, the CFRP plate and the sleeve did not slide at all with respect to the wedge under 2,800 MPa loading (7.62 mm – 7.62 mm = 0 mm). Therefore, it showed that CFRP plate did not slip out of the anchor under 3 mm pre-setting and 2,800 MPa tensile loading. As shown in Fig. 5.7a, the maximum elongation in the CFRP plate was found as 0.83 mm (8.45 mm - 7.62 mm = 0.83 mm), which was less than the given ultimate elongation limit of the CFRP plate (1.7%), given by the manufacturer.

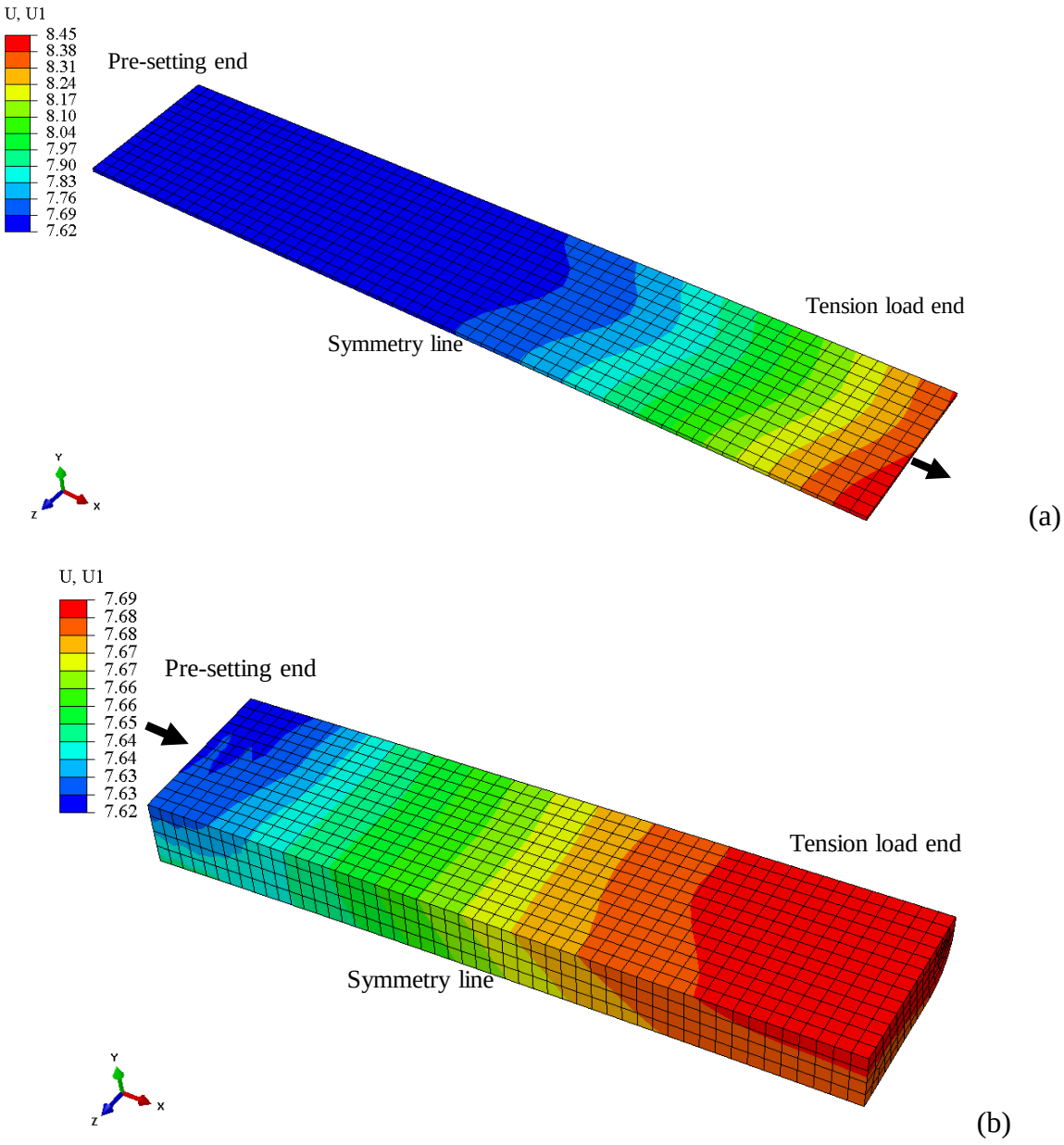

Figure 5.7: (a) Displacement distribution: (a) on the CFRP plate (one-quarter of the CFRP plate) and (b) on the wedge (half of wedge) of the H13 steel solid anchor under 3 mm pre-setting and 2,800 MPa tension loading.

The von Mises stress distribution of the anchor components are shown in Fig. 5.8a (sleeve), Fig. 5.8b (wedge) and Fig. 5.8c (barrel). The maximum von Mises stress values in the sleeve, the wedge and the barrel were the highest in the pre-setting end; and the least in the tension load end of the anchor. The maximum von Mises stress in both the wedge (770 MPa) and the barrel (1,366 MPa) were less than the yield strength of the heat-treated H13 steel, given in Table 5.1 (1,366 MPa). The high stresses in the wedge and the barrel had little effect on the overall performance of the anchor because they were limited to very small areas.

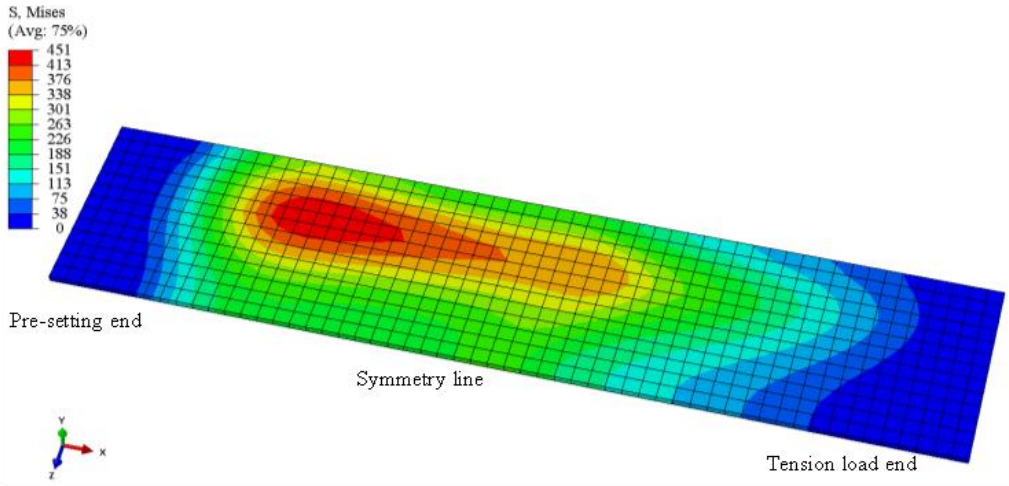

(a)

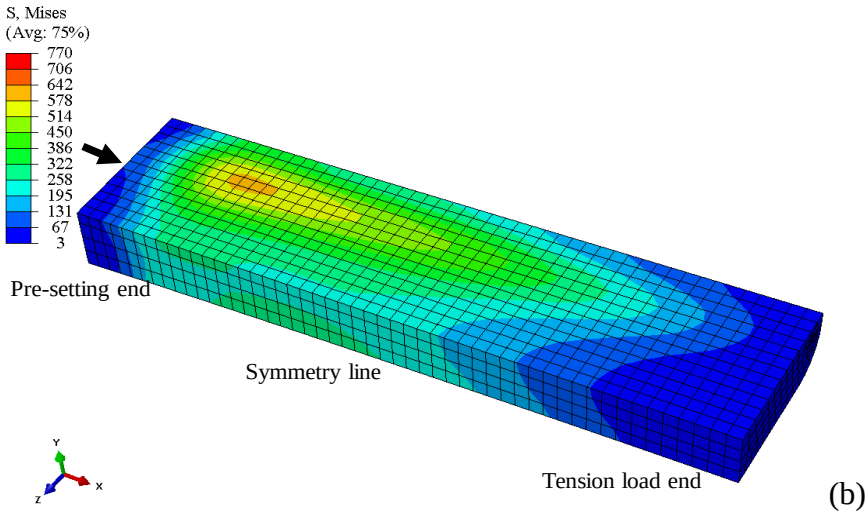

(b)

Figure 5.8: Von Mises stress distribution on: (a) the sleeve (half); (b) the wedge (half); and (c) the barrel (one-quarter) of the solid anchor under 3 mm pre-setting and 2,800 MPa load.

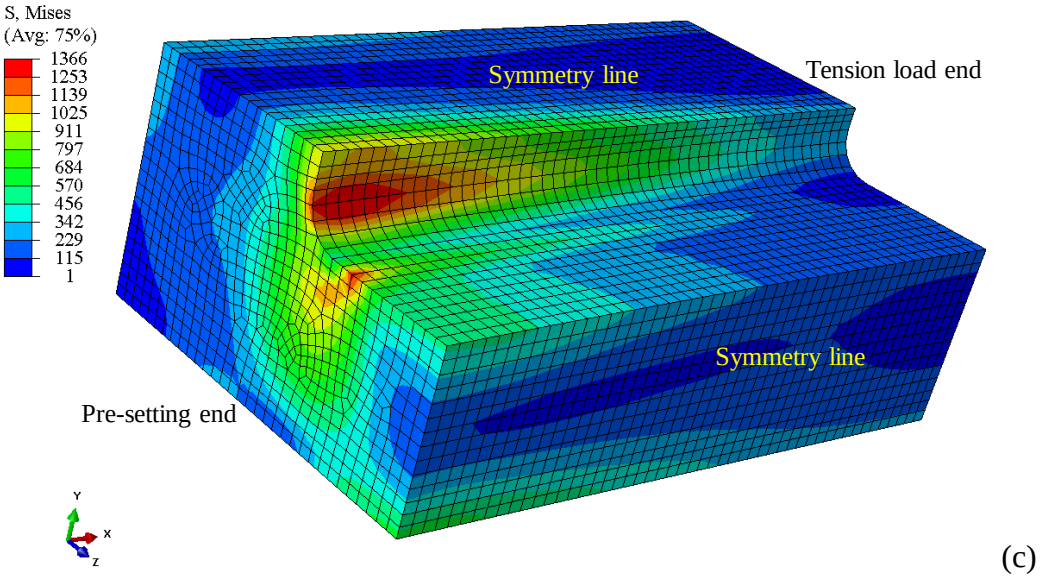

Fig. 5.8 (c): Von Mises stress distribution on the barrel (one-quarter of barrel) of the H13 steel solid anchor under 3 mm pre-setting and 2,800 MPa tension load.

5.5 PARAMETRIC ANALYSIS AND DISCUSSION

Different design parameters were investigated using the numerical model, including the pre-setting distance, the length of the anchor, the interference distance along Y-direction between the barrel and the wedge end points at the loading end, the longitudinal curvature of the barrel and the wedge, and the thickness of the barrel and the wedge. They are briefly discussed in this section. The objective of this parametric study was to demonstrate the effects of different parameters on the anchor performance; and to obtain an optimized anchor design. For presentation purpose, the figures of the parametric study were drawn with the same Y-limit (550 MPa of contact pressure) to show the comparative effects of different parameters.

5.5.1 Effect of Pre-setting Distance

In order to illustrate the effect of the pre-setting distance on the anchor performance, an anchor with 3,000 mm longitudinal curve radius, 0.05 mm interference distance, 25.93 mm minimum thickness barrel at the pre-setting end, 8.05 mm minimum thickness wedge at the loading end and 100 mm length, under a tensile load of 2,800 MPa, was investigated.

In Table 5.4, the maximum total slippage distance is the combined total slippage distance of the wedge, the sleeve and the CFRP plate with respect to the barrel. As demonstrated in Table 5.4, within the pre-setting distance range of 0.32 mm - 7 mm, there was no increase of the contact pressure on the CFRP plate and the von Mises stress in the wedge and the barrel. Within this range, the wedge slid inside the anchor until it self-seat (7.62 mm, as discussed in section 5.4). The self-seating distance was the distance required by the wedge to seat the wedge inside the barrel so that the anchor can carry a high tension load. Above 7.62 mm of pre-setting, the maximum contact pressure on the CFRP plate inside the anchor increased substantially with the increase of the pre-setting distance of the wedge. Above 7.62 mm pre-setting, the von Mises stress in the wedge and the barrel also increased rapidly without any more slippage distance of the wedge (Table 5.4).

The mean contact pressure distributions on the CFRP plate over the length of the anchor under different pre-setting (3 mm, 10 mm and 12 mm) and 2,800 MPa tension load are shown in Fig. 5.9. From Fig. 5.9, the peak of the mean contact pressure for 3 mm pre-setting was closer to the pre-setting end of the anchor than the peak of the larger pre-setting distances (10 mm or 12 mm). In addition, the slope of the 12 mm pre-setting was steeper than that of the 3 mm pre-setting (Fig. 5.9). The peak contact pressure for the 12 mm pre-setting was also very close to the 546 MPa compressive strength of the CFRP plate (Fig. 5.9). This figure establishes the effect of pre-setting on the anchor performance that a larger pre-setting load leads to a larger mean contact pressure on the CFRP plate inside the anchor. This figure also depicts that the

maximum mean contact pressure on the CFRP plate is at the pre-setting end and the minimum mean contact pressure is at the tension load end for all pre-setting distances.

Table 5.4: Effect of pre-setting on the anchor characteristics for an anchor with 3,000 mm longitudinal curve radius, 0.05 mm interference distance, 25.93 mm minimum thickness barrel, 8.05 mm minimum thickness wedge and 100 mm length under 2,800 MPa tensile load.

Pre-setting distance (mm)	CFRP plate max. contact pressure (MPa)	Max. total slippage distance of CFRP, sleeve and wedge (mm)	Wedge max. von Mises stress (MPa)	Barrel max. von Mises stress (MPa)
0.32	393	7.30	769	1,311
3	393	4.62	770	1,366
5	393	2.62	770	1,366
6	393	1.62	770	1,366
7	393	0.62	770	1,366
8	412	0	797	1,431
9	464	0	987	1,662
10	518	0	995	1,693
12	621	0	1,205	2,055
14	728	0	1,847	2,587

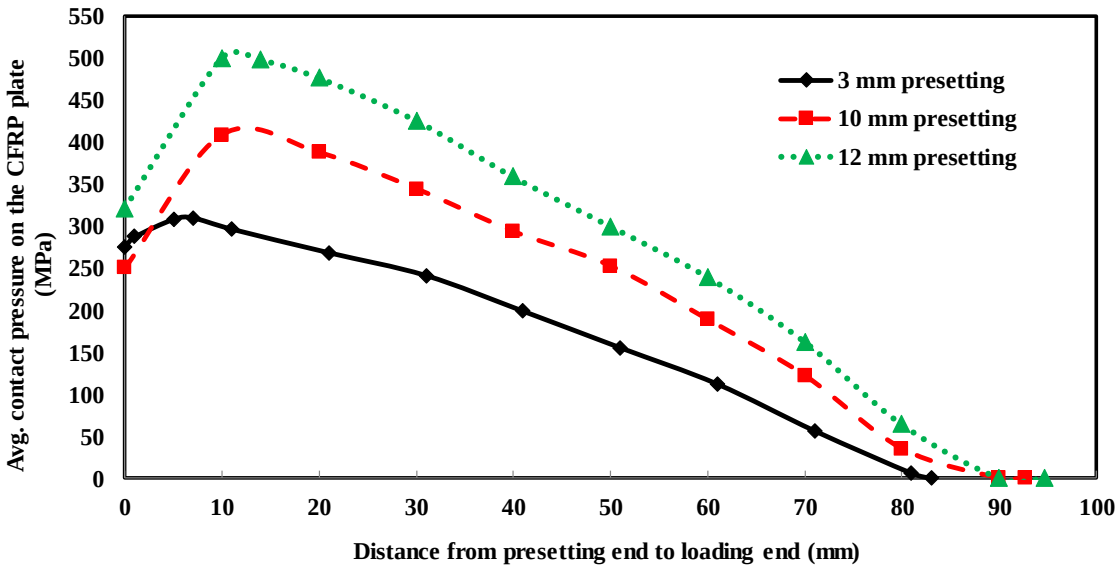

Figure 5.9: Effect of pre-setting on the mean contact pressure on the CFRP plate inside the anchor under different pre-setting loads and 2,800 MPa tension load.

A similar effect of pre-setting distance was observed at the sleeve-wedge and wedge-barrel interfaces as well. The mean contact pressures on both of the sleeve-wedge and wedge-barrel interfaces were the maximum at the pre-setting end and the minimum at the tension loading end. In addition, the mean contact pressure on both of the sleeve-wedge and wedge-barrel interfaces increased with the increase of the pre-setting distance.

A similar effect of pre-setting distance was observed in another anchor that had 2,200 mm longitudinal curve radius, 0.1 mm interference distance, 20 mm minimum thickness barrel, 6.1 mm minimum thickness wedge and 80 mm length. However, the first anchor had a significantly lower contact pressure on the CFRP plate (*e.g.*, 393 MPa compared to 593 MPa, for 3 mm pre-setting) and a significantly lower von Mises stress in the barrel (*e.g.*, 1,366 MPa compared to 2,105 MPa, for 3 mm pre-setting) for all of the pre-setting values. Therefore, it was understood that there were large contributions from other parameters (*i.e.*, longitudinal curve radius, interference distance, length of the anchor, thickness of the barrel and the wedge) on the anchor performance, as well.

5.5.2 Effect of the Anchor-length

The length of the anchor had a significant contribution on the anchor performance under loading. The lengths of the barrel and the wedge were kept same in this thesis; and that length was termed as the anchor-length. In order to demonstrate the effect of the anchor-length, an anchor with 3,000 mm longitudinal curve radius, 0.05 mm interference distance, 25 mm minimum thickness barrel, and 8.05 mm minimum thickness wedge, under 3 mm pre-setting and 2,800 MPa tension load, was investigated. The analysis results with anchor-lengths in the range of 80 mm – 120 mm are presented in Table 5.5. As the anchor-length increased from 80 mm to 120 mm, the concentration of the contact pressure on the CFRP plate was reduced because the pressure was distributed over a larger area of contact. Furthermore, an increased anchor-length led to a heavier and stronger barrel, which provided a larger confinement to the wedge. Subsequently, the wedge slid less in the longer anchors. A longer and stronger barrel also led to a reduced maximum von Mises stress in the barrel.

With an increase of the anchor-length from 80 mm to 120 mm, the maximum contact pressure on the CFRP plate decreased from 506 MPa to 311 MPa; the maximum slippage distance (self-seating distance) of the wedge decreased one-third from 8.43 mm to 2.36 mm; the maximum von Mises stress in the wedge decreased almost half from 1,280 MPa to 694 MPa; and the maximum von Mises stress in the barrel decreased significantly from 1,675 MPa to 1,095 MPa (Table 5.5).

However, one of the goals of this research was to obtain a compact anchor design. Furthermore, an increased length made the anchor heavy, difficult to install and expensive. Hence, an anchor-length was chosen such that the contact pressure on the CFRP plate stayed within the 546 MPa compressive strength of the CFRP plate and the maximum von Mises stress in both barrel and wedge stayed within the 1,366 MPa yield strength of H13 steel. Therefore, an anchor-length of 100 mm was chosen for the final anchor design.

Table 5.5: Effect of the anchor-length on the anchor performance for an anchor with 3,000 mm longitudinal curve radius, 0.05 mm interference distance, 25 mm minimum thickness barrel and 8.05 mm minimum thickness wedge under 3 mm pre-setting and 2,800 MPa load

Length of anchor (mm)	CFRP plate max. contact pressure (MPa)	Wedge max. von Mises stress (MPa)	Barrel max. von Mises stress (MPa)
80	506	1,280	1675
90	444	1,072	1,593
100	393	770	1,366
120	311	694	1,095

5.5.3 Effect of Interference Distance between Barrel and Wedge in Longitudinal Profile

The interference distance along the Y-direction between the barrel and the wedge end points at the loading end (Δ_{VD}), as shown in Fig. 5.10, is an important anchor design parameter. Different interference distance values within the range of 0.05-0.5 mm were considered for this study on an anchor with 3,000 mm longitudinal curve radius, 25 mm minimum thickness barrel, 8.05 mm minimum thickness wedge and 100 mm length under 3 mm pre-setting and 2,800 MPa tension load. The comparative longitudinal anchor profile of one-quarter of the anchor is shown in Fig. 5.10 for 0.05 mm and 0.5 mm interference distances. With a decrease of the interference distance from 0.5 mm to 0.05 mm, the maximum contact pressure on the CFRP plate decreased from 432 MPa to 393 MPa (Table 5.6); the maximum total slippage distance decreased from 5.34 mm to 4.62 mm (Table 5.6); the maximum von Mises stress in the wedge decreased from 947 MPa to 770 MPa; and the maximum von Mises stress in the barrel decreased from 1,532 MPa to 1,366 MPa. Figure 5.11 shows the mean contact pressure distribution on the CFRP plate for 0.05 mm and 0.5 mm interference distances. In addition, the total contact area between barrel and wedge was larger in the anchor with a smaller interference

distance of 0.05 mm than that of 0.5 mm (Fig. 5.10). As shown in Fig. 5.11, the effective contact pressure area in the CFRP plate was also larger (0-80 mm) in the anchor with a smaller interference distance of 0.05 mm than the anchor with a larger interference distance of 0.5 mm (0-50 mm). Therefore, an interference distance of 0.05 mm was chosen over larger interference distances for the final anchor design.

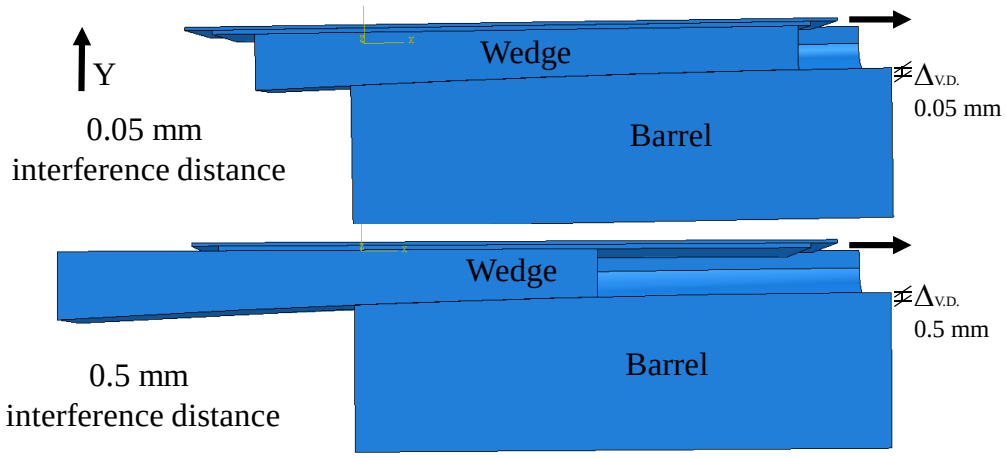

Figure 5.10: Comparative longitudinal anchor-profiles with different interference distances (Δ_{VD}).

Table 5.6: Effect of the interference distance between barrel and wedge ends at the loading end for an anchor with 3,000 mm longitudinal curve radius, 25 mm minimum thickness barrel, 8.05 mm minimum thickness wedge and 100 mm length at 3 mm pre-setting and 2,800 MPa.

Interference distance (mm)	CFRP plate max. contact pressure (MPa)	Maximum total sliding distance of wedge, sleeve and CFRP plate (mm)
0.5	432	5.34
0.2	397	4.73
0.1	394	4.64
0.05	393	4.62

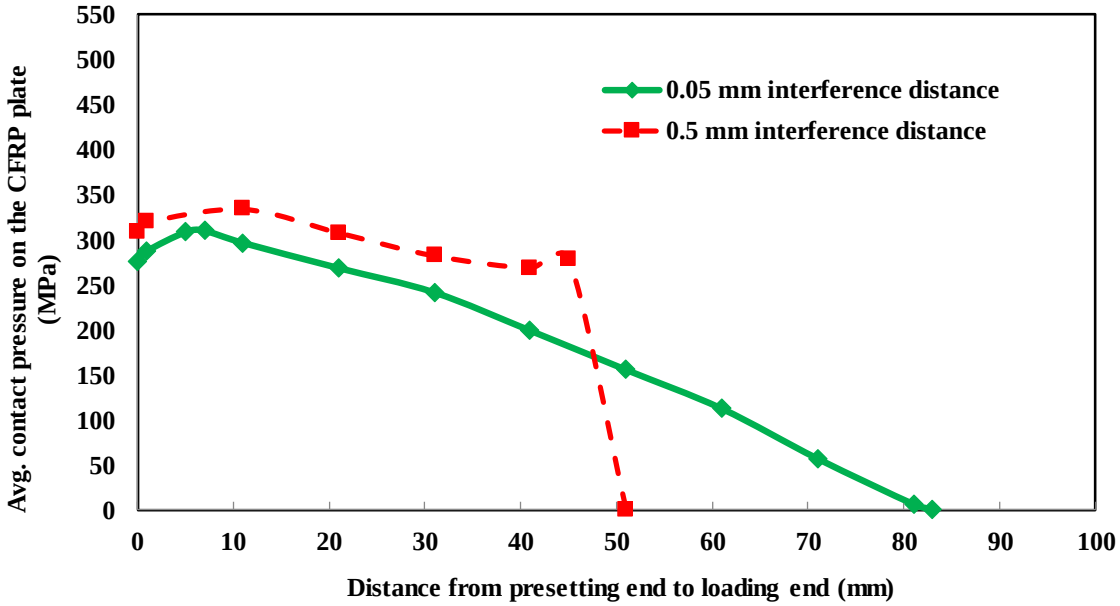

Figure 5.11: Effect of the interference distance between the barrel and wedge end (Δ_{VD}) on the contact pressure of the CFRP plate under 3 mm pre-setting and 2,800 MPa tension load over the length of the CFRP plate.

5.5.4 Effect of Longitudinal Curve Radius

The effect of the longitudinal curve radius of the barrel and the wedge on the anchor performance was investigated numerically keeping the other parameters fixed: pre-setting distance, interference distance, anchor-length, barrel and wedge thickness. In this thesis, the longitudinal curve radius was kept the same for both the barrel and the wedge. The numerical analysis results of the anchors with longitudinal curve radius of 1600 mm, 2200 mm, 2600 mm and 3000 mm are shown in Table 5.7.

In an anchor with a smaller longitudinal radius of 1,600 mm, the 11.97 mm thick (thickness in the pre-setting end) wedge tried to enter into a smaller (11.13 mm thick) barrel-opening under loading. In a larger radius (3,000 mm) anchor, the 10.29 mm thick wedge tried to enter into a smaller (9.67 mm thick) barrel-opening under loading. The difference between the wedge-

thickness and the barrel-opening were 0.84 mm and 0.62 mm for the 1,600 mm and 3,000 mm longitudinal radius anchors, respectively. Hence, this difference was less in the larger longitudinal radius anchor. Therefore, under a pre-setting of 3 mm and a tensile load of 2,800 MPa, with an increased longitudinal radius in the wedge and the barrel, the self-seating distance of the wedge inside the anchor increased; and the maximum von Mises stresses in the barrel and the wedge increased; and the maximum contact pressure on the CFRP plate also increased (Table 5.7).

Two different anchor designs with the same longitudinal curve radius (for 1600 mm, 2200 mm, 2600 mm and 3000 mm) were also compared (Table 5.7). For all of these longitudinal curve radii, it was found that the anchor with 0.05 mm interference distance, 100 mm length, 25 mm minimum thickness barrel, and 8.05 mm minimum thickness wedge exhibited a significantly lower contact pressure on the CFRP plate and a lower von Mises stress in the barrel than that of an anchor with 0.1 mm interference distance, 80 mm length, 20 mm minimum thickness barrel and 6.1 mm minimum thickness wedge (Table 5.7). Therefore, the combined effect of the longitudinal curve radius, the interference distance, the anchor-length and the barrel/wedge thickness was more critical than that of the longitudinal curve radius itself.

Figure 5.12 shows the mean contact pressure distribution on the CFRP plate for anchors with 1600 mm, 2200 mm and 3000 mm longitudinal curve radius for an anchor with an interference distance of 0.05 mm, minimum barrel thickness of 25 mm and minimum wedge thickness of 8.05 mm and length of 100 mm. From Fig. 5.12, the peak of the mean contact pressure on the CFRP plate was located closest to the pre-setting end for the largest radius (3,000 mm) anchor. For the smallest radius (1,600 mm) anchor, the peak of the mean contact pressure was located almost 10 mm away from the pre-setting end. One of the basic objectives of this anchor design concept was to ensure that the location of the peak of the contact pressure was as close as possible to the pre-setting end. Therefore, although the peak mean contact pressure was higher for the largest radius (3,000 mm), it was still chosen as the final longitudinal curve radius.

Table 5.7: Effect of the longitudinal curve radius on the anchor design

Anchor modelling criteria	Long. curve radius (mm)	CFRP plate max. contact pressure (MPa)	Max. slip of wedge, sleeve and CFRP plate (mm)	Barrel max. von Mises stress (MPa)
0.05 mm interference distance, 100 mm long anchor, 25 mm min. thick barrel, 8.05 mm min. thick wedge.	3,000	393	4.62	1,366
	2,600	376	3.48	1263
	2,200	356	2.32	1,170
	1,600	312	0.59	1,088
0.1 mm interference distance, 80 mm long anchor, 20 mm min. thick barrel, 6.1 mm min. thick wedge.	3,000	610	11.66	2,264
	2,600	609	7.84	2,189
	2,200	593	5.6	2,105
	1,600	518	1.81	1,915

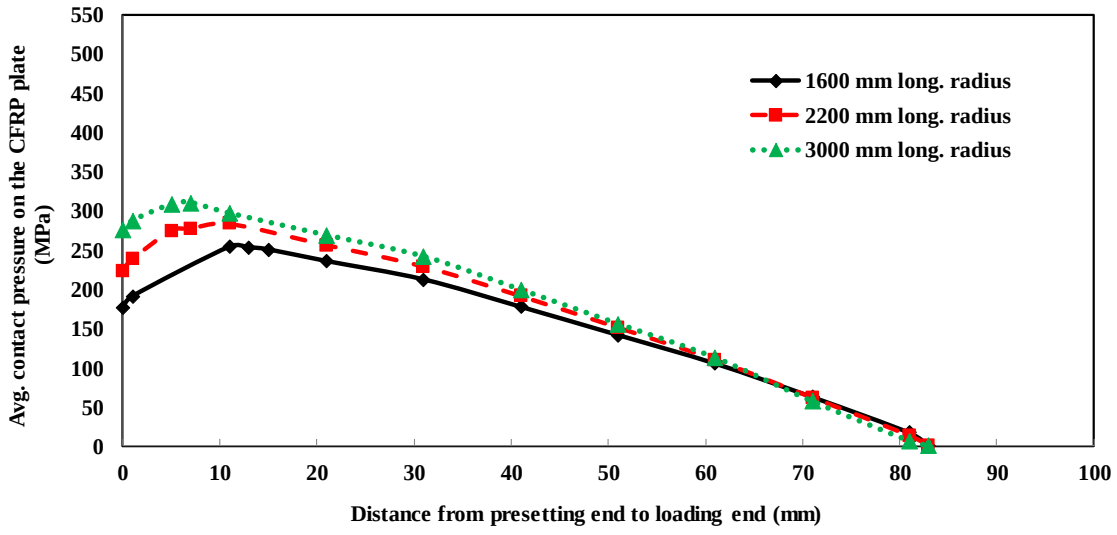

Figure 5.12: Effect of the longitudinal radius on the mean contact pressure on the CFRP plate under loading (3 mm pre-setting and 2,800 MPa tension) over the length of the anchor.

5.5.5 Effect of Thickness of Barrel

Barrel thicknesses (minimum thickness) between 12.93 mm and 25.93 mm at the pre-setting end were investigated. The mean contact pressures on the CFRP plate for different thicknesses of barrel were almost the same along the length of the plate. On the contrary, as illustrated in Table 5.8 and Fig. 5.13, with an increased barrel thickness, the self-seating distance of the wedge inside the anchor under loading decreased, and the maximum von Mises stresses in the barrel and the wedge decreased, and the maximum contact pressure on the CFRP plate also decreased. Under loading, for a thinner barrel, as the barrel deformed, there were localized stress concentrations which caused a larger maximum stress at the barrel-wedge interface. This led to a larger maximum contact pressure on the CFRP plate for an anchor with a thinner barrel. Furthermore, for a thinner barrel (12.93 mm or 15.93 mm), the maximum von Mises stress in the barrel was more than the yield strength of the heat-treated high-strength steel (1,366 MPa). Therefore, a thicker barrel (25.93 mm) was selected for the optimum anchor design.

Table 5.8: Effect of the thickness of barrel on the anchor behaviour for an anchor with 3,000 mm longitudinal curve radius, 0.05 mm interference distance, 8.05 mm thick wedge and 100 mm length under 2,800 MPa tensile load.

Minimum Barrel thickness (mm)	CFRP plate max. contact pressure (MPa)	Maximum total slip of wedge, sleeve and CFRP plate (mm)	Wedge max. von Mises stress (MPa)	Barrel max. von Mises stress (MPa)
12.93	459	9.05	1,135	2,249
15.93	440	7.37	1,001	1,647
20.93	403	5.63	927	1,481
22.93	399	5.18	811	1,367
25.93	393	4.62	770	1,366

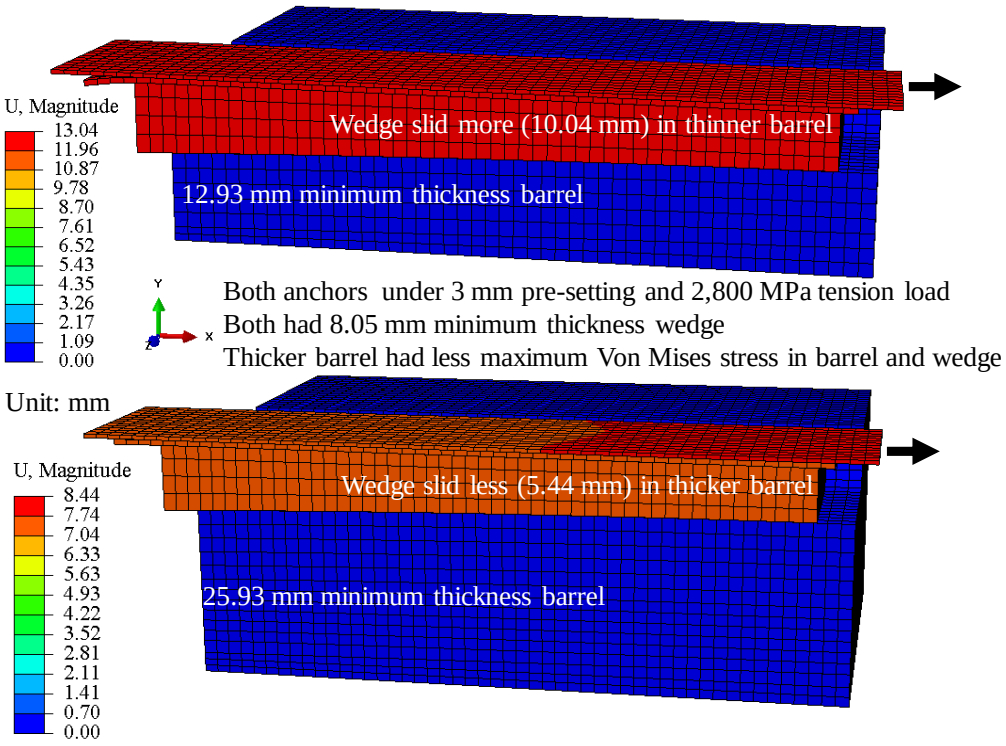

Figure 5.13: The comparative wedge displacement for different barrel thicknesses. It explains the less von Mises stress in barrel and wedge, and less maximum contact pressure in CFRP plate in the thicker barrel anchor under 3 mm pre-setting and 2,800 MPa tension load.

5.5.6 Effect of Thickness of Wedge

Wedge thicknesses (minimum thickness at the loading end) between 6.05 mm and 15.05 mm were investigated. For the same confinement provided by the barrel (25.93 mm thick barrel), the maximum contact pressure on the CFRP plate decreased from 431 MPa to 323 MPa; and the maximum von Mises in the barrel increased from 1,339 MPa to 1,462 MPa with the increase of the minimum thickness of the wedge from 6.05 mm to 15.05 mm (Table 5.9). Similar results were obtained for other anchor designs with different longitudinal curve radii (3,000 mm and 2,200 mm) and interference distances (0.05 mm and 0.1 mm).

Two different anchor designs with the same wedge thickness of 6 mm were investigated. The anchor with 3,000 mm longitudinal curve radius, 0.05 mm interference distance, 25.93 mm minimum thickness barrel and 100 mm length exhibited a significantly lower maximum contact pressure on the CFRP plate (431 MPa compared to 582 MPa) and a significantly lower maximum von Mises stress in both the barrel (1,339 MPa compared to 2,267 MPa) and the wedge (745 MPa compared to 1,224 MPa) than the anchor with 2,200 mm longitudinal curve radius, 0.1 mm interference distance, 20 mm thick barrel and 100 mm length. Considering that an increased wedge thickness led to a heavier anchor, a minimum wedge thickness of 8.05 mm at the loading end was chosen over the thicker wedges for the final anchor design.

Table 5.9: Effect of the thickness of wedge on the anchor behaviour for an anchor with 3,000 mm longitudinal curve radius, 0.05 mm interference distance, 25.93 mm thick barrel and 100 mm length under 3 mm pre-setting and 2,800 MPa tensile load.

Wedge min. thickness (mm)	CFRP plate max. contact pressure (MPa)
6.05	431
8.05	393
10.05	364
13.05	334
15.05	323

5.5.7 Combined Effect of Thickness of Barrel, Barrel Sidewall and Wedge

A combined effect of the thicknesses of the barrel, the barrel sidewall and the wedge on the anchor performance was investigated for the same longitudinal radius (3,000 mm), interference distance (0.05 mm) and pre-setting distance (3 mm) in the anchor (Table 5.10). The anchor with a thicker barrel, barrel sidewall and wedge had a significantly less maximum contact

pressure on the CFRP plate (393 MPa, compared to 458 MPa) and a significantly less maximum von Mises stress in the barrel (1,366 MPa, compared to 1,670 MPa).

On the contrary, for a bolted anchor, the barrel sidewall thickness required to be thick enough to accommodate the bolt-holes inside the barrel sidewall. At least, a distance equal to the half of a bolt diameter was provided in each side of the bolt-holes in order to avoid cracks originated from the bolt-holes. This dominated the thickness of the barrel sidewall while finalizing the anchor design. Considering all of these findings, a thicker barrel sidewall (35 mm thick) was chosen in order to accommodate the bolt-holes required for the three 22.23 mm (7/8-inch) diameter bolts in the barrel sidewalls.

Table 5.10: The combined effect of the barrel sidewall, barrel and wedge thicknesses for an anchor with 3,000 mm longitudinal radius and 0.05 mm interference distance under 3 mm pre-setting and 2,800 MPa tension load.

Min. barrel thickness (mm)	Min. wedge thickness (mm)	Min. barrel sidewall thickness (mm)	CFRP plate max. contact pressure (MPa)	Barrel max. von Mises stress (MPa)
25.9	8.05	35	393	1,366
20	6.05	30	458	1,670

5.5.8 Sensitivity Study

A sensitivity study was carried out to investigate the effect of the plastic properties of the annealed copper sleeves on the anchor performance. The numerical model results were compared with the elastic and elastic-plastic behaviour of the annealed copper sleeve in the anchor. It was found that the results in the two models were close, with the anchor with the elastic-plastic sleeve had a slightly higher contact pressure on the CFRP plate (Table 5.11). With elastic-plastic annealed copper, the maximum von Mises stress in the sleeve was 80 MPa, which was more than the yield strength (45 MPa) but less than the ultimate strength (210 MPa)

of annealed copper. The sleeve deformed during the loading process, but there was negligible effect on the anchor performance. There was no effect on the von Mises stress values of the barrel and the wedge. There was also no effect on the sliding behaviour of any of the components of the anchor.

Table 5.11: Effect of the plastic behaviour of annealed copper sleeves for an anchor with 3,000 mm longitudinal radius, 0.05 mm interference distance and 25.93 mm minimum thickness barrel under 3 mm pre-setting and 2,800 MPa tension load.

Type of annealed copper sleeve in model	CFRP plate max. contact pressure (MPa)
Elastic	393
Elastic-Plastic	416

Another sensitivity study was performed in order to investigate the effect of the Poisson's ratio of the CFRP plate on the anchor performance. From this analysis, it was found that there was no significant effect of the variation of the Poisson's ratio of the CFRP plate on the anchor performance. The maximum contact pressure on the CFRP plate under 3 mm pre-setting and 2,800 MPa tension load was 393 MPa, 384 MPa, 382 MPa and 381 MPa for the transverse Poisson's ratio (v_{23}) value of 0.45, 0.25, 0.17 and 0.1, respectively. There was no change in the total displacement (8.45 mm) and elongation (0.82 mm) values of the CFRP plate inside the anchor for different transverse Poisson's ratio values. There was also no change in the von Mises stress values in the barrel, the wedge and the sleeve under loading for different transverse Poisson's ratio values of the CFRP plate.

5.5.9 Comparative Effect of Different Parameters on the Anchor Design

This section presents the comparative summary graphs originated from the discussions given in the sections 5.5.1 to 5.5.6. Figures 5.14, 5.15 and 5.16 depict the effect of different design parameters on the three critical characteristics of the anchor: the maximum contact pressure on the CFRP plate (Fig. 5.14), the maximum total slip of the wedge, sleeve and CFRP plate, excluding the pre-setting distance (Fig. 5.15), and the maximum von Mises stress in the barrel (Fig. 5.16), respectively. The Y-axis of all six graphs in a set of graphs were kept same (750 MPa of contact pressure in Fig. 5.14, 10 mm of slippage distance in Fig. 5.15, and 2,600 MPa of von Mises stress in Fig. 5.16). This was done in order to have a proper comparison of the effect of each of the six input parameters on the anchor performance.

All of these analyses were carried out under a tension load of 2,800 MPa. During the investigation of the effect of an input parameter on either of these three outputs (contact pressure on CFRP plate, total slippage distance and von Mises stress on the barrel), the remaining five input parameters were kept constant. For instance, during the investigation of the effect pre-setting distance on the contact pressure of the CFRP plate, the remaining five parameters were kept constant (*i.e.*, length of the anchor was 100 mm, interference distance was 0.05 mm, longitudinal curve radius was 3,000 mm, minimum barrel thickness was 25.93 mm, and minimum wedge thickness was 8.05 mm). A range of pre-setting distances between 0.32 mm and 14 mm, a range of anchor-lengths between 80 mm and 120 mm, a range of interference distances between 0.05 mm and 0.5 mm, a range of longitudinal curve radius between 1,600 mm and 3,000 mm, a range of barrel thickness between 12.93 mm and 25.93 mm, and a range of wedge thickness between 6 mm and 15 mm were investigated, and demonstrated in this section.

From these figures, it can be stated that all of these six design parameters have significant effect on the anchor behaviour. The maximum contact pressure on the CFRP plate increased significantly with the increase of the pre-setting distance above 7.62 mm, and with the decrease

of the anchor-length (Fig. 5.14). The maximum contact pressure on the CFRP plate increased slightly with the increase of the interference distance and the longitudinal curve radius; and it decreased slightly with the increase of the barrel and the wedge thicknesses (Fig. 5.14).

The design parameters of the final anchor design were chosen such that the maximum contact pressure on the CFRP plate inside the anchor was neither too low (to avoid slippage of the CFRP plate from the anchor), nor too high, *i.e.*, less than 546 MPa (to avoid premature failure of the CFRP plate inside the anchor).

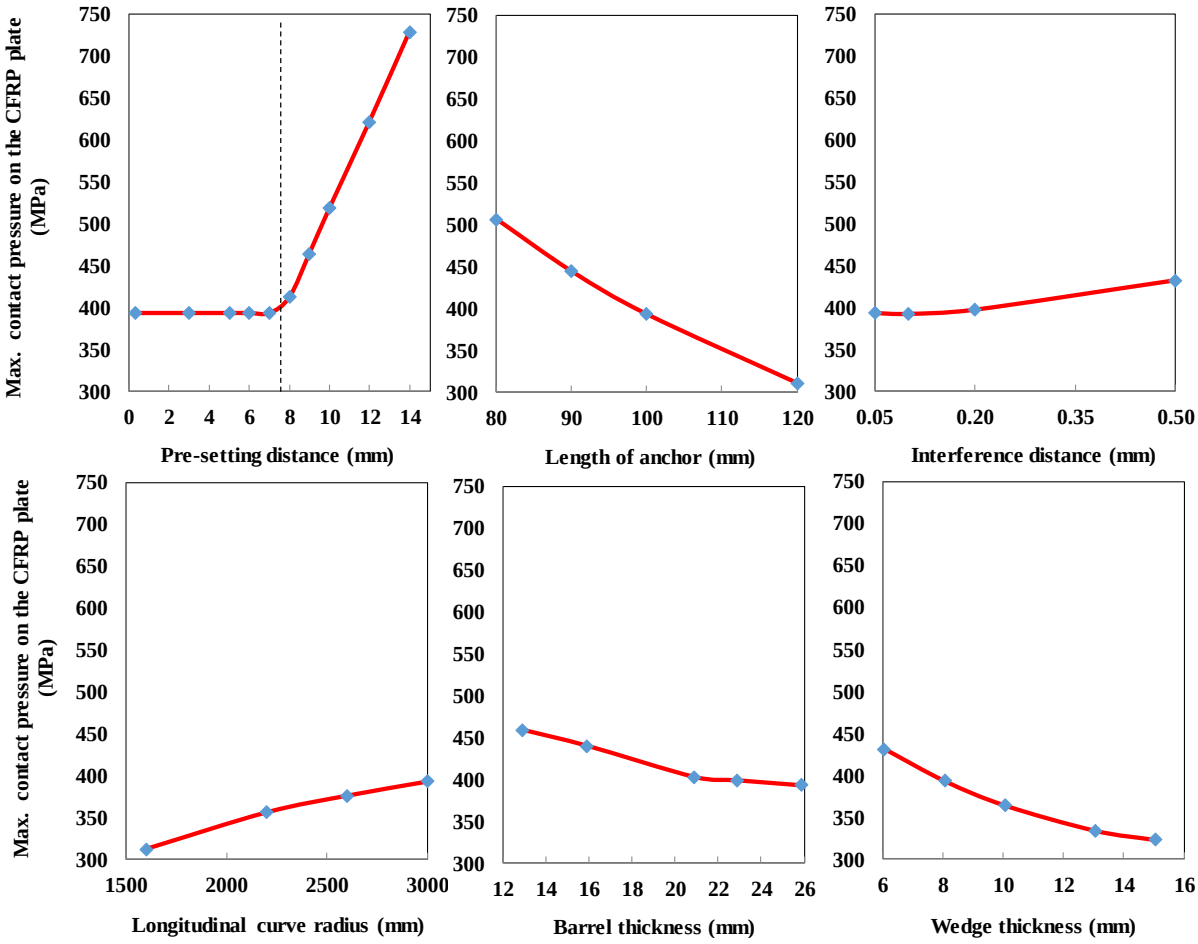

Figure 5.14: Summary of the effect of different design parameters on the maximum contact pressure on the CFRP plate inside the anchor under 2,800 MPa tension load.

From Fig. 5.15, the wedge slid for 7.62 mm in order to self-seat inside the barrel. Therefore, above 8 mm pre-setting, there was no more displacement of the wedge inside the anchor under loading. This total slippage distance or the self-seating distance decreased with the increase of the anchor-length and the barrel-thickness; and it increased with the increase of the longitudinal curve radius and the thickness of the wedge (Fig. 5.15).

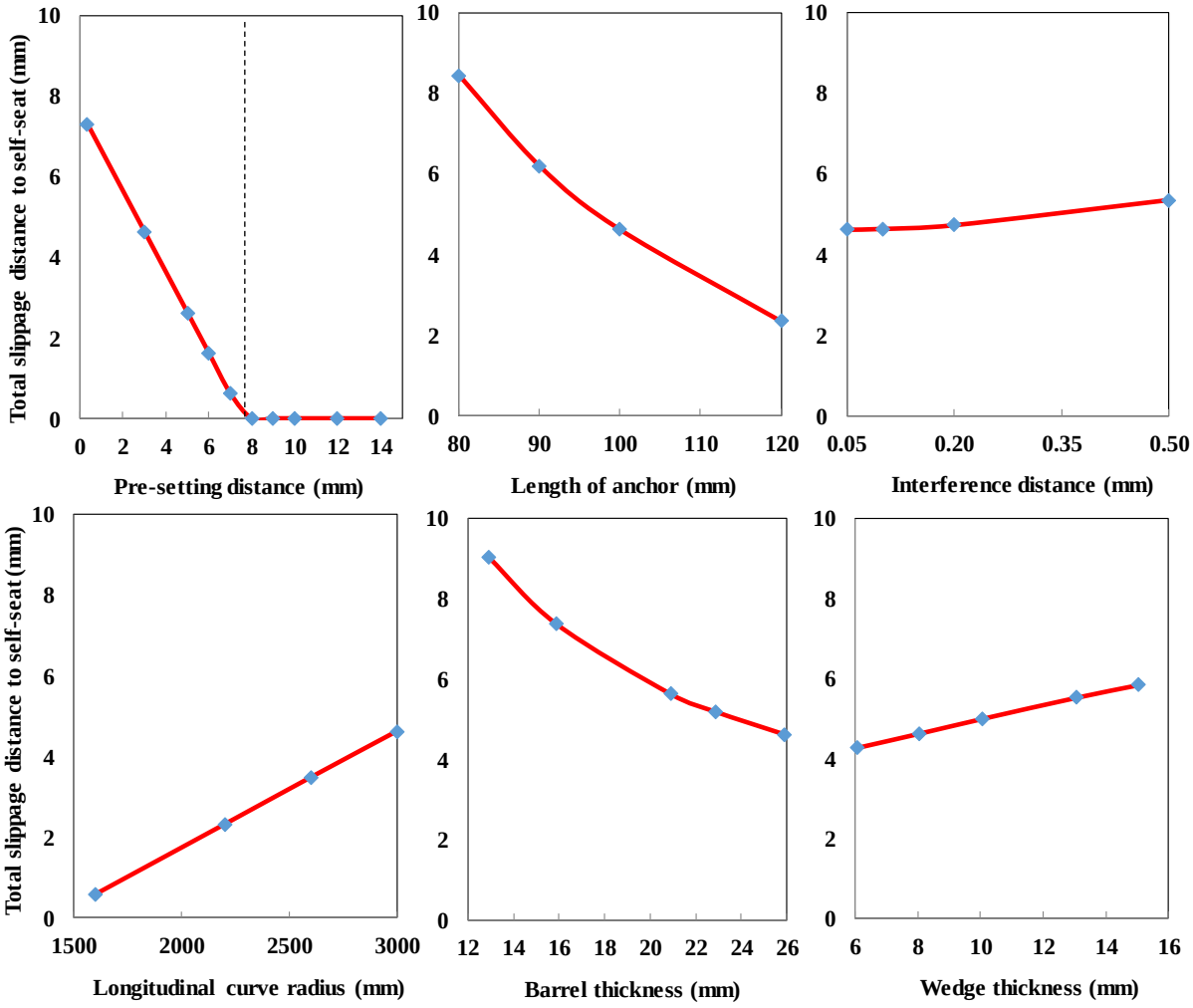

Figure 5.15: Summary of the effect of different design parameters on the maximum total slippage distance of the wedge, the sleeve and the CFRP plate to self-seat under 2,800 MPa tension load.

The pre-setting distance, the barrel-thickness and the anchor-length had significant effects on the maximum von Mises stress in the barrel in the anchor (Fig. 5.16). The maximum von Mises stress in the barrel increased significantly with the increase of the pre-setting distance above 7.62 mm, and with the decrease of the anchor-length and the barrel-thickness. The maximum von Mises stress in the barrel increased slightly with the increase of the interference distance, the longitudinal curve radius and the wedge-thickness. The parameters of the final anchor design were chosen such that the maximum von Mises stress in the barrel of the anchor was less than the yield strength of the heat-treated high-strength H13 steel (1,366 MPa).

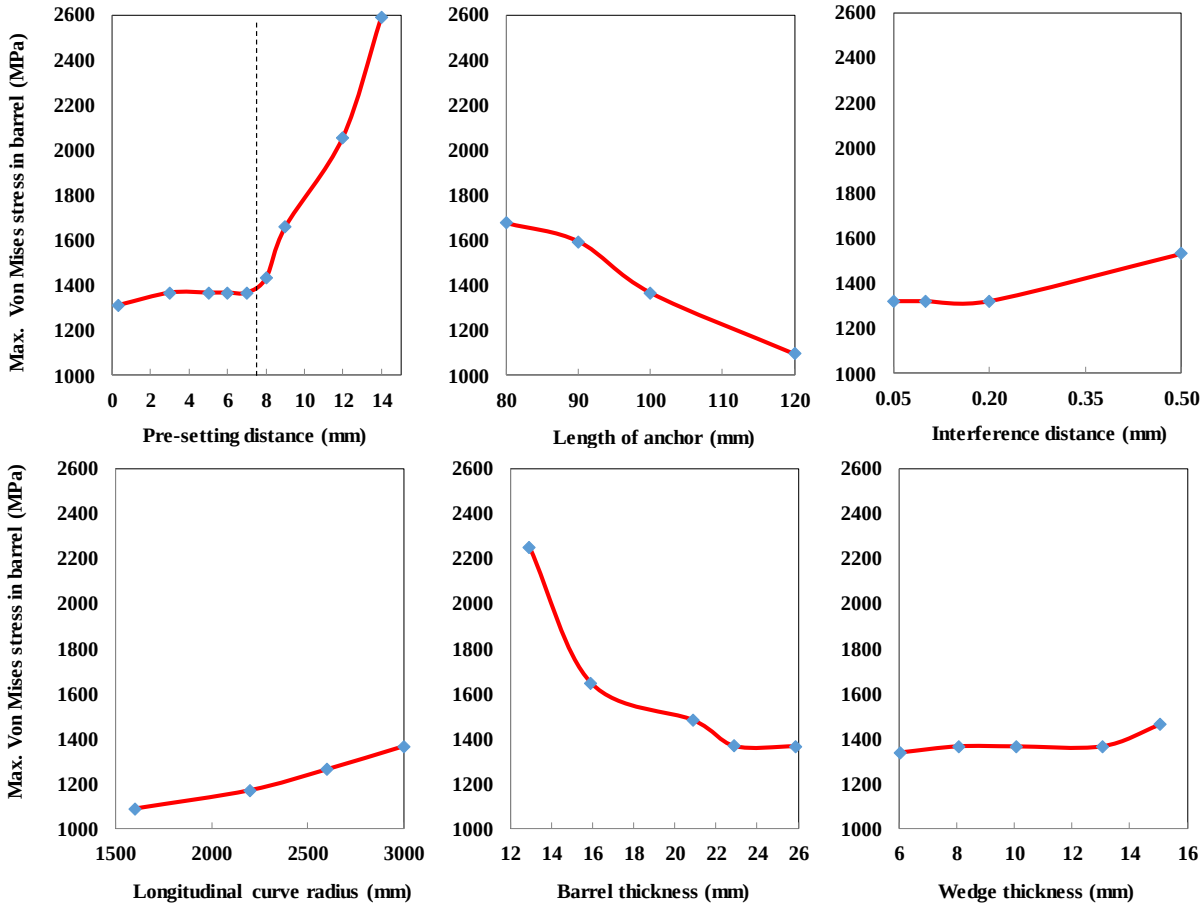

Figure 5.16: Summary of the effect of different design parameters on the maximum von Mises stress in the barrel of the anchor under 2,800 MPa tension load.

5.6 RESULTS OF THE BOLTED ANCHOR (ANCHOR #1)

To ensure that the anchor can be manufactured easily, an anchor design with two pieces of barrel was required. These two pieces were connected through six high strength steel bolts. A three-dimensional FEM model using Abaqus software was developed to accommodate this change in the anchor design. New boundary conditions were applied for this new numerical model to restrict movement at the three bolt-head surfaces in the Y-direction, and at the three cylindrical bolt-bolthole interfaces in the X and the Z-directions, as shown in Fig. 5.3c. This section shows the major analysis results of the H13 steel bolted-anchor or anchor #1 (Fig. 5.17, 5.18, 5.19). The analysis was conducted under a 3 mm pre-setting and 2,800 MPa tension load. The contact pressure distribution on the CFRP plate in this anchor is shown in Fig. 5.17a. The contact pressure was distributed over the entire CFRP plate inside the anchor. The maximum contact pressure on CFRP plate was 369 MPa (Fig. 5.17a) located at the pre-setting end of the CFRP plate. Figure 5.17b shows the uniformly distributed longitudinal stress (S11) distribution on the CFRP plate. There was no slip of the CFRP plate with respect to the sleeve and the wedge. The maximum elongation in the CFRP plate was 0.84 mm (Fig. 5.17c). The maximum von Mises stress in the barrel was at the bolt-nut interface at the pre-setting end of the anchor (Fig. 5.18a). Since the bolt-hole surface at the pre-setting end was in contact with bolt, the maximum stress was located there. The maximum von Mises stress in the wedge was 658 MPa (Fig. 5.18b), which was within the yield strength of the heat-treated H13 steel (Table 5.1).

The failure criteria of the CFRP plate inside the bolted anchor #1 under 3 mm pre-setting and 2,800 MPa tension load using the ‘Maximum Stress Theory’ and the ‘Tsai-Hill Theory’ over the length of the CFRP plate are shown in Fig. 5.19 and Table 5.12. Both the maximum mean contact pressure (297 MPa) and the maximum mean longitudinal stress (2,800 MPa) were within the limit, satisfying the ‘Maximum Stress Theory’. The failure criteria also did not exceed 1.0 satisfying the ‘Tsai-Hill Theory’, as well. Therefore, there was no failure in the CFRP plate inside the anchor #1 under 2,800 MPa tensile loading (Table 5.12).

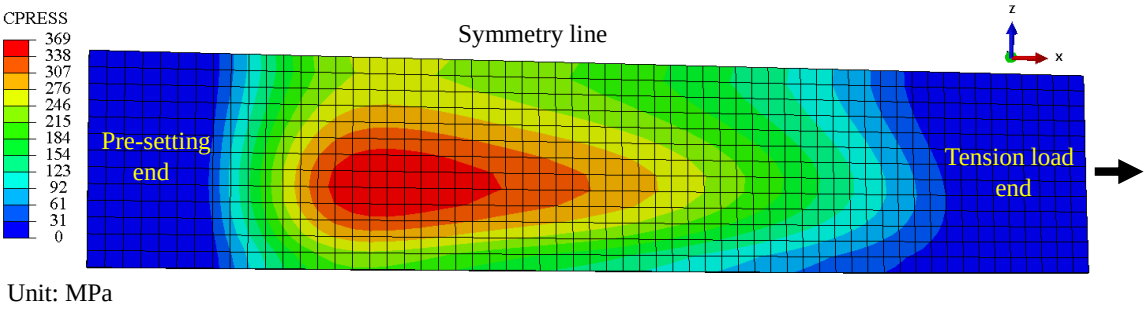

(a)

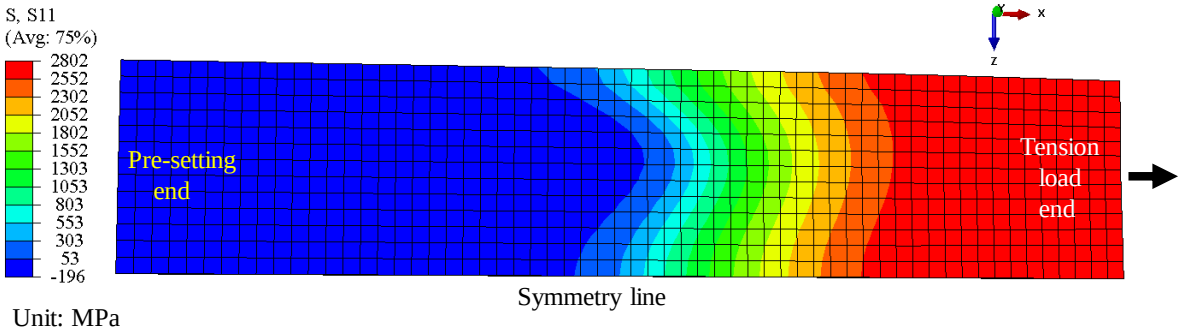

(b)

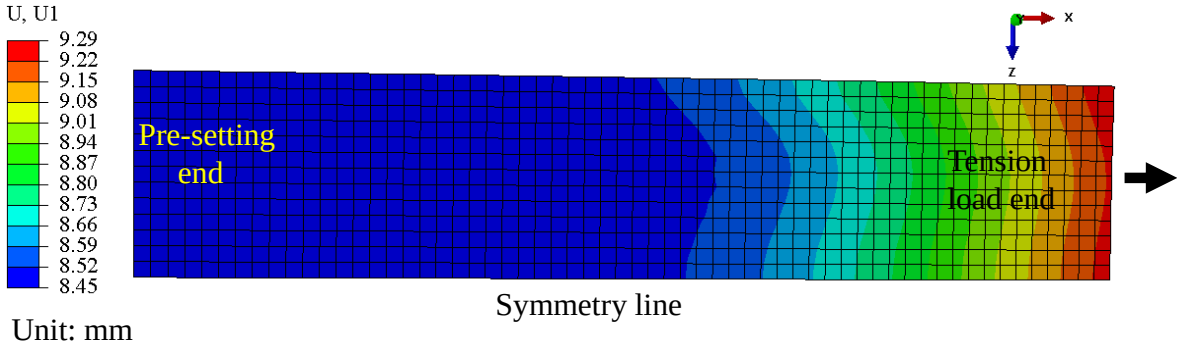

(c)

Figure 5.17: (a) The contact pressure distribution, (b) the longitudinal stress (S11) distribution and (c) the displacement distribution on the CFRP plate inside the anchor #1 (bolted H13 steel anchor) with bolts under 3 mm pre-setting and 2,800 MPa tension load.

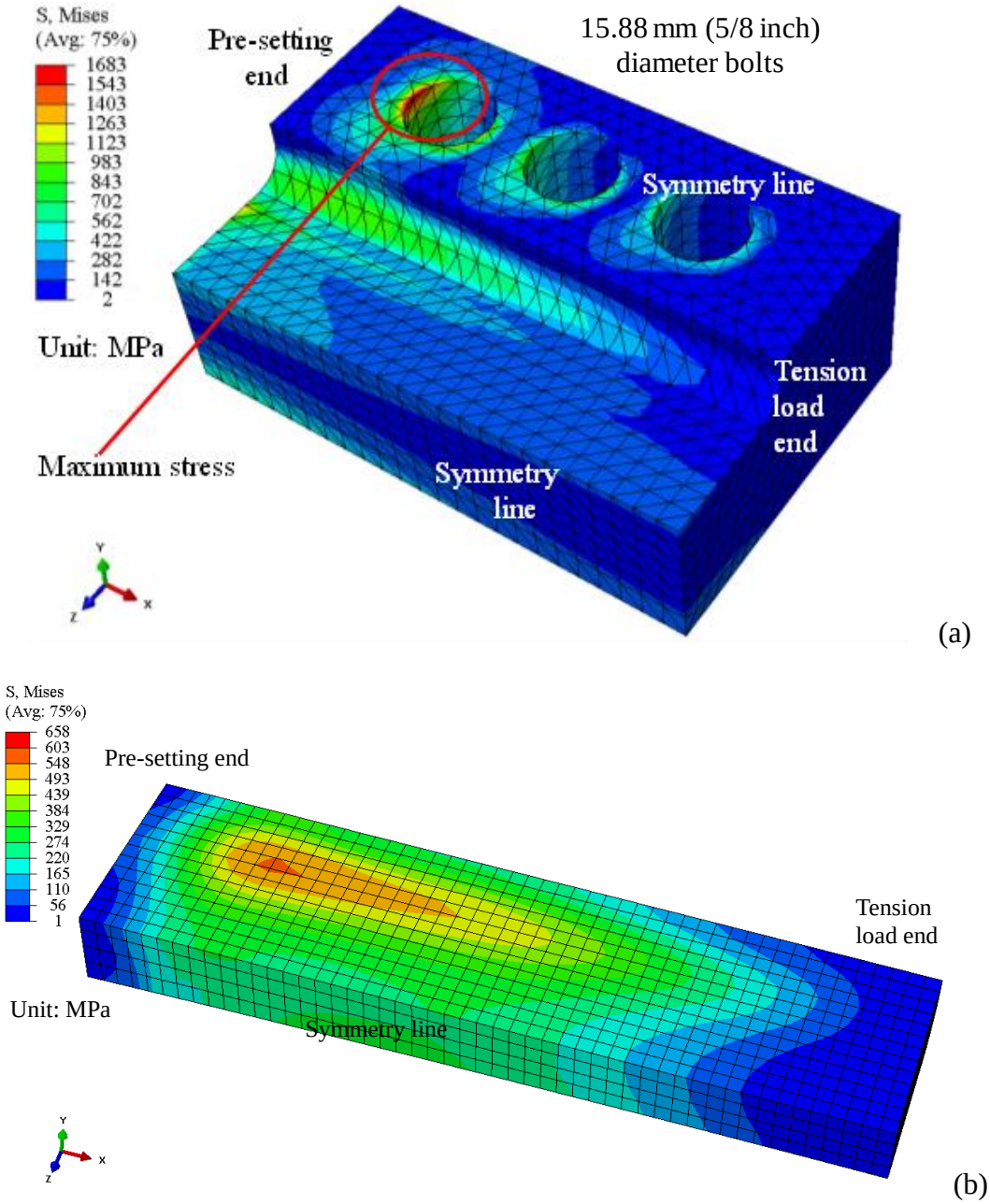

Figure 5.18: Von Mises stress distribution in (a) the barrel (one-quarter of the barrel) and (b) the wedge (half of the wedge) for the anchor #1 (bolted H13 steel anchor) with bolts under 3 mm pre-setting and 2,800 MPa tension load.

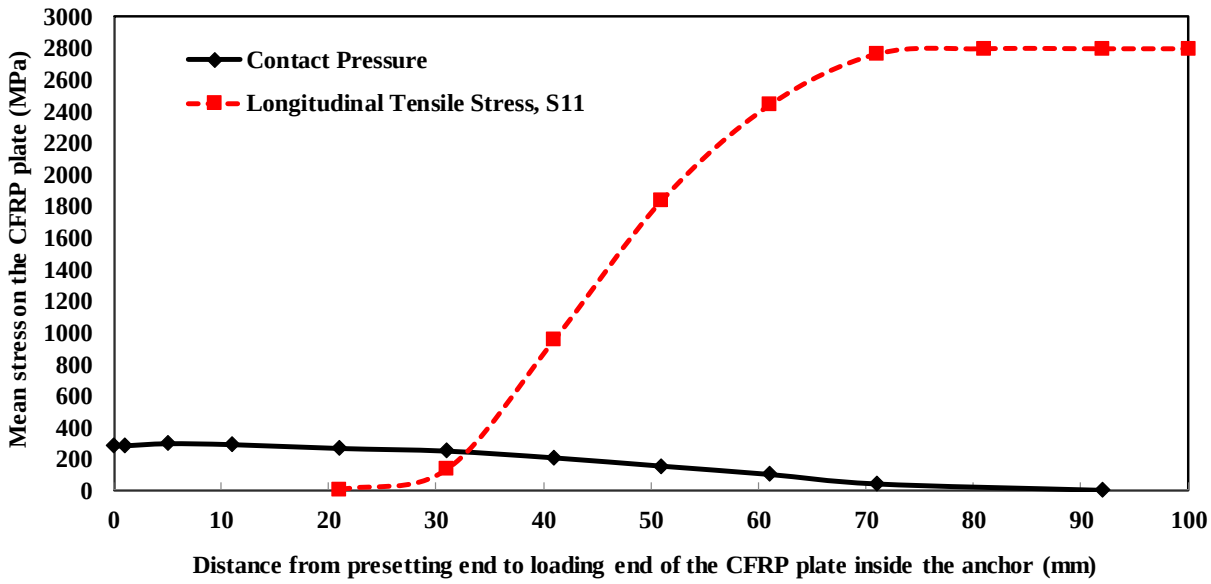

Figure 5.19: The mean contact pressure and the longitudinal stress distribution in the CFRP plate inside the anchor #1.

Table 5.12: Assessment of the failure criteria of the CFRP plate in bolted anchor #1 under 3 mm pre-setting and 2,800 MPa tension load using the Maximum Stress Theory and the Tsai-Hill Theory

Distance in anchor, X (mm)	Mean contact pressure on CFRP plate (MPa)	Mean long. tensile stress in CFRP plate (MPa)	Checking failure of CFRP plate using 'Maximum Stress Theory'	Checking failure of CFRP plate using 'Tsai-Hill Theory'
1	283	N/A	$\sigma_L < \sigma_{Lu}$, $\sigma_T < \sigma_{Tu}$, OK	0.270 <=1, OK
5	297	N/A	$\sigma_L < \sigma_{Lu}$, $\sigma_T < \sigma_{Tu}$, OK	0.295 <=1, OK
11	291	N/A	$\sigma_L < \sigma_{Lu}$, $\sigma_T < \sigma_{Tu}$, OK	0.283 <=1, OK
21	266	0	$\sigma_L < \sigma_{Lu}$, $\sigma_T < \sigma_{Tu}$, OK	0.238 <=1, OK
31	249	132	$\sigma_L < \sigma_{Lu}$, $\sigma_T < \sigma_{Tu}$, OK	0.207 <=1, OK
41	206	954	$\sigma_L < \sigma_{Lu}$, $\sigma_T < \sigma_{Tu}$, OK	0.234 <=1, OK
51	154	1,838	$\sigma_L < \sigma_{Lu}$, $\sigma_T < \sigma_{Tu}$, OK	0.474 <=1, OK
61	101	2,441	$\sigma_L < \sigma_{Lu}$, $\sigma_T < \sigma_{Tu}$, OK	0.763 <=1, OK
71	41	2,766	$\sigma_L < \sigma_{Lu}$, $\sigma_T < \sigma_{Tu}$, OK	0.967 <=1, OK
92	0	2,800	$\sigma_L < \sigma_{Lu}$, $\sigma_T < \sigma_{Tu}$, OK	1.000 <=1, OK
100	0	2,800	$\sigma_L < \sigma_{Lu}$, $\sigma_T < \sigma_{Tu}$, OK	1.000 <=1, OK

5.7 RESULTS OF THE ANCHOR #2 (STAINLESS STEEL ANCHOR)

After the results of the first set of tension tests showed that the tested CFRP plate anchor achieved the ultimate tensile strength of the CFRP plate, an optimized anchor design with a less mass was considered. A corrosion resistant anchor made of heat-treated stainless steel having a reduced barrel thickness was modelled. The yield strength of the heat-treated 440C stainless steel (1,896 MPa) is also higher than that of the heat-treated H13 steel (1,366 MPa). Therefore, the minimum thickness of the barrel at the pre-setting end of the new anchor was reduced by 5 mm to 20.93 mm. It also reduced the anchor mass by approximately 1 kg. The material properties of heat-treated stainless steel, as shown in Table 5.1, were used while modelling the barrel and the wedge in the new numerical model.

The major results obtained from the analysis of the heat-treated stainless steel anchor under a 3 mm pre-setting and 2,800 MPa tension load are shown in Fig. 5.20, 5.21 and 5.22. The maximum contact pressure on CFRP plate was found as 374 MPa at the pre-setting end (Fig. 5.20a). The contact pressure was distributed all over the CFRP plate that was inside the anchor. Both the longitudinal stress (S11) and the displacement were uniformly distributed on the CFRP plate (Fig. 5.20b, 5.20c). There was no slip of the CFRP plate from the anchor under loading. The maximum elongation in the CFRP plate was 0.82 mm (Fig. 5.20c). The maximum von Mises stress in the barrel was 1,858 MPa at the bolt-nut interface at the pre-setting end bolt-hole (Fig. 5.21). This was less than the yield strength of heat-treated stainless steel (1,896 MPa). The maximum von Mises stress in the wedge (742 MPa) was also less than the yield strength of heat-treated stainless steel. The wedge slid 6.49 mm in order to set itself inside the anchor under 3 mm pre-setting and 2,800 MPa tension load.

The failure criteria of the CFRP plate inside this anchor #2 under 3 mm pre-setting and 2,800 MPa tension load using the ‘Maximum Stress Theory’ and the ‘Tsai-Hill Theory’ over the length of the CFRP plate are shown in Fig. 5.22 and Table 5.13; and they show that there was no failure in the CFRP plate in the anchor #2 under loading.

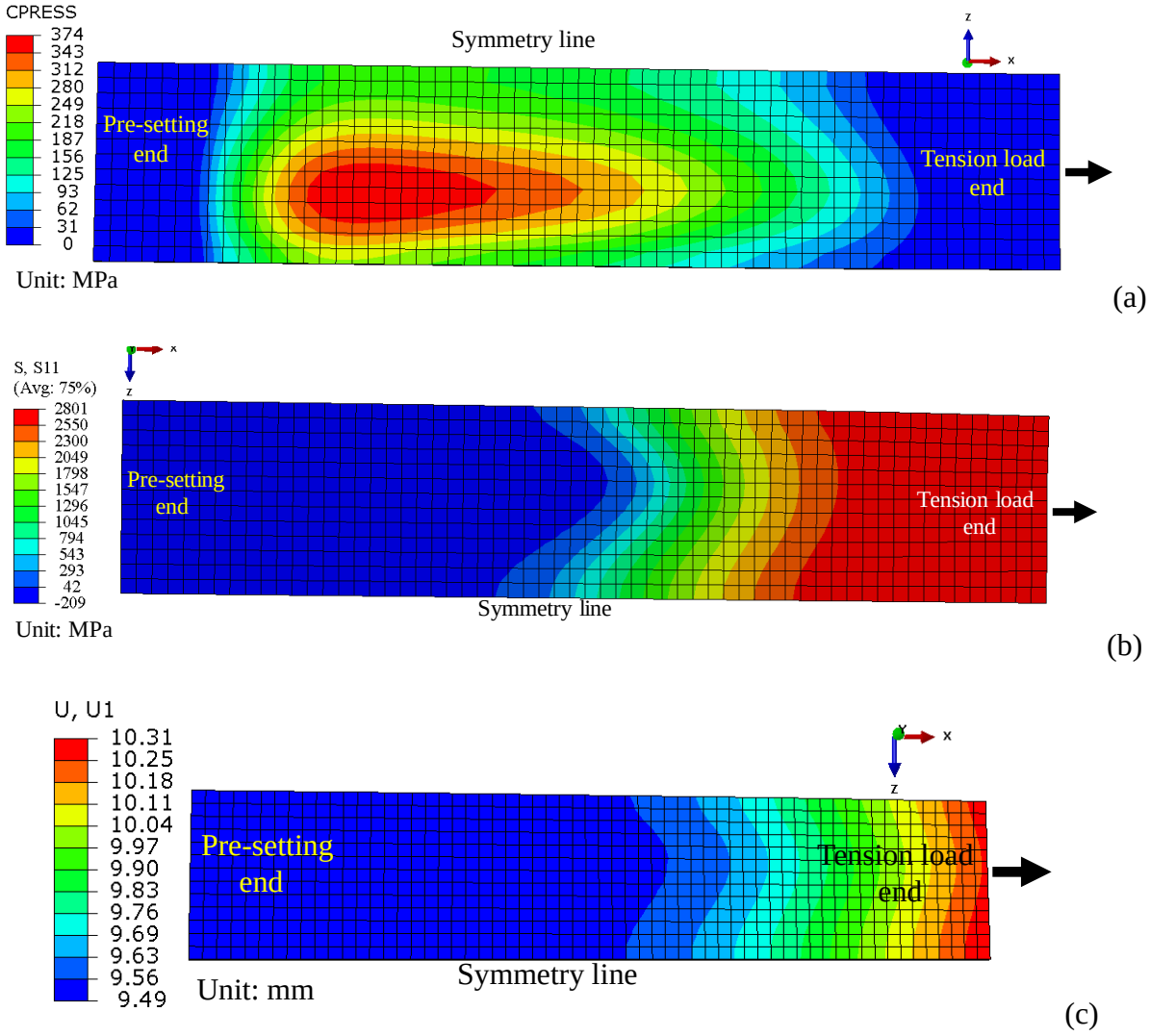

Figure 5.20: (a) The contact pressure distribution, (b) the longitudinal stress (S11) distribution and (c) the displacement distribution on the CFRP plate inside the anchor #2 (stainless steel anchor) with bolts under 3 mm pre-setting and 2,800 MPa tension loading.

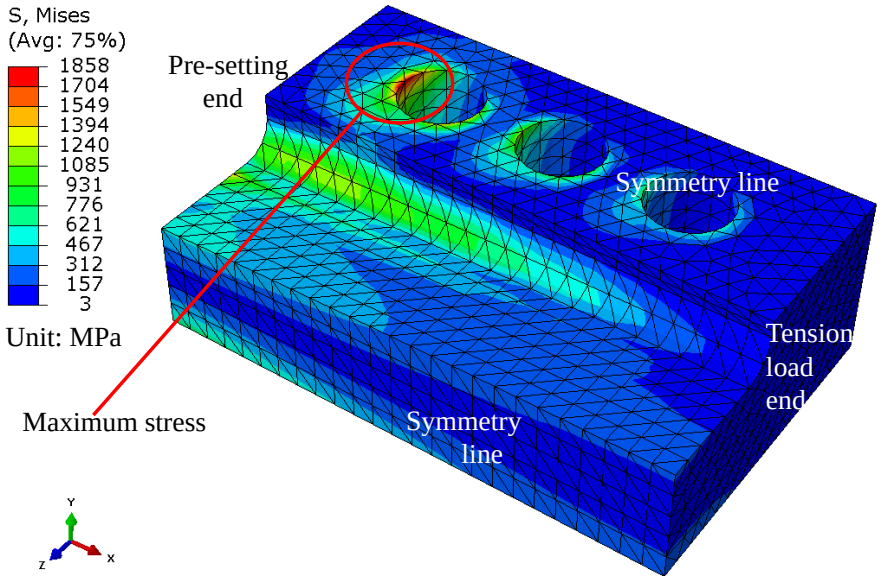

Figure 5.21: Von Mises stress distribution on the barrel (one-quarter of the barrel) for the bolted anchor#2 (stainless steel anchor) under 3 mm pre-setting and 2,800 MPa tension load.

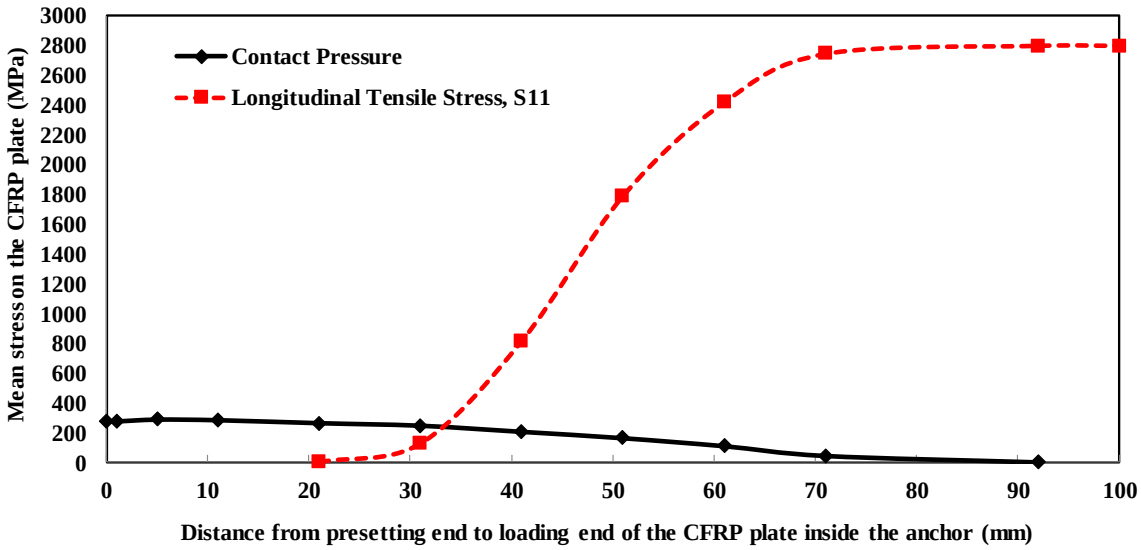

Figure 5.22: The mean contact pressure and the longitudinal stress distribution in the CFRP plate in the anchor #2.

Table 5.13: Checking the failure criteria of the CFRP plate in bolted anchor #2 under 3 mm pre-setting and 2,800 MPa tension load using the Maximum Stress Theory and the Tsai-Hill Theory.

Distance in anchor, X (mm)	Mean contact pressure on CFRP plate (MPa)	Mean long. tensile stress in CFRP plate (MPa)	Checking failure of CFRP plate using 'Maximum Stress Theory'	Checking failure of CFRP plate using 'Tsai-Hill Theory'
1	275	N/A	$\sigma_L < \sigma_{Lu}$, $\sigma_T < \sigma_{Tu}$, OK	0.255 <=1, OK
5	287	N/A	$\sigma_L < \sigma_{Lu}$, $\sigma_T < \sigma_{Tu}$, OK	0.277 <=1, OK
11	283	N/A	$\sigma_L < \sigma_{Lu}$, $\sigma_T < \sigma_{Tu}$, OK	0.269 <=1, OK
21	263	0	$\sigma_L < \sigma_{Lu}$, $\sigma_T < \sigma_{Tu}$, OK	0.233 <=1, OK
31	246	127	$\sigma_L < \sigma_{Lu}$, $\sigma_T < \sigma_{Tu}$, OK	0.202 <=1, OK
41	205	817	$\sigma_L < \sigma_{Lu}$, $\sigma_T < \sigma_{Tu}$, OK	0.205 <=1, OK
51	162	1,791	$\sigma_L < \sigma_{Lu}$, $\sigma_T < \sigma_{Tu}$, OK	0.460 <=1, OK
61	109	2,420	$\sigma_L < \sigma_{Lu}$, $\sigma_T < \sigma_{Tu}$, OK	0.753 <=1, OK
71	43	2,746	$\sigma_L < \sigma_{Lu}$, $\sigma_T < \sigma_{Tu}$, OK	0.953 <=1, OK
92	0	2,800	$\sigma_L < \sigma_{Lu}$, $\sigma_T < \sigma_{Tu}$, OK	1.000 <=1, OK
100	0	2,800	$\sigma_L < \sigma_{Lu}$, $\sigma_T < \sigma_{Tu}$, OK	1.000 <=1, OK

5.8 RESULTS OF THE ANCHOR #3 FOR 1.4 MM CFRP PLATE

In this research, the anchors were primarily developed for the 1.2 mm thick CFRP plates having an ultimate tensile strength of 2,800 MPa and a modulus of elasticity of 165,000 MPa. At this stage, the anchor was investigated numerically to examine its capacity to prestress the commercially available 50 mm × 1.4 mm high-modulus (210,000 MPa) CFRP plates. The ultimate tensile strength of this plate was 2,900 MPa. Therefore, the analysis was carried out at 3 mm pre-setting and 2,900 MPa tension load. The anchor #1 was modified in order to prestress the 1.4 mm thick CFRP plates. In the updated numerical model, a 0.7 mm thick annealed copper sleeve (similar to 22-gauge copper sheet) was used instead of 0.8 mm thick sleeve. The analysis results of this anchor #3 showed that the maximum contact pressure in the CFRP plate was 428 MPa (less than 546 MPa), and the contact pressure was distributed over the entire CFRP plate with no significant stress concentration. For self-seating purpose, the wedge slid 10.33 mm with respect to the barrel. The self-seating distance of the wedge in this anchor was larger than that of anchor #1 and #2. This was due to the higher tensile stress (2,900 MPa) applied on the CFRP plate in the numerical model of this anchor #3. The reason for the application of this higher tensile load was the higher ultimate tensile strength of the 1.4 mm thick CFRP plate (2,900 MPa). There was no sliding of the CFRP plate with respect to the sleeve and the wedge. The elongation of the CFRP plate was 0.82 mm. The maximum von Mises stresses were 1,895 MPa and 833 MPa in the barrel and the wedge, respectively. The failure criteria of the CFRP plate under a 3 mm pre-setting and 2,900 MPa tension load using the ‘Maximum Stress Theory’ and the ‘Tsai-Hill Theory’ over the length of the CFRP plate are shown in Table 5.14 and Fig. 5.23; and they show that there was no failure anywhere in the CFRP plate inside this anchor #3 under loading.

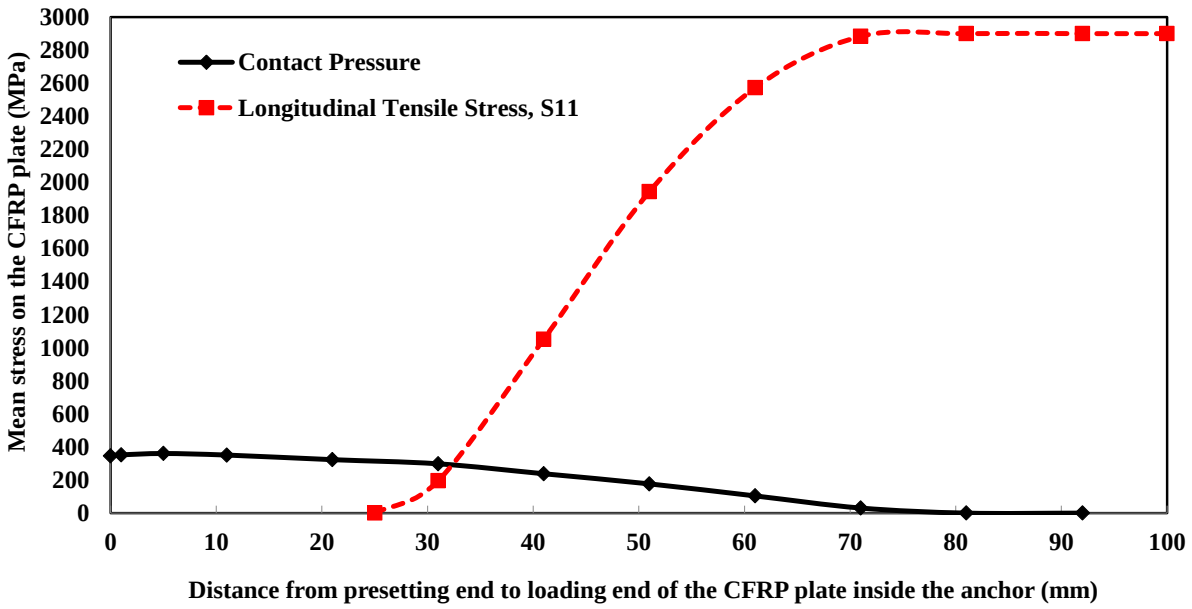

Figure 5.23: The mean contact pressure and longitudinal pressure distribution in the CFRP plate for anchor #3.

Table 5.14: Assessment of the failure criteria of the CFRP plate in bolted anchor #3 under 3 mm pre-setting and 2,900 MPa tension load using the Maximum Stress Theory and the Tsai-Hill Theory

Distance in anchor, X (mm)	Mean contact pressure on CFRP plate (MPa)	Mean long. tensile stress in CFRP plate (MPa)	Checking failure of CFRP plate using 'Maximum Stress Theory'	Checking failure of CFRP plate using 'Tsai-Hill Theory'
0	346	N/A	$\sigma_L < \sigma_{Lu}$, $\sigma_T < \sigma_{Tu}$, OK	0.401 <=1, OK
1	352	N/A	$\sigma_L < \sigma_{Lu}$, $\sigma_T < \sigma_{Tu}$, OK	0.416 <=1, OK
5	360	N/A	$\sigma_L < \sigma_{Lu}$, $\sigma_T < \sigma_{Tu}$, OK	0.436 <=1, OK
11	351	N/A	$\sigma_L < \sigma_{Lu}$, $\sigma_T < \sigma_{Tu}$, OK	0.413 <=1, OK
21	323	0	$\sigma_L < \sigma_{Lu}$, $\sigma_T < \sigma_{Tu}$, OK	0.350 <=1, OK
31	298	195	$\sigma_L < \sigma_{Lu}$, $\sigma_T < \sigma_{Tu}$, OK	0.296 <=1, OK
41	238	1052	$\sigma_L < \sigma_{Lu}$, $\sigma_T < \sigma_{Tu}$, OK	0.292 <=1, OK
51	177	1944	$\sigma_L < \sigma_{Lu}$, $\sigma_T < \sigma_{Tu}$, OK	0.513 <=1, OK
61	104	2572	$\sigma_L < \sigma_{Lu}$, $\sigma_T < \sigma_{Tu}$, OK	0.791 <=1, OK
71	31	2883	$\sigma_L < \sigma_{Lu}$, $\sigma_T < \sigma_{Tu}$, OK	0.981 <=1, OK
81	0	2900	$\sigma_L < \sigma_{Lu}$, $\sigma_T < \sigma_{Tu}$, OK	1.000 <=1, OK
92	0	2,900	$\sigma_L < \sigma_{Lu}$, $\sigma_T < \sigma_{Tu}$, OK	1.000 <=1, OK
100	0	2,900	$\sigma_L < \sigma_{Lu}$, $\sigma_T < \sigma_{Tu}$, OK	1.000 <=1, OK

5.9 A COMPARATIVE DISCUSSION FOR DIFFERENT ANCHOR MODELS

5.9.1 Longitudinal Stress-Displacement Relationship and Effect of Bolted Anchor

The longitudinal stress-displacement behaviour of the CFRP plate anchor was investigated for both solid and bolted anchors. In both cases, an anchor with a longitudinal curve radius of 3,000 mm, an interference distance of 0.05 mm, a length of 100 mm, a minimum barrel thickness of 25.93 mm at the pre-setting end, and a minimum wedge thickness of 8.05 mm at the loading end was used. A coefficient of friction of 0.07 was used at the barrel-wedge interface for this study [149]. At the beginning of the analysis, a 3 mm pre-setting was applied to the wedge of the anchor. This was followed by applying 1 mm tension displacement on the CFRP plate in each step. Afterwards, the longitudinal stress (S11) in the CFRP plate in each step was listed. Subsequently, the longitudinal stress-displacement curves for the solid anchor and the bolted anchor #1 were compared (Fig. 5.24). From the previous failure criteria investigations given by Tables 5.3, 5.12, 5.13 and 5.14, both the solid and the three bolted anchors carried 2,800 MPa longitudinal tensile stress (S11) without any premature failure.

From Fig. 5.24, initially, the longitudinal stress values for both anchors increased rapidly. Subsequently, the slopes changed exhibiting a larger total displacement of the wedge, sleeve and CFRP plate (self-seating distance). Furthermore, for the same stress values, there was slightly more total displacement (self-seating distance of the wedge) in the bolted anchor than that of the solid anchor (Fig. 5.24).

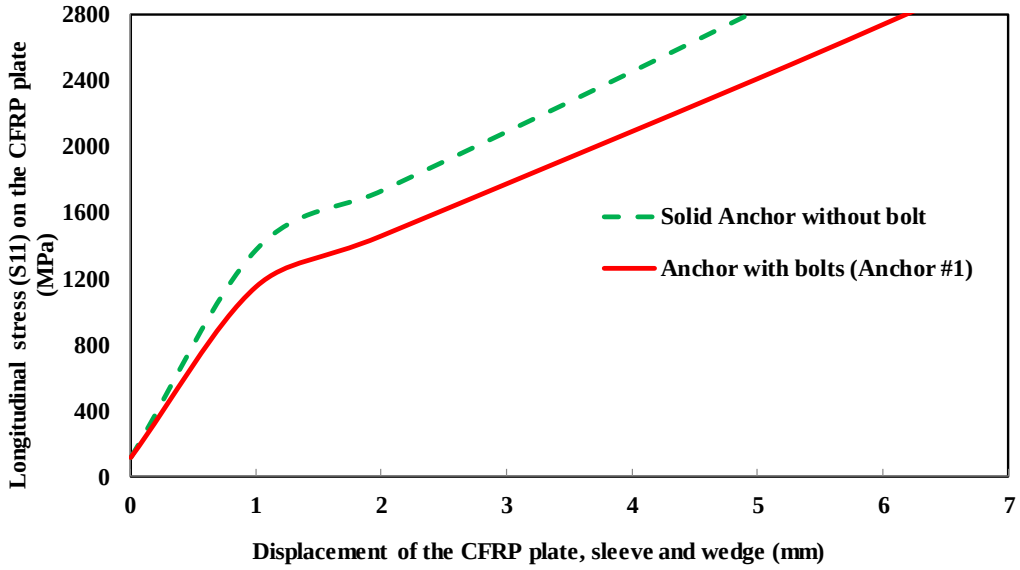

Figure 5.24: The longitudinal stress (S11) on CFRP plate vs. displacement curve for the CFRP plate anchor for 3 mm pre-setting distance for an anchor with longitudinal curve radius of 3,000 mm, an interference distance of 0.05 mm, a minimum barrel-thickness of 25.93 mm and a coefficient of friction of 0.07 between the barrel and the wedge.

Because of manufacturing ease, a two-part barrel instead of an one-part solid barrel was required to be made. Subsequently, the two parts of the barrel were connected using six bolts. The performance of the solid anchor was compared with the performance of the bolted anchor with two-part barrel (Table 5.15). The CFRP plate in the bolted anchor had a slightly lower contact pressure (Table 5.15) and a slightly larger total displacement of the wedge than that of the solid anchor. The larger displacement was due to a larger self-seating distance of the wedge in the bolted anchor, as shown in Fig. 5.24. The maximum von Mises stress in the wedge of the bolted anchor was less than that of the solid anchor. This was due to the less confinement provided by the bolts in the bolted anchor, compared to the one-piece-barrel solid anchor. The maximum von Mises stress in the barrel of the bolted anchor was larger than that of the solid anchor. This was due to the localized stress concentration at the bolt-nut interface at the pre-setting end bolt in the bolted anchor.

Table 5.15: Effect of using bolts for an anchor with 3,000 mm longitudinal curve radius, 0.05 mm interference distance, 25.93 mm minimum thickness barrel, 8.05 mm minimum thickness wedge and 100 mm length under 3 mm pre-setting and 2,800 MPa tension load.

Anchor type	CFRP plate max. contact pressure (MPa)
Solid (no bolt)	393
Bolted (6 bolts)	369

5.9.2 Effect of the type of the CFRP Plate on the Anchor Performance

The effect of different CFRP plates on the anchor performance was investigated (Table 5.16). Two CFRP plates were used for this comparative analysis. The first CFRP plate had a thickness of 1.2 mm, an ultimate tensile strength of 2,800 MPa and a modulus of elasticity of 165,000 MPa. The second CFRP plate was a high modulus plate having a thickness of 1.4 mm, an ultimate tensile strength of 2,900 MPa and a modulus of elasticity of 210,000 MPa. For this comparative analysis, a CFRP plate anchor of 3,000 mm longitudinal radius, 3 mm pre-setting distance, 8.05 mm thick wedge, 0.05 mm interference distance and 25.93 mm thick barrel was used. For the thinner plate, two annealed copper sleeve plates of 0.8 mm thickness were used. On the contrary, for the thicker CFRP plate (1.4 mm thick), two annealed copper sleeve plates of 0.7 mm thickness were used in order to accommodate the additional thickness of the CFRP plate inside the anchor. The anchor for the 1.4 mm thick CFRP plate had a slightly higher contact pressure (Table 5.16) and a slightly higher total displacement (due to the slippage of wedge inside the anchor in order to self-seat) than that of the anchor for the 1.2 mm thick CFRP plate. The von Mises stress in the barrel of the anchor for 1.4 mm CFRP plate was higher than that of the anchor for 1.2 mm CFRP plate. This was due to the higher ultimate tensile strength of the 1.4 mm CFRP plate. The failure criteria of the CFRP plate were satisfied for both of the anchors; and the CFRP plates did not fail in either of the anchors in the FEM model.

Table 5.16: Effect of using different types of CFRP plate in the anchor

CFRP plate type	Sleeve thickness (mm)	CFRP plate max. contact pressure (MPa)
1.2 mm thick CFRP plate with E = 165,000 MPa	0.8	369
1.4 mm thick CFRP plate with E = 210,000 MPa	0.7	428

5.9.3 Comparison among the Tested Anchors in the Numerical Analysis

Table 5.17 shows the comparative anchor properties of the three anchors, obtained from this numerical analysis, that were tested for the tension tests afterwards. In all of these anchors, the failure criteria of the CFRP plate were satisfied; and the CFRP plate did not fail in any of these anchors in the FEM numerical model.

Table 5.17: Comparison among the three bolted anchors

Anchor	Material	Min. barrel thickness (mm)	CFRP plate max. contact pressure (MPa)
Anchor #1	Heat-treated H13 steel	25.93	369
Anchor #2	Heat-treated stainless steel	20.93	374
Anchor #3 for 1.4 mm CFRP plate	Heat-treated H13 steel	25.93	428

5.10 SUMMARY

Based on the parametric analysis and the optimization study results and considering the manufacturability, the CFRP plate anchor made of heat-treated H13 steel with bolts with a longitudinal curve radius of 3,000 mm, a minimum barrel thickness of 25.93 mm, a barrel side wall thickness of 35 mm, a minimum wedge thickness of 8.05 mm, and a transverse curve radius of 6 mm for both barrel and wedge was selected as the final design for experimental testing. In addition, a second bolted anchor, made of heat-treated stainless steel, with a minimum barrel thickness of 20.93 mm, a longitudinal curve radius of 3,000 mm, a transverse curve radius of 6 mm, a barrel sidewall thickness of 35 mm, and a minimum wedge thickness of 8.05 mm was also selected for experimental testing, as the corrosion-resistant option.

CHAPTER 6
ANALYTICAL MODELLING

6.1 INTRODUCTION

In order to estimate the capacity of a friction-based CFRP plate anchor, the proper understanding of the shear stress generated inside the anchor is necessary. The shear stress is a function of the coefficient of friction and the contact pressure [151]. It is very difficult to measure the contact pressure between different component surfaces inside the CFRP plate anchor experimentally without damaging the anchor. In addition, a high contact pressure concentration can cause a premature failure of the CFRP plate inside the anchor under loading. Therefore, an analytical model was required to investigate the contact pressure distribution on the CFRP plate surface inside the anchor; and also to predict a preliminary starting thickness of the barrel of the anchor before performing a detailed, time-consuming and expensive numerical modelling and experimental investigation of the newly designed anchor.

The contact pressure distribution on the CFRP plate surface depends on the geometry and the material properties (*i.e.,* modulus of elasticity and Poisson's ratio) of different components of the anchor, in addition to the loading (*i.e.,* uniformly distributed load) and the boundary conditions. The concept of the Beam on Elastic Foundation, along with Hooke's law, Theory of Elasticity and Winkler Spring Model, was used to develop this mathematical model. This chapter illustrates the development of the mathematics-based analytical model. The results are presented and compared with the finite element modelling (FEM) outcomes.

6.2 MODEL DESCRIPTION

The new CFRP plate anchor has four components: a steel outer barrel with a hollow rectangular cross-section, two steel wedges, two annealed copper sleeves and the CFRP plate in the middle of the two sleeves (Fig. 6.1). The inner surface of the barrel and the outer surface of the wedges

have a longitudinal circular profile of 3,000 mm radius along their length. Since the objective was to protect the CFRP plate inside the anchor under loading, the analytical model in this chapter focused on the contact pressure between the CFRP plate and the sleeve plate.

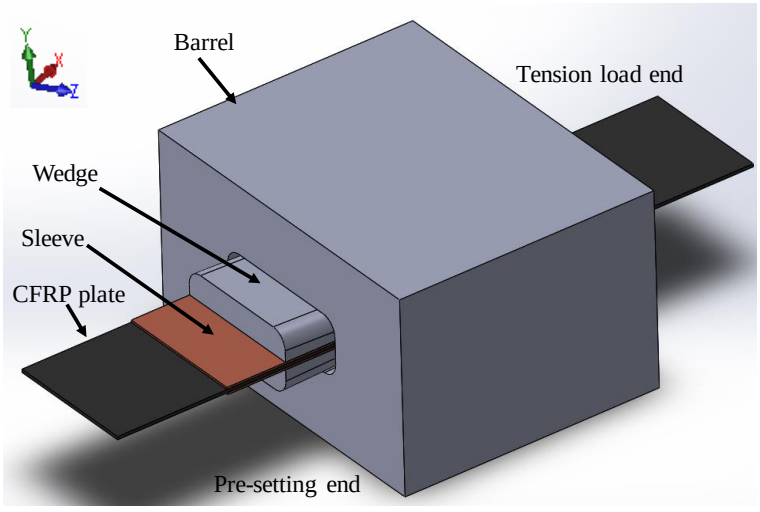

(a)

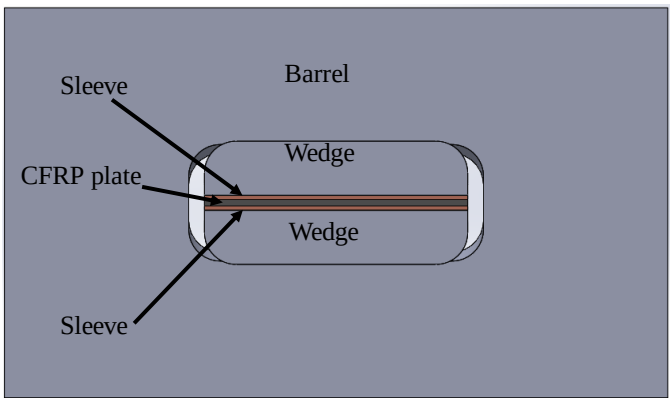

(b)

Figure 6.1: Different components of the anchor: outer steel barrel, two steel wedges, two annealed copper sleeves (each 0.8 mm thick) and the CFRP plate (1.2 mm thick) in the middle in (a) the 3-D view and (b) the cross-section.

Figure 6.2 shows the schematic diagram of the deflected shape of the anchor outer barrel. The solid lines show the deflected shape and the dotted lines show the original barrel shape. P is the pressure acting on the barrel and the Δ is the deflection of the barrel. The inner components

of the anchor (two wedges, two annealed copper sleeves and the CFRP plate, combined) have a thicker dimension than the barrel opening. When the larger size inner components are pushed inside the smaller barrel opening, it creates pressure (P) on the barrel components and that causes the deflection (Δ). In this process, it was assumed that the four right angle corners of the barrel would remain right angles (90^o angle) after deformation. In addition, the deflections are caused primarily by the bending of the members; and slightly by the deformation of the barrel sidewalls (Δ_v). Details of the model are described in Sections 6.2.1 - 6.2.7. The full program file of the analytical model is given in Appendix A.

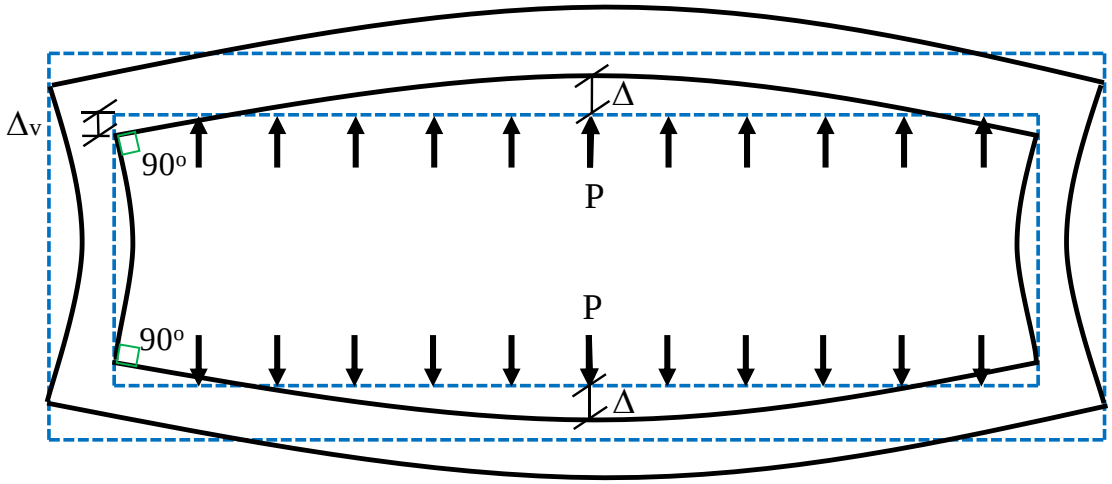

Figure 6.2: Schematic deflection diagram of the anchor barrel under loading (hollow rectangular cross-section barrel under contact pressure from larger size inner components: two wedges, two sleeves and a CFRP plate). The dotted lines are the shape before deflection.

6.2.1 Model Assumptions

The Hooke's law for plane stress and the Theory of Elasticity were used to develop this theoretical analytical model. According to Schepis [152], because of symmetry, the centers of the interfaces do not move parallel to the interface. So it can be assumed that all strains parallel to the interfaces are zero (*i.e.*, $\varepsilon_x = 0$ at the top and bottom wall of the barrel). There are three other basic assumptions in this analytical model:

1. The right angles formed by any two sides of the barrel remain right angles.
2. Bending causes a majority portion of the stresses in the barrel.
3. Elastic deformation occurs in the vertical sidewalls of the barrel.

All of the components of the anchor were considered as beams. All of the contact pressures transferred from one component to another were considered as uniformly distributed pressures. The CFRP plate (half thickness), the sleeve (full thickness) and the wedge (full thickness) were considered as beams with uniformly distributed load supported on an elastic foundation. The top and bottom walls of the barrel were considered as beams with uniformly distributed load supported by fixed supports at the two ends (two corners of the barrel). Elastic deformation (Δ_v) occurs in the vertical sidewalls of the barrel as well. The deflections in the other members (wedges, sleeves and half of the CFRP plate) are caused by bending of the beam.

When pressure is applied on the top and bottom beam of the barrel by the inner components, the four corners of the barrel move (Fig. 6.2). The top beam of the barrel tends to bend upward and the bottom beam of the barrel bends downward. The angle between all beams stays at a 90^o angle even after the deflection, following the assumptions given by Schepis [152]. In addition, the top and bottom beams of the barrel have the contact pressures only due to bending of the members.

6.2.2 Bending of a Beam by Uniform Load

According to Timoshenko and Goodier [153], the deflection of a beam (Δ) with narrow rectangular cross-section and supported at the two ends, due to the bending of the beam under an uniform load, as shown in Fig. 6.3, is given by:

$$\Delta = \frac{5}{24}\frac{P.\left(\frac{L}{2}\right)^4}{E.I}\left[1 + \frac{12}{5}\frac{c^2}{\left(\frac{L}{2}\right)^2}\left(\frac{4}{5} + \frac{\upsilon}{2}\right)\right] \tag{6.1}$$

where, P is the uniformly distributed pressure on the beam (barrel), L is length of the beam (barrel) under loading, I is the moment of inertia of the beam, c is the half-depth of the beam cross-section, E is the modulus of elasticity, and υ is the Poisson's ratio of the material.

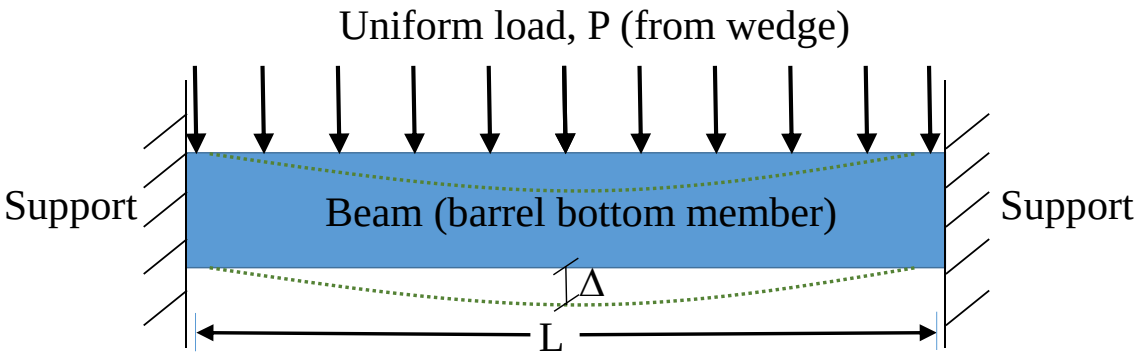

Figure 6.3: Uniform load on beam supported at two ends. The dotted line shows the deformed shape.

6.2.3 Bending of an Uniformly Loaded Beam on Elastic Foundation

The deflection of a beam (Δ) resting on a solid elastic foundation under an uniformly distributed load (P), as shown in Fig. 6.4, was given by Chyu [154]:

$$\Delta = P.\frac{2 - [exp(-b.n).cos(b.n)] - [exp(-b.m).cos(b.m)]}{2.k} \tag{6.2}$$

where, m and n are the beginning and end locations of the load along the length of the beam. For the maximum deflection in the beam resting on an elastic foundation,

$$m = 0;\ n = L$$

From Chyu [154], the parameter, b depends on the modulus of subgrade reaction (k) of the foundation material, the modulus of elasticity (E) of the beam material, and the dimensions of the beam:

$$b = \left(\frac{k}{4.E.\left(\frac{Length\ .\ thickness^3}{12}\right)} \right)^{1/4}$$

(6.3)

By replacing m and in the equation (6.2), the deflection can be found as:

$$\Delta = P.\frac{1 - [exp(-b.L).cos(b.L)]}{2.k}$$

(6.4)

Where, P is the uniformly distributed load, and L is the length of the beam (width of the CFRP plate, sleeve and wedge). Here, the deflection of the beam resting on an elastic foundation is a function of length (*L*) and modulus of subgrade reaction (*k*) of the foundation material. The unit of *k* was N/m^3 in SI units. In this equation, the value of *k* for any given material can be calculated through the equations given in sections 6.2.4 (isotropic material) and 6.2.5 (orthotropic material).

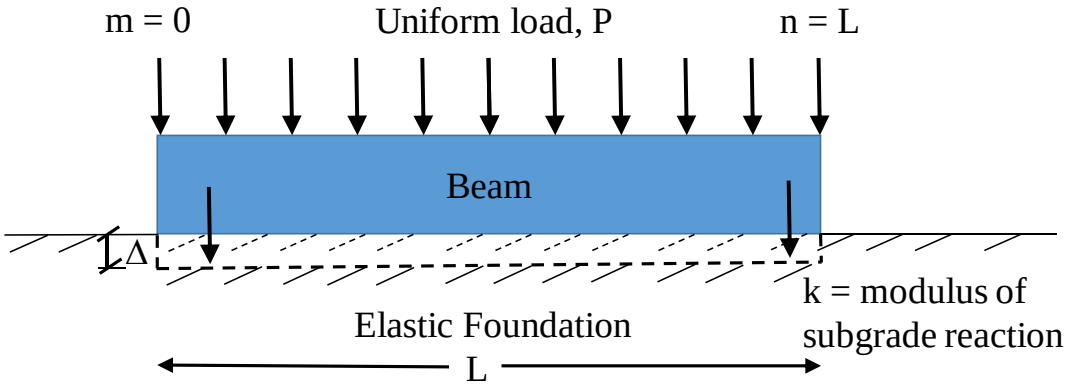

Figure 6.4: Uniform load on beams supported on elastic foundation. The dotted line shows the deformed shape.

6.2.4 Modulus of Subgrade Reaction for Isotropic Sleeve and Wedge

In order to use the equation (6.4) to calculate the deflection, the value of the modulus of subgrade reaction (*k*) for sleeve and wedges needs to be determined (Fig. 6.4). Both sleeve (annealed copper) and wedge (steel) are isotropic materials. An equation to correlate the modulus of subgrade reaction (*k*) with the modulus of elasticity (*E*) and the Poisson's ratio (υ) of a material is a crucial step in this mathematical modelling.

According to Wang [155] and Schepis [152], from Hooke's law and the theory of elasticity, the stress in the y direction (σ_y) for plane stress:

$$\sigma_y = \frac{E}{(1 - \upsilon^2)}(\varepsilon_y + \upsilon\varepsilon_x) \tag{6.5}$$

Where, ε_y and ε_x are the strains in the y and x directions, respectively.

Re-writing the equation (6.5) in terms of strain in the y direction, and considering strain in the x direction, $\varepsilon_x = 0$ (based on the discussion in section 6.2.1),

$$\varepsilon_y = \frac{\sigma_y(1 - \upsilon^2)}{E} \tag{6.6}$$

According to the Winkler Spring Model, since there is no shear transmission between adjacent springs [156], the displacement of a beam resting on an elastic foundation is proportional to the pressure between the plate and the subgrade at the same point, as shown in equation (6.7):

$$k = \frac{P}{\Delta} = \frac{\sigma_y}{\Delta} \tag{6.7}$$

Here, *P* is the resisting pressure of the foundation ($P = \sigma_y$) and Δ is the deflection of the plate [156].

According to Timoshenko and Woinowsky-Krieger [157], if there is friction between the plate and the elastic foundation, which is the case in the anchor, the actual displacement of the subgrade depends on the nature of the subgrade and the length of the plate. This parameter, *k* is not a constant and not a fundamental property of a given material. The value of *k* depends on the modulus of elasticity, the Poisson's ratio and the contact surface area. The value of *k* decreases with the increase of the loaded area [158]. The deflection at a point in the subgrade depends not only on the stress, but it is also influenced by the decreasing stress with the increasing distance from the center of the plate. Considering all of the above and using the Winkler Spring Model, for a square flexible footing resting on an isotropic, homogeneous, linear, elastic and solid material carrying a vertical uniform load, as shown in Fig. 6.4, the modulus of subgrade reaction (*k*) was derived by Lusas [158] as:

$$k = \frac{P}{\Delta} = \frac{E}{0.95\, h\, (1 - \upsilon^2)} \tag{6.8}$$

Here, E is the modulus of elasticity, υ is the Poisson's ratio and h is the length of the equivalent square area under loading. In order to use this equation for rectangular area, the equivalent length of the contact area or loaded area (*h*) was given as [159]:

$$h = \sqrt{Length \times width} \tag{6.9}$$

6.2.5 Modulus of Subgrade Reaction for Orthotropic CFRP plate

In order to use the equation (6.4) to calculate the deflection of the CFRP plate, the value of the modulus of subgrade reaction (*k*) for the CFRP plate is required (Fig. 6.4 and 6.5). CFRP plate is an orthotropic material having a higher strength and modulus of elasticity in the longitudinal direction than that of the other two directions. For any orthotropic material, for the bending of

a beam supported by an elastic foundation, the modulus of subgrade reaction (*k*) depends on the elasticity of the material and the dimensions of the beam [160].

According to Biot [160], for the bending of beams resting on elastic foundation, the basic assumption is that the foundation consists of a large number of small springs; and the deflection of the beam is proportional to the reaction of the elastic foundation. The width of the beam is $2b_1$ (Fig. 6.5). The maximum bending moment location is given by the fundamental length of the beam (a_1), as shown in the equation (6.10). The relationship among the maximum bending moment, the fundamental length (a_1) and the length of the plate (l) was obtained by Biot [160]:

$$M_{max} = 0.353\ Pl = 0.385\ Pa_1 \tag{6.10}$$

According to Biot [160], for a beam with a uniformly distributed load and sitting on an elastic foundation, the modulus of subgrade reaction (*k*) for an orthotropic material is:

$$k = 0.710\ E\ \frac{b_1}{a_1} \tag{6.11}$$

Where, the half-width of the CFRP plate (b_1) was 25 mm, as shown in Fig. 6.5. The fundamental length of the CFRP plate (a_1), as shown in Fig. 6.5, was calculated by Biot [160] for the maximum bending moment location in the beam for the equivalent loading on the elastic foundation from the equation (6.10):

$$a_1 = \frac{Length\ of\ the\ plate}{1.09} \tag{6.12}$$

Here, the length of the plate was considered as the length of the anchor, which was 100 mm.

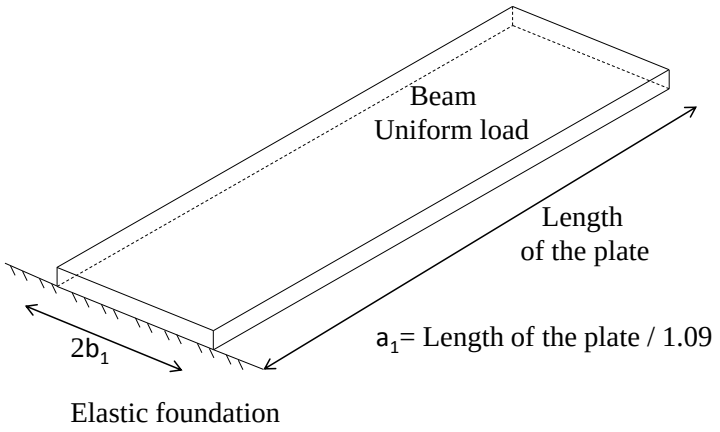

Figure 6.5: Bending of beam with uniform load resting on an elastic foundation.

The value of *k* obtained from equation (6.11) can be put in the equation (6.4) to obtain the deflection of the CFRP plate.

6.2.6 Minimum Required Barrel Wall Thickness

Using Hooke's law and the theory of elasticity, Schepis [152] derived an equation for the minimum required rectangular barrel wall thickness for fitting a rectangular box inside of another hollow rectangular tube to create a pressure seal. For his derivation, Schepis [152] considered that the centers of the interfaces did not move parallel to the interface because of symmetry. So it was assumed that all strains parallel to the interfaces were zero (ε_x=0). There were three major assumptions for his derivation:

1. The four corners of the barrel did not move;
2. The stresses induced in barrel were due to bending only;
3. The right angles formed by any two sides in the barrel remained right angles.

According to Schepis [152], the thickness of the rectangular barrel wall required for a rectangular pressure seal was:

$$t \geq \frac{1}{3.5}\left[\left(\frac{E_{core}}{E_{barrel}}\right)\frac{b_0^4}{a_0 \times (1 - v_{core}^2)}\right]^{\frac{1}{3}} \tag{6.13}$$

where, E_{core} and E_{barrel} represents the modulus of elasticity of the core (wedge, sleeve and CFRP plate) and the barrel, respectively. ν_{core} is the Poisson's ratio of the core (wedge, sleeve and CFRP plate). a_0 and b_0 are the shorter and longer dimension of the barrel opening, respectively.

$$E_{core} = \frac{E_{CFRP}t_{CFRP} + E_{Cu}t_{Cu} + E_{steel}t_{steel}}{t_{total}} \tag{6.14}$$

$$\upsilon_{core} = \frac{\upsilon_{CFRP}t_{CFRP} + \upsilon_{Cu}t_{Cu} + \upsilon_{steel}t_{steel}}{t_{total}} \tag{6.15}$$

Here, E_{core} and υ_{core} are the equivalent modulus of elasticity and the equivalent Poisson's ratio of the core of the anchor, respectively. The core consists of the CFRP plate, the annealed copper sleeve plate and the steel wedge. E_{CFRP}, E_{cu} and E_{steel} are the modulus of elasticity of the CFRP plate, annealed copper and steel, respectively. υ_{CFRP}, υ_{cu} and υ_{steel} are the Poisson's ratio of the CFRP plate, annealed copper and steel, respectively. t_{CFRP}, t_{cu} and t_{steel} are the thickness of the CFRP plate, annealed copper and steel, respectively. It is worth mentioning that the thickness of the wedge varies nonlinearly along the length.

6.2.7 Model Description in whole Anchor

The anchor was divided into ten sections longitudinally to accommodate the varying thickness of the barrel and the wedges. The analytical modelling was performed for each of these ten sections to obtain the contact pressures on the CFRP plate at different sections over the length of the anchor (Fig. 6.6).

Deflection of the steel barrel obtained using the equation (6.1) was as follows:

$$y_{barrel} = f(P_3, L, E_{steel}, v_{steel}, t_{barrel}) - \left(\frac{H_{halfbarrel}}{E_b}\frac{P_3.L_{contact}}{2.t_{barrelwall}}\right) \quad (6.16)$$

During the calculation of the deflection of the barrel, the axial deformation of the two sidewalls was considered and incorporated in the equation (6.16). The axial deformation of the barrel depended on the force acting on the barrel sidewall, the height of the half of the barrel ($H_{halfbarrel}$), the area of the barrel sidewall, and the modulus of elasticity of the barrel material (E_b). The force acting on the barrel sidewall was calculated by multiplying the contact pressure on the inner surface of the barrel (P_3) with the contact area. This contact area was calculated from the contact surface length ($L_{contact}$). The area of the barrel sidewall was calculated from the thickness of the barrel sidewall ($t_{barrelwall}$).

The deflection of the other components of the anchor (CFRP plate, annealed copper sleeve and steel wedge) obtained using the equation (6.4) were as follows:

$$y_{CFRP} = f(P_1, k_{CFRP}, b_{cu}, L)$$

$$y_{Cu-sleeve} = f(P_2, k_{Cu}, b_w, L)$$

$$y_{wedge} = f(P_3, k_{steel}, b_b, L) \quad (6.17)$$

Where, P_1, P_2 and P_3 are the contact pressures at the CFRP-sleeve interface, sleeve-wedge interface and wedge-barrel interface, respectively. In addition, b_{cu}, b_w and b_b are the b-parameter values of the sleeve, wedge and barrel, respectively. E_{steel} is the modulus of elasticity of the barrel material (steel). v_{steel} is the Poisson's ratio of the barrel material (steel). t_{barrel} is the half of the thickness of the barrel top and bottom walls. k_{Cu} is the modulus of subgrade reaction of the sleeve material (copper), calculated using the Equation 6.8, since copper is an isotropic material. k_{steel} is the modulus of subgrade reaction of the wedge material (steel), calculated

using the Equation 6.8, since steel is an isotropic material. k_{CFRP} is the modulus of subgrade reaction of CFRP plate, calculated using the Equation 6.11.

Four boundary conditions were applied to solve the above four equations (6.16 and 6.17):

Relative deflection, $\text{Inter}_1 = y_{CFRP} - y_{Cu\text{-}sleeve}$

Relative deflection, $\text{Inter}_2 = y_{CFRP} - y_{wedge}$

Relative deflection, $\text{Inter}_3 = y_{wedge} - y_{Barrel} - \delta$

Pressure at the outer surface of the barrel, $P_4 = 0$.

Here, δ is the difference between the original longitudinal radius of the wedge and the matching longitudinal radius of the inner surface of the barrel at a specific location.

The Maple software [161] was used to solve the above mentioned equations. The Maple program file is also shown in Appendix A.

6.3 RESULTS AND DISCUSSION

The theoretical mathematics-based analytical model provided a good assessment of the contact pressure distribution on the CFRP plate in contact with the annealed copper sleeve surface. The results obtained from the FEM-based numerical model matched with the results from the analytical model for the contact pressure distribution on the CFRP plate surface for all three pre-setting distances of 10 mm, 12 mm and 17.32 mm (Fig. 6.6). The contact pressure distribution at the sleeve-wedge interface also matched in both the numerical and the analytical results for 10 mm, 12 mm and 17.32 mm pre-setting distances. The contact pressure at the CFRP-sleeve interface was the highest at the pre-setting end; decreased over the length of the anchor; and was the lowest at the tension load end. The characteristics were valid for all three different pre-setting values – 10 mm, 12 mm, and the full pre-setting of 17.32 mm (Fig. 6.6). The contact pressures at the sleeve-wedge interface and wedge-barrel interface were also the highest at the pre-setting end and the lowest at the loading end for all three pre-setting

distances. Therefore, the anchor design was in the right track avoiding the stress concentration at the tension load end; and it was ensured that the highest stress was on the pre-setting end of the anchor components.

The average contact pressure on the CFRP plate for 10 mm, 12 mm and 17.32 mm pre-setting distances, obtained from the FEM numerical model, are shown in three-dimensional graphs in Fig. 6.7. Figure 6.7 also shows that the contact pressure distribution is similar to the analytical model results, as shown in Fig. 6.6. Therefore, it can be stated that this analytical model is an important tool to quantify the contact pressure distribution on the CFRP plate inside the anchor rapidly.

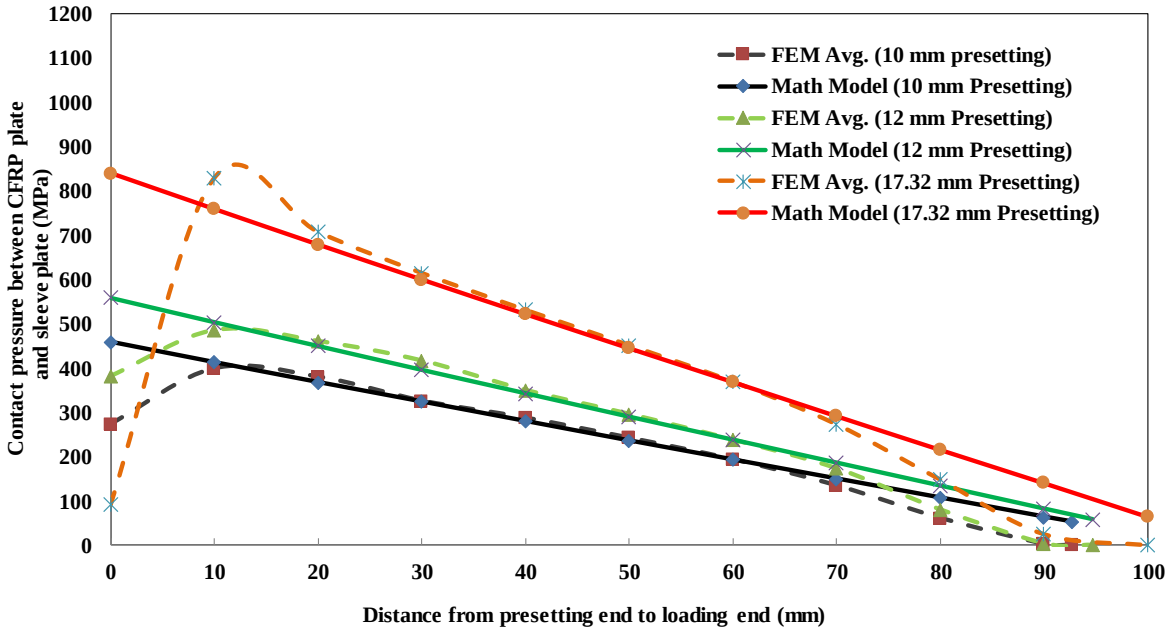

Figure 6.6: Comparative contact pressure distribution on the CFRP plate surface for 10 mm, 12 mm and 17.32 mm pre-setting load from the analytical model and the numerical model.

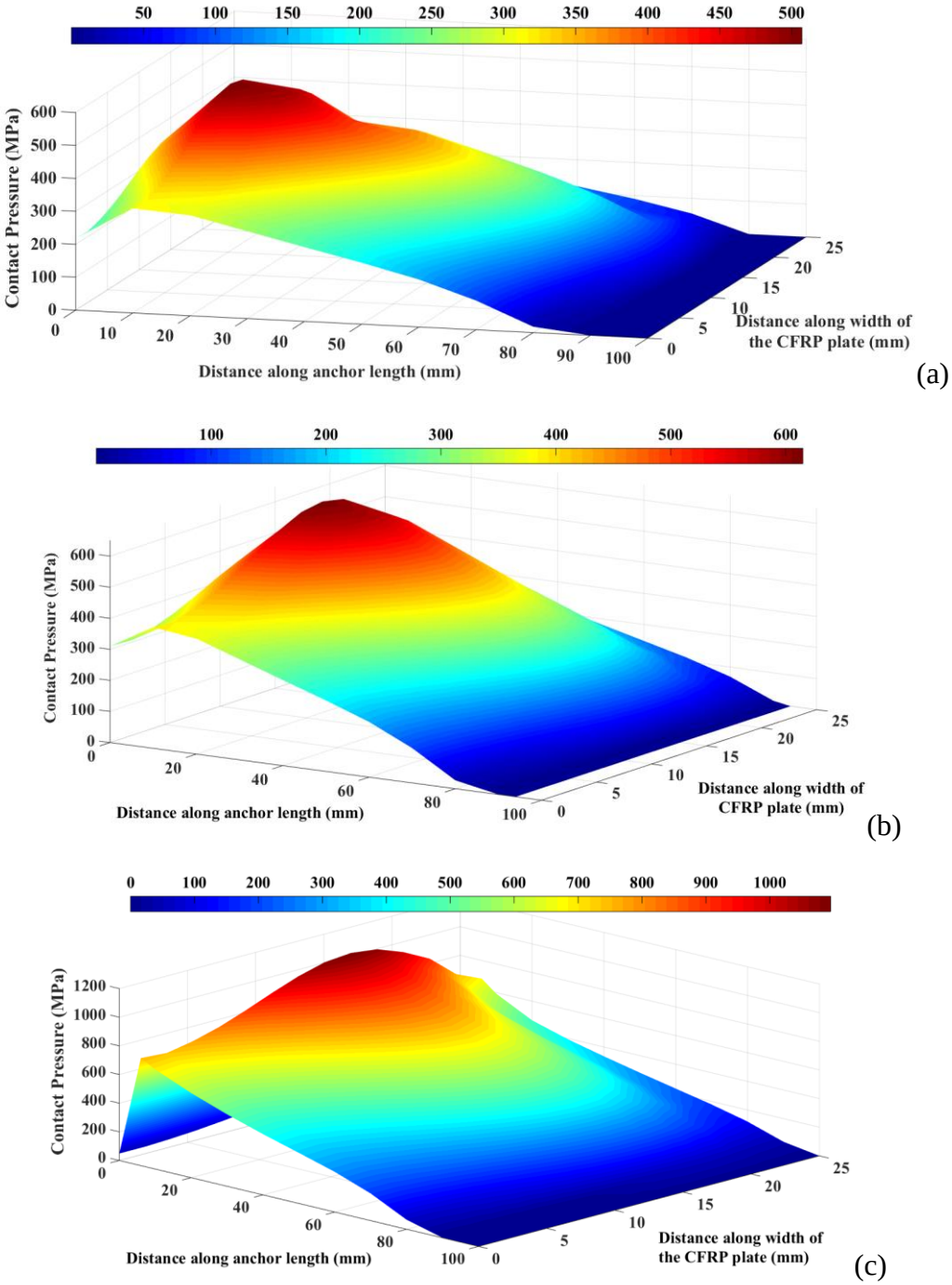

Figure 6.7: Three dimensional contact pressure distribution from the FEM model on half of the CFRP plate surface for (a) 10 mm, (b) 12 mm, and (c) 17.32 mm pre-setting distances.

The preliminary minimum required barrel thickness was estimated in the analytical model using the equation (6.13) before proceeding to the time consuming numerical modelling and parametric study. Using the equation (6.13), the top and bottom wall thickness of the barrel at the loading end was found as 23.03 mm. At this end, the shorter dimension of the barrel opening (a_0) was 18.8 mm, the longer dimension of the barrel opening (b_0) was 56 mm, the equivalent modulus of elasticity of the core was 180,878 MPa (using equation 6.14) and the equivalent Poisson's ratio of the core was 0.31 (using equation 6.15). At the pre-setting end of the anchor, a_0 was 22.13 mm, b_0 was 56 mm, the equivalent modulus of elasticity and the equivalent Poisson's ratio of the core were 180,878 MPa and 0.31, respectively. Hence, at this end, the top and bottom wall thickness of the barrel was 21.95 mm.

These barrel thicknesses (23.03 mm at the loading end and 21.95 mm at the pre-setting end) were used as the preliminary dimensions of the barrel while starting the time consuming FEM numerical analysis, the parametric study and the optimization process of the anchor design. It can be noted that the final barrel-thickness of the optimized anchor #2 was 22.60 mm and 20.93 mm at the loading end and the pre-setting end, respectively.

6.4 SIGNIFICANCE OF ANALYTICAL MODELLING AND SUMMARY

The mathematics-based analytical model validated the FEM-based numerical model results with the same contact pressure values on the CFRP plate for different pre-setting loads. It also showed that the contact pressure was the maximum at the pre-setting end and the minimum at the loading end for all anchor components. The contact pressure on the CFRP plate surface inside the anchor was calculated using this theoretical analytical model to ensure that the CFRP plate would not fail under loading during the experimental investigation. The analytical model also quantified the preliminary minimum required barrel thickness as a start point for the time-consuming and expensive detailed numerical and experimental investigation process in this thesis.

CHAPTER 7
ANCHOR TENSION TEST: EXPERIMENTAL PROGRAM

7.1 INTRODUCTION

An extensive experimental study was conducted to evaluate the performance of the anchor system, to verify the analytical and the numerical model results of the anchor models, and to show the capability of the anchors in carrying a high tensile load. This chapter discusses the test specimens, test setup, instrumentation, test procedure, and test program. A total of twenty-nine successful tension tests were carried out on three different new anchors; and the results of the experimental studies are discussed in Chapter 8. A part of this chapter has been adapted from Mohee *et al.* [162].

7.2 TEST SPECIMEN

7.2.1 Design and Manufacturing of the Anchor

This section presents the design and manufacturing process of the new CFRP plate anchor, particularly the anchor #1 (bolted H13 steel anchor with a minimum barrel thickness of 25.93 mm). Initially, the new CFRP plate anchor was developed and analyzed in the numerical model considering a solid one-piece barrel for the anchor. However, for ease of manufacturing, it was determined that the rectangular cross-section barrel with the given longitudinal circular profile of 3,000 mm radius was not possible to manufacture with a high precision at a low cost. Therefore, a two-piece rectangular barrel, connected by at least six high strength steel bolts, was chosen for manufacturing the anchor.

Based on the FEM model results presented in Chapter 5 (Fig. 5.8c), the maximum von Mises stress in the barrel of the anchor was 1,366 MPa. Hence, a steel was chosen such that the yield strength was equal or higher than 1,366 MPa. Several steel types were considered to make the new anchor. The most common and commercially available high strength steels were 4140,

4340 and H13 steel. The 4140 steel was slightly cheaper than the H13 steel, but the strength of the 4140 steel was below the minimum required yield strength (1,366 MPa). On the contrary, the 4340 steel had sufficient strength, but it was two times more expensive than the H13 steel. Therefore, the heat-treated H13 steel, which has a yield strength (F_y) of 1,366 MPa and an ultimate strength (F_u) of 1,580 MPa [163], [164], was chosen to make the barrel and the wedges of the anchor. The heat treatment process applied to the H13 steel to obtain this strength was:

Step 1: Heating the barrel/wedges at 1010ºC (1850ºF) for 1 hour;

Step 2: Oil quenching;

Step 3: Tempering twice for 2 hours at 593ºC (1100ºF).

The anchor dimension was 126 mm × 100 mm × 74 mm (Fig. 7.1a). It had a mass of approximately 7 kg. Two annealed copper plates of 21 gauge (0.81 mm thick) were used as sleeves in each anchor (Fig. 7.1b). The annealing of the copper plates was done at 500ºC for one hour, followed by air-cooling [163], [164].

For manufacturing the anchor, the detail geometry of all of the components (barrel, wedges and sleeves) were required. Both the barrel and the wedges had a longitudinal circular profile with a radius of 3,000 mm. The center of the longitudinal circular profile in the barrel was located along the barrel-end-line at the tension load end. The center of the circular profile in the wedges was 17.32 mm away from the end of wedge towards the loading end. The wedges had a thickness of 8.05 mm at the tension load end and 10.29 mm at the pre-setting end. The longitudinal profile of the wedges is shown in Fig. 7.2a. The barrel had a 56 mm wide opening. The opening was 18.8 mm thick in the loading end and 22.13 mm thick in the pre-setting end (free end). The barrel had a sidewall thickness of 35 mm, sufficient to accommodate the 15.88 mm diameter bolts and to facilitate the tightening of the bolts. The barrel had a thickness of 25.93 mm in the pre-setting end and 27.6 mm in the tension load end. Both barrel and wedges had a transverse curve in all of the corners with a radius of 6 mm in order to avoid stress concentrations in the corners. The wedges had two small threaded bolt-holes at the pre-setting

end for 5 mm long #4-40 (40 threads per inch) bolts (Fig. 7.1a) to connect the wedges to the aluminum plate for the LVDT spring installation, as discussed in Section 7.4.

The outer side of the wedges facing the barrel surface had a very smooth surface (Fig. 7.2a). The flat side of the wedges facing the annealed copper sleeve was sandblasted to increase the coefficient of friction between the wedges and the sleeves (Fig. 7.1a, 7.2b).

Initially, threaded M8 bolts were chosen for the anchor. However, two M8 bolts at the pre-setting end of the anchor broke into half during the first tension test. Subsequently, higher strength and larger diameter bolts were chosen for the anchor. Grade 8 bolts with an ultimate tensile strength of 1,034 MPa (150,000 psi) and a diameter of 15.88 mm (5/8-inch) were used. Initially, 102 mm long bolts were used. Later, 89 mm (3.5 inch) long bolts were used to make the anchor compact, lighter and cheaper. They were coarse threaded (11 threads per inch) bolts. The bolts had a head length of 16 mm, thread length of 52 mm and a mass of 0.16 kg, each.

Initially, threaded bolt-holes were chosen for the anchor to reduce the dimension and weight of the anchor. But after the bolts broke in the first test, nuts were chosen over the threaded bolt-holes in the anchor. Grade 5 nuts were used in the initial tension tests, but they broke each time. Hence, grade 8 hexagonal nuts of 2.38 mm (15/16-inch) diameter and 1.39 mm (35/64-inch) length were used. These were the equivalent nuts for the 15.88 mm (5/8-inch) diameter bolts. The nuts were coarse threaded (11 threads per inch, NC type). The nuts were made of cadmium and chromate plated steel. A typical drawing of the anchor is given in Fig. 7.3.

A torque of 243 N-m (179 ft-lb) was applied on all six 15.88 mm (5/8-inch) diameter bolts in both of the anchors (testing anchor and bottom anchor) before each test [165]. Any larger torque would break the bolts and the nuts. Any smaller torque would not be sufficient for the anchor to carry the desired 2,800 MPa tension load. The torque value depended on the bolt diameter and the bolt surface condition. This was the torque value for the lubricated surface of bolts and nuts. Therefore, oil was used in bolts and nuts before applying torque each time [165].

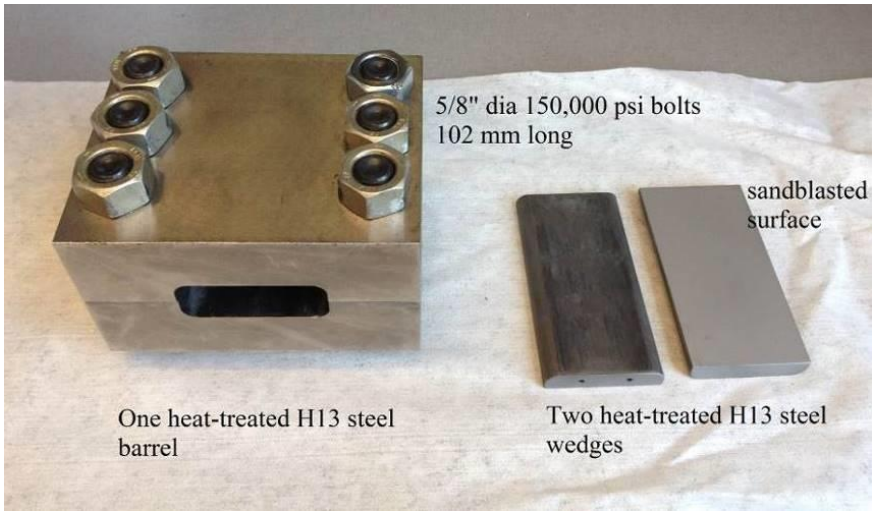

(a)

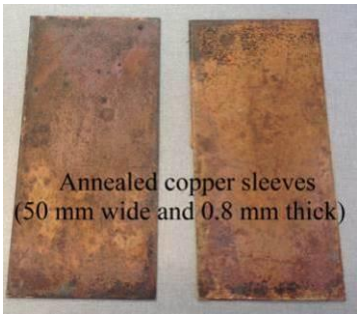

(b)

Figure 7.1: Components of the anchor: (a) barrel and wedges, (b) sleeves.

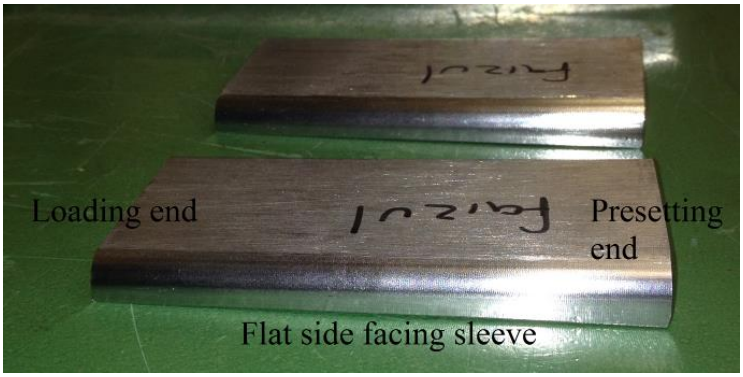

(a)

(b)

Figure 7.2: (a) Longitudinal profile of wedges, (b) sandblasting of the flat side of wedges.

7.2.2 Lighter Stainless Steel Anchor (Anchor #2)

After the successful tension tests of anchor #1, the anchor design was optimized to be corrosion-resistant and to have a lower mass. Since the primary use of the new CFRP plate anchor and prestressed CFRP plate was to replace corroded steel, it was ideal to design an anchor that was corrosion-resistant itself. In addition, the thickness of the barrel was reduced by 5 mm to reduce the mass of the anchor. The mass of this new anchor was 6 kg. Therefore, a second anchor (anchor #2), made of stainless steel, was experimentally investigated.

The stainless steel of type 440C was chosen to make this optimized and corrosion-resistant anchor. The nominal composition of 440C stainless steel consists of 1.1% carbon, 17% Cr and 0.75% Mo, and remaining are Fe, by weight. As shown in Fig. 5.21 in Chapter 5, the maximum von Mises stress in the barrel in the numerical model was found as 1,858 MPa. Hence, a stainless steel was chosen such that the yield strength was higher than 1,858 MPa. Therefore, the heat-treated stainless steel of type 440C with a yield strength (F_y) of 1,896 MPa and an ultimate strength (F_u) of 1,975 MPa was used to make the barrel and the wedges of this anchor [164]. The Rockwell hardness number of the anchor components after heat treatment was 57 HRC. The heat treatment processes to obtain this strength were as follows [163], [164]:

Step 1: Heating the two barrel pieces and the two wedges at 1040ºC for 1 hour;
Step 2: Oil quenching;
Step 3: Tempering at 315ºC for 2 hours.

The barrel was 100 mm long, 126 mm wide and 64 mm thick. Figure 7.3a and 7.3b show the cross section of the barrel in the tension load end and the pre-setting end (free end), respectively. Figure 7.3c shows the longitudinal section of the barrel. The inner profile of the barrel had a longitudinal curve with a 3,000 mm radius. The barrel had 2 parts connected by six 15.88 mm diameter bolts. The wedges were 100 mm long and 50 mm wide. They were 8.05 mm thick at the loading end (Fig. 7.4a and 7.4b) and 10.29 mm thick at the free end

(Fig. 7.4a and 7.4b). The wedges also had a longitudinal circular profile with a radius of 3,000 mm and a transverse curve of 6 mm radius. There were two small threaded bolt-holes in the free end of the wedges for two 5 mm long #4-40 bolts to connect the aluminum clamp. The physical anchor #2, gripping the CFRP plate, is shown in Fig. 7.5.

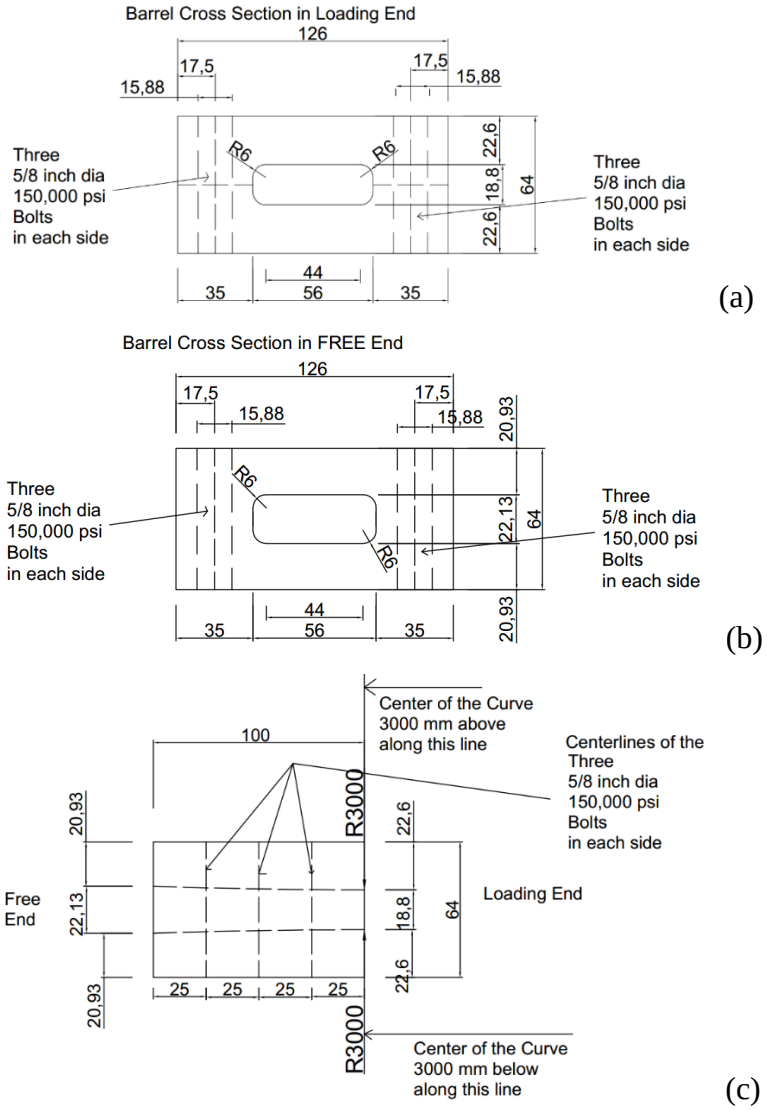

Figure 7.3: Cross section of the optimized stainless steel anchor barrel at (a) loading end, (b) free end, (c) Longitudinal section of the optimized stainless steel anchor barrel.

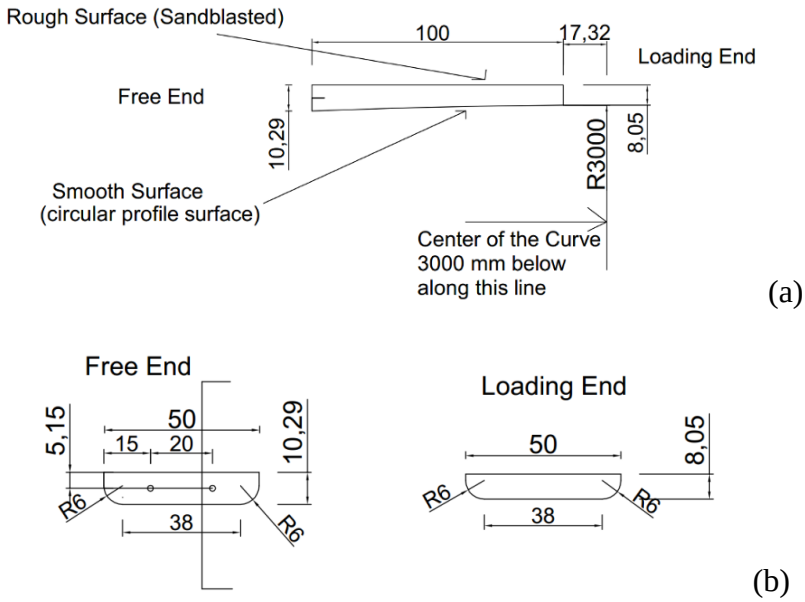

Figure 7.4: (a) Longitudinal section and (b) cross-section of the wedge in anchor #2.

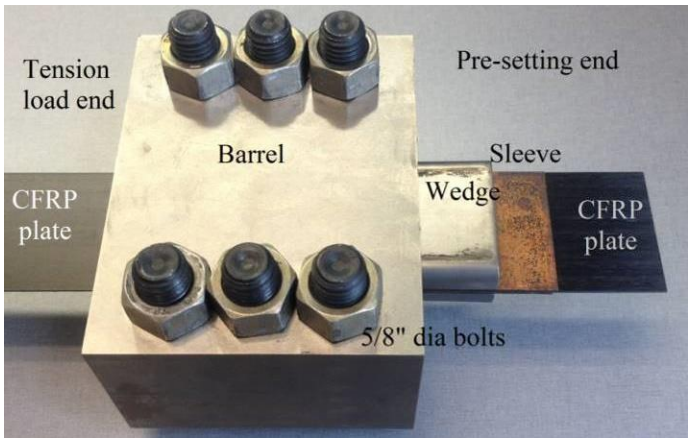

Figure 7.5: Optimized stainless steel anchor (anchor #2) for CFRP plate.

7.2.3 Anchor #3 For 1.4 mm Thick High Modulus CFRP Plate

The newly developed anchor #1 was slightly modified for prestressing the 1.4 mm CFRP plate. Instead of the 21-gauge copper plate, the 22-gauge (0.71 mm thick) annealed copper sleeves were used in anchor #3 to test the 1.4 mm thick high modulus (210,000 MPa) CFRP plates.

7.2.4 3D Printing

Two anchor prototypes were manufactured using 3D printing in a filament based additive manufacturing process. The first prototype was a preliminary base anchor. The second prototype was a full scale anchor with the exact same dimension as the anchor #1. The 3D printing was done upward in a extruder-based machine. The 3D printing machine (the MakerBot Replicator 3D printing machine) and the 3D printing processes of the barrel and the wedge are shown in Fig. 7.6a, 7.6b and 7.6c, respectively.

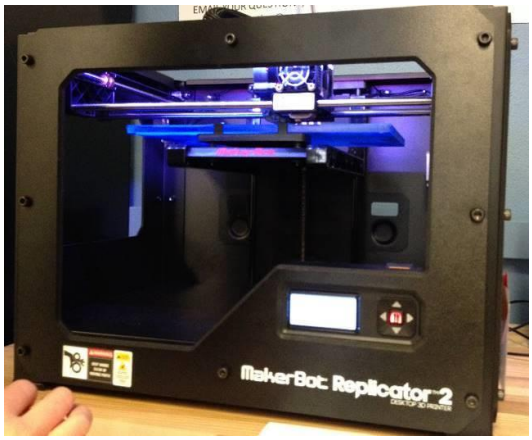

(a)

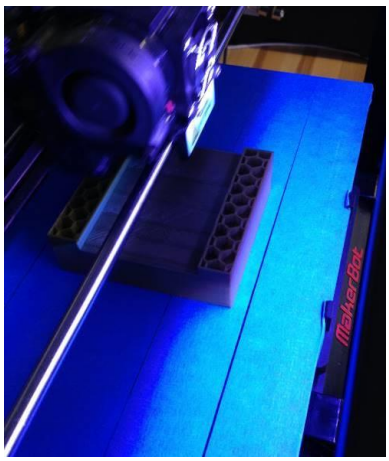

(b)

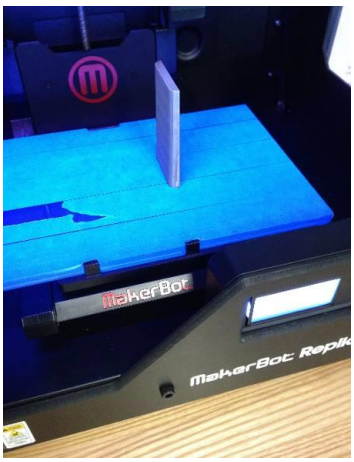

(c)

Figure 7.6: (a) The 3D printing machine, (b) 3D printing process of the barrel, and (c) wedge just after finishing the 3D printing.

During 3D printing, a 15% infill in a honeycomb pattern was used to provide the internal structural support of the wedge and the barrel. The number of shells was two; and the layer height was 0.1 mm. Therefore, the sidewall thickness of each of the prototypes was 0.2 mm. The 'high' resolution and the 'slower' printing speed were used for the printing to ensure a high quality 3D print. The filament used in 3D printing worked as a plastic welding rod. The filament material used for this printing was PLA (Poly Lactic Acid), which is a bioplastic material derived from corn. PLA is a hard and strong material with a low thermal expansion. A heating temperature of 230^{o}C was used to melt the PLA filament for the 3D printing process. Both of the 3D printed anchors are shown in Fig. 7.7.

Both of the 3D printed anchors (Fig. 7.7) were widely used to visualize the anchor concept and to understand the application of the anchor for the prestressing process of the CFRP plate. The second full scale anchor (Fig. 7.7b) was used to design the different test setup components (*e.g.,* exact dimensions of the steel base plate) of the tension test machine. The 3D printed anchor was also used to figure out the pre-setting load application procedure before manufacturing the actual steel anchor. The 3D printed prototypes were also used to explain to the machine shop technicians exactly what was intended to make in the machine shop; and to determine the best manufacturing process of the anchor, as discussed in section 7.2.1.

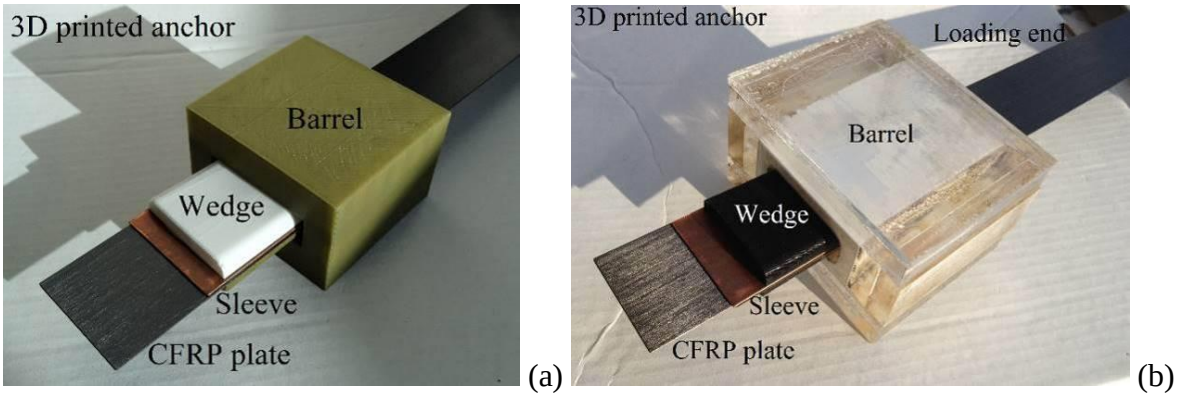

Figure 7.7: The 3D printed anchor prototype before manufacturing the actual anchor.

7.2.5 Bolt-Based Clamping Anchor as the Preliminary Dead End Anchor

Initially, three tension tests were conducted on the new anchor using a clamping anchor at the dead-end (bottom end). In order to perform the tension test of the newly developed anchors, a new reusable and bolt-based clamp anchor was designed (Fig. 7.8) and manufactured (Fig. 7.9) to grip the CFRP plate at the dead end (bottom end). Two cold rolled 1018 steel plates, each 25.4 mm thick, were used to make the clamp anchor. The CFRP plate, epoxied with two 0.81 mm thick copper plates, were placed inside two serrated steel plates connected by eight bolts (12.7 mm diameter and grade 5 bolts). To increase the coefficient of friction between the copper plates and this anchor, 5.7 mm thick hard steel files were put inside the pockets of the steel plates. A 3 mm chamfer was kept in the steel plates at the loading end. Four small (6 mm diameter) holes were kept in the outer surface of the steel plates so that the file pieces could be pushed out of the anchor pieces, if required. This dead end anchor was 203 mm long, 110 mm wide and 25.4 mm thick (Fig. 7.8 and 7.9).

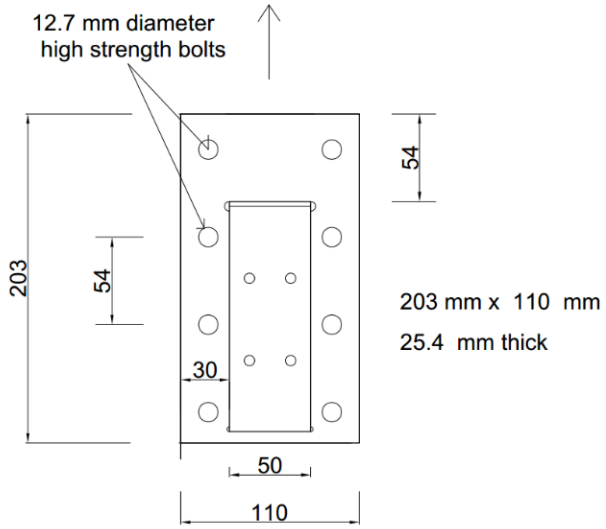

Figure 7.8: Bolt-based clamp anchor used as the dead end anchor in the initial tension tests.

The applied torque on the bolts was uniformly distributed to avoid any stress concentration on the CFRP plate inside this anchor. The top two bolts at the loading end were not torqued (to

avoid stress concentration at the loading end). The second row of bolts had a lower torque of 95 N.m; and the bottom row of bolts, at the free end, had a higher torque of 135 N.m.

Two 0.81 mm thick (21 gauge) copper sleeves were used to protect the CFRP plate from the hard steel of this anchor (Fig. 7.9a). This also helped the files in the anchor to have a better grip on the CFRP plate, which was epoxied to the copper plates. Figure 7.9 shows the step-by-step process of this new clamping anchor: two anchor parts (Fig. 7.9a), CFRP plate with copper sleeves (Fig. 7.9a) and the CFRP plate and the copper plates inside the clamping anchor (Fig. 7.9b).

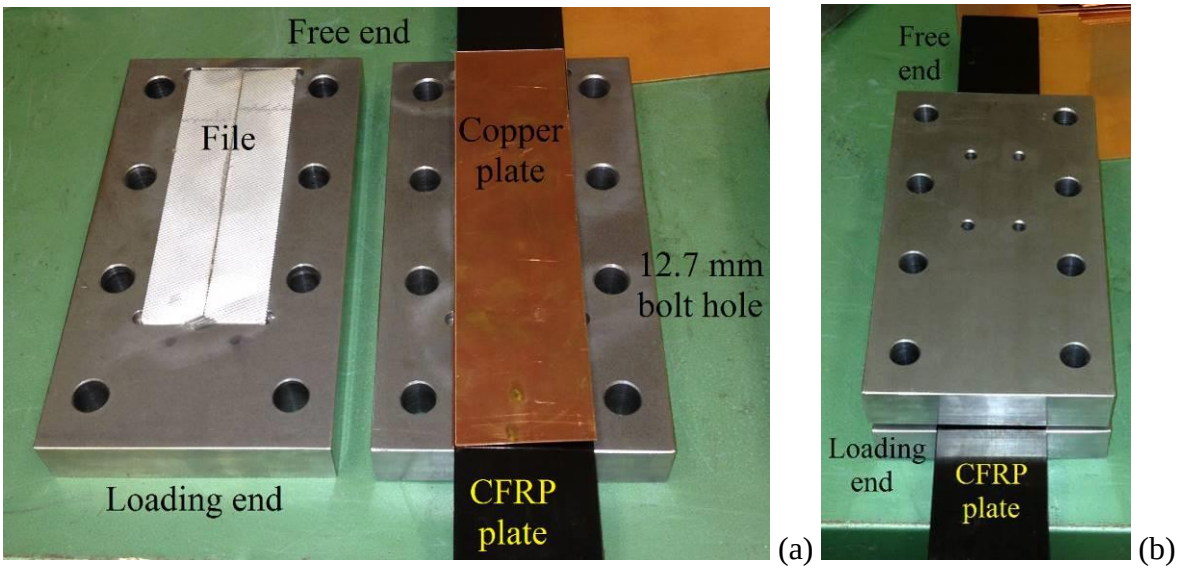

Figure 7.9: Bolt-based clamp anchor used as the dead end anchor in the first set of tension tests: (a) clamps with copper plates, (b) clamp anchor set with CFRP plate.

7.3 EXPERIMENTAL SETUP AND PROCEDURE

7.3.1 Loading Rig and Tension Test Setup

This section describes the tension test setup and the loading rig. The 250 kN capacity tension test machine, as shown in Fig. 7.10a, was used for the tension test of the new CFRP plate anchors. The loading frame was attached to MTS servo controlled hydraulic system. The tension test machine had two steel plates – top plate and bottom plate, 300 mm apart vertically from each other (Fig. 7.10b). The top plate was 19 mm thick. The bottom plate was designed (Fig. 7.11), made in machine shop (Fig. 7.12), and installed in the tension test machine (Fig. 7.10b). The two plates were connected by four 25.4 mm diameter and 450 mm long threaded high strength steel bars (Fig. 7.10b). The horizontal opening between two long steel bars was 105 mm, through which the anchor was inserted. The new bottom plate was made of cold rolled 1018 mild steel. It was 50.8 mm thick, 200 mm long and 200 mm wide (Fig. 7.10b, 11). The plate was made with an 8 mm wide and 128 mm long slot in the middle so that the CFRP plate could pass through the slot (Fig. 7.11). The length of the slot was designed such that the anchor could be centered with the center of this base plate. A 3D printed full-scale anchor was used to design this new base plate (Fig. 7.12b) to determine the exact dimension of the slot, the bolt-hole locations and diameter, the requirement of the second steel plate beside the main steel base plate, etc. Because of the presence of the long and wide slot in this plate, there was a high risk of bending the plate under loading. Therefore, a new 200 mm long and 25.4 mm thick steel plate was designed (Fig. 7.11) and made (Fig. 7.12) to protect the new base plate (bottom plate) from bending. The second plate was connected to the base plate by four 12.7 mm diameter and 19.05 mm long bolts - two bolts in each side of the slot. The upper plate was attached to a load cell mounted to the MTS actuator. The test anchor was placed on top of the bottom steel base plate. Both the upper and the lower base plates were levelled using a level.

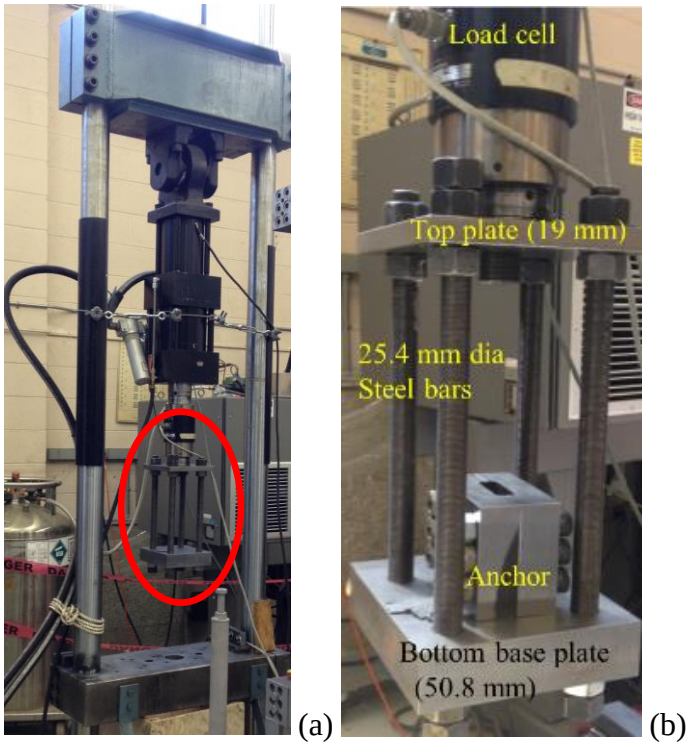

Figure 7.10: Tension test loading rig: (a) full setup, (b) zoomed view.

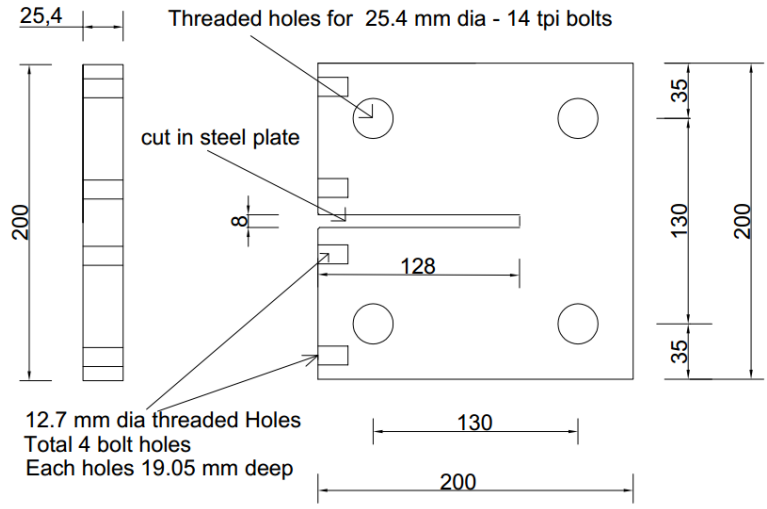

Figure 7.11: Steel bottom base plate for the tension test setup. The anchor sat on this steel base plate during the tension tests.

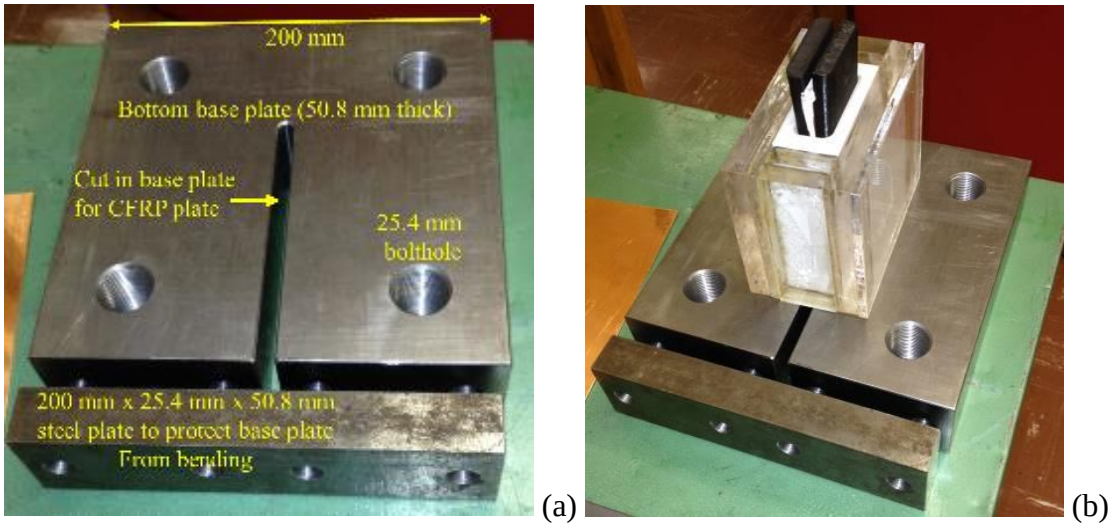

Figure 7.12: (a) The new steel bottom base plate for the tension test setup; and (b) a 3-D printed prototype of the anchor sits on the steel base plate.

The bottom end of the CFRP plate was gripped by either a clamping anchor (as described in section 7.2.5) or the newly developed anchor #1. The bottom anchor was supported by a 150 mm thick steel bearing plate in the tension test machine frame (Fig. 7.10a). This thick bearing plate had a central hole so that the CFRP plate could pass through the hole.

7.3.2 Pre-setting of the Anchor

To pre-set the anchor, the wedges were pushed into the barrel of the anchor by a pre-defined distance prior to applying the load. The wedges were marked at the pre-defined distance (17 mm and 5 mm from the pre-setting end of the wedge for moderate and high pre-setting, respectively); and the wedges were pushed until that mark was reached. This was conducted in order to ensure that the CFRP plate would not slide through the anchor because of a lack of contact pressure on the CFRP plate inside the anchor. The pre-setting rig (Fig. 7.13a) was used to pre-set the wedges inside the anchor. A pressure dial gage set in the pre-setting machine was used to measure the pre-setting force applied through the 101.6 mm diameter shaft of the pre-setting rig. Two high strength flat steel plates were used to transfer the pre-setting force from

the pre-setting rig to the wedges (Fig. 7.13a, and b). In the tests investigating no pre-setting, the wedges were hammered lightly into the barrel before the tests. Before making the steel anchors, a full scale 3D printed anchor prototype was used to understand the pre-setting process of the anchor. The pre-setting machine was also used to push the wedges out of the anchor in a direction opposite to the pre-setting direction after each tension test.

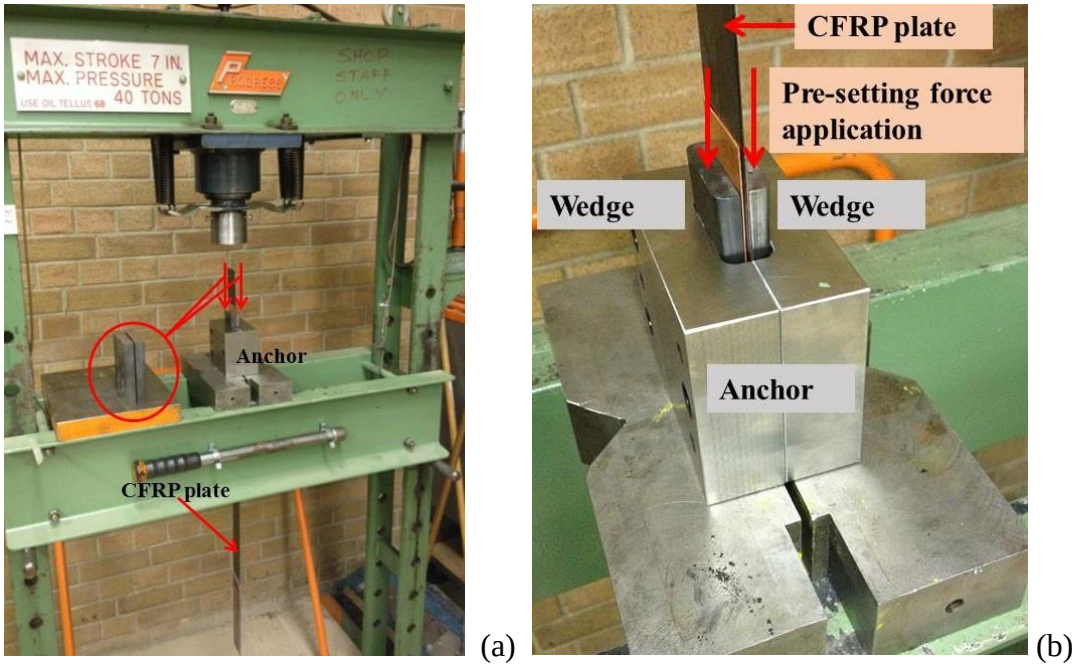

(a) (b)

Figure 7.13: Pre-setting rig and the procedure to pre-set wedges inside the anchor barrel.

The pre-setting force ($F_{presetting}$) applied on the two wedges was calculated by multiplying the pressure (P_{shaft}) observed in the pre-setting machine dial gauge with the cross-sectional area of the shaft of the pre-setting machine (D_{shaft}), as shown in the equation (7.1):

$$F_{presetting} = P_{shaft} \frac{\pi \, . \, D_{shaft}{}^2}{4} \tag{7.1}$$

The shaft diameter of the pre-setting machine (D_{shaft}) was 101.6 mm and the pressure (P_{shaft}) was read from the pre-setting machine gauge for a given pre-setting distance: (1) regular pre-setting (17 mm of the wedge outside of the barrel), and (2) high pre-setting (5 mm of the wedge outside of the barrel).

Table 7.1: The equivalent pre-setting force required for a given pre-setting distance in terms of wedges outside of the anchor in the pre-setting end for anchor #1

Type of pre-setting	Length of wedge outside of barrel after application of the pre-setting force (mm)	Equivalent pre-setting force applied on the two wedges (kN)
Moderate	17	37
High	5	110

7.4 INSTRUMENTATION, APPARATUS AND METHODOLOGY

An MTS 458.20 micro-console, 458.91 micro-profiler and 458.13 AC controller were used to operate the tension test machine. Displacement control with 150 mm stroke was used. A loading rate of 0.6 mm/min was used for the tension tests. One specimen was tested at a faster extension rate of 4 mm/min to examine the effect of the loading rate on the anchor capacity. Figure 7.14 shows the schematic instrumentation diagram of the tension test. As shown in Fig. 7.14, the bottom steel plate stayed fixed and the top steel plate moved upward during the tension test creating tension in the CFRP plate. The tests were terminated upon the failure of the test specimen.

Two calibrated linear variable differential transformer (LVDT), Transtek model #243 LVDTs with a capacity of 21 mm each, were used to measure displacement during the tension tests (Fig. 7.15a). The first LVDT was connected to the CFRP plate using a LVDT clamp to measure the displacement between the CFRP plate and the barrel (Fig. 7.14). This reflected the total

sliding distance of the wedges, sleeve and CFRP plate inside the barrel. The second LVDT was also connected to the CFRP plate using the LVDT clamp to measure displacement between the CFRP plate and a wedge (Fig. 7.14). This was the combined sliding distance of the CFRP plate and the sleeve. In some tests, strain gauges were used in order to verify the failure stress obtained from the load cell. The strain gauges had a gauge length of 5 mm, a gauge width of 1.5 mm, a gauge resistance of 120 ± 0.5 Ω, a transverse sensitivity of 0%, and had a pre-attached 5 meter long vinyl lead wire to connect to the data acquisition system (Fig. 7.15b). The LVDTs, the load cell and the strain gauge were connected to the Labview data acquisition system.

A new LVDT clamp was designed (Fig. 7.16a) and manufactured (Fig. 7.16b) to hold the two LVDTs and to connect them with the CFRP plate. Fig. 7.16c shows the LVDT clamp holding a LVDT. The new LVDT clamp was made of aluminum. There were two circular openings in the clamp to place the LVDTs. The diameter of the circular openings (19.05 mm diameter) was made such that it was exactly the same as the diameter of the LVDTs used in the experiments (Fig. 7.16). It had two parts connected by bolts. All of these bolts were #10-32 bolts (32 threads per inch). All of these bolts were 43 mm long. Two bolts in the two ends were used to tighten and loosen the grip on the LVDTs. Two bolts in the middle were used to tighten the LVDT clamp to the CFRP plate. The middle surface between the two parts was made rough in order to increase the friction between the CFRP plate and the LVDT clamp so that the CFRP plate would not slip during the tests (Fig. 7.16a, b). The length of the clamp was also made such that the CFRP plate could fit between the two middle bolt-holes (Fig. 7.16a, b). The center-to-center distance between the two middle bolts was 62 mm, which was larger than the CFRP plate width (50 mm).

A new ice hockey-stick shaped plate, made of aluminum, was designed (Fig. 7.17a) and manufactured (Fig. 7.17b) to hold the LVDT spring. This was used to measure the displacement between the CFRP plate and the wedge during the tension tests. This aluminum plate was connected to a wedge by two #4-40 bolts. The bolt-hole locations were matched with

the wedge dimension in the pre-setting end. The center-to-center distance between the two bolt-holes was 20 mm. The bolt-holes were 15 mm away from the end of the wedge (Fig. 7.17). The extended L-part of the aluminum plate was also designed such that it could reach the spring of the LVDT connected to the CFRP plate using the LVDT clamp (Fig. 7.14 and 7.17). The L-shape in this aluminum plate was required in order to accommodate the thickness of the wedge (10.29 mm), the diameter of the LVDT (19.05 mm), and the thickness of the LVDT clamp (18 mm); and thus to accommodate the LVDT spring within the 40 mm × 40 mm L-shape area.

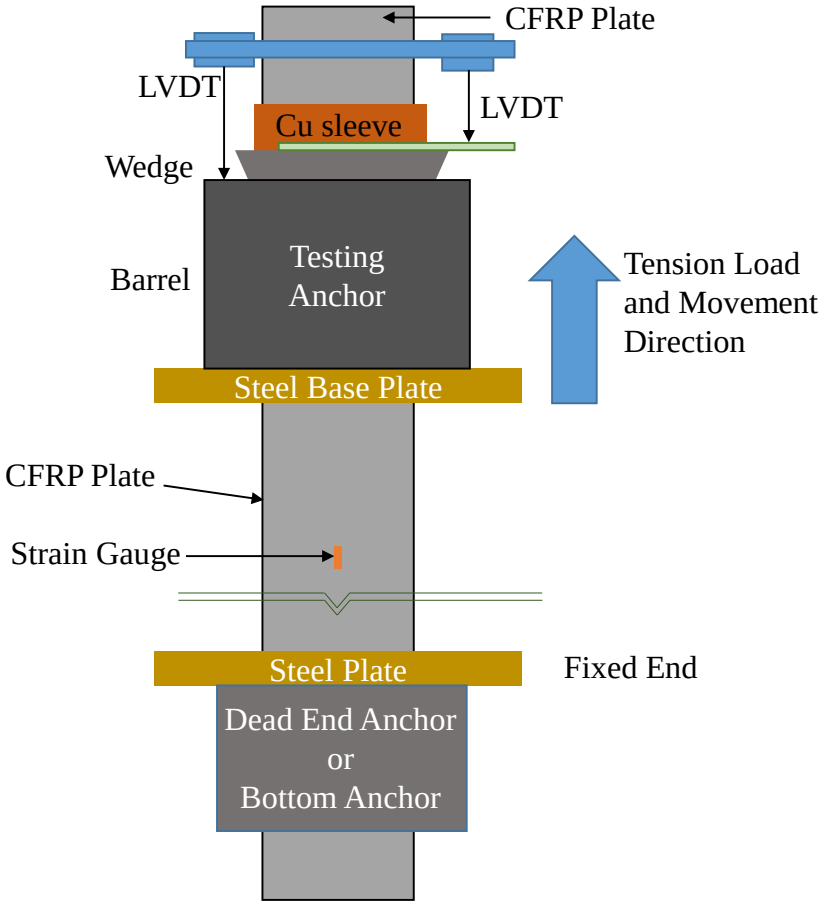

Figure 7.14: Schematic instrumentation for the tension test (not drawn to scale).

(a)

(b)

Figure 7.15: (a) LVDT, and (b) strain gauge.

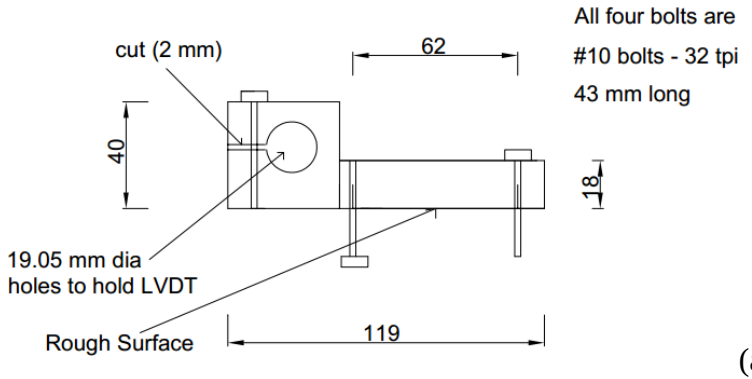

(a)

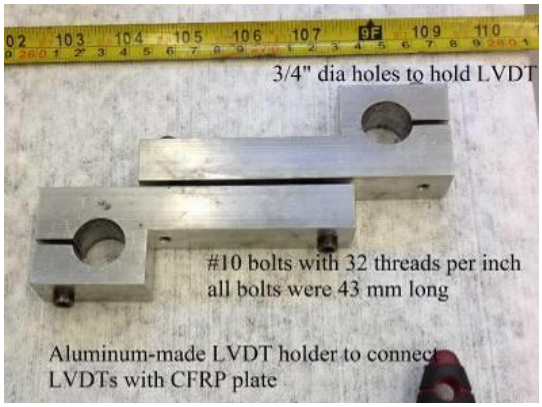

(b)

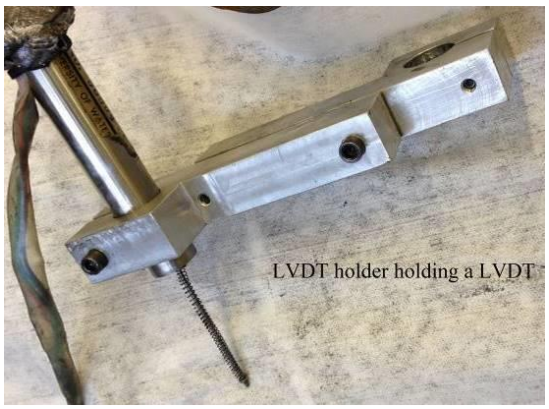

(c)

Figure 7.16: (a) Sketch of the LVDT clamp to make it; (b) aluminum-made clamp to hold LVDTs during the tension tests; (c) LVDT clamp with the LVDT together.

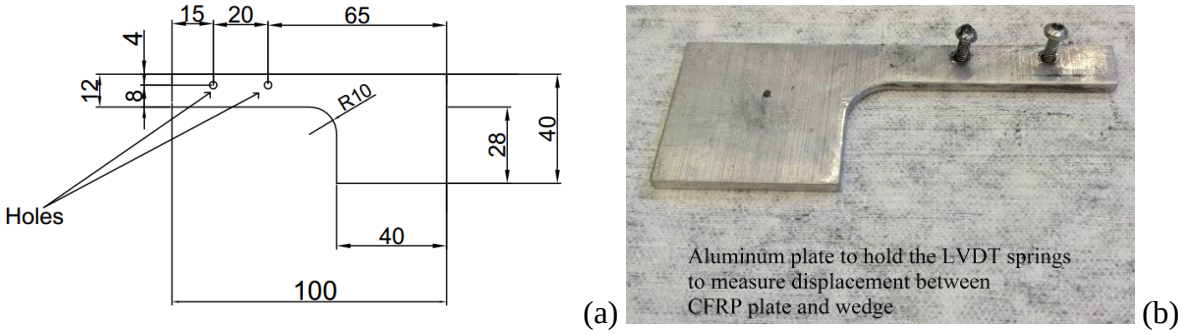

(a) (b)

Figure 7.17: (a) sketch of the aluminum plate and (b) aluminum plate to hold LVDT spring to measure displacement between CFRP plate and wedges during the tension tests.

7.5 TEST SAMPLE PREPARATION AND TEST PROCEDURE

CFRP plates of 970 mm length and 50 mm width were used as the test samples. Before each test, the CFRP plate, the barrel and the wedges of both of the anchors and the annealed copper sleeves were cleaned using Acetone or Isopropanol to ensure no particles or residues impacted the friction coefficient during the tension tests. To facilitate the movement of wedges inside the barrel, and thus to ensure a proper grip on the CFRP plate inside the anchor, a thin layer of lubricant (DOW Molykote G-n Metal Assembly Paste, high pressure lubricant) was applied on the outer surface of the wedges and on the inner surfaces of the barrel before each test. This lubricant reduced the frictional force in the surfaces immediately upon application; and protected the surfaces against fretting wear and corrosion.

Two neoprene spacers, each 1 mm thick, were used on each side of the wedges to keep the wedges centered and aligned with the barrel (Fig. 7.18). A centerline was marked on the wedges and the barrel to match their centerlines. In addition, a level was used during the pre-setting process to keep the CFRP plate straight and vertical.

The 50.8 mm thick steel base plate in the tension test machine was levelled before each test (Fig. 7.18). A 130 mm of length of the CFRP plate was kept outside of the testing anchor in

order to accommodate the LVDT clamp and to accommodate any potential slippage distance of the CFRP plate. Figure 7.19 shows the experimental setup from two different angles.

The wedges were kept at a distance of 17 mm outside of the barrel in the tests (except the tension tests that investigated the effect of pre-setting). In the tests investigating no pre-setting, the wedges were hammered lightly into the barrel before the tests.

After the pre-setting, the testing anchor and the CFRP plate assembly was placed in the tension test machine. A level was used to make the steel base plate horizontal and the CFRP plate straight and vertical. Subsequently, the bottom anchor was placed under the steel beam of the tension test machine to hold the CFRP plate at the bottom end. At the beginning of each tension test, a 2-4 kN of preliminary tension load was applied manually to set the wedges in the bottom anchor.

Different safety measures were taken for the tension tests. Two wooden safety boxes were made and used all around the test setup to contain the CFRP fibres after rupture. A thick rubber piece was placed under the test setup to ensure that the bottom anchor and the floor would not be damaged. Two 12 mm thick steel plates (200 mm $\times$ 50 mm each) were used on top of the bottom anchor to ensure that the wedges would not slide out of the barrel of the bottom end anchor. A 150 mm long wood piece was kept on top of the testing anchor to protect the LVDTs and the anchor from sudden jumping after the tensile rupture of the CFRP plate.

After each test, all of the bolts and bolt threads were examined after each test to check if they broke. All of the nuts and nut threads were also checked for damage. Since some of the initial grade 5 nuts broke during the initial tension tests, grade 8 nuts were used in the later tests.

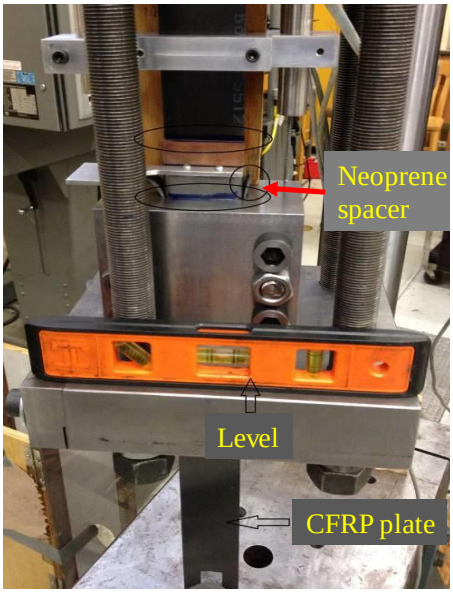

Figure 7.18: Level was used to make the CFRP plate vertical and the steel base plate horizontal. Neoprene spacers were used in the space between barrel and wedges.


(a)

(b)

Figure 7.19: Experimental setup for the tension test of the anchor #2.

7.6 TEST PROGRAM

A total of twenty-nine successful tension tests on the three newly developed anchors were performed in this test program (Table 7.2). Out of these twenty-nine tests, twenty-two tests were carried out on the anchor #1, three tests were carried out on the stainless steel anchor (anchor #2) and four tests were carried out on the anchor #3 using 1.4 mm thick CFRP plate, as listed in Table 7.2. Using anchor #1, a total of twenty-two successful tests were carried out in order to investigate the effect of different parameters on the performance of the anchor. The parameters include the pre-setting distance, the wedge width, the type of the bottom-end-anchor, the roughness and the loading rate (Table 7.3).

Table 7.2: Tension test experimental program for the three new CFRP plate anchors

Anchor	Material	CFRP plate type	No. of specimens
Anchor #1	Heat-treated H13 steel	1.2 mm thick, 2,800 MPa strength and 165,000 MPa modulus of elasticity	22
Anchor #2	Heat-treated 440C stainless steel		3
Anchor #3	Heat-treated H13 steel	1.4 mm thick, 2,900 MPa strength and 210,000 MPa modulus of elasticity	4

Table 7.3: Tension test experimental program for anchor #1 (bolted H13 steel anchor)

Testing criteria	Test details	No. of specimens
Pre-setting distance	Regular pre-setting (17 mm of wedge outside)	3
	High pre-setting (5 mm of wedge outside)	3
	No pre-setting	2
Wedge width	Full width (55.5 mm wide wedges)	3
Bolt-based clamping anchor at the bottom end	Bolt-based clamping anchor at the bottom end	3
Use of the new anchor at the bottom end	Regular pre-setting (17 mm of wedge outside)	3
Roughness	Rough surface wedge	1
Loading rate	Slow (0.6 mm/min)	3
	Fast (4 mm/min)	1

7.7 TEST PARAMETERS

During the tension tests, the following output parameters were investigated:

1. The ultimate tension load capacity of the anchor.
2. The failure mode of the anchor. The desirable failure mode was the tensile rupture of the CFRP plate in brush mode in the mid-length outside of the anchors.
3. The amount of sliding in the CFRP plate, the sleeves and the wedges.
4. The effect of pre-setting on the anchor capacity.
5. The effect of the application of a bolt-based clamping anchor and the new anchor in the bottom end (dead end) on the anchor performance.
6. The effect of using the full width (55.5 mm wide) wedges and the wedges with 3 mm gap on the anchor capacity.
7. The effect of using sandblasting on the outer surface of the wedges.
8. The effect of the loading rate on the anchor capacity.

CHAPTER 8
ANCHOR TENSION TEST: RESULTS AND DISCUSSION

8.1 INTRODUCTION

This chapter presents the tension test results of the developed anchor systems. A total of twenty-nine successful tension tests were conducted on the three newly developed CFRP plate anchors. The primary aim of these tests was to show the use and the capability of the anchors to carry high tensile load and to validate the numerical models. In this chapter, the effects of different parameters on the anchor performance are also highlighted. The failure modes of the anchors during the tests are also explored and discussed in detail. A part of this chapter has been adapted from Mohee *et al.* [162].

8.2 RESULTS OF THE TENSION TEST

8.2.1 General Performance of the Anchor

This section presents the results of the experimental study. A total of twenty-two successful tests were carried out to investigate the effect of different parameters (*i.e.*, pre-setting distance, type of bottom anchor, width and roughness of wedges and load rate) on the performance of the anchor #1. Two additional distinct anchors (anchors #2 and #3) were also tested for their tensile capacity and failure mode. Anchors #1 and #2 were tested with 1.2 mm thick CFRP plates having a guaranteed tensile strength of 2,800 MPa; and anchor #3 was tested with 1.4 mm thick CFRP plates having a guaranteed tensile strength of 2,900 MPa.

Figure 8.1 shows a typical tension load-displacement curve to explain the anchor performance. The X-axis represents the total slip of the wedge including the sleeve and the CFRP plate with respect to the barrel. Due to pre-setting, an anchor carries an initial tension load before the wedges begin to slide. In Fig. 8.1, the zone 1 represents the region of zero slip behaviour of the anchor that is controlled by the pre-setting level. After reaching that load level (70 kN in

Fig. 8.1), the wedges slide with respect to the barrel (zone 2) until the wedges reach the steel base plate that supports the anchor (18 mm sliding zone 2, as shown in Fig. 8.1) similar to real-life applications. Once the wedges reach the supporting base plate, there is no more displacement of the wedges and the CFRP plate; and the anchor carries more tension load until the CFRP plate ruptures (zone 3 in Fig. 8.1).

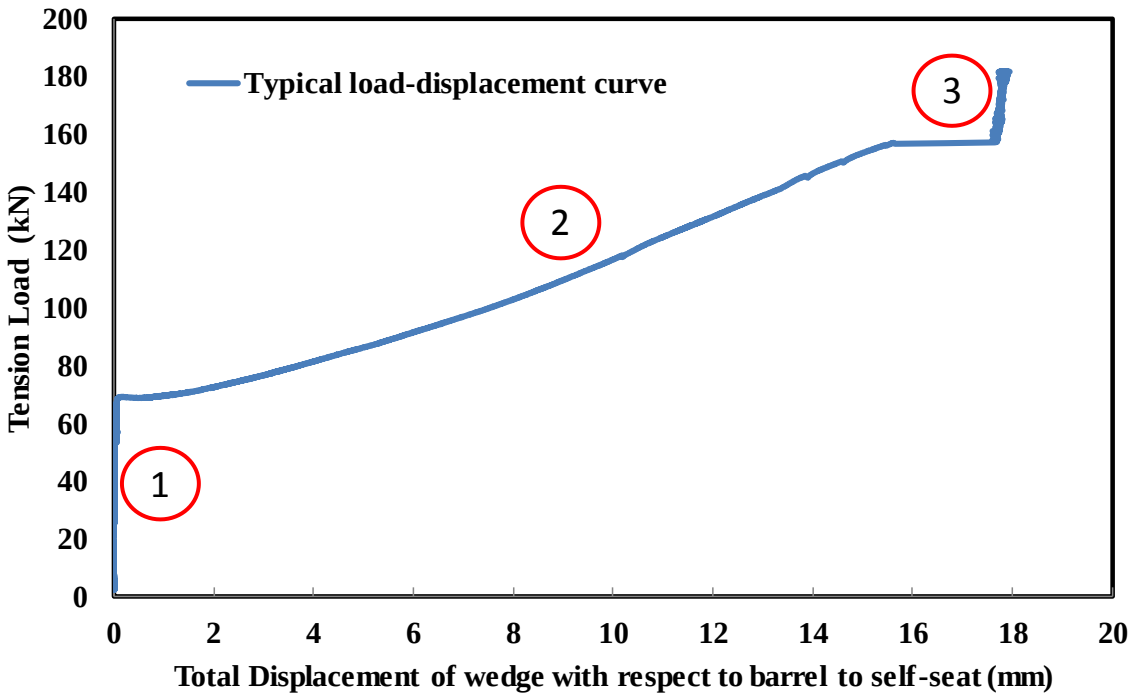

Figure 8.1: A typical tension load vs. displacement behaviour of the new anchors.

8.2.2 Tension Test Results for the H13 Steel Anchor #1

This section shows the tension test results with anchor #1 at both ends of the CFRP plate. The anchors had an ultimate tensile capacity of 187±6 kN, which was equal to 111% of the guaranteed ultimate tensile strength of the CFRP plate, provided by the manufacturer. The failure mode of the anchor was the tensile rupture of the CFRP plate at the free length outside of the anchors (Fig. 8.2). A pre-setting load of 37 kN was applied on the wedges before the application of the tension load.

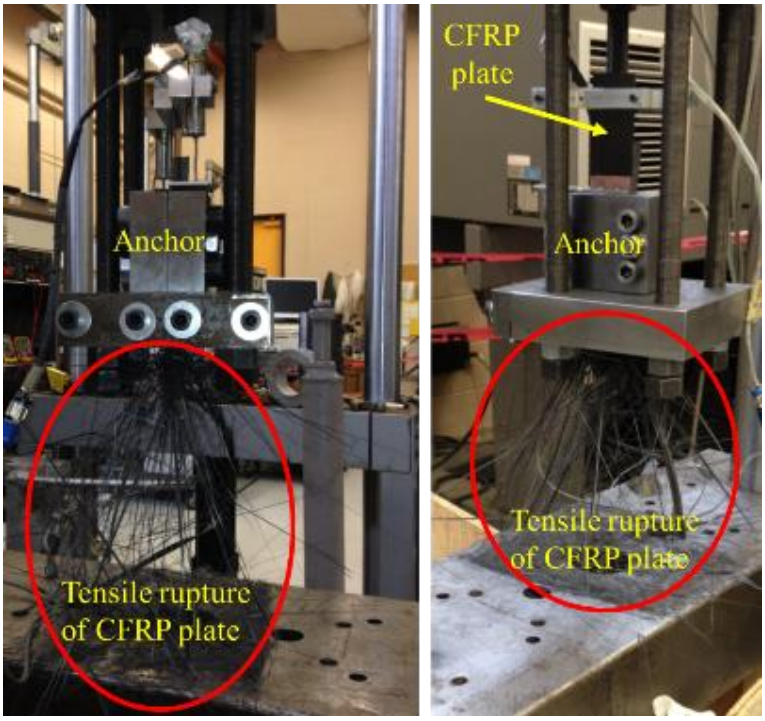

Figure 8.2: Failure of CFRP plate outside of the anchor #1.

The tension load vs. displacement relationships are shown in Fig. 8.3 (displacement between the CFRP plate and the barrel) and Fig. 8.4 (displacement between the CFRP plate and the wedges). Most of the displacement was due to the sliding of the wedges together with sleeve and CFRP plate (16-17 mm) with respect to barrel (Fig. 8.3). The sliding distance of the wedges depended on the exact pre-setting distance before the tests. The wedges slid all the way to the end of the barrel until they were stopped by the supporting steel base plate in the tension test machine. From Fig. 8.4, it can be seen that the CFRP plate and the sleeve moved less than 3 mm during the tension tests. As shown in Fig. 8.5, the initial location of the CFRP plate was marked before the test and the photo was taken after the test indicating that the CFRP plate did not slide during the tension tests.

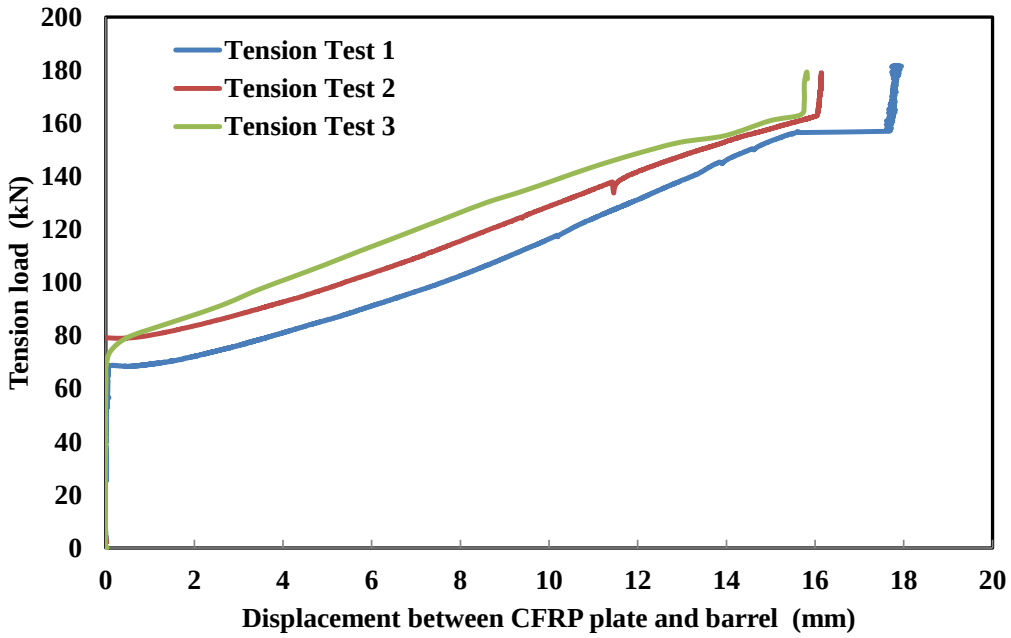

Figure 8.3: Tension load vs. displacement curve for the anchor #1 (H13 steel anchor) for displacement between CFRP plate and barrel

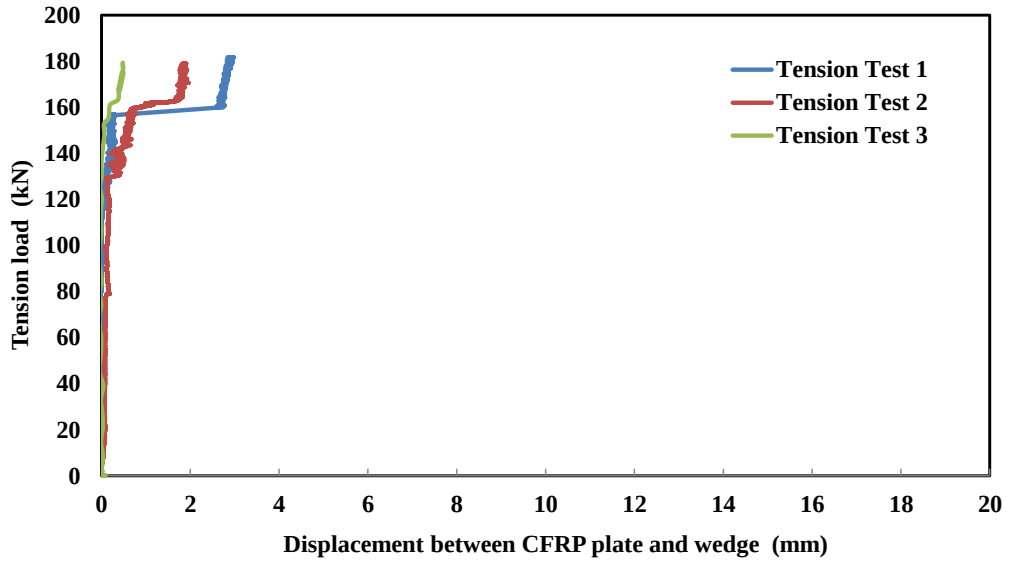

Figure 8.4: Tension load vs. displacement curve for the anchor #1 (H13 steel anchor) for displacement between CFRP plate and wedge.

Figure 8.5: CFRP plate did not move from the anchor (as shown in the circle) and wedges slid all the way to the end of barrel during the tension test.

8.2.3 Tension Test Results for the Stainless Steel Anchor (Anchor #2)

This section presents the tension test results of anchor #2, the 10 mm thinner and 1 kg lighter anchor. Three tension tests were carried out on the heat-treated stainless steel anchor #2. The anchor #1 was used to fix the CFRP plate at the bottom end. Figure 8.6a shows the relationship between the tension load and the displacement between the CFRP plate and the barrel; while Fig. 8.6b shows the relationship for the displacement between the CFRP plate and the wedges. As shown in Fig. 8.6a, the wedges slid all the way to the end of the barrel (16-17 mm, depending on the pre-setting distance). The CFRP plate and the sleeve together moved less than 2.73 mm (Fig. 8.6b). The ultimate tensile strength of anchor #2 was 183-194 kN, which was equal to 109-115% of the guaranteed tensile strength of the CFRP plate. The failure mode was the tensile rupture of the CFRP plate in the free length outside and away from the anchor.

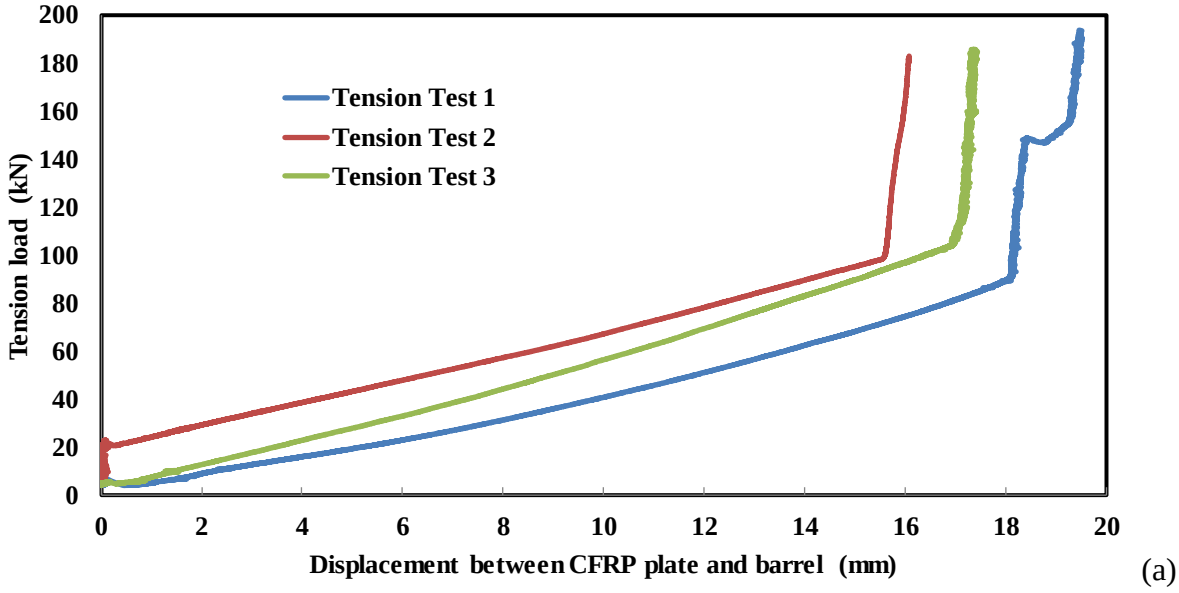

(a)

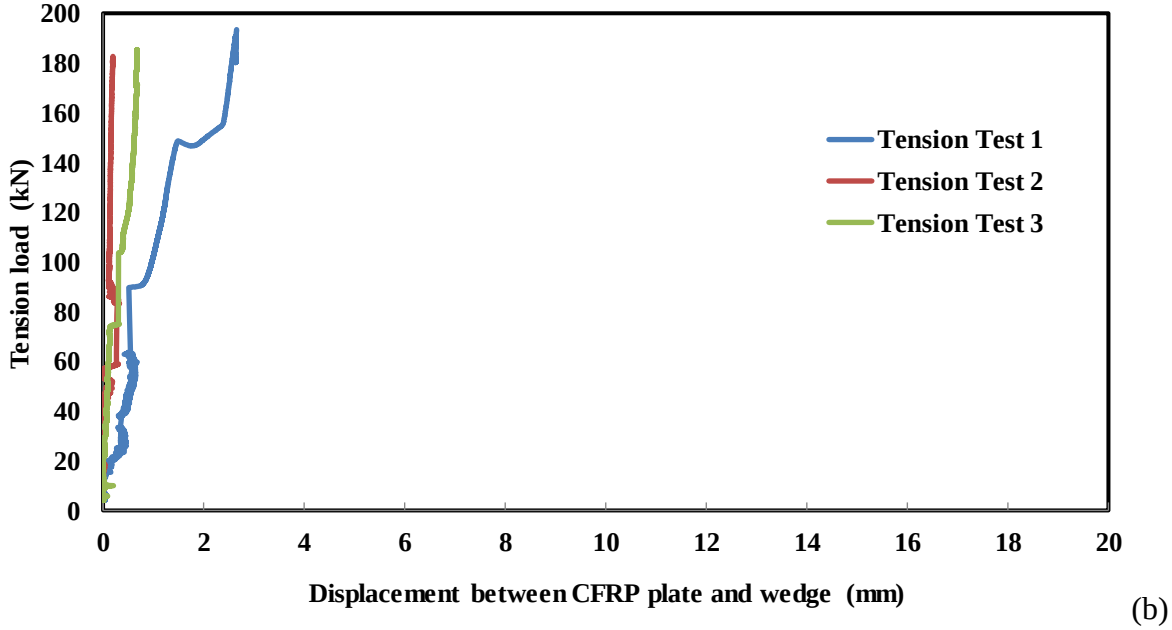

(b)

Figure 8.6: Tension load vs. displacement curve for the anchor #2 (stainless steel anchor) for displacement (a) between CFRP plate and barrel, and (b) between CFRP plate and wedge.

8.2.4 Test Results for Anchor #3 Testing 1.4 mm Thick High Modulus CFRP Plate

Four tension tests were carried out on the new anchor #3 for prestressing the 1.4 mm thick, high modulus (210,000 MPa) and a guaranteed tensile strength of 2,900 MPa (203 kN for 50 mm wide plate) CFRP plate. One test was conducted with 21-gauge (0.81 mm thick) annealed copper sleeves, and three tests were performed with 22-gauge (0.71 mm thick) annealed copper sleeves. In Fig. 8.7, the Tension Test 1 is the test with the 21-gauge sleeve, and the Tension Tests 2-4 represent the tests with 22-gauge sleeves.

With 21-gauge (0.81 mm thick) annealed copper sleeves, the ultimate tensile capacity of the anchor was 184 kN, which was 91% of the CFRP plate capacity (Tension Test 1 in Fig. 8.7). Using the thinner sleeve plate of 0.71 mm thick (22-gauge), the tensile capacity of the anchor was improved to 225-237 kN, which was equal to 111-117% of the guaranteed tensile strength of the 1.4 mm thick CFRP plate (2,900 MPa or 203 kN). The failure mode in all cases was the tensile rupture of the CFRP plate outside of the anchor in the free length.

Figure 8.7 illustrates the relationship between the tension force and the displacement between the barrel and the CFRP plate. The wedges slid 16-17 mm (Fig. 8.7). Only a small combined sliding distance of <3mm was measured for the CFRP plate and the sleeves during the tension tests. The sliding distance of the wedges was a function of the pre-setting distance before the tests.

These tests showed that although this 1.4 mm thick CFRP plate had a much higher tensile load capacity (203 kN) than the 1.2 mm thick CFRP plate (168 kN), the newly developed anchor #3 had a sufficient strength to prestress the 1.4 mm thick CFRP plate to 100% of its tensile capacity.

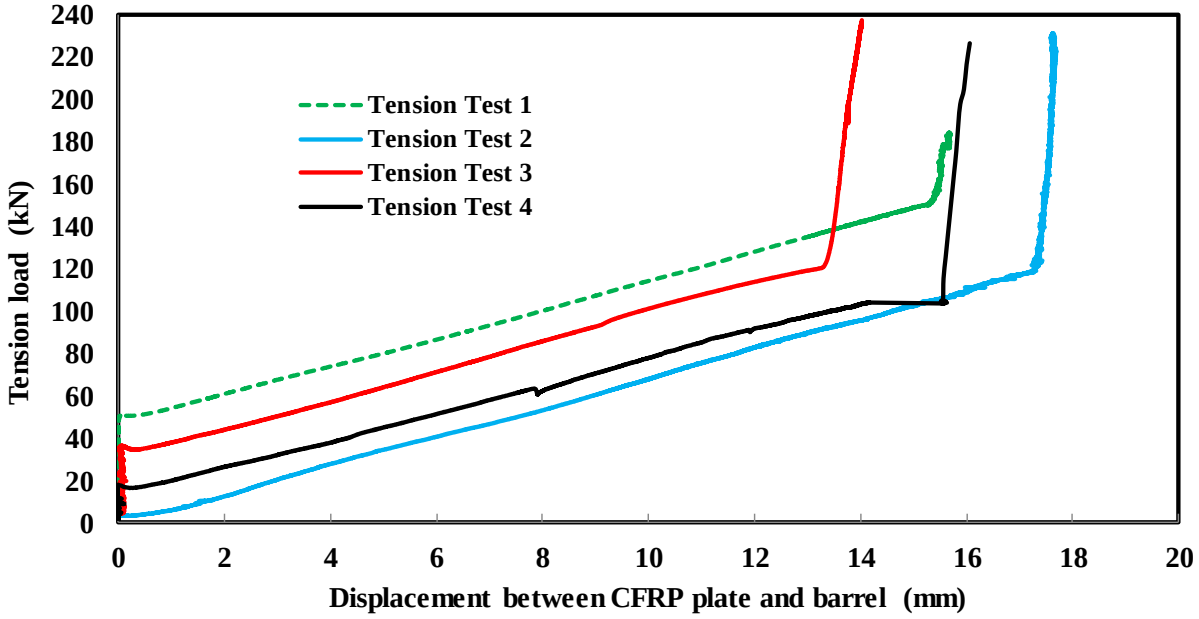

Figure 8.7: Tension load vs. displacement for anchor #3 with 1.4 mm thick CFRP plate for the displacement between the CFRP plate and the barrel.

8.2.5 Tension Test Results Using Clamping Anchor as Dead-End Anchor

Three tension tests were carried out on the new heat-treated H13 steel anchor #1 using a bolt-based clamping anchor at the dead-end (bottom end). The relationship of load vs. displacement of the CFRP plate relative to the barrel is shown in Fig. 8.8. The main component of displacement was the sliding of the wedges along the sleeve and the CFRP plate (4-7 mm) with respect to the barrel. From the mark on the CFRP plate and the sleeve, the CFRP plate and the sleeve had a negligible displacement (<5 mm) relative to the wedges. In these tests, the wedges did not slide to the end of the barrel in the test anchor. The wedges slid the least compared to the tension tests when the newly developed anchor was used as the bottom anchor as well, described in the prior sections. This was due to the lower tension capacity of the anchor system.

The testing anchor, with the bolted clamping anchor in the dead-end, carried a tensile load of 124 ± 20 kN, which was equal to 60-83% of the ultimate tensile strength of the CFRP plate (168 kN or 2,800 MPa). The failure mode was the tensile rupture of the CFRP plate just outside of the clamping bottom anchor. This was attributed to the stress concentration accumulated in the CFRP plate caused by the dead-end clamping anchor. In addition, during the application of torque (as high as 135 N.m) at the dead-end anchor before the test, the CFRP plate was twisted and some fibres cracked. Therefore, in order to avoid this premature failure in all subsequent tests, the newly developed anchor (anchor #1) was used as the bottom end anchor, as discussed in sections 8.2.2-8.2.4.

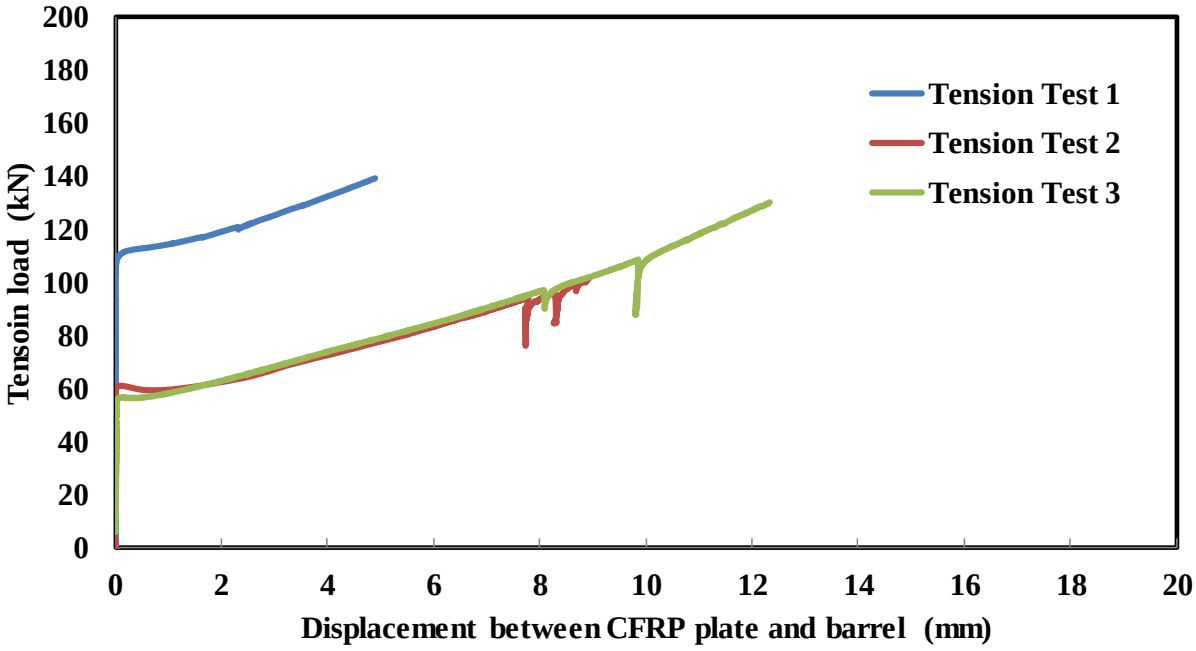

Figure 8.8: Tension load vs. displacement curve between the CFRP plate and the barrel using the clamping anchor at the bottom end.

8.2.6 Summary of Results

The summary of all of the tension test results of all of the anchors is shown in Tables 8.1 and 8.2. Table 8.1 shows the effect of different design parameters on the performance of anchor #1. The mean failure load of the anchor with no pre-setting was 190±6 kN. In the case of the anchor #1 with a high pre-setting, the mean failure load was 191±4 kN. The mean failure load of the anchor #1 with 50 mm wide wedges was found as 187±6 kN, while the mean failure load of the anchor #1 with 55.5 mm wide wedges was found as 177±9 kN. There were minor local damages during the tests of the anchors with 55.5 mm wide wedges (Table 8.1). The mean failure load of the anchor #1 was 187±6 kN, with the new anchor at the bottom end. On the contrary, when a clamping anchor was used as the dead-end anchor (bottom anchor), the anchor #1 failed at 124±20 kN, on average.

Anchor #1 was the 7 kg heat-treated H13 steel anchor and anchor #2 was the 6 kg heat-treated stainless steel anchor. Both anchor #1 and #2 were designed for the 1.2 mm thick CFRP plate. Anchor #3 was the heat-treated H13 steel anchor for prestressing the 1.4 mm thick high-modulus CFRP plate. The failure mode of all of these anchors was the tensile rupture of the CFRP plate at its free length outside of the anchor (Table 8.2). All of the anchors exceeded the guaranteed ultimate tensile capacity of the CFRP plate (168 kN for 1.2 mm thick CFRP plate and 203 kN for 1.4 mm thick CFRP plate). The mean failure load of the anchor #1 (187±6 kN) was same as the mean failure load of the anchor #2 (187±5 kN). In contrast, the mean failure load of the anchor #3 was significantly larger (231±6 kN) than both anchor #1 and #2. This was due to the larger thickness (1.4 mm) and strength (2,900 MPa) of the CFRP plate used in the anchor #3. Table 8.1 and 8.2 also shows the failure loads in terms of the percentage of the guaranteed ultimate tensile strength (GUTS) of the CFRP plate.

Table 8.1: Summary of tension test results for different design parameters in anchor #1

Testing criteria	Mean Failure Load (kN)	Failure Mode
No pre-setting	190±6 (113%)	Tensile rupture of CFRP plate
Regular pre-setting	180±1 (107%)	
High pre-setting	191±4 (114%)	
Full width (55.5 mm) wedges	177±9 (105%)	Tensile rupture of CFRP plate, local damage in barrel and wedge
Bolt-based clamping anchor at the bottom end	124±20 (74%)	Tensile rupture of CFRP plate just outside of bottom end anchor

Table 8.2: Summary of tension test results for all three new CFRP plate anchors

Anchor	Mean Failure Load (kN)	Failure Mode
Anchor #1	187±6 (111%)	Tensile rupture of CFRP plate
Anchor #2	187±5 (111%)	Tensile rupture of CFRP plate
Anchor #3	231±6 (114%)	Tensile rupture of CFRP plate

8.3 DISCUSSIONS

8.3.1 Mode of Failure

The failure mode in the tension tests for the three anchors was the tensile rupture of the CFRP plate outside of the anchor, as shown in Fig. 8.9. At the end of the tests, the CFRP plate broke suddenly in a brush mode and the fibres spread apart (Fig. 8.9). The safety box contained all of the fibres during this failure. A wooden piece placed on the tested anchor protected the anchor and the LVDTs from the sudden jumping of the anchor after the abrupt failure of the CFRP plate.

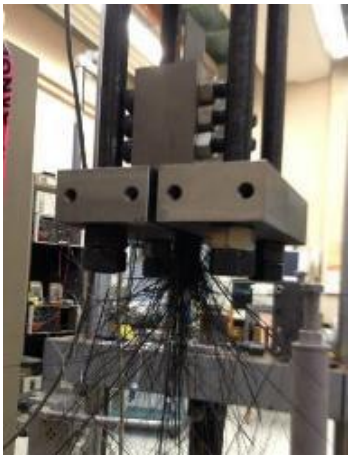

(a)

(b)

(c)

Figure 8.9: Tensile rupture of CFRP plate for (a) anchor #1, (b) anchor #2, (c) anchor #3.

Post-mortem investigation of the anchors illustrated that the two pieces of the barrel bent and moved away from each other slightly (0.95 mm), at the pre-setting end of the anchor barrel, as shown in Fig. 8.10. This was mainly to accommodate the larger wedges sliding through the smaller barrel opening. The bending of the testing anchor and the bottom anchor are shown in Fig. 8.10a and 8.10b, respectively. This spreading apart led to a larger tensile stress in the bolts connecting the barrel pieces; and it led to an elongation of the bolts, particularly the two bolts at the pre-setting end. The spreading apart of the two barrel parts and the elongation of the bolts allowed the wedges to slide through the barrel opening until it reached the steel base plate. Hence, the contact pressure on the CFRP plate stayed within the compressive strength of the plate, and this whole mechanism led the CFRP plate to carry load up to its ultimate tensile capacity of 2,800 MPa.


(a)

(b)

Figure 8.10: Bending of the two parts of the barrel after tension test: (a) testing anchor, and (b) bottom anchor.

The numerical model results, as shown in Chapter 5, show that the maximum von Mises stress in the barrel occurred at the barrel bolthole-bolt thread and the bolt-nut connections. A similar observation was made during the tension tests as well. In some tests, the threads of the bolts broke and they could not be re-used. Figure 8.11a shows the broken-thread bolts after tension test. Threads of grade 5 nuts broke in almost all tests and they could not be re-used (Fig. 8.11b).

Therefore, grade 8 nuts were used in the subsequent tests. However, grade 8 nuts broke at the pre-setting end of the anchor in some tests (Fig. 8.11b).

(a)

(b)

Figure 8.11: Threads of (a) bolts, (b) nuts broke during the tension tests.

During all of the tension tests, the annealed copper sleeves in the anchor were squeezed, flattened (Fig. 12a, b) and elongated towards the width (Fig. 12c) under the high contact pressure inside the anchor. As well, some carbon fibre debris from the CFRP plate accumulated on the sleeve surfaces (Fig. 12a). This was caused by the minor slippage (<3 mm) of the CFRP plate that occurred under 180+ kN tensile load (Fig. 8.12a, c) resulting in ploughing of the CFRP plate and carbon fibre debris accumulated on the annealed copper sleeve plates (Fig. 8.12a).

 (a)  (b)  (c)

Figure 8.12: (a) Annealed copper sleeve (in contact with CFRP plate) after the tension test; (b) the sleeve was squeezed; (c) the sleeve flattened and widened during the tension tests.

During the testing of anchor #3 with the 1.4 mm thick and high modulus CFRP plate, when the 21-gauge (0.81 mm thick) sleeves were used, the CFRP plate broke at a lower load (184 kN or 91% of the capacity of the 1.4 mm thick CFRP plate). In addition, the CFRP plate broke into a few longitudinal pieces (Fig. 8.13a) instead of the brush-mode failure. This was because of the large stress concentration on the CFRP plate inside the anchor with a thicker sleeve (Fig. 8.13b). The CFRP plates failed in the regular brush-mode, as described in Fig. 8.9, when a thinner (0.71 mm thick) sleeve was used.

 (a)

 (b)

Figure 8.13: The 1.4 mm thick CFRP plate broke at a lower load; and broke longitudinally into a few longitudinal pieces inside the anchor when 0.81 mm copper sleeve was used.

The effect of using one and two extra nuts in the pre-setting end of the bottom anchor on the displacement of the CFRP plate was examined. If two extra nuts were used at the bottom end anchor, the displacement of the wedges inside the barrel of the bottom anchor was less; and the ultimate strength of the anchor remained unchanged. Use of one extra nut caused a longitudinally differential displacement in the CFRP plate, and thus caused an unwanted premature failure of the CFRP plate.

8.3.2 Effect of Pre-Setting

Eight tension tests were carried out to investigate the effect of pre-setting using three levels of pre-setting. Three tests were conducted with high pre-setting (12.32 mm pre-setting or 5 mm of wedges were outside of the barrel). Three tests were performed with moderate pre-setting (0.32 mm pre-setting or 17 mm of wedges outside of the barrel). In addition, two tests were carried out without any pre-setting. The latter represented the most challenging condition of gripping the plate by relying on the self-seating of the anchor under tensile loading. In all three cases, the ultimate tensile strength of the anchor was more than 180 kN exceeding the guaranteed tensile strength of the CFRP plate (168 kN). The failure mode was the tensile rupture of the CFRP plate at its free length outside of the anchors in all cases (Fig. 8.9).

As shown in Fig. 8.14 and 8.15a, during high pre-setting, the anchor carried 120 kN of tension load without any slippage of wedges or any other components of the anchor. In the case of moderate pre-setting, the anchor carried 80 kN of tension load without any slippage. On the contrary, in the case of no pre-setting, the slippage of wedges (along with sleeve and CFRP plate) started from the beginning even before taking any tension load (solid line in Fig. 8.14 and 8.16a). In all three cases, the wedges (along with sleeve and CFRP plate) reached the end of the barrel and the steel base plate at around 150-160 kN tension load range, followed by the tension rupture of the CFRP plate above 180 kN load (Fig. 8.14).

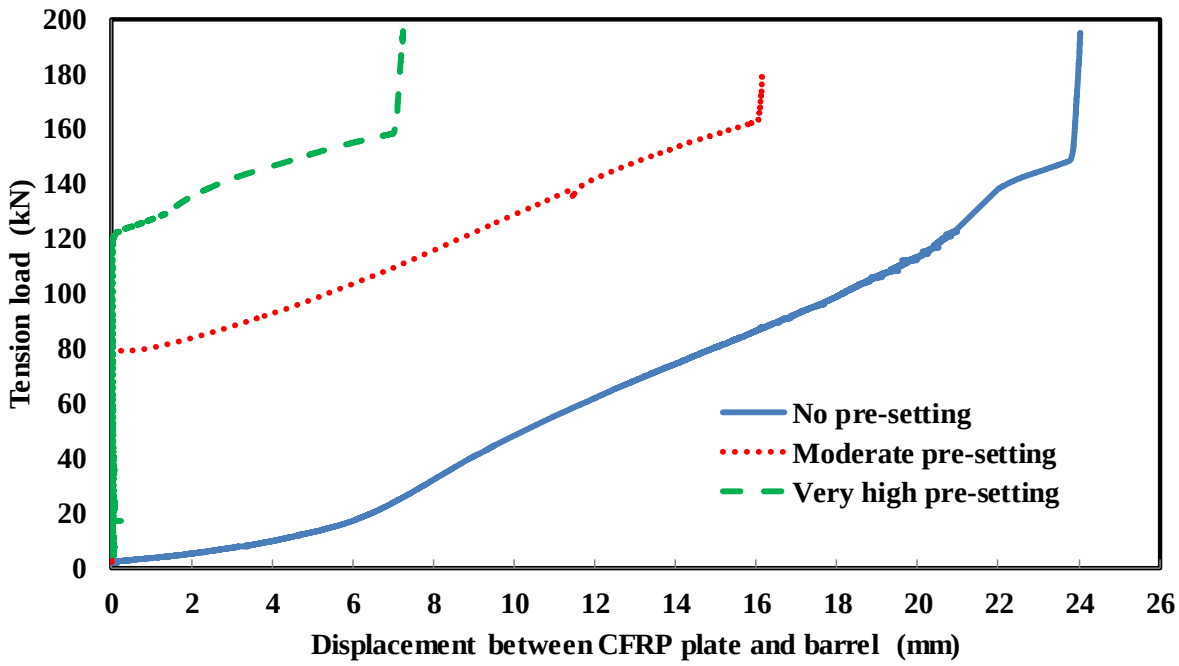

Figure 8.14: The effect of pre-setting distance on the performance of anchor #1 using three levels of pre-setting distances.

The tension load vs. displacement relationships for the high pre-setting (Fig. 8.15) and no pre-setting (Fig. 8.16) show that there was no significant effect of pre-setting on the ultimate tension load capacity of the anchor. In all of these tests, the failure load was more than 180 kN, which was more than the guaranteed tensile strength of the CFRP plate, and the failure mode was the tensile rupture of the CFRP plate. For high pre-setting, the failure load of the anchor was 189-196 kN, which was equal to 112-117% of the ultimate tensile strength of the CFRP plate. For no pre-setting, the anchors carried an ultimate tensile capacity of 185-195 kN, which was equal to 110-116% of the ultimate tensile strength of the CFRP plate. In both cases, no slip of the sleeve or the CFRP plate occurred (Fig. 8.15b and 8.16b).

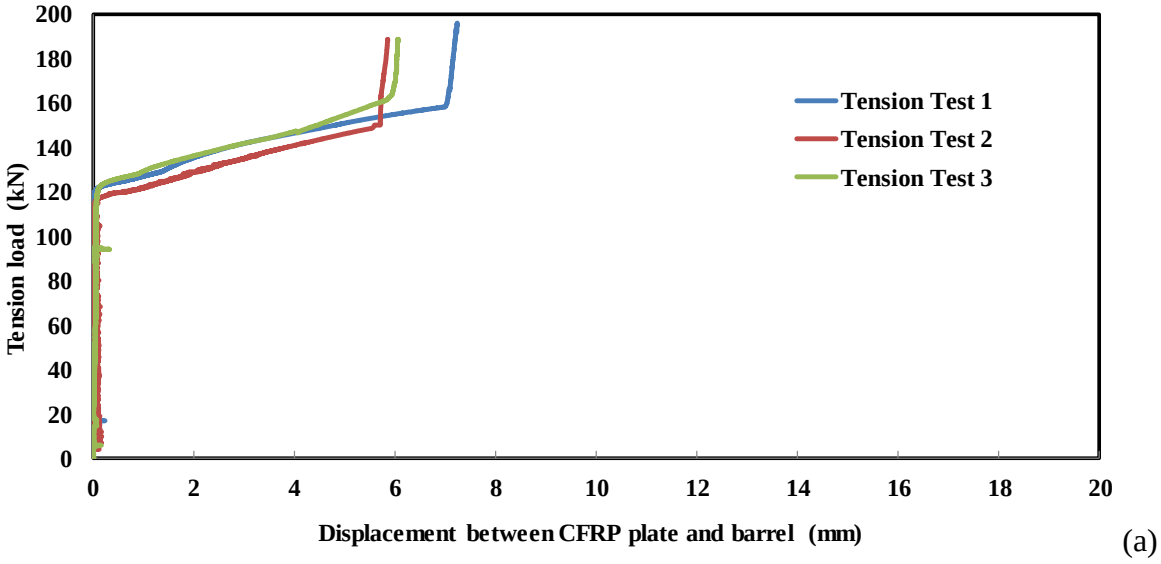

(a)

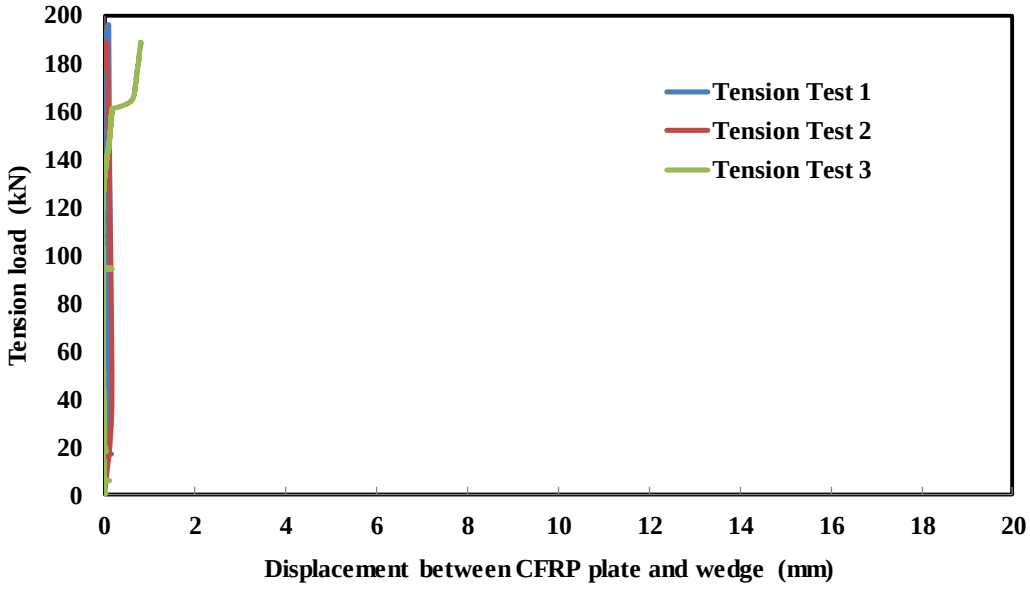

(b)

Figure 8.15: The effect of high pre-setting on the tension load capacity of anchor #1: for displacement between (a) CFRP plate and barrel, and (b) CFRP plate and wedge.

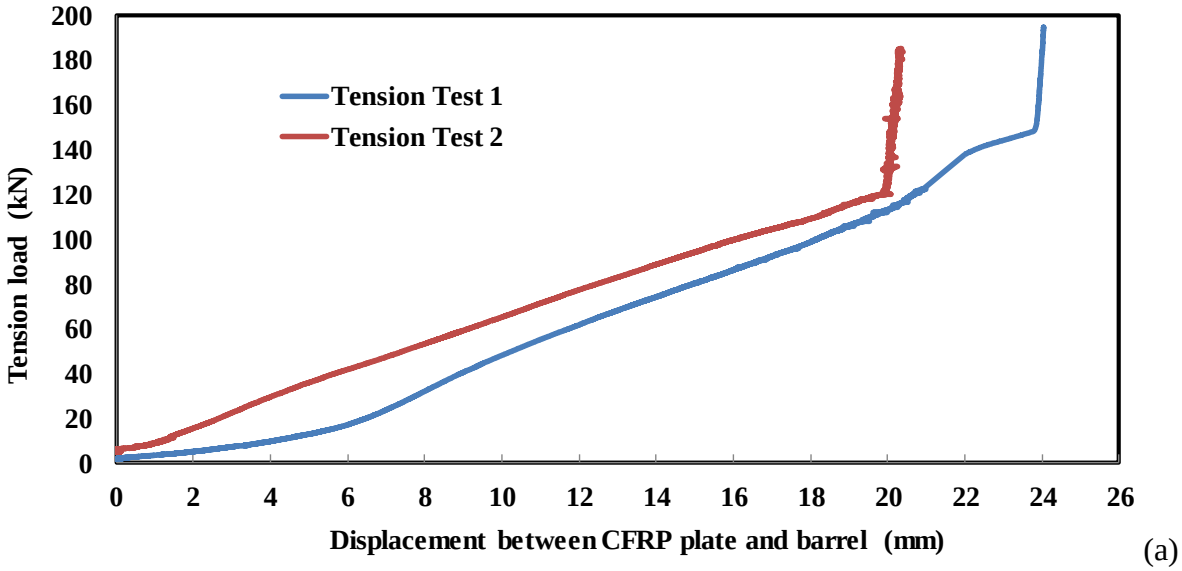

(a)

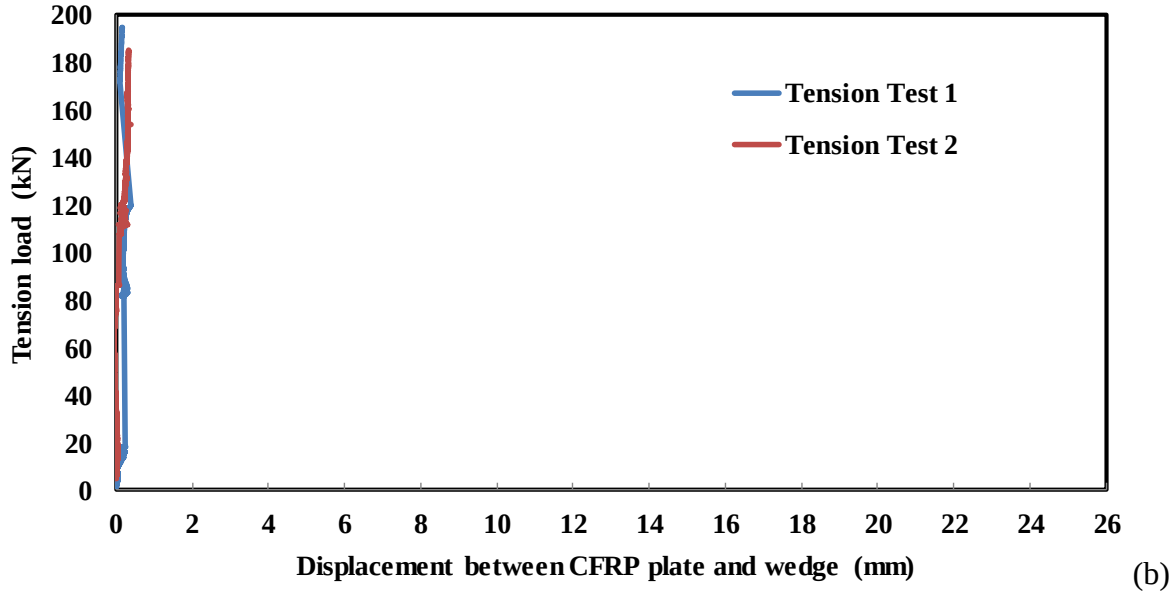

(b)

Figure 8.16: The effect of having no pre-setting on the tension load capacity of anchor #1: for displacement between (a) CFRP plate and barrel, and (b) CFRP plate and wedge.

When no pre-setting was used, the wedges were hammered inside the anchor; and the anchor still carried a load more than the ultimate tensile strength of the CFRP plate. This shows that there is no requirement of using an expensive pre-setting rig machine at the construction site

in order to install this anchor. This is a significant improvement in the construction industry using the CFRP plate, since all of the existing anchors require an additional costly pre-setting machine for the installation of the anchor at the site.

8.3.3 Effect of Width of Wedges

Three tests were carried out to investigate the effect of full width (55.5 mm wide) wedges on the anchor performance. The pre-setting force required for the regular pre-setting (17 mm of wedge outside of barrel) was 113.5 kN when 55.5 mm wide wedge was used in the anchor. This was significantly higher than that of the anchor with 50 mm wide wedges (37 kN).

Figure 8.17 shows the tension force vs. displacement for the anchor with 55.5 mm wide wedges. In this anchor, the wedges slid all the way to the end of the barrel, similar to the reduced wedge width anchor (Fig. 8.17a). However, the sleeves and the CFRP plate together slid 2-4 mm, which was slightly larger than that of the anchor #1 (Fig. 8.17b). This was due to the extra friction surface area between the barrel and the two wedges.

The average failure load in this anchor #1 with 55.5 mm wide wedges was 177±9 kN, which was less than the average failure load with 50 mm wide wedges (187±6 kN), but more than the guaranteed tensile strength of the CFRP plate (168 kN). This was primarily due to the localized stress concentration at the barrel-wedge interface at the pre-setting end, and thus on the CFRP plate inside the anchor at the pre-setting end (Fig. 8.18 and 8.19). Wider wedges caused localized stress concentrations in both the barrel and the wedges in the pre-setting end at the barrel-wedge interface, particularly in the two corners, as shown by the circles in Fig. 8.18 (wedges) and Fig. 8.19 (barrel). Under 2,800 MPa tensile loading, the wedges, the sleeves and the CFRP plate were under high contact pressure and expanded in the lateral direction. These caused the stress concentration at the two sides at the pre-setting end where the ratio of the wedge thickness and the barrel opening was the highest and there was no open space to expand. A larger gap between the barrel sidewalls and wedge sidewall could solve this issue. But a

larger gap would increase the corrosion potential of the anchor and the weight of the anchor; and a larger radius transverse curve in the barrel and the wedge would increase the total weight of the anchor. Although there were local damages in both wedges and barrel; the anchor still achieved a tensile capacity of 101-111% of the ultimate tensile strength of the CFRP plate. The failure mode of the anchor was the tensile rupture of the CFRP plate in its free length just outside of the testing anchor.

The advantage of using the full width (55.5 mm wide) wedge was to close the gap between the wedge and the barrel and consequently, to reduce the risk of corrosion in this anchor. Furthermore, since there was no gap, there was no requirement of using the extra neoprene spacers, and it was easier to keep the wedges straight and aligned inside the barrel. Although there were these advantages, since there were some minor local stress concentrations (Fig. 8.18, 8.19) in this anchor with the full width wedges, and since the 3 mm gap led to a lower anchor weight, the anchor #1 with 50 mm wide wedges was a more suitable design option.

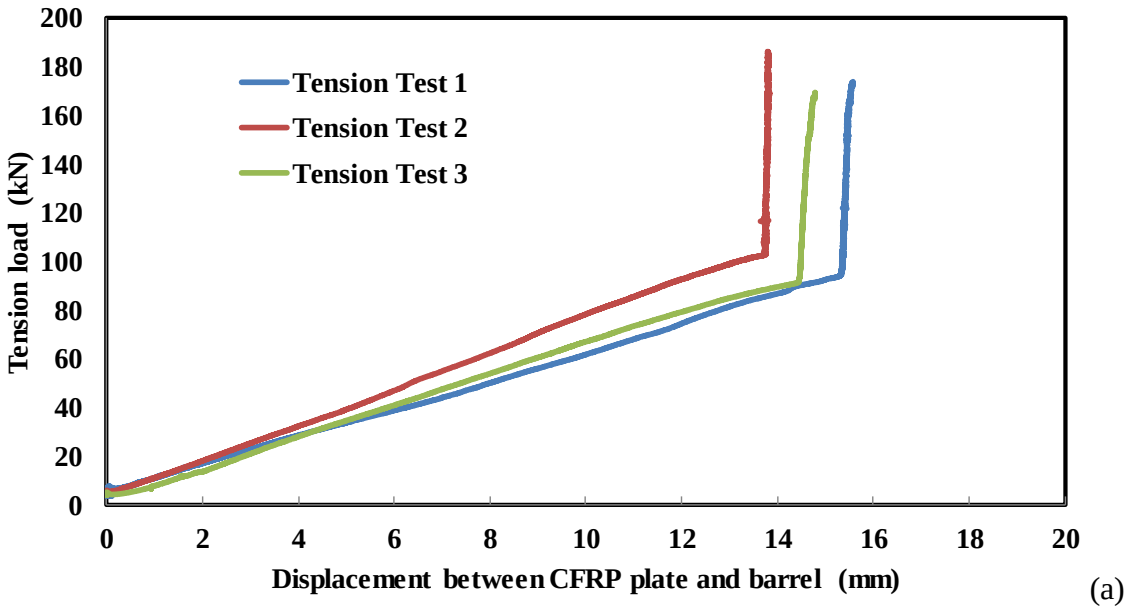

(a)

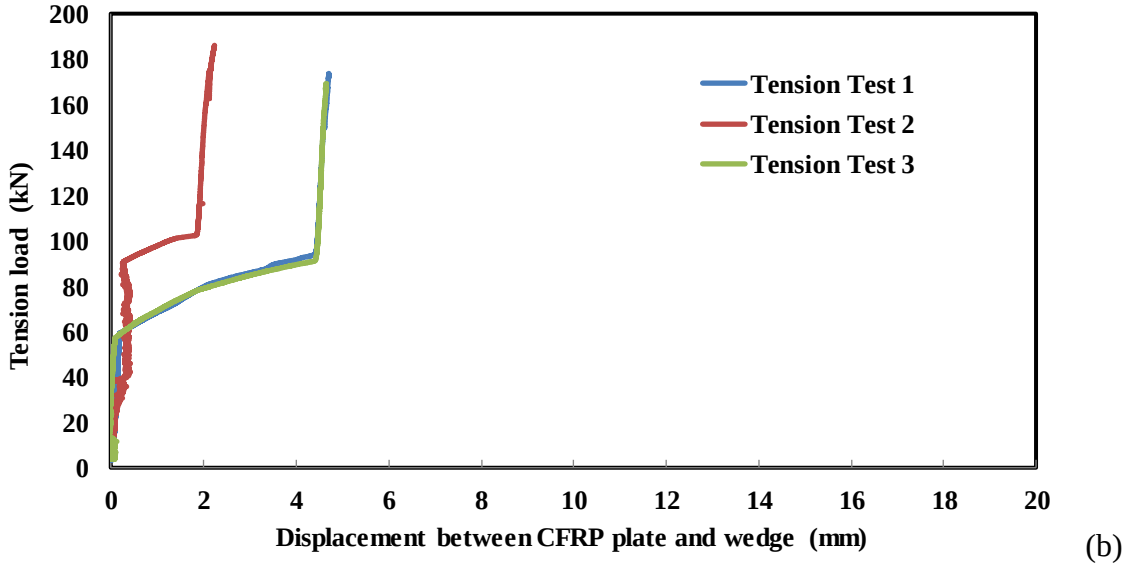

(b)

Figure 8.17: The tension load vs. displacement curve for anchor with 55.5 mm wide wedges for displacement between (a) CFRP plate and barrel, and (b) CFRP plate and wedge.

Figure 8.18: Local damage in the wedges of the anchor in the pre-setting end after test for the H13 steel anchor # 1 with 55.5 mm wide (full width) wedges.

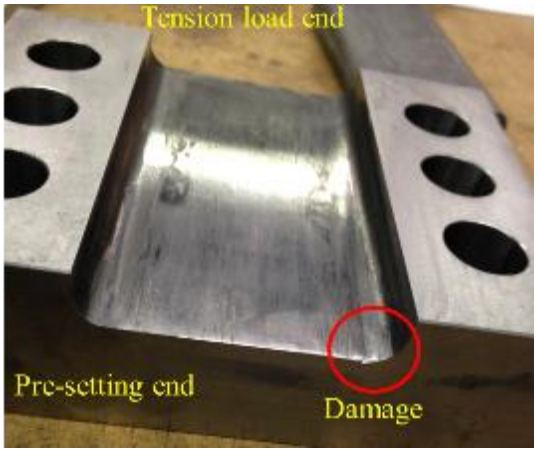

Figure 8.19: Local damage in the barrel of the anchor in the pre-setting end after test for the H13 steel anchor #1 with 55.5 mm wide (full width) wedges.

8.3.4 Effect of the Bottom End Anchor

At the early stage of the test program, a clamping anchor was used at the lower end opposite to the investigated anchor (anchor #1). Pre-mature failure occurred at 60-83% of the ultimate capacity of the CFRP plate. During these tests, a significant stress concentration accumulated in the loading end of the CFRP plate from the dead-end clamping anchor. In addition, during

the application of torque (as high as 135 N.m) at the dead-end anchor before the test, the CFRP plate was twisted and some fibres in the CFRP plate cracked. Both of these matters contributed and led to an early rupture of the CFRP plate. Therefore, the clamping anchor was replaced by the designed anchor (Anchor #1). The ultimate capacity of anchor #1 increased significantly to 111% of the ultimate capacity of the CFRP plate by using anchor #1 at both ends of the plate. Based on this performance, anchor #1 was used as the bottom end anchor in all of the subsequent tests.

8.3.5 Effect of Wedge Roughness

The effect of roughness of the wedge surfaces on the anchor performance was investigated by performing one tension test with machined rough surface wedges and the results were compared to the tests with regular wedges with a sandblasted surface. The wedges had the roughness as a result of the manufacturing process. The direction of the roughness was perpendicular to the tension load direction (Fig. 8.20). During the tension test of the anchor with these rough surface wedges, the rough surface wedges had a strong grip on the soft annealed copper sleeves. Hence, there was no displacement between the wedge and the sleeve in the anchor. On the contrary, the CFRP plate slid 9.23 mm out of the testing anchor above 134.57 kN, which was 80% of the ultimate tensile strength of the CFRP plate.

After the wedges reached the steel base plate of the tension test machine, there was absolutely no slippage of the sleeves with respect to the very rough wedges. At this stage, instead of the CFRP plate carrying the additional tension load and instead of the tensile rupture of the CFRP plate at more than 100% tension load, the CFRP plate slid with respect to the sleeves, and the CFRP plate slid out of the anchor at 80% tension load level.

Given the poor performance of this anchor, the wedges with machined rough surface were not used in the subsequent tests for all of the three anchors and the wedges with a sandblasted surface were used instead.

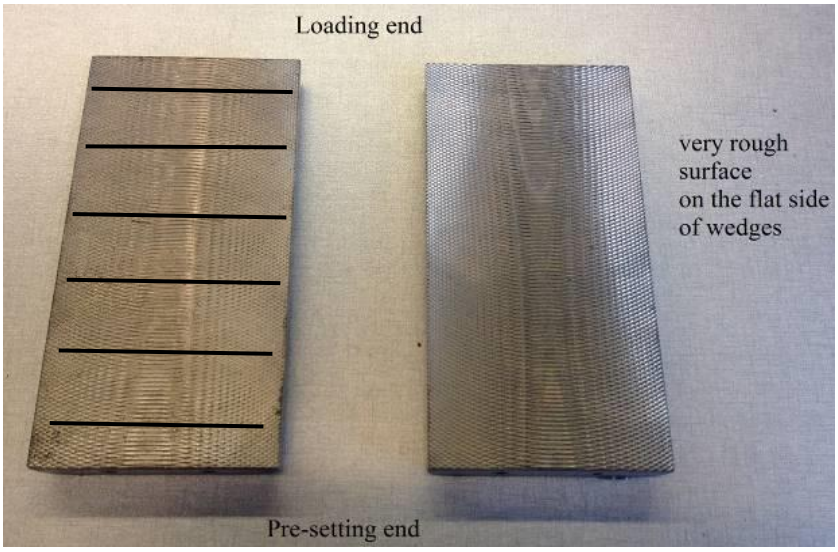

Figure 8.20: Very rough surface on the flat side of the wedges to increase coefficient of friction between wedge and sleeves.

8.3.6 Effect of Load Rate

The effect of load rate on the performance of the anchor is important factor, considering a potential accidental high loading rate in the construction site. The loading rate during the tension test was examined and there was no effect on the anchor performance. Two load rates were tested: a slower load rate of 0.6 mm/min (0.01 mm/sec) and a faster load rate of 4 mm/min. The mean ultimate tensile load for the anchor #1 with 0.6 mm/min load was 180.38 kN; and the capacity of the anchor with 4 mm/min load rate was 179.35 kN. In both cases, the failure mode of the anchor was the tensile rupture of the CFRP plate outside of the anchor. In both cases, the wedges slid all the way to the barrel end and the CFRP plate slid only a small distance (1-3 mm). Therefore, there was no significant effect of the load rate on the anchor performance and the anchor design is safe at a potential accidental high loading rate.

8.4 COMPARISON WITH THE NUMERICAL MODEL RESULTS

This section presents a comparison between the numerical modelling and the experimental investigation results for the bolted anchor #1 (Fig. 8.21). Since lubricant with a low coefficient of friction was used at the barrel-wedge interface during the tension tests, in order to simulate a similar behaviour for the anchor in the numerical model, a coefficient of friction of 0.01 was used at the barrel-wedge interface in the numerical model [114], [148]. In the numerical analysis, a 3 mm pre-setting was applied to the wedge. Subsequently, 1 mm tension displacement was applied in each loading step; and the longitudinal stress in the CFRP plate was recorded. The tension load-displacement curve obtained from the numerical analysis for the anchor #1 was compared to the test results (Fig. 8.21). The numerical model results show that the anchor #1 had a capacity of 186 kN for a total displacement of the wedge, the sleeve and the CFRP plate (self-seating distance) of 16 mm. From the experimental results, the tensile capacity of the anchor #1 was found as 181 kN along with a total displacement of 16.14 mm. Therefore, the numerical model and the experimental results for the bolted anchor #1 exhibited a similar tensile strength of the anchor for a similar total displacement (Fig. 8.21).

In the theoretical numerical model, at the beginning of the analysis, the wedges were already in place at 17.32 mm away from the pre-setting end of barrel. Therefore, the initial tension load after the pre-setting load at the beginning of the load-displacement curve was small (25 kN at Fig. 8.21). On the contrary, in the tension tests, in order to put the wedges at that location (17.32 mm away from the pre-setting end of the barrel), some pre-setting force was required to push the wedges. This was due to the presence of local asperities and irregular shapes generated from the cutting process and the manufacturing process of the anchor components. This pre-setting load led the anchor to carry some tension load at the beginning (80 kN in Fig. 8.21). The reason behind the slight difference at the end of the two curves (at 16 mm displacement in Fig. 8.21) was that there was a steel base plate under the anchor during the tension tests for safety; and the wedges could not slide anymore after reaching the base plates.

On the contrary, there was no boundary conditions for the wedges at this level in the numerical model; therefore, the wedges were allowed to slide even after reaching the base plate level. This led to the slightly different curve shape at 16 mm displacement level in Fig. 8.21.

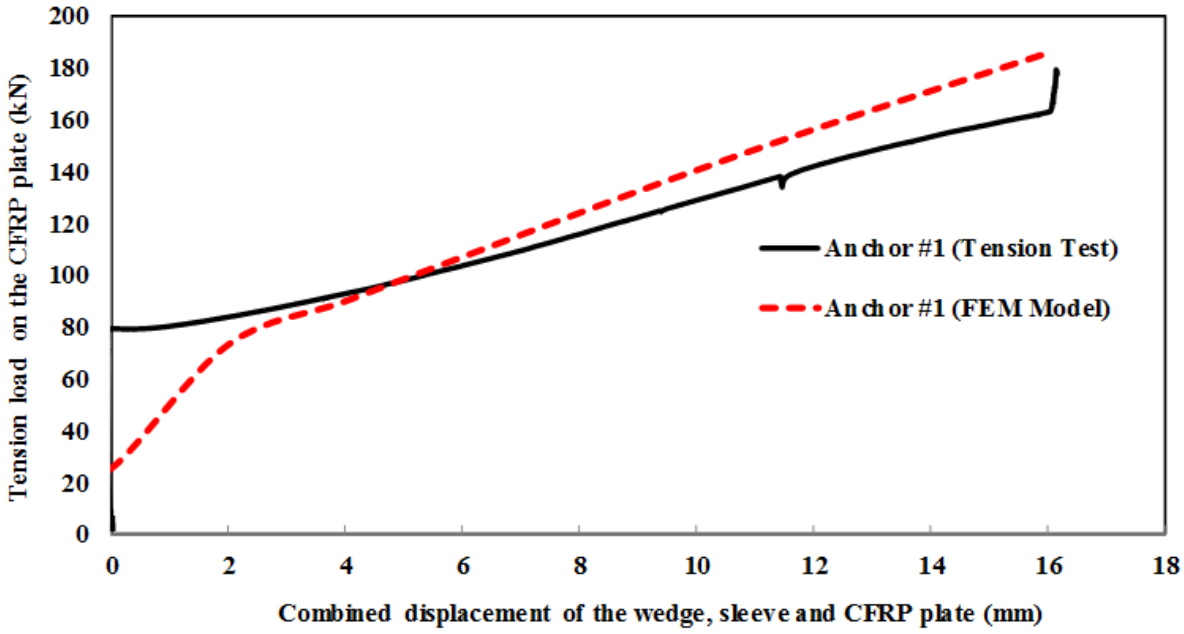

Figure 8.21: Comparative tension load vs. displacement curve from the numerical modelling and the experimental investigation results for anchor #1.

A similar tension load-displacement relationship was also obtained for both anchor #2 and anchor #3 from both the FEM numerical model and the experimental investigation results.

Since both the practical strength and displacement values matched with the theoretical strength and displacement values given by the numerical model results, the experimental study validated the numerical model results.

8.5 SUMMARY

The test results showed that all three anchors had a strength of more than 2,800 MPa, which was the guaranteed tensile strength of the CFRP plate, given by the manufacturer. The failure mode of all of the anchors was the tensile rupture of the CFRP plate outside of the anchor at the free length. There was no significant slippage of the CFRP plate or the sleeve in the anchor under loading. In some cases, some of the anchor nuts and bolt threads were damaged. Several design parameters were investigated in this test program to explore their effect on the anchor performance. The parameters included the pre-setting load, the width and the roughness of the wedges, two types of dead-end anchorage, the load rate, and the effect of the CFRP plate thickness and modulus of elasticity. It was also determined that the new anchors did not require any extra pre-setting equipment for its installation at site. Manual hammering of the wedges inside the anchor was sufficient for the anchor to carry the required load. Both the 1.2 mm thick CFRP plate with 2,800 MPa tensile strength and 165,000 MPa modulus of elasticity and the 1.4 mm thick CFRP plate with 2,900 MPa tensile strength and 210,000 MPa modulus of elasticity were successfully tested using the new anchors. For corrosion resistance, the heat-treated stainless steel anchor was developed and also successfully tested for the tensile capacity. Through these experimental studies, the numerical model was validated. Finally, through these experimental studies, the practical applicability of the newly developed anchors was shown.

CHAPTER 9
CONCLUSIONS AND RECOMMENDATIONS

9.1 GENERAL

This thesis describes the friction test, the analytical and numerical analysis, the parametric study and optimization, the 3-D printing, the material selection and manufacturability study, and the experimental investigation of three innovative, mechanical, epoxy-free, high-strength, prestressing anchors for CFRP plates. Based on the literature review, there was no high-strength anchor available for the commercially available and popular 50 mm wide CFRP plates. There were several disadvantages in all of the available CFRP plate anchors including low strength, long waiting time, long anchor-length, not being reusable, heavy weight, and requirement of heat-treatment machine at site. Therefore, the development of new effective CFRP plate anchors was required and carried out in this research.

The major applications of this new CFRP plate anchor include: (1) the new construction and the repair, rehabilitation and retrofitting of aging infrastructure by prestressing CFRP plate reinforcement in corroded bridges, buildings, tunnels, dams, marine structures and other structures; (2) the design of lighter and more fuel-efficient cars, ultra-high-speed trains, airplanes and satellites; and (3) a wider use of different composite materials in different industries (*e.g.*, automotive, aviation, space and shipbuilding industries).

The new CFRP plate anchors were developed for the popular 50 mm wide and 1.2-1.4 mm thick CFRP plates. To develop the new anchor, friction tests were carried out to investigate the tribological behaviour and the coefficient of friction values between the CFRP plate and two types of copper plates: as-received and annealed. A mathematics-based analytical model was developed to predict the contact pressure distribution on the CFRP plate inside the anchor under loading using Maple software. Several FEM models of the new anchors were created and analyzed for different design parameters using Abaqus software. A detailed parametric

study was performed using the numerical model to optimize the anchor design. For ease of manufacturing of the anchor, the numerical model was further updated and analyzed to incorporate anchor bolts. A numerical model for a corrosion-resistant anchor, made of stainless steel, was also created and analyzed. An experimental study on the three newly developed anchors was carried out to determine the tensile strength and the failure mode; and to show the capability of the new anchors to carry the high tensile load. A series of tension tests was also carried out on the anchor #1 to investigate the effects of different design parameters on the anchor performance.

9.2 SUMMARY AND CONCLUSIONS

The research work was conducted in four major steps: friction tests, analytical modelling, numerical modelling and tension tests. Through this research, the following conclusions were reached.

9.2.1 Friction Tests

- The frictional behaviour of CFRP plates in contact with as-received and annealed copper plates was characterized experimentally within the contact pressure range of 50-175 MPa.
- Within the 50-175 MPa contact pressure range, the static coefficient of friction between the CFRP plate and the as-received copper plate was found as 0.31.
- The static coefficient of friction between the CFRP plate and the annealed copper plate decreased from 0.39 to 0.30 with the increase of contact pressure from 50 MPa to 175 MPa.
- The softer annealed copper plates exhibited a higher coefficient of friction value (0.30-0.39) than the harder as-received copper plates (0.30-0.31) in the 50-175 MPa contact pressure range.

- For the as-received copper plate, the shear stress vs. normal stress (contact pressure) relationship obtained at the contact pressure range of 50 MPa-175 MPa was: $\tau = 0.31\sigma$.
- For the annealed copper plate, the shear stress vs. normal stress relationship obtained at the contact pressure range of 50 MPa-175 MPa was: $\tau = 1.02\ \sigma^{0.76}$.

9.2.2 Mathematics-based Analytical Modelling

- A unique analytical model was created to predict the contact pressure distribution on the CFRP plate inside the anchor under loading.
- It showed that the contact pressure was the maximum at the pre-setting end and the minimum at the tension load end of the anchor in all anchor components.
- The analytical model also quantified the preliminary barrel thickness as a starting point for the detailed numerical modelling and optimization of the anchor design.

9.2.3 FEM-based Numerical Modelling

- Finite element numerical models of the three new anchors were developed.
- The longitudinal profile radius of the barrel and the wedge, the length of the barrel and the wedge, the thickness of the barrel and the wedge, the pre-setting distance and the interference distance between the barrel and the wedge at the loading end had significant effects on the anchor performance.
- Based on the numerical model results, in all anchor components, the maximum contact pressure was at the pre-setting end and the minimum contact pressure was at the tension load end of the anchor.
- The contact pressure on the CFRP plate increased significantly with the increase of pre-setting distance; and decreased significantly with the increase of the anchor-length.
- The location of the peak contact pressure on the CFRP plate moved towards the pre-setting end with the increase of the longitudinal curve radius of the barrel and the wedge.

- Under a specific tensile loading, the contact pressure on the CFRP plate increased with the increase of the interference distance between the barrel and the wedge; and decreased with the increase of the thickness of the barrel and the wedge.
- The von Mises stress on the barrel increased significantly with the increase of the pre-setting distance; decreased significantly with the increase of the length of the anchor and the thickness of the barrel, under a specific tensile loading.
- There was no slip of the CFRP plate from the anchor under 2,800 MPa tension load.
- Based on the parametric analysis and the optimization study results and considering the manufacturability, the final design of the CFRP plate anchor (anchor #1), made of heat-treated H13 steel with bolts, was selected with the following parameters: a longitudinal curve radius of 3,000 mm, an interference distance of 0.05 mm, an anchor-length of 100 mm, a minimum barrel thickness of 25.93 mm at the pre-setting end, a transverse curve radius of 6 mm for both barrel and wedge, a barrel sidewall thickness of 35 mm, and a minimum wedge thickness of 8.05 mm at the loading end.
- A second bolted anchor (anchor #2), made of heat-treated stainless steel, with a minimum barrel thickness of 20.93 mm at the pre-setting end, a longitudinal curve radius of 3,000 mm, an interference distance of 0.05 mm, an anchor-length of 100 mm, a transverse curve radius of 6 mm for both barrel and wedge, a barrel sidewall thickness of 35 mm, and a minimum wedge thickness of 8.05 mm at the loading end, was selected as an optimum anchor design, particularly as the corrosion-resistant option.
- A third bolted anchor (anchor #3) similar to the anchor #1, made of heat-treated H13 steel and a 22-gauge annealed copper sleeve, was selected for prestressing the 1.4 mm thick high modulus CFRP plates.

9.2.4 Experimental Investigations on the Three New Anchors

- The tension test results showed that all of the three anchors had a strength of more than 100% of the guaranteed ultimate tensile strength of the CFRP plate.
- The average failure load was 187±6 kN, 187±5 kN and 231±6 kN for anchor #1, #2 and #3, respectively.
- The failure mode of all of the anchors was the tensile rupture of the CFRP plate in the free length outside of the anchors.
- There was no significant slip of the CFRP plate or the sleeves in the anchor under the failure loading.
- It was also determined that a manual hammering of the wedges inside the anchor was sufficient for the anchor to carry the high load.
- This experimental study results validated the numerical model results of the anchors.
- Finally, through this experimental study, the practical applicability of the newly developed anchors was shown.

9.2.5 Summary

The primary contribution of this research work is that three innovative mechanical anchors were developed, analyzed, optimized, manufactured and tested for prestressing the 50 mm wide CFRP plates. The anchor #1 was developed to prestress the 1.2 mm thick and 165,000 MPa modulus of elasticity CFRP plates. The anchor #2 was the corrosion-resistant option for prestressing the 1.2 mm CFRP plates. The anchor #3 was developed for prestressing the 1.4 mm thick and 210,000 MPa modulus of elasticity CFRP plates. All of the three anchors were capable of carrying a load more than 100% of the guaranteed ultimate tensile strength of the CFRP plate with no significant slip of the CFRP plate from the anchor.

9.3 RECOMMENDATIONS FOR FUTURE STUDY

Based on the findings in this thesis, there are many interesting opportunities in the areas of structural engineering and materials for further investigation. The potential future research originating from this PhD are as follows:

- An experimental investigation (fatigue test) can be carried out to determine the fatigue life of the newly developed anchors under different stress conditions. The stress vs. number of cycles (S-N) curve and the strain vs. number of cycles (ε-N) curve for the anchors can be developed.
- The behavior of the anchor under a long term (10-15 years) [6] load can be studied to monitor and predict long term characteristics of the anchor.
- A study on the wedge and CFRP plate slip behaviour under repeated (fatigue) loads and under sustained long term load can be investigated experimentally.
- An experimental study of the anchor performance using shims or adjustable (moveable) anchors should be performed.
- An experimental study of the anchor performance with the application of force seating of the wedges inside the "live end" anchor should be conducted with two of the newly developed anchors installed in concrete beams.
- The development of an anchor connection system to attach the newly developed anchor systems to the structure in both external bonded (EB) and near surface mounted (NSM) methods in concrete structures and also in the steel structures can be studied.
- Similar other anchors can also be developed for the other commercially available composite materials.
- The resiliency of the new anchor under extreme conditions, *e.g.*, corrosion, nuclear radiation, acid-attack, alkali-attack, sulphate attack, vibrating condition, freeze-thaw, extreme cold temperature and high temperature, can be experimentally investigated.

- Another promising avenue of research is the investigation of the performance of components of super tall building structures made of prestressed ultra-high-strength concrete and prestressed CFRP plate reinforcement using the new CFRP plate anchors for both static and dynamic wind, earthquake, aircraft impact and tornado-generated missile impact loads.

REFERENCES

[1] S. Mirza, "Danger Ahead: The coming collapse of Canada's municipal infrastructure, A Report for the Federation of Canadian Municipalities," 2007.

[2] R. Reid, "The Infrastructure Crisis," *Civil Engineering Magazine*, 2008.

[3] F. M. Mohee, A. Al-Mayah, and A. Plumtree, "Anchors for CFRP plates: State-of-the-art review and future potential," *Compos. Part B Eng.*, vol. 90, pp. 432–442, 2016.

[4] H. N. Garden and L. C. Hollaway, "An experimental study of the influence of plate end anchorage of carbon fibre composite plates used to strengthen reinforced concrete beams," *Compos. Struct.*, vol. 42, pp. 175–188, 1998.

[5] T. C. Triantafillou and N. Deskovic, "Prestressed FRP Sheets as External Reinforcement of Wood Members," *J. Struct. Eng.*, vol. 118, no. 1843, pp. 1270–1284, 1992.

[6] J. Michels, E. Martinelli, C. Czaderski, and M. Motavalli, "Prestressed CFRP Strips with Gradient Anchorage for Structural Concrete Retrofitting: Experiments and Numerical Modeling," *Polymers (Basel).*, vol. 6, no. 1, pp. 114–131, Jan. 2014.

[7] J. Rytter, G. Portnov, and V. Kulakov, "Anchoring and a load transfer technique in uniaxial tension of unidirectional high-strength composites," *Mech. Compos. Mater.*, vol. 41, no. 3, pp. 217–228, 2005.

[8] G. G. Portnov, V. L. Kulakov, and a. K. Arnautov, "Grips for the transmission of tensile loads to a FRP strip," *Mech. Compos. Mater.*, vol. 49, no. 5, pp. 457–474, 2013.

[9] S. L. Burtscher, "Wedge Anchorage for CFRP Strips," no. August, pp. 446–453, 2008.

[10] ACI440, *Report on Fiber-Reinforced Polymer (FRP) Reinforcement*. 2007.

[11] D. S. Avery, D.P., Samborsky D.D., Mandell, J.F., Cairns, "Compression Strength of Carbon Fibre Laminates Containing Flaws with Fibre Waviness," in *Proceedings ASME Wind Energy Symposium*, 2004, pp. 54–63.

[12] ACI, "ACI 440.1R-06 : Guide for the Design and Construction of Structural Concrete

Reinforced with FRP Bars : Reported by ACI Committee 440," 2006.

[13] CNR, "Guide for the Design and Construction of Externally Bonded FRP Systems for Strengthening Existing Structures," 2004.

[14] ISIS, *FRP Rehabilitation of Reinforced Concrete Structures - Design Manual 4*, no. 4. ISIS Canada Research Network, 2008.

[15] M. Motavalli, "FRP Strengthening of Masonry," in *Fibre Composites, FS12*, 2004.

[16] Fib, *Externally bonded FRP reinforcement for RC structures*. Federation Internationale du Beton, Switzerland, 2001.

[17] H. Ku, H. Wang, N. Pattarachaiyakoop, and M. Trada, "A review on the tensile properties of natural fiber reinforced polymer composites," *Compos. Part B Eng.*, vol. 42, no. 4, pp. 856–873, Jun. 2011.

[18] V. Dhand, G. Mittal, K. Y. Rhee, and D. Hui, "A short review on basalt fiber reinforced polymer composites," *Compos. Part B Eng.*, no. December, Dec. 2014.

[19] V. Fiore, T. Scalici, G. Di Bella, and a. Valenza, "A review on basalt fibre and its composites," *Compos. Part B Eng.*, vol. 74, pp. 74–94, Jan. 2015.

[20] C. E. Bakis *et al.*, "Fiber-Reinforced Polymer Composites for Construction—State-of-the-Art Review," *J. Compos. Constr.*, vol. 6, no. 2, pp. 73–87, May 2002.

[21] G. Koronis, A. Silva, and M. Fontul, "Green composites: A review of adequate materials for automotive applications," *Compos. Part B Eng.*, vol. 44, no. 1, pp. 120–127, Jan. 2013.

[22] L. . Hollaway, "The evolution of and the way forward for advanced polymer composites in the civil infrastructure," *Constr. Build. Mater.*, vol. 17, no. 6–7, pp. 365–378, Sep. 2003.

[23] L. C. Hollaway, "A review of the present and future utilisation of FRP composites in

the civil infrastructure with reference to their important in-service properties," *Constr. Build. Mater.*, vol. 24, no. 12, pp. 2419–2445, Dec. 2010.

[24] B. Täljsten, "FRP strengthening of concrete structures: new inventions and applications," *Prog. Struct. Eng. Mater.*, vol. 6, no. 3, pp. 162–172, Jul. 2004.

[25] M. Motavalli and C. Czaderski, "FRP composites for retrofitting of existing Civil Structures in Europe: state-of-the-art review," in *Composites & Polycon 2007, American Composite Manufacturers Association, Tampa, Fl, USA.*, 2007.

[26] Z. Wu, W. Xin, Z. Xing, and M. Noori, "State-of-the-art review of FRP composites for major construction with high performance and longevity," *Int. J. Sustain. Mater. Struct. Syst.*, 2014.

[27] A. Nanni, "North American design guidelines for concrete reinforcement and strengthening using FRP: principles, applications and unresolved issues," *Constr. Build. Mater.*, vol. 17, no. 6–7, pp. 439–446, Sep. 2003.

[28] G. Portnov, C. E. Bakis, E. Lackey, and V. Kulakov, "FRP reinforcing bars - designs and methods of manufacture (review of patents)," *Mech. Compos. Mater.*, vol. 49, no. 4, pp. 381–400, 2013.

[29] A. Napoli, L. C. Bank, V. L. Brown, E. Martinelli, F. Matta, and R. Realfonzo, "Analysis and design of RC structures strengthened with mechanically fastened FRP laminates: A review," *Compos. Part B Eng.*, vol. 55, pp. 386–399, Dec. 2013.

[30] S. C. Chin, N. Shafiq, and M. F. Nuruddin, "FRP as strengthening material for Reinforced Concrete beams with openings — A review," *KSCE J. Civ. Eng.*, vol. 19, no. 1, pp. 213–219, Aug. 2014.

[31] A. P. Rathod and T. P. Vora, "Fiber reinforced polymer reinforcement for construction - state of the art review," *Int. J. Res. Eng. Technol.*, vol. 4, no. 2, pp. 2319–2322, 2015.

[32] X.-L. Zhao and L. Zhang, "State-of-the-art review on FRP strengthened steel

structures," *Eng. Struct.*, vol. 29, no. 8, pp. 1808–1823, Aug. 2007.

[33] J. G. Teng, T. Yu, and D. Fernando, "Strengthening of steel structures with fiber-reinforced polymer composites," *J. Constr. Steel Res.*, vol. 78, pp. 131–143, Nov. 2012.

[34] M. Kamruzzaman, M. Z. Jumaat, N. H. R. Sulong, and a B. M. S. Islam, "A review on strengthening steel beams using FRP under fatigue.," *ScientificWorldJournal.*, vol. 2014, no. August 2007, p. 702537, Jan. 2014.

[35] A. Shaat, D. Scbnercb, A. Fam, and S. Rizkalla, "Retrofit of Steel Structures Using Fiber Reinforced Polymers (FRP): State-of-the-Art," no. 919, 2003.

[36] M. R. F. Coelho, J. M. Sena-Cruz, and L. a. C. Neves, "A review on the bond behavior of FRP NSM systems in concrete," *Constr. Build. Mater.*, May 2015.

[37] S. Y. Seo, L. Feo, and D. Hui, "Bond strength of near surface-mounted FRP plate for retrofit of concrete structures," *Compos. Struct.*, vol. 95, pp. 719–727, 2013.

[38] SIKA, "Prestressing Systems for Structural Strengthening with Sika CarboDur," 2015.

[39] ACI, "ACI 440.4R-04 : Prestressing Concrete Structures with FRP Tendons : Reported by ACI Committee 440," pp. 1–35, 2004.

[40] Gregor Schwegler, "Patent US 6851232_Reinforcement Device for Supporting Structures_SIKA FRP plate anchorage system.pdf," 2005.

[41] S. V. Grelle and L. H. Sneed, "Review of Anchorage Systems for Externally Bonded FRP Laminates," *Int. J. Concr. Struct. Mater.*, vol. 7, no. 1, pp. 17–33, Mar. 2013.

[42] R. Kalfat, M. Asce, and S. T. Smith, "Anchorage Devices Used to Improve the Performance of Reinforced Concrete Beams Retrofitted with FRP Composites : State-of-the-Art Review," *J. Compos. Constr.*, vol. 17, no. February, pp. 14–33, 2013.

[43] M. R. Taha and N. G. Shrive, "New Concrete Anchors for Carbon Fiber-Reinforced Polymer Post-Tensioning Tendons — Part 1 : State-of-the-Art Review / Design," *ACI*

Struct. J., no. 100, 2003.

[44] J. W. Schmidt, A. Bennitz, B. Täljsten, P. Goltermann, and H. Pedersen, "Mechanical anchorage of FRP tendons – A literature review," *Constr. Build. Mater.*, vol. 32, pp. 110–121, Jul. 2012.

[45] I. a. Rubinsky and A. Rubinsky, "A preliminary investigation of the use of fibre-glass for prestressed concrete," *Mag. Concr. Res.*, vol. 6, no. 17, pp. 71–78, Sep. 1954.

[46] W. Figeys *et al.*, "Feasibility of a novel system to prestress externally bonded reinforcement," *Mater. Struct.*, vol. 44, no. 9, pp. 1655–1669, Mar. 2011.

[47] P. França and A. Costa, "New anchoring device for prestressing CFRP laminates," in *3rd fib International Congress*, 2010.

[48] M. Maier and H. Andra, "Tensioning Device for strip-shaped tension members, United States Patent, Patent No. US 2005/0252116 A1," 2005.

[49] H. Andra, M. Maier, and R. Beyerlein, "Anchoring for Strip-shaped Traction Elements on Supporting Structures, United States Patent, Patent No. US 7,658,041 B2," 2010.

[50] H. Andra, M. Maier, and D. Sandner, "Clamping Device for a Band-shaped Tensional Member, United States Patent, Patent No. US 6,584,738 B1," 2003.

[51] G. M. Raftery and A. M. Harte, "Low-grade glued laminated timber reinforced with FRP plate," *Compos. Part B Eng.*, vol. 42, no. 4, pp. 724–735, 2011.

[52] A. Borri, G. Castori, and M. Corradi, "Intrados strengthening of brick masonry arches with composite materials," *Compos. Part B Eng.*, vol. 42, no. 5, pp. 1164–1172, 2011.

[53] HughesBrothers, "Carbon Fiber Reinforced Polymer (CFRP) Laminates - Aslan 400 series," 2011.

[54] S&P, "S&P CFRP - Laminates and S&P slot-applied laminates, Technical data sheet," pp. 1–6, 2014.

[55] M. T. El-Mihilmy and J. W. Tedesco, “Analysis of Reinforced Concrete Beams strengthened with FRP Laminates,” *J. Struct. Eng.*, vol. 126, no. June, pp. 684–691, 2000.

[56] M. Arduini and A. Nanni, “Behaviour of Precracked RC Beams strengthened with Carbon FRP Sheets,” *J. Compos. Constr.*, vol. 1, no. 2, pp. 63–70, 1997.

[57] B. Täljsten, “Strengthening concrete beams for shear with CFRP sheets,” *Constr. Build. Mater.*, vol. 17, no. 1, pp. 15–26, Feb. 2003.

[58] H. Nordin and B. Täljsten, “Testing of hybrid FRP composite beams in bending,” *Compos. Part B Eng.*, vol. 35, no. 1, pp. 27–33, Jan. 2004.

[59] H. Saadatmanesh and M. Malek, “Design Guidelines for Flexural Strengthening of RC Beams with FRP Plates,” *J. Compos. Constr.*, vol. 2, no. 4, pp. 158–164, 1998.

[60] D. J. Oehlers, I. S. T. Liu, and R. Seracino, “Shear deformation debonding of adhesively bonded plates,” in *Proceedings of the Institution of Cvil Engineers, Structures & Buildings 158, February 2005*, 2005, no. February, pp. 77–84.

[61] D. J. Oehlers, “FRP plates adhesively bonded to reinforced concrete beams: Generic debonding mechanisms,” *Adv. Struct. Eng.*, vol. 9, no. 6, pp. 738–750, 2006.

[62] S. . Smith and J. . Teng, “FRP-strengthened RC beams. I: review of debonding strength models,” *Eng. Struct.*, vol. 24, no. 4, pp. 385–395, Apr. 2002.

[63] S. . Smith and J. . Teng, “FRP-strengthened RC beams. II: assessment of debonding strength models,” *Eng. Struct.*, vol. 24, no. 4, pp. 397–417, Apr. 2002.

[64] L. C. Holloway and J. G. Teng, *Strengthening and rehabilitation of civil infrastructures using fibre-reinforced polymers (FRP) composites*. Cambridge: Woodead Publishing Limited., 2008.

[65] H. B. Pham and R. Al-Mahaidi, “Prediction Models for Debonding Failure Loads of

Carbon Fiber Reinforced Polymer Retrofitted Reinforced Concrete Beams," *J. Compos. Constr.*, vol. 10, no. February, pp. 48–59, 2006.

[66] M. Z. Jumaat and M. D. A. Alam, "Experimental and numerical analysis of end anchored steel plate and CFRP laminate flexurally strengthened reinforced concrete (r . c .) beams," vol. 5, no. 2, pp. 132–144, 2010.

[67] V. L. Kulakov, Y. M. Tarnopol'skii, A. K. Arnautov, and J. Rytter, "Stress-strain state in the zone of load transfer in a composite specimen under uniaxial tension," *Mech. Compos. Mater.*, vol. 40, no. 2, pp. 91–100, 2004.

[68] H. Yuzuru, K. Takayuki, T. Nobuaki, K. Kazuhiro, K. Akira, and T. Masahiro, "FRP Plate with Anchor Implement, Japanese Patent, Patent Number: 2006-097462," 2006.

[69] Yuzuru, "Japanese Patent for anchor of CFRP plate." 2006.

[70] F. Fischli, R. Clenin, A. De Silva, and P. Chaemmangkang, "Strengthening of structures with the carbostress system," in *Asia-Pacific Conference on FRP in Structures (APFIS 2007), International Institute for FRP in Construction*, 2007, no. Apfis, pp. 387–392.

[71] C. Czaderski and M. Motavalli, "40-Year-old full-scale concrete bridge girder strengthened with prestressed CFRP plates anchored using gradient method," *Compos. Part B Eng.*, vol. 38, no. 7–8, pp. 878–886, Oct. 2007.

[72] C. Czaderski, E. Martinelli, J. Michels, and M. Motavalli, "Effect of curing conditions on strength development in an epoxy resin for structural strengthening," *Compos. Part B Eng.*, vol. 43, no. 2, pp. 398–410, Mar. 2012.

[73] C. Czaderski-forchmann, "Strengthening of reinforced concrete members by prestressed, externally bonded reinforcement with gradient anchorage, PhD Thesis, ETH Zurich," ETH Zurich, 2012.

[74] M. Motavalli, C. Czaderski, and K. Pfyl-lang, "Prestressed CFRP for Strengthening of Reinforced Concrete Structures : Recent Developments at Empa , Switzerland," *J.*

Compos. Constr., vol. 15, no. 2, pp. 194–205, 2011.

[75] C. Czaderski, K. Soudki, M. Motavalli, and M. Asce, "Front and Side View Image Correlation Measurements on FRP to Concrete Pull-Off Bond Tests," no. August, pp. 451–463, 2010.

[76] J. Michels, J. Sena-Cruz, C. Czaderski, and M. Motavalli, "Structural Strengthening with Prestressed CFRP Strips with Gradient Anchorage," *J. Compos. Constr.*, vol. 17, no. 5, pp. 651–661, Oct. 2013.

[77] E. Martinelli, C. Czaderski, and M. Motavalli, "Modeling in-plane and out-of-plane displacement fields in pull-off tests on FRP strips," *Eng. Struct.*, vol. 33, no. 12, pp. 3715–3725, Dec. 2011.

[78] M. Deuring, "Verstärken von Stahlbeton mit gespannten Faserverbundwerkstoffen, PhD Thesis, ETH Zürich," 1993.

[79] S&P, "S&P pre-stressing system: gradient achorage method," 2015.

[80] K. Y. Tan, G. Tumialan, and A. Nanni, "Evaluation of externally bonded CFRP systems for the strengthening of RC slabs," pp. 1–11, 2003.

[81] N. Eshwar, A. Nanni, and T. J. Ibell, "Performance of two anchor systems of externally bonded fiber-reinforced polymer laminates," *ACI Mater. J.*, vol. 105, no. 1, pp. 72–80, 2008.

[82] S&P, "Guide for the application of S&P FRP Systems," 2006.

[83] S. L. Burtscher, "Anchoring for pre-tensioned and/or stressed tensile elements, United States Patent Application, Patent No. US 2007/ 0221894 A1.," 2007.

[84] A. Vorwagner, S. L. Burtscher, G. Grass, and C. Freund, "Application of Prestressed Near Surface Mounted Carbon Fibre Reinforced Polymer (PNSM)," in *First Middle East Conference on Smart Monitoring, Assessment and Rehabilitation of Civil*

Structures, 8-10 February 2011, Dubai, UAE, 2011, pp. 1–9.

[85] A. Vorwagner, "Entwicklung eines effizienten und dauerhaften Verankerungssystems für vorgespannte eingeschlitzte Kohlefaserlamellen zur Bauteilverstärkung, Institut für Hochbau und Technologie," 2012.

[86] A. Vorwagner and S. L. Burtscher, "Wedge Anchorage for Near Surface Mounted Applications - Stregthening of Structures by Using Prestressed Carbon Fibre Reinforced Strips," in *Talk: fib - 3rd International Congress and Exhibition, Washington, USA; 2010-05-29 - 2010-06-02; in: "3rd International fib Congress and Exhibition,"* 2010.

[87] A. Vorwagner and S. L. Burtscher, "Improvement of Serviceability by Strengthening with Prestressed NSM," in *Talk: IABSE Symposium Venice 2010, Venedig; 2010-09-22 - 2010-09-24; in: "IABSE Symposium Venice 2010 - Large Structures and Infrastructures for Environmentally Constrained and Urbanised Areas,"* 2010.

[88] A. Vorwagner, S. L. Burtscher, and J. Kollegger, "Experimental Investigation of Strengthened Beams by using Prestressed near Surface Mounted Carbon Fiber Strips," in *fib Symposium Prague 2011, Prag; 08.06.2011 - 10.06.2011; in: "Concrete engineering for excellence and efficiency, proceedings Volume 2,"* 2011.

[89] D. Duthinh and M. Starnes, *Strengthening of reinforced concrete beams with carbon FRP*. 2001.

[90] H. Andra, M. Maier, and R. Beyerlein, "Anchoring for strip-shaped traction elements on supporting structures," United States Patent, Pub. No.: US 2006/0272246 A1, 2006.

[91] H. Andra and M. Maier, "Method of installing tension members on supporting structures, and apparatus for performing the method, United States Patent, Patent No. US 7,296,385 B2," 2007.

[92] H. Andra, G. Konig, and M. Maier, "Tie anchor for a strip-type tension member, United States Patent, Patent No. US 7,441,380 B2," 2008.

[93] M. Maier, D. Sandner, and H. Andra, “Method and apparatus for strengthening/ restoring a reinforced/ prestressed concrete structure, United States Patent, Patent No. US 6,385,940 B1,” 2002.

[94] H. Andra and M. Maier, “Post-strengthening with externally bonded prestressed CFRP strips,” in *IABSE Congress report, 16th Congress of IABSE, Lucerne*, 2000, pp. 1507–1514.

[95] S&P, “Publikationen / Bücher FRP Tragwerkverstärkung - VORSPANNEN (V) Publications / Books FRP strengthening systems - prestressing Publikationen / Bücher FRP Tragwerkverstärkung - VORSPANNEN (V) Publications / Books FRP strengthening systems - prestressing,” 2015.

[96] S&P, “S&P pre-stressing system,” 2015.

[97] P. Fernandes, C. Fernandes, P. Silva, and E. Júlio, “Flexural response of HSC girders strengthened with non- and prestressed CFRP laminates,” in *FRPRCS-11*, 2013, pp. 1–9.

[98] I. Stöcklin and U. Meier, “Strengthening of concrete structures with prestressed and gradually anchored CFRP,” in *FRPRCS-6: proceedings of the Sixth Inter‐ national Symposium on FRP Reinforcement for Concrete Structures, FRPRCS-6, Singapore. Singapore:World Scientific*, 2003.

[99] I. Stöcklin, U. Meier, and G. Pietro Terrasi, “Making better use of the strength of advanced materials in structural engineering,” in *CICE01: proceedings od the FRP Composites in Civil Engineering, CICE01, Hong Kong, China. Hong Kong: Elsevier*, 2001.

[100] M. R. Garcez, L. C. Meneghetti, and L. C. P. S. Filho, *Applying Post-Tensioning Technique to Improve the Performance of FRP Post-Strengthening, Chapter 4*, no. 1980. 2013.

[101] K. Brosens, “Anchorage of externally bonded steel plates and CFRP laminates for the strengthening of concrete elements, PhD Thesis,” Katholieke Universiteit Leuven, 2001.

[102] W. Figeys, L. Schueremans, D. Van Gemert, K. Brosens, and J. Dereymaeker, “Feasibility study of a novel prestressing system for FRP-laminates,” pp. 1175–1180, 2009.

[103] E. Verstrynge, K. De Wilder, R. Timmermans, L. Schueremans, and L. Vandewalle, “Retrofitting of think concrete slabs with various types of externally bonded reinforcement,” in *8th International Conference on Structural Analysis of Historical Constructions, October 15-17 2012, Wroclaw, Poland*, 2012.

[104] W. Figeys, “Shear modeling of steel cord reinforced polymer, prestressing and bonding technology for externally bonded reinforcement, PhD Thesis,” katholieke Universiteit Leuven, 2008.

[105] Guo, “Active prestressed carbon fiber plate reinforcing system, Chinese Patent, Patent No. CN 203065976 U,” 2013.

[106] F. Mohee, A. Al-Mayah, and A. Plumtree, “Friction Characteristics of CFRP Plates in Contact with Copper Plates under High Contact Pressure,” *J. Compos. Constr.*, p. 4016022, 2016.

[107] G. Portnovs, “Gripping device for transmission of tensile load to an elastic strip, European Patent Appllication, Patent No. EP 2602399 A1,” 2013.

[108] G. Portnov and C. E. Bakis, “Analysis of stress concentration during tension of round pultruded composite rods,” *Compos. Struct.*, vol. 83, no. 1, pp. 100–109, Mar. 2008.

[109] G. G. Portnov, V. L. Kulakov, and A. K. Arnautov, “A refined stress-strain analysis in the load transfer zone of flat specimens of high-strength unidirectional composites in uniaxial tension 1. Theoretical analysis,” *Mech. Compos. Mater.*, vol. 42, no. 6, pp. 547–

554, 2006.

[110] G. G. Portnov, V. L. Kulakov, and A. K. Arnautov, “A refined stress-strain analysis in the load transfer zone of flat specimens of high-strength unidirectional composites in uniaxial tension 2. Finite-Element Parametric Analysis,” *Mech. Compos. Mater.*, vol. 43, no. 1, pp. 29–40, 2007.

[111] G. G. Portnov, V. L. Kulakov, and A. K. Arnautov, “A refined stress-strain analysis in the load transfer zone of flat specimens of high-strength unidirectional composites in uniaxial tension 3. Effect of Grip Misalignment,” *Mech. Compos. Mater.*, vol. 43, no. 6, pp. 503–512, 2007.

[112] M. E. Cunningham, S. V. Schoultz, and J. M. Toth, “Effect of end-tab design on tension specimen stress concentrations,” in *Recent Advances in Composite in the United States and Japan, ASTM STP 864*, 1985, pp. 253–262.

[113] A. Al-Mayah, K. Soudki, and A. Plumtree, “Effect of Sandblasting on Interfacial Contact Behavior of Carbon-Fiber-Reinforced Polymer-Metal Couples,” *J. Compos. Constr.*, vol. 9, no. 4, pp. 289–295, 2005.

[114] A. Al-Mayah, “Interfacial behaviour of CFRP-metal couples for wedge anchor systems,” University of Waterloo, 2004.

[115] U. Meier, “Securing of reinforcing strips,” 1995.

[116] E. Y. Sayed-Ahmed and N. G. Shrive, “A new steel anchorage system for post-tensioning applications using carbon fibre reinforced plastic tendons,” *Can. J. Civ. Eng.*, vol. 25, no. 1, pp. 113–127, 1998.

[117] X. Ning and M. R. Lovell, “On the Sliding Friction Characteristics of Unidirectional Continuous FRP Composites,” *J. Tribol.*, vol. 124, no. 1, pp. 5–13, 2002.

[118] N. P. Suh, *Tribophysics*. 1986.

[119] N. P. Suh and N. Saka, “Tribology: friction , wear and lubrication: Basic mechanisms – Technology : Design , manufacture , maintenance,” 2004.

[120] R. M. Overney, “Tribology Fundamentals,” 2008.

[121] H. G. Howell, “The Laws of Static Friction,” pp. 589–591.

[122] J. Howell, H. G., and Mazur, “J. Textile Inst.,” *J. Text. Inst.*, vol. T59, 1953.

[123] T. Tsukizoe and N. Ohmae, “Friction and Wear of Advanced Composite Materials,” *Fibre Sci. Technol.*, vol. 18, pp. 265–286, 1983.

[124] O. Jacobs, K. Friedrich, G. Marom, K. Schulte, and H. D. Wagner, “Fretting wear performance of glass-, carbon-, and aramid-fibre/epoxy and peek composites,” *Wear*, vol. 135, pp. 207–216, 1990.

[125] W. Z. Nie and J. Li, “Effect of carbon fibre content on friction and wear properties of carbon fibre reinforced PA6 composites,” *Plast. Rubber Compos.*, vol. 39, no. 1, pp. 10–15, 2010.

[126] I. F. Brown and C. J. Burgoyne, “The friction and wear of Kevlar 49 sliding against aluminium at low velocity under high contact pressures,” *Wear*, vol. 236, pp. 315–327, 1999.

[127] J. P. Giltrow and J. K. Lancaster, “The role of the counterface in the friction and wear of carbon fibre reinforced thermosetting resins,” *Wear*, vol. 16, pp. 359–374, 1970.

[128] S. M. Mahdavian, Y. W. Mai, and B. Cotterell, “Friction, metallic transfer and debris analysis of sliding surfaces,” *Wear*, vol. 82, pp. 221–232, 1982.

[129] T. C. Ovaert, “On the wear behavior of longitudinally (parallel) oriented unidirectional fiber reinforced polymer composites,” *Tribol. Trans.*, vol. 38, no. 1, pp. 27–34, 1995.

[130] J. K. Lancaster, “Polymer-based bearing materials: The role of fillers and fibre reinforcement,” *Tribology*, vol. 5, no. 6, pp. 249–255, 1972.

[131] N. Sung and N. Suh, “Effect of fiber orientation on friction and wear of fiber reinforced polymeric composites,” vol. 53, pp. 129–141, 1979.

[132] T. Tsukizoe and N. Ohmae, “Wear performance of unidirectionally oriented carbon-fibre-reinforced plastics,” *Tribol. Int.*, no. August, pp. 171–176, 1975.

[133] M. Shimbo, “Frictional behaviour of cured epoxide resins,” vol. 91, 1983.

[134] N. K. Myshkin, M. I. Petrokovets, and a. V. Kovalev, “Tribology of polymers: Adhesion, friction, wear, and mass-transfer,” *Tribol. Int.*, vol. 38, no. 11–12, pp. 910–921, Nov. 2005.

[135] F. Van De Velde and P. De Baets, “The friction and wear behaviour of polyamide 6 sliding against steel at low velocity under very high contact pressures,” *Wear*, 1997.

[136] S. Matsunaga and T. Matsubara, “Effects of Reciprocation Number on the Friction Behaviors of Carbon / Epoxy for Various Fiber Orientations and High Contact Pressures,” in *Proc. ICCM-13, Beijing*, 2001, pp. 1–10.

[137] J. Schön, “Coefficient of friction of composite delamination surfaces,” *Wear*, vol. 237, no. 1, pp. 77–89, 2000.

[138] J. Schön, “Coefficient of friction and wear of a carbon fiber epoxy matrix composite,” *Wear*, vol. 257, no. 3–4, pp. 395–407, Aug. 2004.

[139] J. Schön, “Coefficient of friction for aluminum in contact with a carbon fiber epoxy composite,” *Tribol. Int.*, vol. 37, no. 5, pp. 395–404, May 2004.

[140] I. C. Roselmant and D. Tabor, “The friction of carbon fibres,” *J. Phys. D Appll. Phys.*, vol. 9, 1976.

[141] A. Al-Mayah, K. Soudki, and A. Plumtree, “Effect of Sleeve Material on Interfacial Contact Behavior of CFRP-Metal Couples,” *J. Mater. Civ. Eng. ASCE*, vol. 16, no. 6, pp. 825–830, 2006.

[142] A. Al-Mayah, K. Soudki, and A. Plumtree, “Effect of rod profile and strength on the contact behavior of CFRP-metal couples,” *Compos. Struct.*, vol. 82, no. 1, pp. 19–27, 2008.

[143] A. Sikder, “Tribo-testing applications in automotive and effective characterization of the tribo-tests,” 2014.

[144] D. Kwon, H. Park, S. Ghosh, and C. Lee, “Recrystallization of the copper films deposited by pulsed electroplating on ECR plasma-cleaned copper seed layers,” *J. Korean Phys. Soc.*, vol. 44, no. 5, pp. 1108–1112, 2004.

[145] F. M. Mohee, A. Al-Mayah, and A. Plumtree, “Development of an Innovative Prestressing CFRP Plate Anchor: Numerical Modelling and Parametric Study,” *Compos. Struct.*, 2017.

[146] C. Harper, *Handbook of plastic, elastomers & composites*. McGraw-Hill, New York, 2002.

[147] Matweb, “Material property data.” .

[148] A. Al-Mayah, K. Soudki, and A. Plumtree, “Novel Anchor System for CFRP Rod: Finite-Element and Mathematical Models,” *J. Compos. Constr.*, vol. 11, no. 5, pp. 469–476, 2007.

[149] A. Al-Mayah, K. Soudki, and A. Plumtree, “Mechanical Behavior of CFRP rod Anchors under Tensile Loading,” *J. Compos. Constr.*, vol. 5, no. 2, pp. 128–135, 2001.

[150] I. M. Daniel and O. Ishai, *Engineering Mechanics of Composite Materials*. Oxford University Press, Inc., 1994.

[151] I. Press, “Friction characteristics of CFRP plates in contact with copper plates under high contact pressure, in-press,” *J. Compos. Constr.*, 2016.

[152] A. J. Schepis, “On the Theory of Shrink Fits with Application to Waveguide Pressure

Seals," *Bell Syst. Tech. J.*, vol. May, pp. 885–907, 1962.

[153] S. P. Timoshenko and J. N. Goodier, *Theory of Elasticity*, 3rd Editio. McGraw-Hill, Inc., New York, 1970.

[154] J.-J. Chyu, *Elastic Beam Calculations Handbook*. J. Ross Publishing, 2009.

[155] C. T. Wang, *Applied Elasticity*. McGraw-Hill, New York, 1953.

[156] E. Ventsel and T. Krauthammer, *Thin Plates and Shells: theory, Analysis, and Applications*. Marcel Dekker, Inc., 2001.

[157] S. P. Timoshenko and S. Woinowsky-Krieger, *Theory of Plates and Shells*, 2nd Editio. McGraw-Hill, Inc., New York.

[158] Lusas, *The Calculation of Modulus of Subgrade Reaction for a "Winkler Spring" model*. Finite Element Analysis Ltd., 2013.

[159] S. K. Gupta and A. Gangal, *Learning Composite Mathematics*. 2015.

[160] M. A. Biot, "Bending of an infinite beam on an elastic Foundation," *J. Appl. Math. Mech.*, vol. 203, p. A-1-A-7, 1937.

[161] J. J. O'Connor, *A Maple Handbook*. 2005.

[162] F. M. Mohee, A. Al-Mayah, and A. Plumtree, "Development of a Novel Prestressing Anchor for CFRP Plates: Experimental Investigations," *Compos. Struct.*, 2017.

[163] ASM, *Source Book on Industrial Alloy and Engineering Data*. American Society for Metals (ASM), 1978.

[164] ASM, *Metals Handbook*. American Society for Metals (ASM), 1995.

[165] ASTM, *Socket head cap screw (ASTM A574) torque chart*. fastenal.com, 2016.

APPENDIX A

MATHEMATICS-BASED ANALYTICAL MODEL

$$y := unapply\left(combine\left(\frac{5}{24}\cdot\frac{(p\cdot l^4)}{E\cdot\left(\frac{(2\cdot l)\cdot(2\cdot t)^3}{12}\right)}\cdot\left(1+\frac{12}{5}\cdot\frac{t^2}{l^2}\cdot\left(\frac{4}{5}+\frac{v}{2}\right)\right)\right), p, l, E, t, v\right);$$

$$(p, l, E, t, v) \to \frac{5}{32}\,\frac{p\,l^3\left(1+\frac{12}{5}\,\frac{t^2\left(\frac{4}{5}+\frac{1}{2}\,v\right)}{l^2}\right)}{E\,t^3} \quad \textbf{(1)}$$

$$yElasticFoundation := unapply\left(combine\left(\left(p\cdot\left(\frac{2-(\exp(-b\cdot 1)\cdot\cos(b\cdot l))-(\exp(-b\cdot 0)\cdot\cos(b\cdot 0))}{2\cdot k}\right)\right)\right), p, k, b, l\right);$$

$$(p, k, b, l) \to \frac{1}{2}\,\frac{p-p\,e^{-b\,l}\cos(b\,l)}{k}$$

$DELTA := 0.2834;$

$$0.2834 \quad \textbf{(3)}$$

$tw := 9.3503;$

$$9.3503 \quad \textbf{(4)}$$

$tb := 26.5331;$

$$26.5331 \quad \textbf{(5)}$$

$L3 := 92.68;$

$$92.68 \quad \textbf{(6)}$$

$$\textbf{(7)}$$

$L1 := 50;$

$$50 \quad \textbf{(8)}$$

$Lwb1 := 38;$

$$38$$

$$\textbf{(10)}$$

$L2 := 38;$

$$38 \quad \textbf{(11)}$$

$Lwb2 := 19;$

$$19 \quad \textbf{(12)}$$

$p4 := 0;$

========== CFRP Plate ==========

$Efrp := 9500;$

9500 **(13)**

$Efrplong := 165000;$

165000 **(14)**

(15)

$$kfrp := \frac{0.71 \cdot \left(\frac{L1}{2}\right) \cdot Efrp}{\frac{100}{1.09}};$$

1838.012500

$$tfrp := \frac{1.2}{2};$$

0.6000000000

$lengthfrp := 10;$

10 **(18)**

$$bfrp := \left(\frac{kcu}{4 \cdot Efrplong \cdot \frac{lengthfrp \cdot tfrp^3}{12}}\right)^{0.25};$$

$0.05386366369\ kcu^{0.25}$ **(19)**

========== Copper Sleeve ==========

$Ecu := 117000;$

117000 **(20)**

$tcu := 0.8;$

0.8 **(21)**

$vcu := 0.31;$

0.31 **(22)**

$$kcu := \frac{Ecu}{\text{sqrt}(L3 \cdot 50)} \cdot \frac{1}{0.95 \cdot (1 - vcu^2)};$$

2001.538072

$lengthcu := 10;$

10 **(24)**

(25)

$$bcu := \left(\frac{kfrp}{4 \cdot Ecu \cdot \frac{lengthcu \cdot tcu^3}{12}}\right)^{0.25};$$

0.3097444071 **(26)**

========== Wedge ==========

$Ew := 200000;$

$vw := 0.30;$

$$0.30 \quad (27)$$

$$kw := \frac{Ew}{\text{sqrt}(L3 \cdot 50)} \cdot \frac{1}{0.95 \cdot (1 - vw^2)};$$

$$3398.497724$$

$tw;$

$$9.3503$$

$$(31)$$

$lengthw := 10;$

$$10 \quad (32)$$

$$bw := \left(\frac{kcu}{4 \cdot Ew \cdot \frac{lengthw \cdot tw^3}{12}} \right)^{0.25};$$

$$0.04377686122 \quad (33)$$

========== Barrel ==========

$Eb := 200000;$

$$200000 \quad (34)$$

$vb := 0.30;$

$$0.30 \quad (35)$$

$lengthb := 10;$

$$10 \quad (36)$$

$$tb2 := \frac{tb}{2};$$

$$13.26655000 \quad (37)$$

$$bb := \left(\frac{kw}{4 \cdot Eb \cdot \frac{\text{lengthb} \cdot tb^3}{12}} \right)^{0.25};$$

$$(38)$$

$Hhalfbarrel := 37;$

$$37 \quad (39)$$

$tbarrelwall := 35;$

$$35 \quad (40)$$

$$yb2 := \frac{Hhalfbarrel}{Eb} \cdot \frac{p3 \cdot L2}{2 \cdot tbarrelwall};$$

$$\frac{703}{7000000}\ p3 \quad (41)$$

(42)

========== Individual Sections are done, now starting solving equations ========

$yfrp := unapply(yElasticFoundation((p1), kfrp, bcu, L1), p1);$

$$p1 \rightarrow 0.0002720330202\ p1 \quad (43)$$

$ycu := unapply(yElasticFoundation((p2), kcu, bw, L1), p2);$

$$p2 \rightarrow 0.0002660265650\ p2 \quad (44)$$

$yw := unapply\left(yElasticFoundation\left(\frac{p3}{2}, kw, bb, Lwb1\right), p3\right);$

$$p3 \rightarrow 0.00005362539645\ p3 \quad (45)$$

(46)

$yb := unapply\left(y\left(\frac{p3}{2}, Lwb2, Eb, tb2, vb\right) - yb2, p3\right);$

$$p3 \rightarrow -0.00009800555743\ p3 \quad (47)$$

$inter1 := yfrp(p1) - ycu(p2);$

$$0.0002720330202\ p1 - 0.0002660265650\ p2 \quad (48)$$

$inter2 := ycu(p2) - yw(p3);$

$$0.0002660265650\ p2 - 0.00005362539645\ p3 \quad (49)$$

$inter3 := yw(p3) - yb(p3) - DELTA;$

$$0.0001516309539\ p3 - 0.2834 \quad (50)$$

$inter4 := yb(p3);$

$$-0.00009800555743\ p3 \quad (51)$$

$solve(\{inter1, inter2, inter3\}, \{p1, p2, p3\});$

$$p1 = 368., p2 = 377 \quad (52)$$